NASA-CR-174,657
NASA CR-174657
Creare TN-371

ANALYTICAL AND EXPERIMENTAL INVESTIGATION OF RUBBING INTERACTION IN LABYRINTH SEALS FOR A LIQUID HYDROGEN FUEL PUMP

by
Francis X. Dolan
Francis E. Kennedy
Erland M. Schulson

CREARE R&D INCORPORATED
prepared for

NATIONAL AERONAUTICS AND SPACE ADMINISTRATION

NASA Lewis Research Center
Contract NAS 3-23276

Engineering Research and Development
Computer Systems and Software

1. Report No.	2. Government Accession No.	3. Recipient's Catalog No.
CR 174657		

4. Title and Subtitle	5. Report Date
Analytical and Experimental Investigation of Rubbing Interaction in Labyrinth Seals for a Liquid Hydrogen Fuel Pump	August 1984
	6. Performing Organization Code
7. Author(s)	8. Performing Organization Report No.
Francis X. Dolan, Francis E. Kennedy, Erland M. Schulson	TN-371
	10. Work Unit No.
9. Performing Organization Name and Address	11. Contract or Grant No.
Creare R&D Inc. Box 71 Hanover, NH 03755	NAS 3-23276
	13. Type of Report and Period Covered
12. Sponsoring Agency Name and Address	Final
NASA LeRC 21000 Brookpark Road Cleveland, OH 44135	14. Sponsoring Agency Code

15. Supplementary Notes

Project Manager, Robert C. Bill, NASA Lewis Research Center
Cleveland, Ohio

16. Abstract

A combined analytical and experimental program was carried out to address issues related to the observed cracking of the titanium knife edges on the labyrinth seals of the liquid hydrogen fuel pump in the Space Shuttle main engine.

Finite element analysis of the thermal response of the knife edge in sliding contact with the wear ring surface shows that interfacial temperatures can be quite high and they are significantly influenced by the thermal conductivity of the surfaces in rubbing contact.

Thermal shock experiments were carried out using a test specimen similar to the knife edge geometry. These tests demonstrate that cracking of the titanium alloy is possible in a situation involving repeated thermal cycles over a wide temperature range, as might be realized during a rub in the liquid hydrogen fuel pump.

High-speed rub interaction tests were conducted using a representative knife edge and seal geometry over a broad range of interaction rates. Alternate materials were also experimentally evaluated. These tests provide information which can be used to design improved labyrinth seals for the HPFP of the SSME. In particular, plasma-sprayed aluminum-graphite was found to be significantly better than presently used aluminum alloy seals from the standpoint of rub performance. Ion nitriding the titanium alloy knife-edges was also found to improve rub performance compared to the untreated baseline.

17. Key Words (Suggested by Author(s))	18. Distribution Statement
cryogenic rub interaction labyrinth seal titanium alloy thermal fatigue crack initiation	

19. Security Classif. (of this report)	20. Security Classif. (of this page)	21. No. of Pages	22. Price*
Unclassified	Unclassified		

* For sale by the National Technical Information Service, Springfield, Virginia 22161

NASA-C-168 (Rev. 10-75)

N85-18084#

TABLE OF CONTENTS

TABLE OF CONTENTS (Continued)

LIST OF TABLES

LIST OF FIGURES

LIST OF FIGURES (Cont'd)

This Page Intentionally Left Blank

SUMMARY

A combined program of analysis and experimentation has been carried out to address issues related to the observed cracking of the titanium knife edges on the labyrinth seals of the liquid hydrogen fuel pump in the Space Shuttle main engine. The cracking is believed to be caused by combined thermal and mechanical stresses in the knife edge which occur during rub interaction between the knife edge and mating wear ring of the labyrinth seal.

A steady-state finite element analysis examined the thermal response of the labyrinth seal geometry with a steady heat flux in the contact zone. The heat flux was estimated from a surface plasticity model. The boundary condition for the seal configuration in the analysis assumed an infinite heat sink at the temperature of liquid hydrogen. This analytical method considered the effects of contact geometry (length) and material properties on the steady-state temperature achieved at the interface of the knife edge and wear ring. The preliminary analysis shows that this temperature can be quite high and is significantly influenced by the thermal conductivity of the mating surfaces.

Thermal shock experiments were carried out using titanium test specimens with geometry similar to the knife edge. Individual specimens were cycled, 1, 3 and 10 times between two high temperatures and the temperature of liquid nitrogen. These tests demonstrate that cracking of the titanium alloy is possible in a situation involving repeated thermal cycles over a wide temperature range, as might be realized during a rub in the liquid hydrogen fuel pump.

High-speed rub interaction tests were conducted using a representative knife edge and seal geometry. Tests were carried out with the baseline titanium and aluminum knife edge and wear ring material. Alternate materials were also experimentally evaluated. A total of 15 tests were conducted with the various material combinations, over a wide range of interaction rates. These tests provide information which can be used to design improved labyrinth seals for the high pressure fuel pump of the SSME. In particular, plasma-sprayed aluminum/silicon/graphite was found to be significantly better than presently used aluminum alloy seals from the standpoint of rub performance. Also, nitrogen ion implantation of the titanium alloy knife edge improved rub performance compared to the untreated baseline material.

1 INTRODUCTION

In modern high performance turbomachinery, clearances between the rotating components and the adjacent stationary structures are reduced to a minimum in order to maximize the efficiency of these machines. For instance, a labyrinth seal is used on the shrouded impeller of the High Pressure Fuel Pump (HPFP) of the Space Shuttle Main Engine (SSME) to prevent leakage of liquid hydrogen fuel from the pump discharge to the inlet of the pump. The close clearances are maintained between "knife edges" on the impeller shroud and stationary "wear rings" which are formed in the pump outer case. It has been estimated (Ref. 1) that a decrease in pump efficiency of 1 to 2% is incurred if the labyrinth clearance is increased by 0.127 mm (0.005 inch).

Rubbing wear is a common occurrence in high speed turbomachines as the impellers and shafts are subjected to rapid transients and body forces during engine operation and vehicle maneuvers. The resulting impeller to wear ring relative deflections can be substantially larger than predicted for normal steady operation. As a consequence, the labyrinth knife edges will machine or "abrade" a groove into the opposing wear rings. If the knife edges are able to accomplish this in a manner such that most or all of the material removal is from the wear rings rather than from the knife edges, the net performance loss is minimized upon return of the rotor to its nominal operating position (Ref. 2). One quantitative measure for determining the acceptability of seal wear behavior is the volume wear ratio (VWR). VWR is defined as the ratio of the volume loss of knife edge material during a rub to the loss of wear ring material. Usually, VWR < 0.1 would constitute an acceptable seal wear rate.

During the course of such interactions, it is just as important that the knife edges do not pick up substantial seal material, known as "transfer" or "pickup", since this grooves the wear rings even deeper than the normal-length labyrinth would have. A seal that allows a knife edge to wear it away with minimal occurrence of transfer is known as "abradable". Various abradable seal materials have been developed in recent years for labyrinth and other gas path seals in turbomachinery. These include: low shear strength, plastically deformable materials (Ref. 3), porous sintered metals and fibermetals (Refs. 4, 5), and plasma-sprayed porous ceramics (Ref. 6). Although each of these materials was designed to abrade easily when placed on the stator component of gas path seals, it has sometimes been necessary to add hard or abrasive coatings to the rotor component of the seal to lessen the wear of the rotor component during seal rubs (Refs. 7, 8).

The HPFP was designed with such abradable seals. The stationary wear rings are made of 2024 aluminum alloy and are intended to be sacrificially worn by the Ti-5Al-2.5Sn alloy knife edges on the impeller shroud. However, as described in Reference 1, there is evidence of crack formation in the titanium alloy knife edges as a result of cyclic thermal strains imposed in the course of rub interactions with the wear rings.

Creare R&D Inc. has carried out a program of analysis and experimentation which addresses some of the issues related to the observed cracking of the bill-of-materials (BOM) labyrinth knife edges, and which

examined alternate materials as candidates for the HPFP labyrinth knife edges and wear ring. The objectives of this program were to identify the role of rub interaction in the initiation of impeller knife-edge cracks, and to evaluate alternate seal material/knife edge coating systems. The alternate seal material combinations were assessed from the standpoint of reducing the incidence of cracking as well as retention of minimum clearances. In order to meet these criteria the alternate materials must exhibit low disk heating compared to the baseline combination, and the VWR must also be less than for the baseline materials.

Finite element analysis was used to examine the first stage impeller and wear ring under combined centrifugal, pressure and thermal loads, and to examine the knife edges and adjacent regions of the wear rings with heat generation input from a rub. The basic analysis was extended to consider different rub geometries (contact length) and alternate wear ring materials and treatments to the knife edge.

Experimental investigations of cracking of the labyrinth finger knife edge were carried out in two phases. In the first, test specimens of the titanium alloy were subjected to multiple thermal cycles between either of two elevated temperatures (593°C and 1150°C) and liquid nitrogen temperature (-196°C). These experiments provided a severe thermal shock simulation of a rub interaction followed by cooling of the knife edge in the surrounding cryogen.

The second phase experimental program involved actual rub interactions between rotating knife edges and wear ring specimens in a cryogenic (liquid nitrogen) environment. These tests were conducted with several different coatings and materials on the knife edge and wear ring in order to identify candidate materials for replacement service in the SSME HPFP. For most of the material combinations, tests were conducted at two rates of interaction between the wear ring and the knife edge.

The test specimens from the thermal shock and rubbing tests were metallurgically examined in order to characterize the extent and type of failure or wear of the materials in the different tests.

Section 2 describes the analysis efforts which were carried out in this program and presents results in the form of temperature and stress gradients for the HPFP labyrinth fingers and the wear rings. Thermal profiles for the alternate materials considered in the analysis are also presented.

The experimental investigations are presented in two separate sections. The thermal shock experiments and results are described in Section 3 and Section 4 describes the rub interaction tests, the test hardware and procedures and a summary of test results.

An overall summary and conclusions from the work carried out in this project and recommendations for additional work are presented in Section 5.

Appendix A provides a report on the results of supplementary analysis and experiments carried out on this contract. That work included finite element modeling of the labyrinth fingers and wear ring for cases having

rub lengths of 30° and 360°, and also considered aluminum and copper wear ring materials. Results for some low-speed rub tests and single-pass abradability tests are also presented in Appendix A.

Appendix B provides a brief analysis of the contact angle and wear rate in a rub situation.

Documentation for the materials used in the experimental phases of this program is provided in Appendix C.

Test data for all rub interaction experiments are presented in Appendix D in the form of plots of the temperatures, forces and displacements of the test specimens during the incursion period.

Appendix E describes in detail the metallurgical examination of wear components from one test. Micrographs of all wear specimens are included in Appendix F.

2 PRELIMINARY ANALYTICAL MODELING OF RUB INTERACTION

Finite element methods were used in several stages to analyze the impeller and seal of the HPFP under conditions of normal pump operation and for an assumed rub interaction scenario. This section provides some background information on the models and assumptions used in the analyses and describes results for specific cases.

2.1 Impeller and Wear Ring Analysis

Analyses of the first stage impeller and wear ring were undertaken using the steady-state ANSYS code to determine the levels of stresses under combined centrifugal (impeller only), thermal and pressure loads. Finite element models for the impeller and wear ring were based on pump geometry information provided to Creare by the NASA Project Manager. Pump environmental conditions (temperatures and pressures) were obtained from Reference 9.

The finite element models for the wear ring and impeller are shown in Figures 2-1 and 2-2, respectively, with additional details of the element breakup in the labyrinth fingers shown in Figure 2-3. These models were used to calculate the combined thermal, pressure and centrifugal stresses during a rub.

In these calculations, the temperatures of the surface elements in the rub contact region of the knife edge and wear ring were assumed to be at 260°C (500°F). This interface temperature resulted from a preliminary analysis of the thermal response of the seal components having an imposed steady heat input of 330 kW/cm² (2000 Btu/s-in²). That heat rate was calculated using a surface plasticity model (Ref. 10) that assumes shearing of the aluminum wear ring by the rotating knife edge. When compared with rub energy data from low-speed knife edge tests performed in support of this project (see Appendix A) this heat input rate appears to be high, although temperatures measured in the wear ring during the rub tests (Section 4.6) are higher than this temperature for some tests.

The results of the finite element calculations are shown in Figures 2-4 and 2-5 which display profiles of the combined stresses for the impeller and wear ring. The maximum stress level at the tip of the second labyrinth finger is only about 270 MPa (39,200 psi) while peak stresses in the wear ring surface at the point of rubbing contact are about 488 MPa (70,800 psi). Even imposed cyclically these stress levels are not high enough to initiate cracking in the knife edge.

2.2 Labyrinth Seal Thermal Analysis

A finite element thermal analysis using the ANSYS code was performed to estimate the steady-state temperature distribution at the interface between the labyrinth finger and wear ring during a rubbing contact. The analysis considered different rub contact lengths for the BOM titanium and aluminum materials, and also examined the effects of alternate knife edge and wear ring materials on rub temperatures.

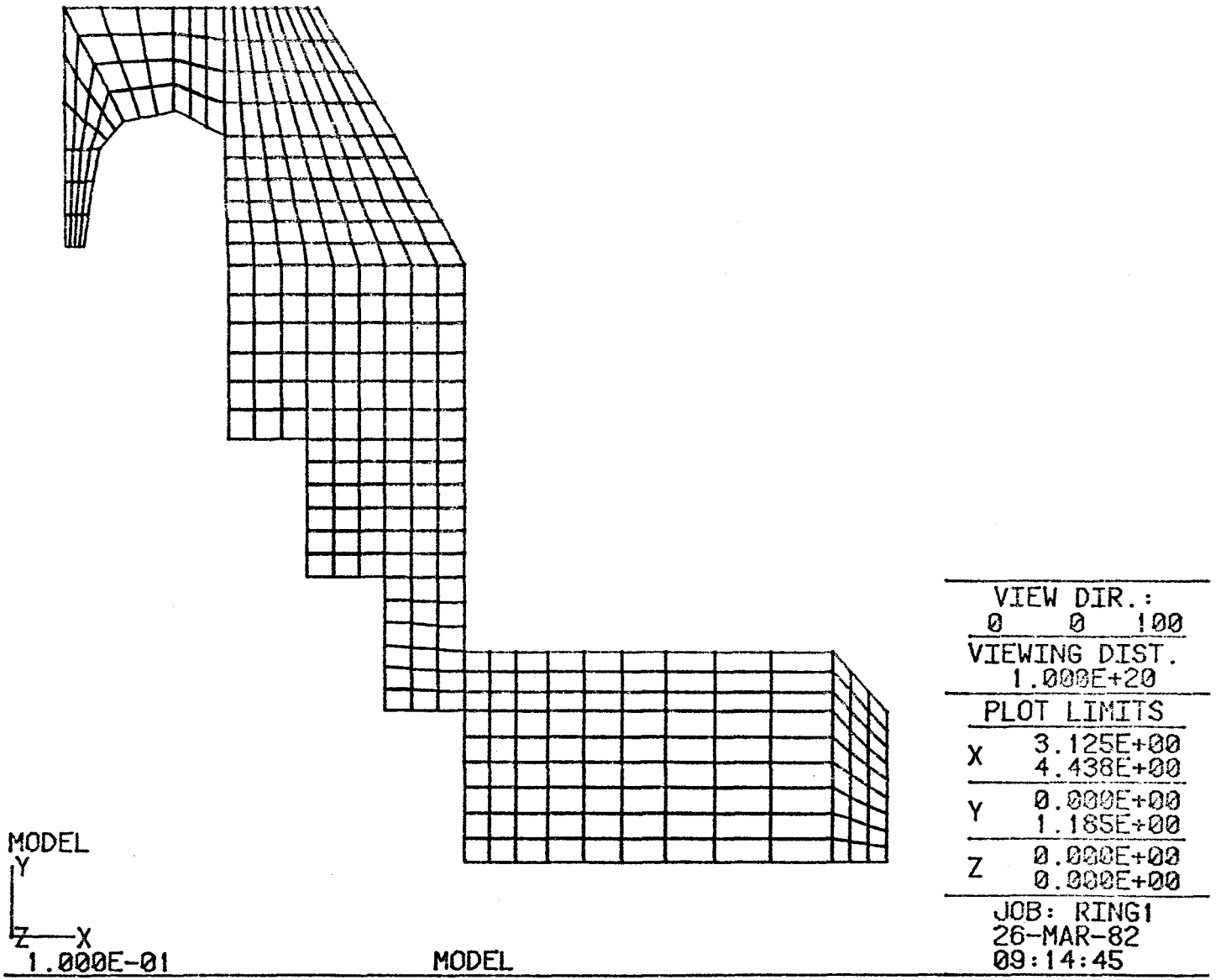

FIGURE 2-1. FINITE ELEMENT MODEL FOR WEAR RING.

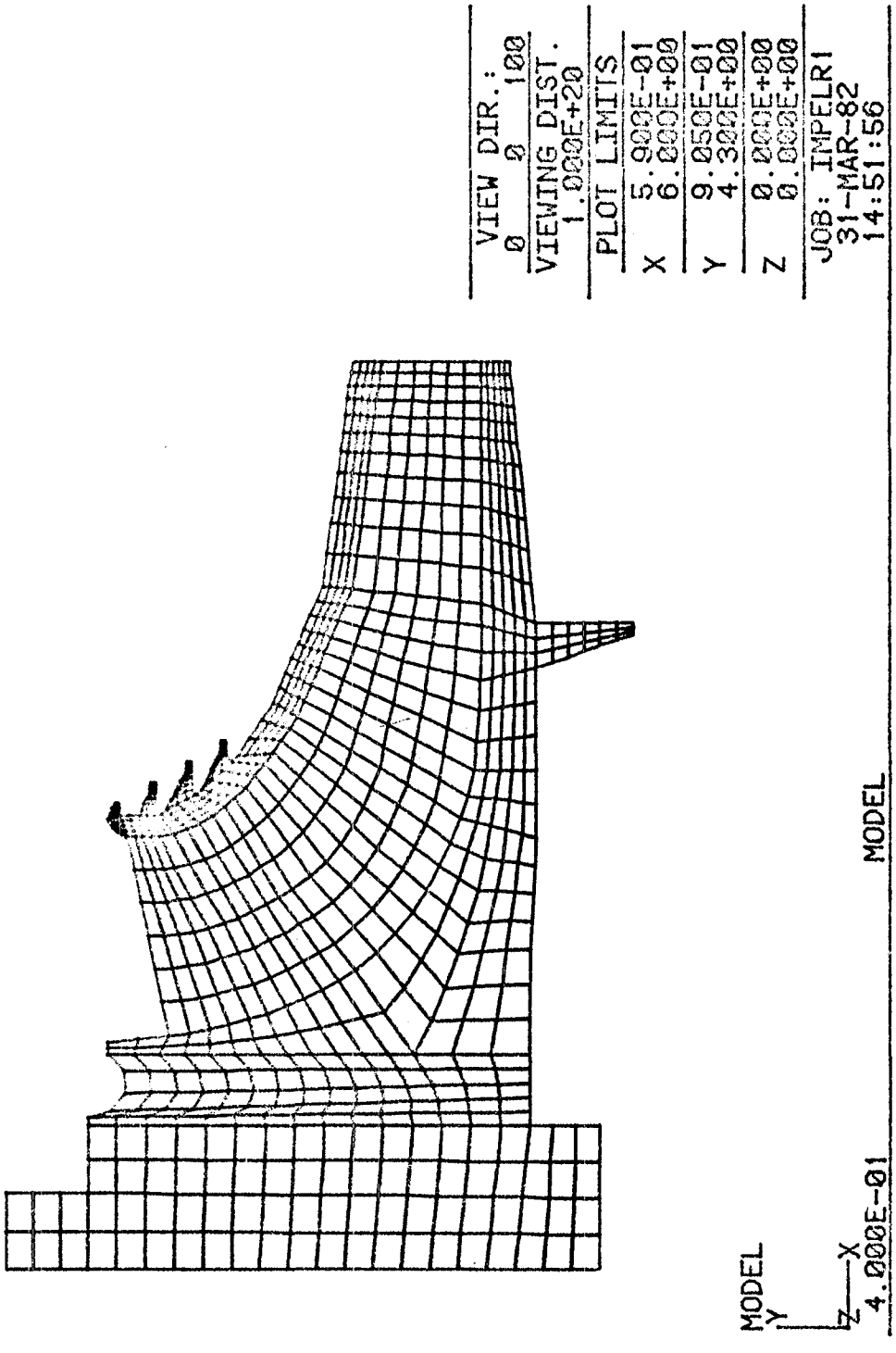

FIGURE 2-2. FINITE ELEMENT MODEL FOR IMPELLER.

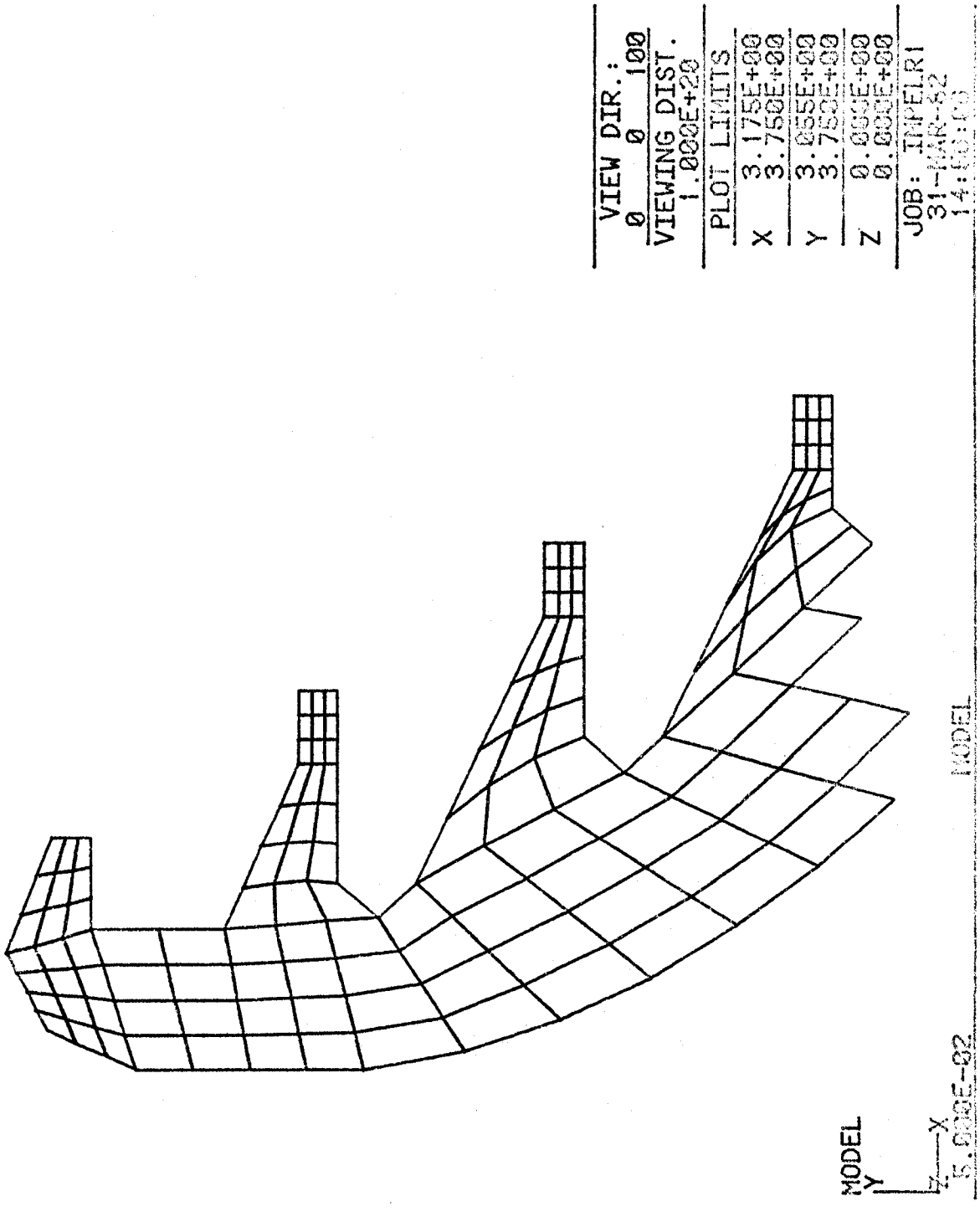

FIGURE 2-3. DETAIL OF FINITE ELEMENT MODEL FOR LABYRINTH FINGERS.

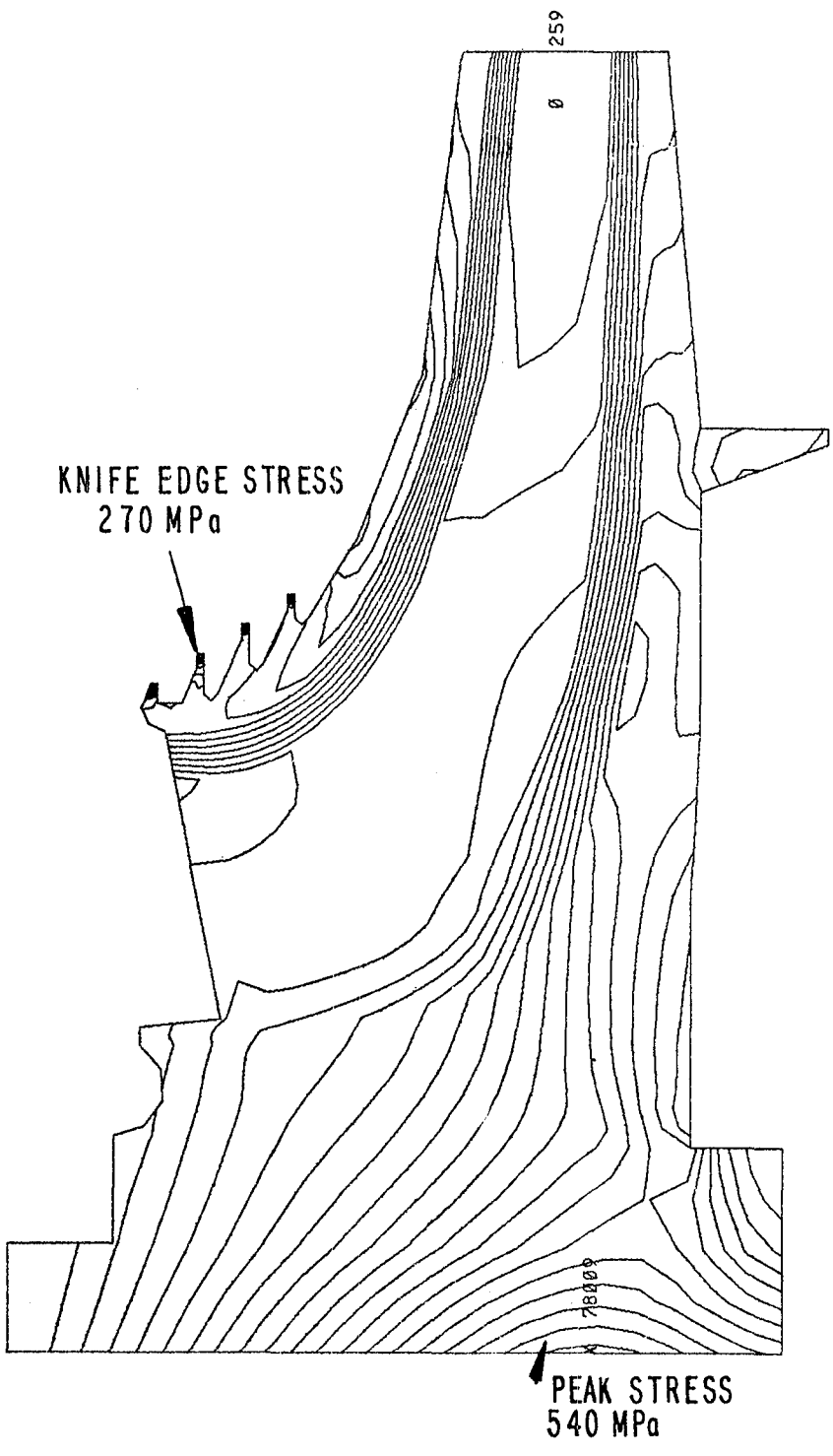

FIGURE 2-4. COMBINED STRESSES ON IMPELLER FOR RUB CONDITION IMPOSING 260° C INTERFACE TEMPERATURE.

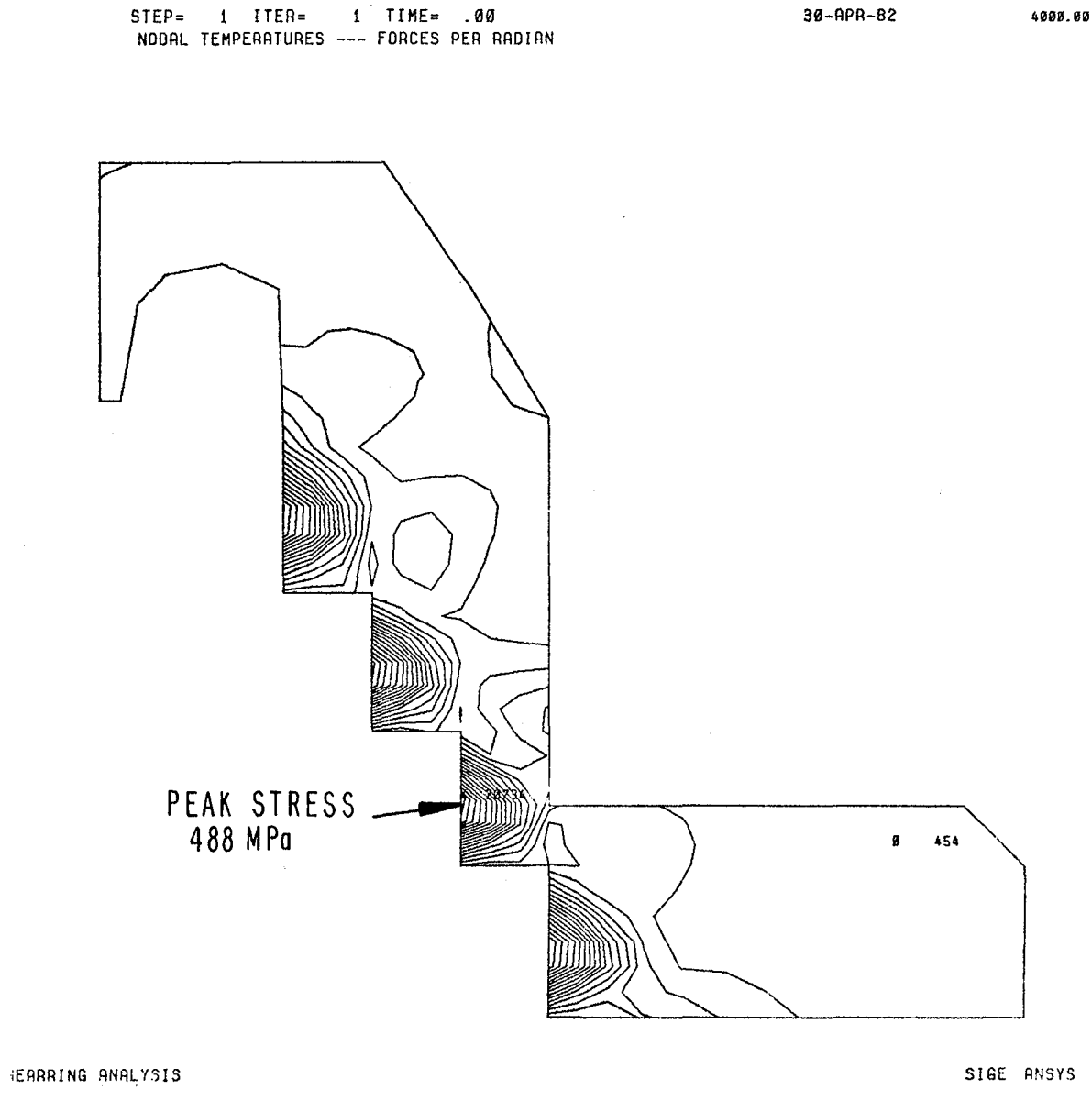

FIGURE 2-5. COMBINED STRESSES ON WEAR RING FOR RUB CONDITION IMPOSING 260° C INTERFACE TEMPERATURE.

The finite element model used in this analysis is shown in Figure 2-6. It is an axisymmetric representation of the labyrinth finger and knife edge, having 316 elements and 392 nodes. A detailed view of the element breakup in the contact zone is shown in Figure 2-7.

The boundary conditions specified in the analysis were:

1. Temperatures of the nodes at the bottom of the labyrinth finger and around the periphery of the wear ring model were specified to be at the temperature of the liquid hydrogen (-226°C).

2. Heat was transferred by convection from the sides of the labyrinth finger and the sides of the wear ring adjacent the contact zone to the surrounding cryogenic fluid. The convective heat transfer coefficient was estimated to be 12 W/cm²°C (0.04 Btu/s-in²-°F) which may be non-conservative, hence underpredicting the interface temperatures. Appendix A provides some further discussion of the effect of heat transfer coefficient on rub temperatures.

A heat flux input of 82 kW/cm² (500 Btu/s-in²) was assumed in the thermal analysis for a rub making contact on the full circumference of the knife edge. This value of heat flux is on the "high side" of expected rub energy dissipation based on previous wear test results provided by the NASA Project Manager and from low-speed wear tests at Dartmouth (Appendix A) and blade interaction tests at Creare.

In the thermal analysis, the heat input was assumed to be applied to the surface elements of either the labyrinth finger or the wear ring with heat flow by conduction into the other member. With this approach it was possible to "bracket" the steady-state interface temperature, without making any assumptions about a heat "split" between the two surfaces.

2.2.1 Effect of Contact Length

Three different rub contact length cases were considered:

1. 360° contact length
2. 180° contact length
3. 30° contact length

The full circumference contact length is somewhat unrealistic since it implies a "shrink-fit" situation. However, it does produce a useful upper bound estimate of interface temperature and provides a baseline for comparisons with alternate materials cases.

The rub contact analysis in Appendix B shows that the length of the wear scar rapidly increases as incursion continues, approaching 130° of arc for an incursion depth of 0.25 mm (0.010 inch). Therefore, the thermal analysis case having a 180° contact length should produce a realistic estimate of interface temperatures.

The 30° rub case provides a base for comparison with the results from the experimental phase (Section 4) which used a wear ring specimen with an arc length of 30°.

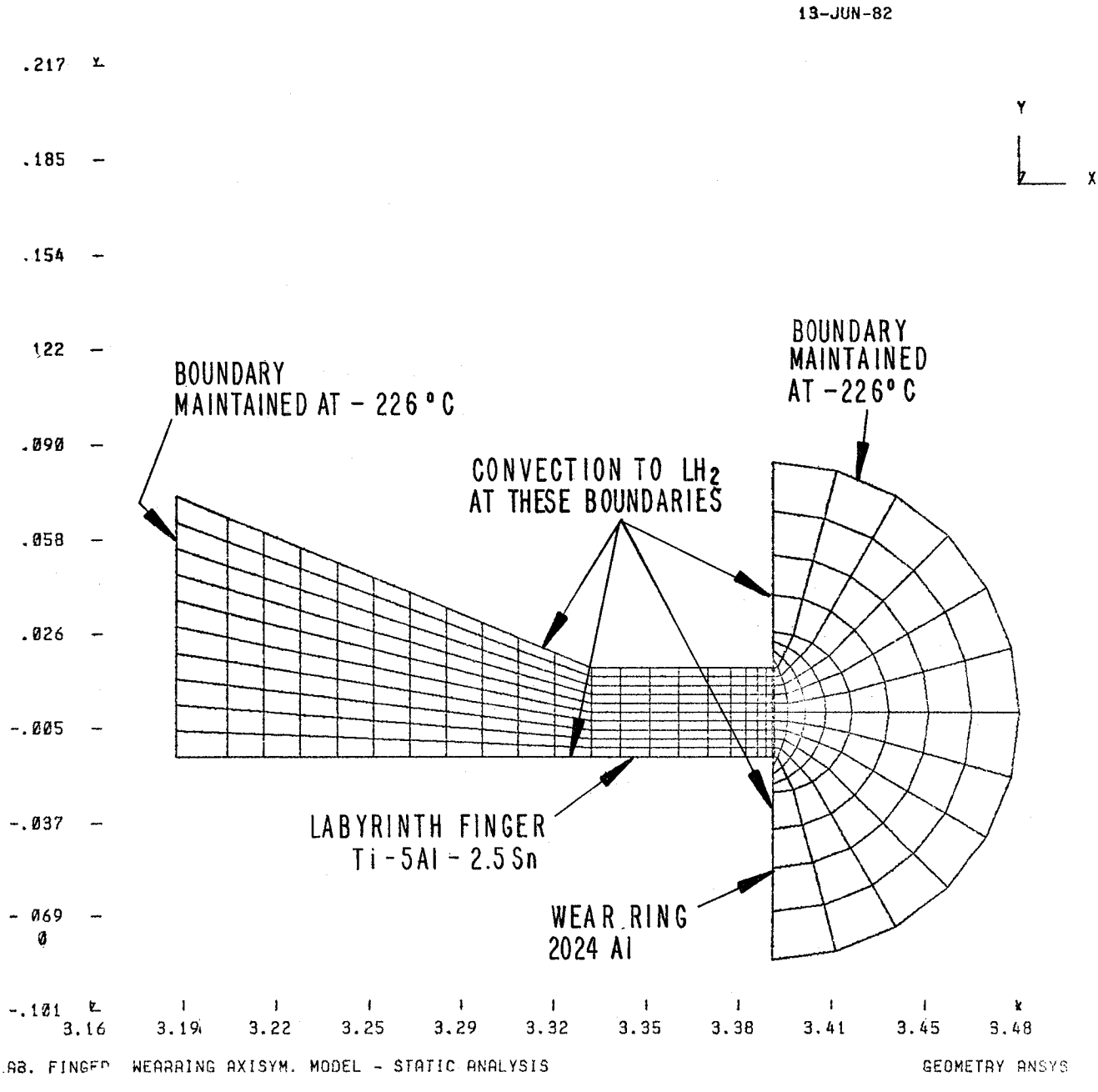

FIGURE 2-6. FINITE ELEMENT MODEL FOR THERMAL ANALYSIS.

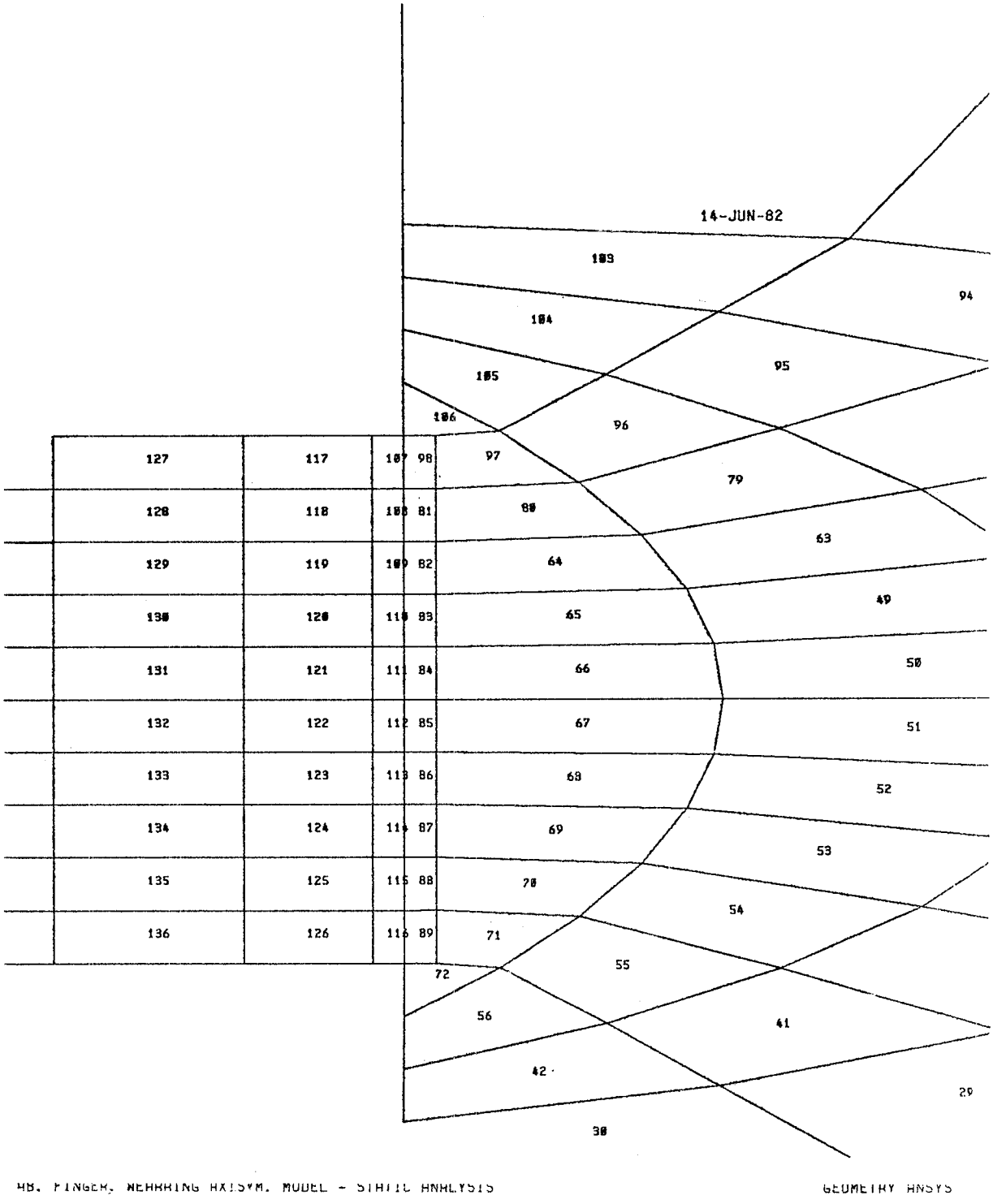

FIGURE 2-7. DETAILS OF FINITE ELEMENT MODEL FOR THERMAL ANALYSIS.

For the cases in which the rub energy was applied to the labyrinth finger, the heat input value was reduced in proportion to the total contact length (constant heat flux).

Results of the thermal analyses for the three contact angle cases are shown in Figures 2-8, 2-9 and 2-10. Peak temperatures occur at the mid-plane of the contact zone and are not greatly different for the two modes of heat application. As expected, interface temperature decreases with decreased contact length.

2.2.2 Alternate Materials Cases

Several alternate materials were investigated as treatments or coatings for the knife edge and as abradable wear ring materials. The cases, materials and material properties considered in this phase of the analysis are presented in Table 2-1. Properties for the BOM aluminum and titanium alloys used for the wear ring and knife edge are shown for comparison purposes.

Thermal analyses were carried out for each alternate material case for a rub contact angle of 360°. The material in the mating component of the seal was selected as the BOM material used in the HPFP---aluminum for the wear ring and titanium for the knife edge.

Results for the 5 alternate materials cases are shown in Figures 2-11 through 2-15. As in the other studies, the analysis considered heat application individually to the knife edge and to the wear ring. Also, the heat flux value assumed for these alternate materials cases was the same (82 kW/cm^2) as for the baseline material cases.

The most notable results are the cases with the magnesia/zirconia wear pad coating (Case 4, Figure 2-13) and the copper wear pad (Case 6, Figure 2-15). In the former, the low conductivity coating results in a very high interfacial temperature, whereas the copper seal surface enhances heat transfer from the rub zone producing a reduction in temperature compared with the baseline case with 2024 aluminum (Figure 2-8).

2.3 Thermal Shock Analysis

A finite element analysis was performed on the test specimen used in the thermal shock tests (see Section 3 for a description of the experiments and the geometry of the specimen). This analysis examined the transient temperature field within the specimen for a step change in boundary temperature and with negligible thermal resistance in the boundary film. The specimen was assumed to be initially at a uniform 593°C (1100°F) and then the boundary temperature was changed to -226°C (-375°F) at time t = 0. The results of this transient analysis indicate that all of the "shocking" action takes place in the first few tenths of a second and the specimen is essentially at thermal equilibrium in less than one second. A similar thermal shock is expected to occur as the knife edge rotates out of the contact zone in a rub interaction and is quenched by the liquid hydrogen.

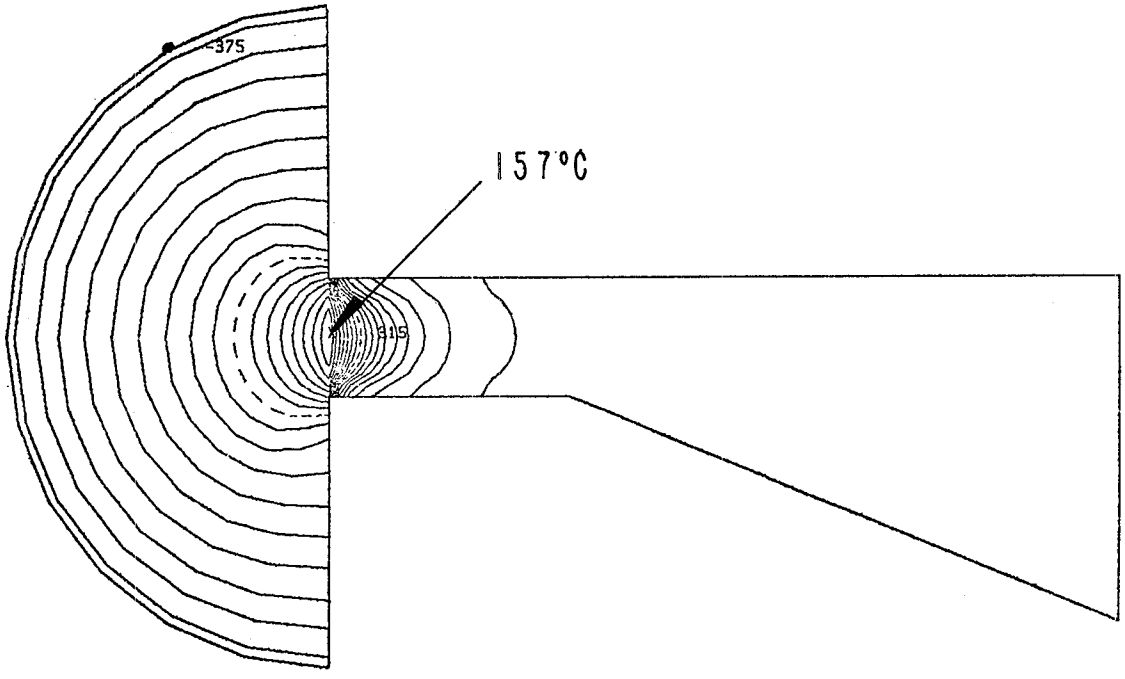

360 DEG. RUB. HEAT APPLIED TO WEARRING TEMP ANSYS

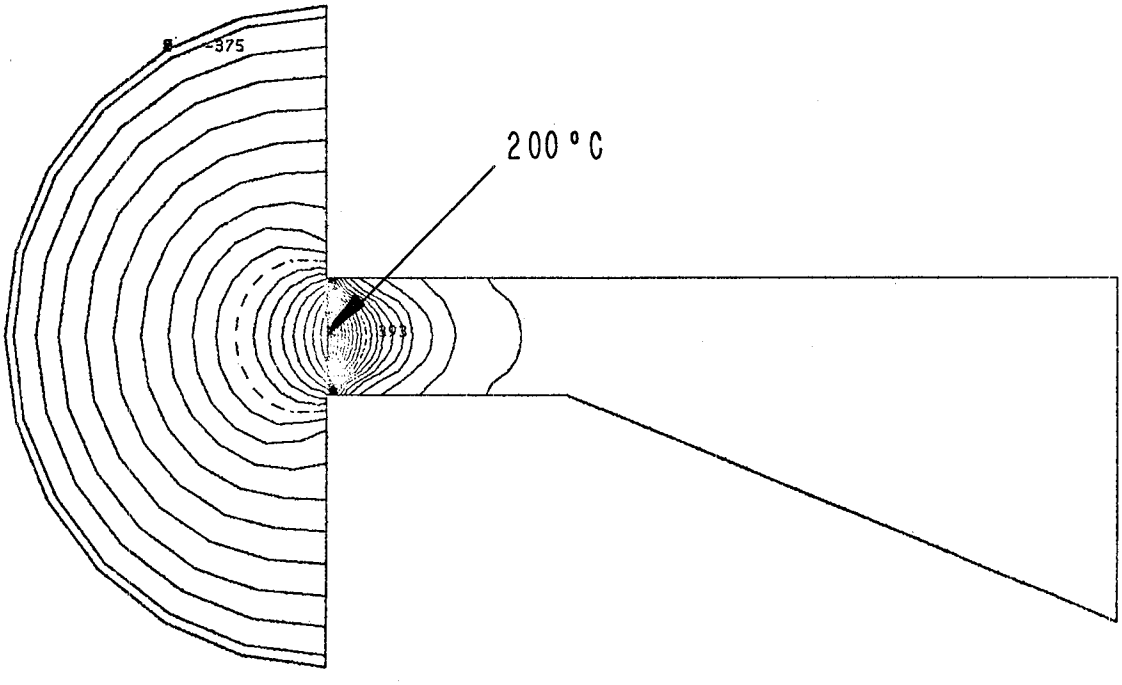

360 DEG. RUB. HEAT APPLIED TO LABYRINTH FINGER TEMP ANSYS

FIGURE 2-8. THERMAL ANALYSIS FOR LABYRINTH SEAL 360° CONTACT LENGTH

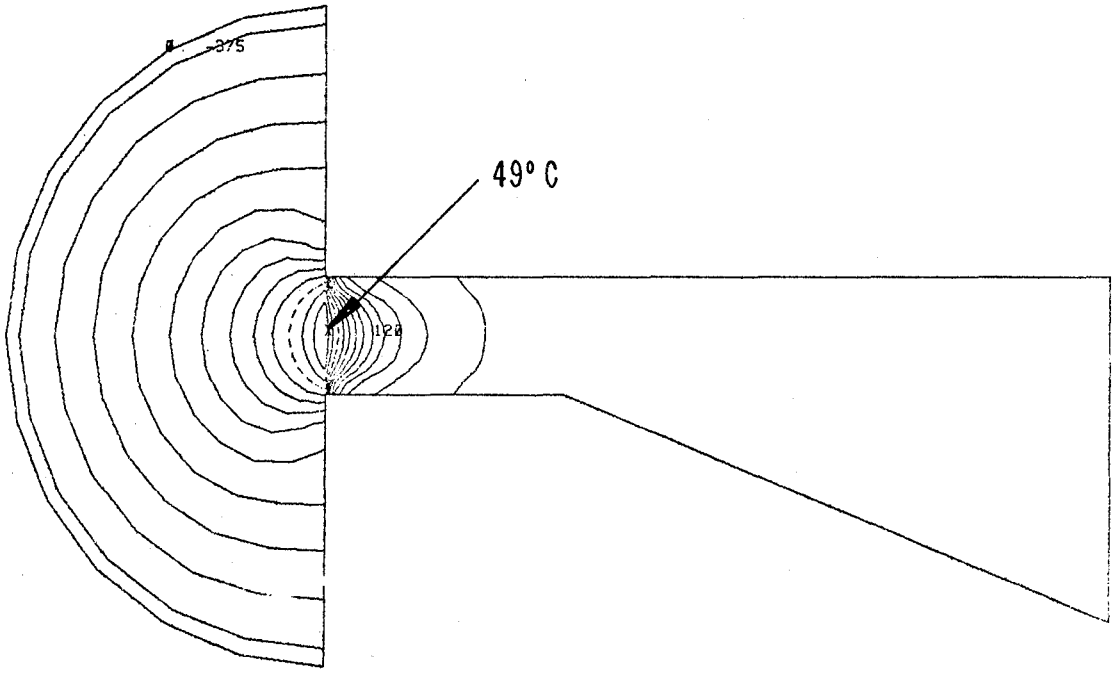

180 DEG. RUB. HEAT APPLIED TO WEARRING TEMP ANSYS

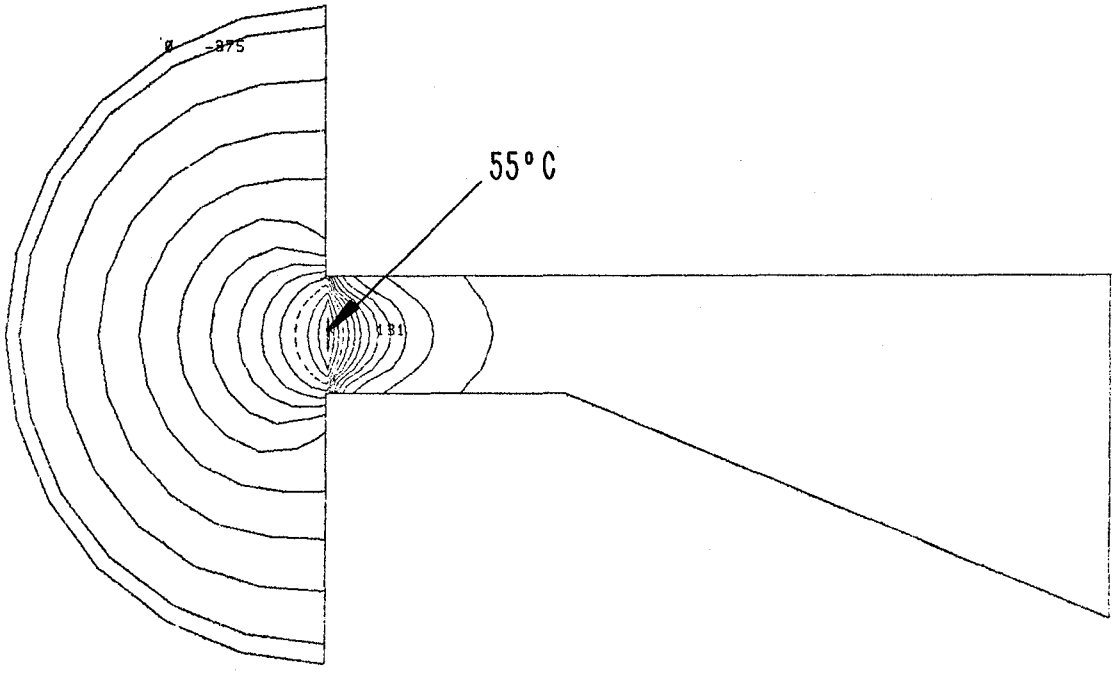

180 DEG. RUB. HEAT APPLIED TO LABYRINTH FINGER TEMP ANSYS

FIGURE 2-9. THERMAL ANALYSIS FOR LABYRINTH SEAL. 180° CONTACT LENGTH

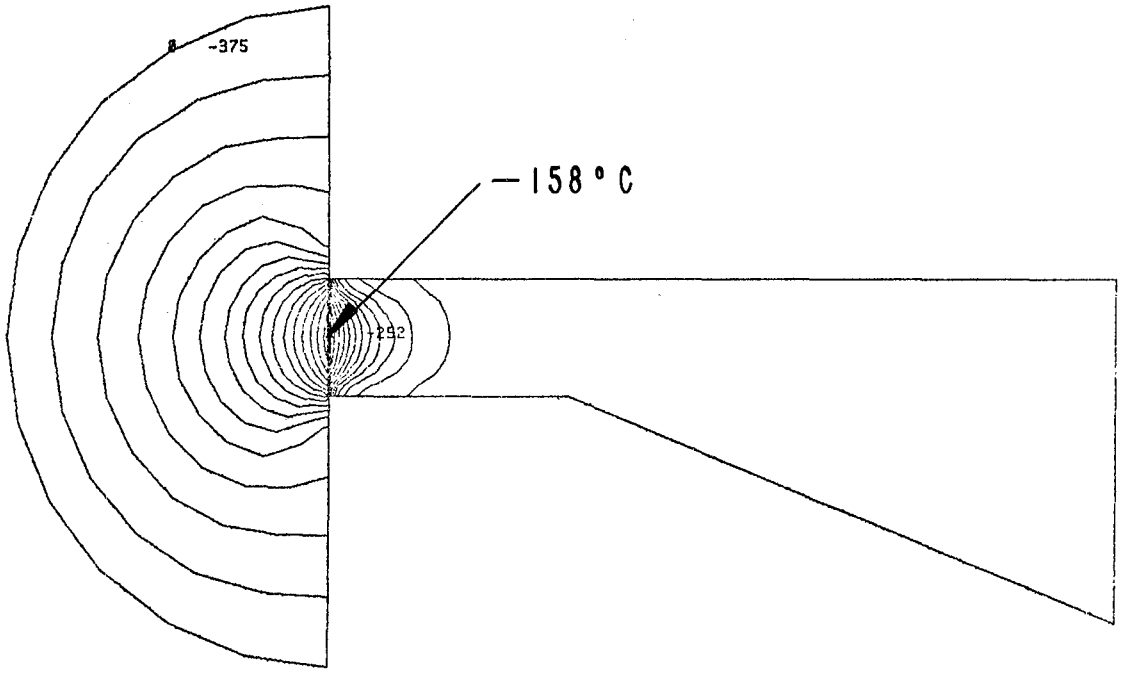

30 DEG. RUB. HEAT APPLIED TO WEARRING

TEMP SYSYS

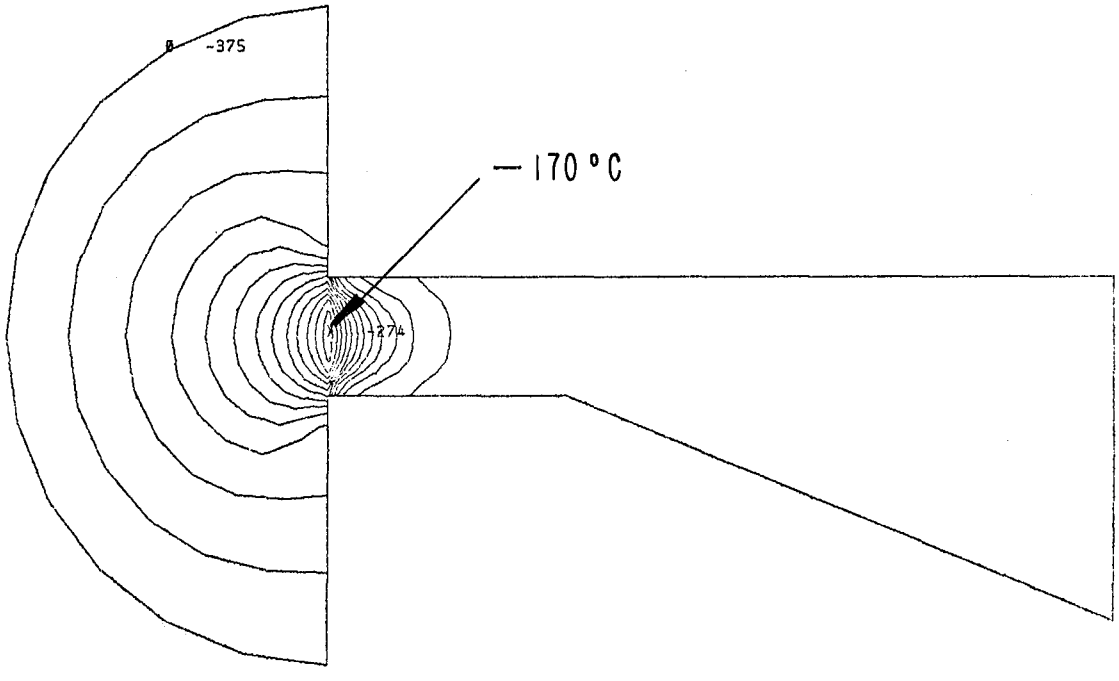

30 DEG. RUB. HEAT APPLIED TO LABYRINTH FINGER

TEMP SYSYS

FIGURE 2-10. THERMAL ANALYSIS FOR LABYRINTH SEAL 30° CONTACT LENGTH

TABLE 2-1 ALTERNATE MATERIALS CASES

Case No.	Materials and Application	Material Properties[1]		
		Density (kg/m^3)	Specific Heat Capacity (J/kg-K)	Thermal Conductivity (W/m-K)
2	Plasma-sprayed ODS coating on knife edge; 0.25 mm thick	8,040	462	14
3	Al_2O_3 knife edge coating 0.15 mm thick	3,880	752	22
4	Magnesia-Zirconia coating on wear ring, 85% dense, 0.76 mm thick	3,600	460	0.82
5	Aluminum-Polyester coating on wear ring, fully dense, 0.76 mm thick	1,385	962	75
6	99.7% pure copper wear ring	8,865	385	396
-	2024 Aluminum, wear ring	2,770	870	112
-	Ti-5Al-2.5Sn, knife edge	4,490	535	7.9

[1] The materials properties listed in this table are evaluated at or near room temperature.

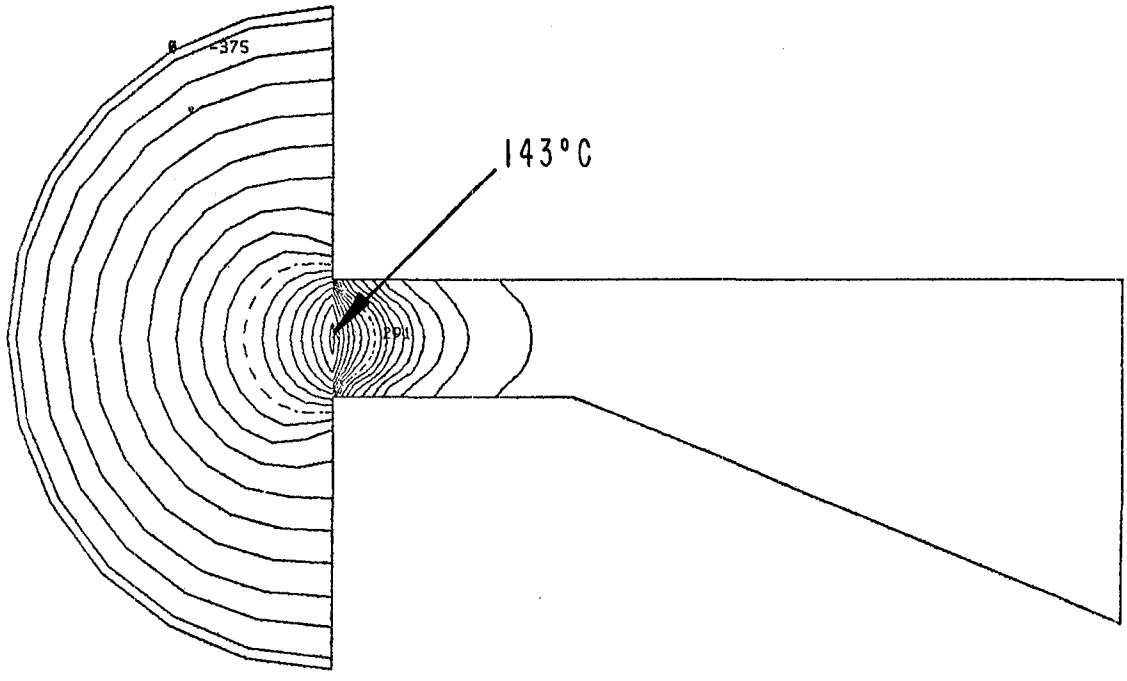

MATERIAL CASE 2A. HEAT APPLIED TO WEARRING TEMP ANSYS

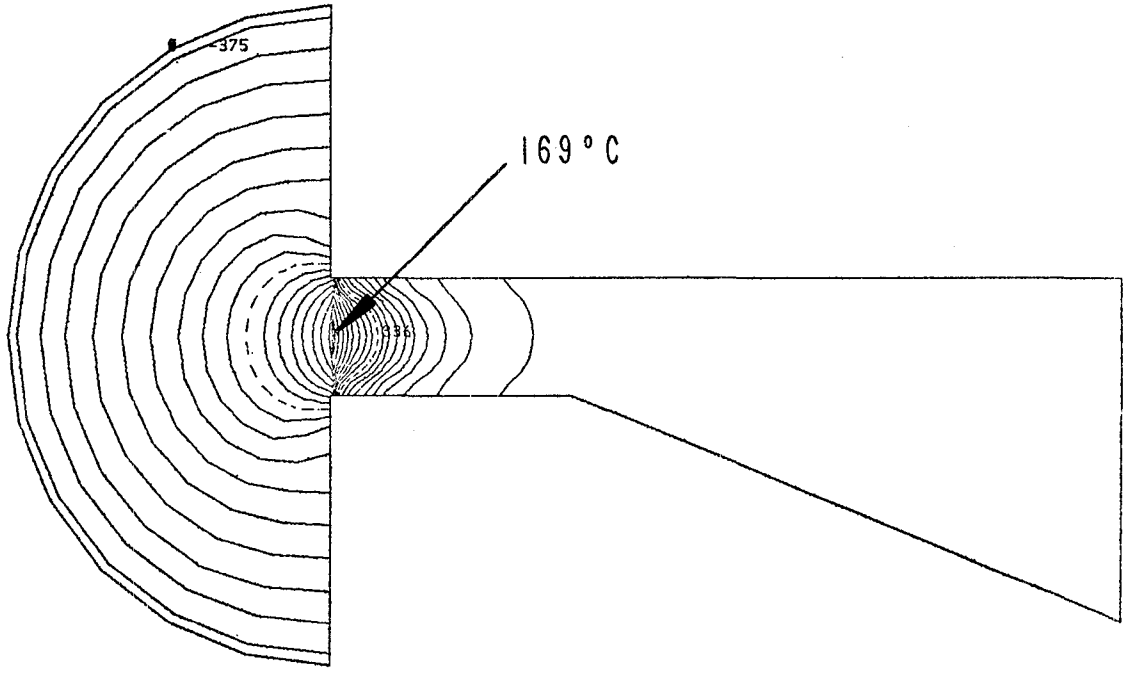

MATERIAL CASE 2B. HEAT APPLIED TO LABYRINTH FINGER TEMP ANSYS

FIGURE 2-11. THERMAL ANALYSIS OF LABYRINTH SEAL WITH ODS KNIFE EDGE COATING

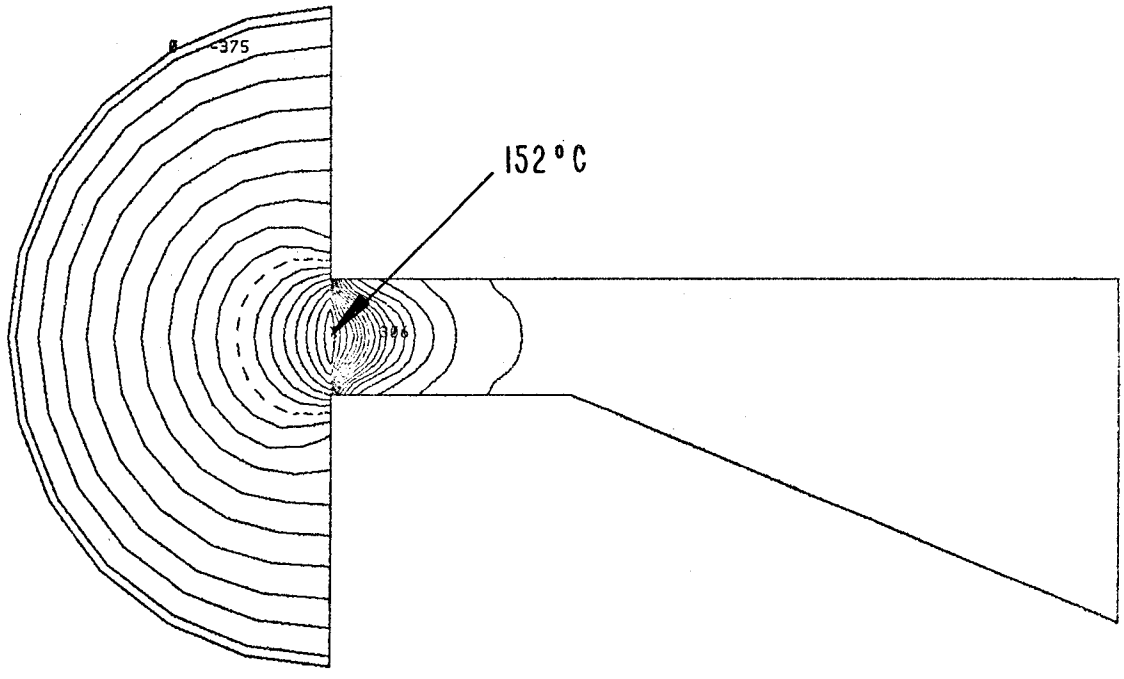

ATERIAL CASE 3A. HEAT APPLIED TO WEARRING TEMP ANSYS

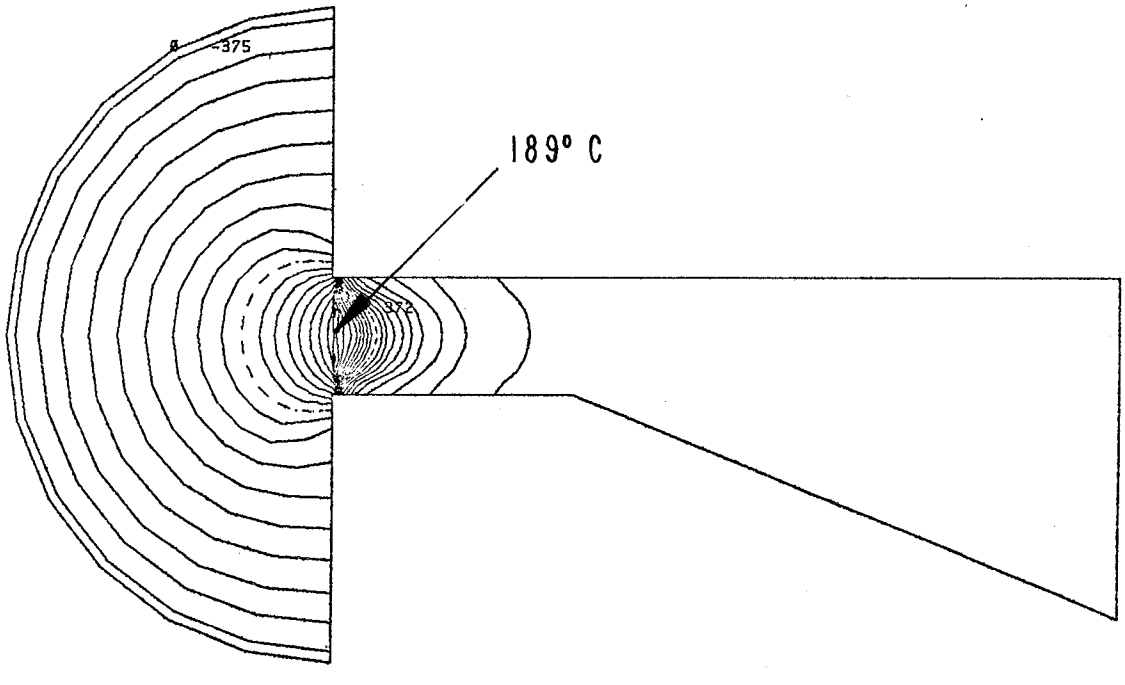

TER. CASE 3B. HEAT APPLIED TO LABYRINTH FINGER TEMP ANSYS

FIGURE 2-12. THERMAL ANALYSIS FOR LABYRINTH SEAL ALUMINUM OXIDE KNIFE EDGE COATING.

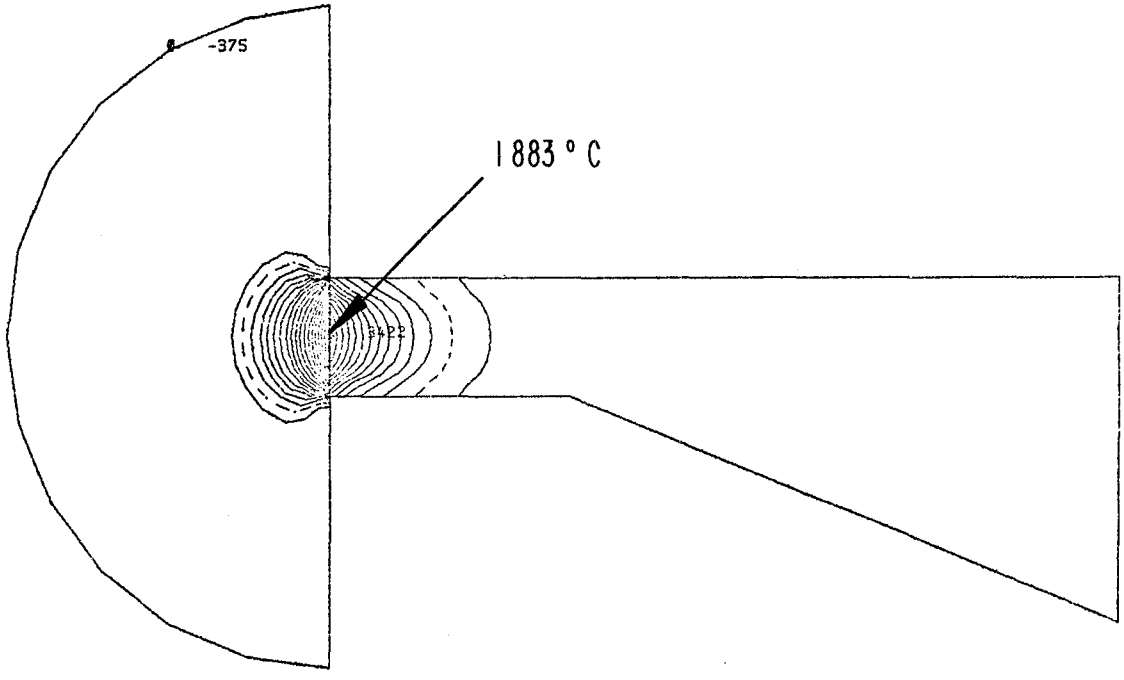

MATERIAL CASE 4A. HEAT APPLIED TO WEARRING TEMP ANSYS

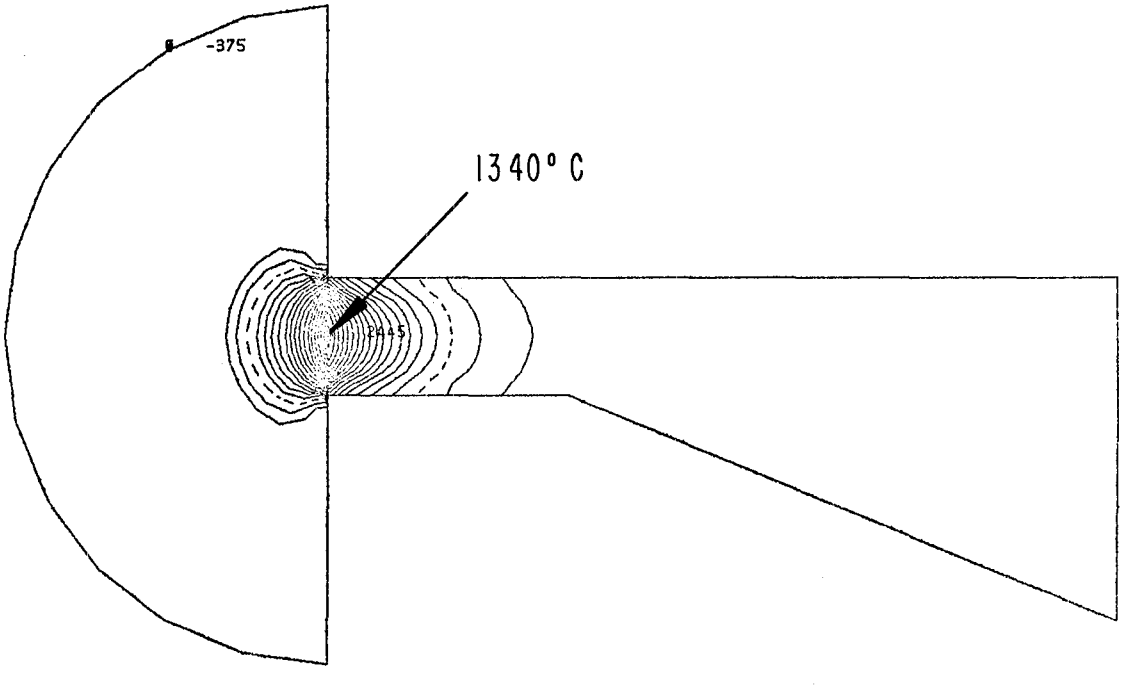

MATERIAL CASE 4B. HEAT APPLIED TO LABYRINTH FINGER TEMP ANSYS

FIGURE 2-13. THERMAL ANALYSIS FOR LABYRINTH SEAL MAGNESIA ZIRCONIA WEAR RING SURFACE

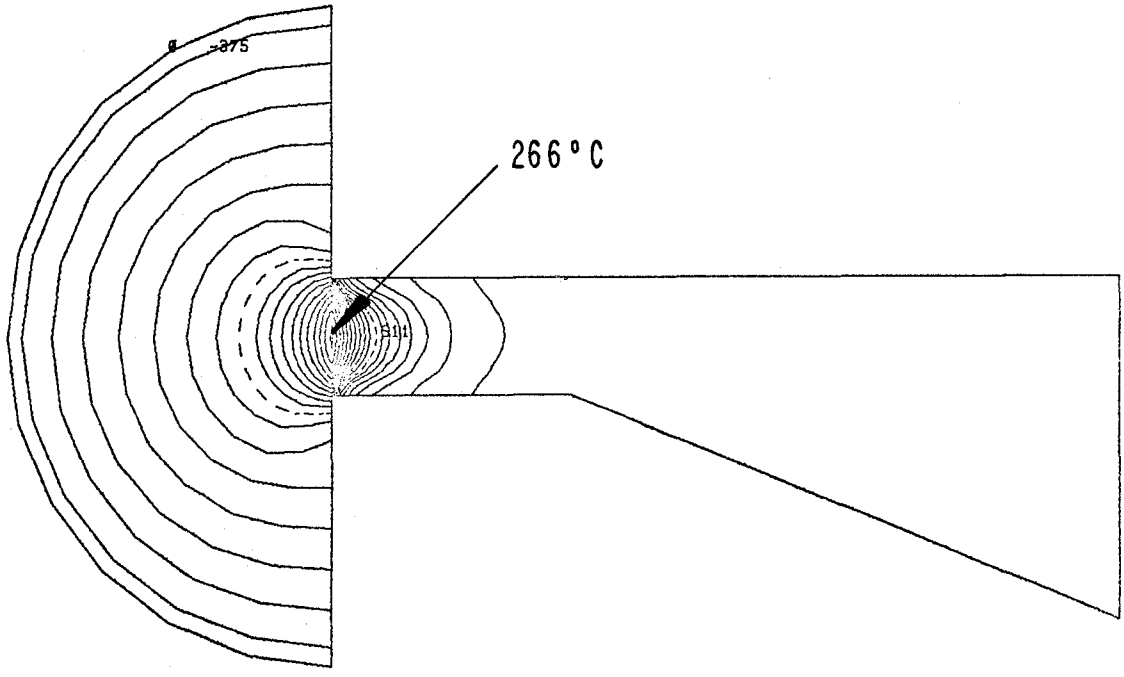

MATERIAL CASE 5A. HEAT APPLIED TO WEARRING

TEMP ANSYS

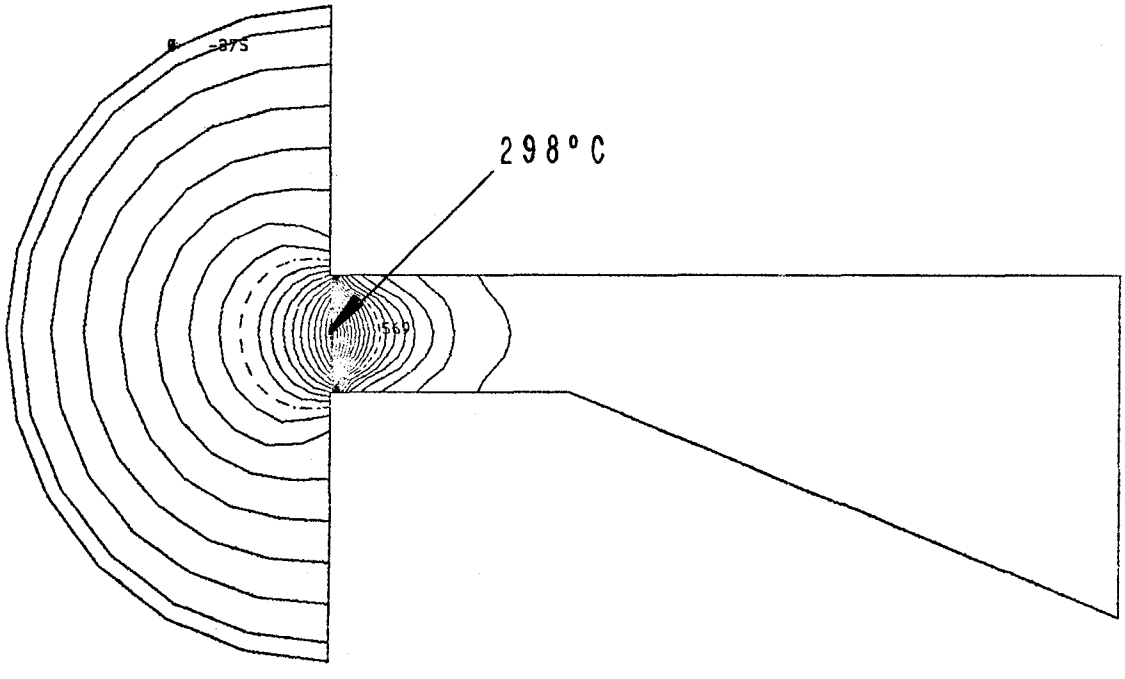

MATERIAL CASE 5B. HEAT APPLIED TO LABYRINTH FINGER

TEMP ANSYS

FIGURE 2-14. THERMAL ANALYSIS FOR LABYRINTH SEAL ALUMINUM-POLYESTER WEAR RING SURFACE

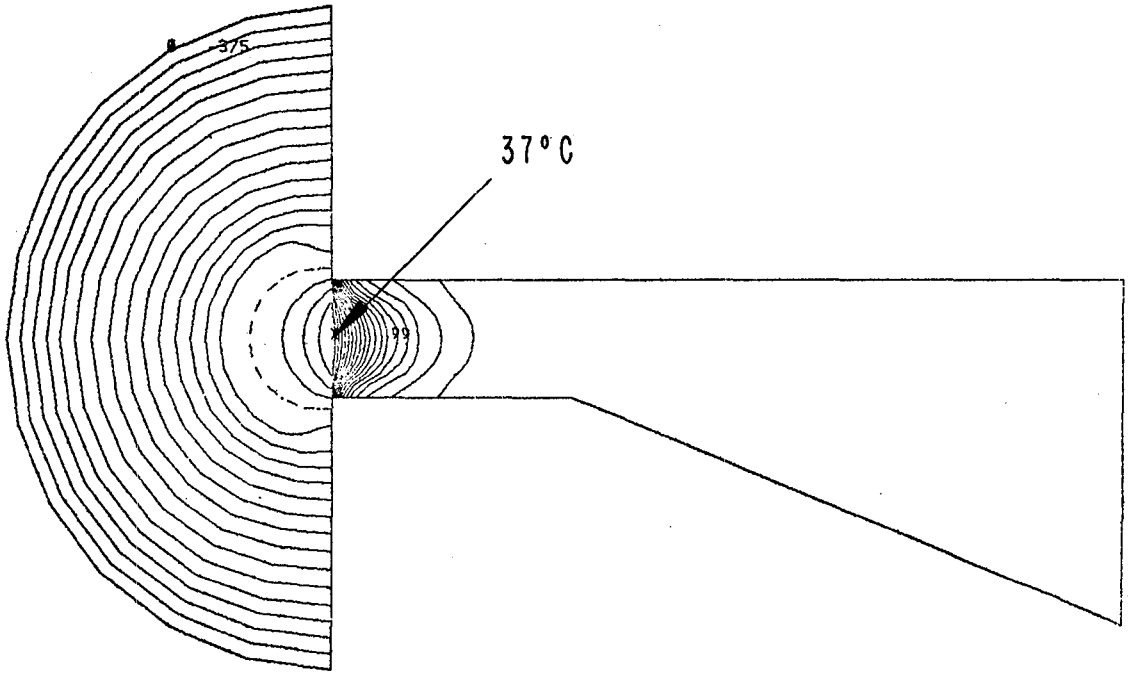

MATERIAL CASE 6A. HEAT APPLIED TO WEARRING TEMP ANSYS

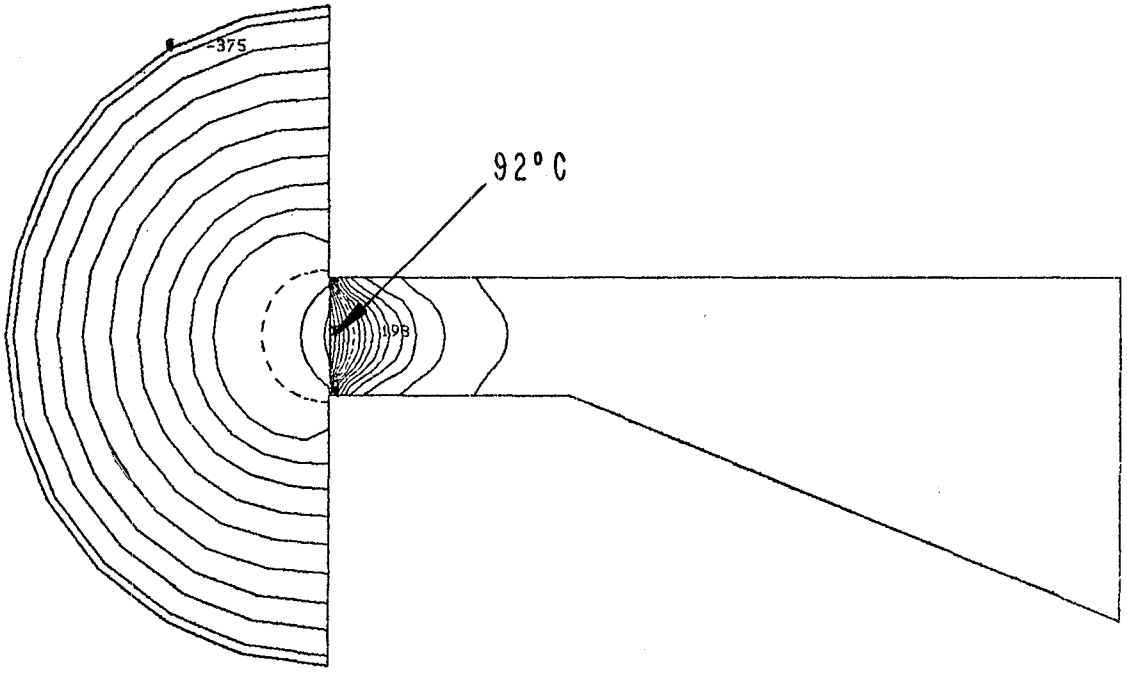

MATERIAL CASE 6B. HEAT APPLIED TO LABYRINTH FINGER TEMP ANSYS

FIGURE 2-15. THERMAL ANALYSIS FOR LABYRINTH SEAL HIGH PURITY COPPER WEAR RING.

3 THERMAL SHOCK EXPERIMENTS

3.1 Background

In a rubbing situation, the labyrinth knife edge is heated locally due to energy dissipation at the wear interface. As the knife edge moves out of the rub zone (assuming that contact occurs over only a portion of the perimeter of the seal) it is subjected to rapid cooling by the surrounding cryogenic fluid (liquid hydrogen). Transient, non-uniform cooling of the knife edge will induce strains in the material which may result in cracking of the knife edge.

A number of variables may be of importance in producing "quench cracks" in the knife edge. Among them are:

1. temperature differential in the thermal cycle
2. rate of cooling
3. metallurgical condition of the specimen (e.g., grain size and orientation)
4. mechanical properties (e.g. thermal expansion coefficient, modulus and ultimate strength)
5. geometry of specimen
6. thermal cycling (fatigue)

Although assumptions can be made for certain of these variables and calculations can be performed which predict the probability for cracking, some uncertainty will still remain regarding thermal cracking for specific situations. In order to gain further insight to this problem, an experimental investigation was undertaken which provided direct evidence of cracking of the titanium alloy in a cryogenic quench.

3.2 Experimental Investigation

A series of experiments was carried out to subject specimens of the Ti-5Al-2.5Sn to thermal cycles between either of two elevated temperatures and the temperature of liquid nitrogen (-196°C). Specimens were cycled 1, 3 and 10 times from each of the elevated temperatures (593°C and 1150°C) and were examined for evidence of cracking after each series of thermal cycles.

The test specimens were fabricated by lathe-turning from a rod of annealed Ti-5Al-2.5Sn, as shown in Figure 3-1. The knife edge width (0.76 mm) and taper approximately match the configuration of the full-size knife edge which should provide a realistic simulation of temperature gradients during quench. A copy of the certificate of analysis for the titanium rod is given in Appendix C-1.

The lower of the two test temperatures (593°C, 1100°F) represents the maximum expected temperature of the knife edge during a "single-pass" rub, based on the high side heat flux estimate used in the thermal analysis and considering heat transfer to the wear ring and to the surrounding environment. The upper temperature (1150°C, 2100°F) is slightly above the α-β transformation temperature for the titanium alloy.

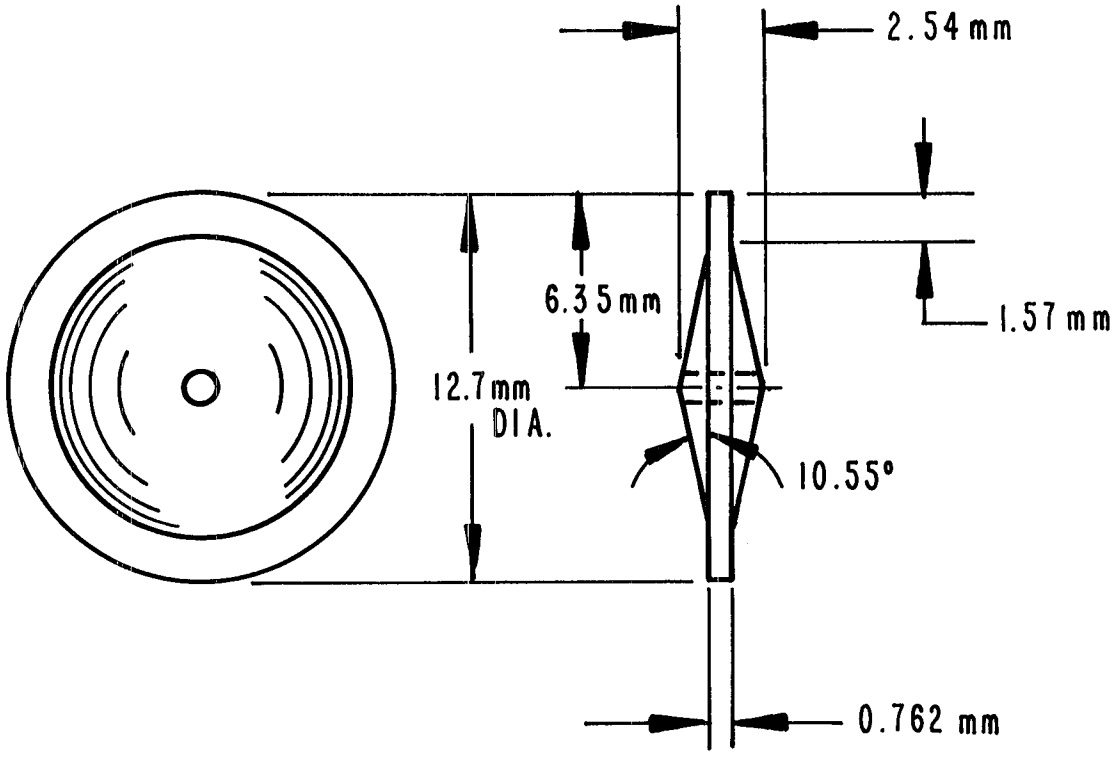

FIGURE 3-1 . THERMAL SHOCK TEST SPECIMEN

Liquid nitrogen was selected as the quench medium for these tests because it was more readily available and has reduced handling risks compared to liquid hydrogen.

The issues of hydride formation and possible effects of hydrides on thermal cracking in the HPFP environment were considered prior to undertaking these tests. The literature on the effect of long-term exposure of titanium alloys to a low temperature hydrogen environment indicates that hydride formation is unlikely (Reference 11) and therefore should not be a contributing factor in the cracking of the knife edge. It also seems unlikely that the short-term exposure of this titanium to hydrogen in the high temperature rub zones would result in any significant hydride formation.

In the quench tests, the specimens were heated in a furnace having an argon gas atmosphere, allowed to hold at temperature for several minutes and then were dropped into a container of liquid nitrogen. After cooling, the specimens were removed from the nitrogen and then examined for cracks using a scanning electron microscope (SEM) at magnifications up to 1000X.

3.3 Test Results

3.3.1 Observations and Data Summary

Despite the protective argon atmosphere during heating, oxidation of the specimens occurred. Its extent was limited, however, as evident from the gold to blue interference colors on the test specimens, indicative of thin (<1μm) films. This result is not surprising given the propensity with which titanium getters oxygen.

Grains were evident to the unaided eye after cycling to the higher temperature. After one cycle the grain diameter was around 0.7 mm; after 10 cycles it was closer to 3 mm. Grains were not seen by eye even after 10 cycles at the lower temperature, presumably because grain growth and thermal etching of grain boundaries were less extensive at 593°C than at 1150°C.

Quenching into liquid nitrogen resulted in a relatively slow extraction of heat from the test specimens. This point was evident from the observation that boiling occurred in the nitrogen bath for up to about 5 to 6 seconds after dropping in the specimen. In fact, the bath bubbled for about 5 seconds, became quiet, bubbled again for about 1 second, and then ceased bubbling. These effects are probably caused by transitions through stages of film and nucleate boiling coupled with thermal conduction within the specimen.

The test specimens which were cycled from 593°C to -196°C did not show any evidence of cracking even for the specimen cycled 10 times. After three of the more extreme shocks (1150°C to -196°C) cracks were seen in one area of the test specimen, near to but in from the periphery (approximately 0.4 mm), Figure 3-2. Several cracks emanating from the periphery were observed in the specimen subjected to 10 of the extreme thermal cycles, as

shown in Figure 3-3. These cracks were distributed more or less uniformly around the circumference of the disk. The results of the thermal shock tests are summarized in Table 3-1 including remarks from the metallurgical examination of the test specimens.

TABLE 3-1 THERMAL SHOCK TEST RESULTS

Thermal Quench Temperature	Number of Cycles	Remarks
593°C/-196°C	1,3,10	no cracking evident at magnifications up to 1000X
1150°C/-196°C	1	no cracking evident
	3	irregular cracks in one area away from periphery of knife edge
	10	numerous cracks up to 0.5 mm in length, emanating from periphery of knife edge, several locations around circumference

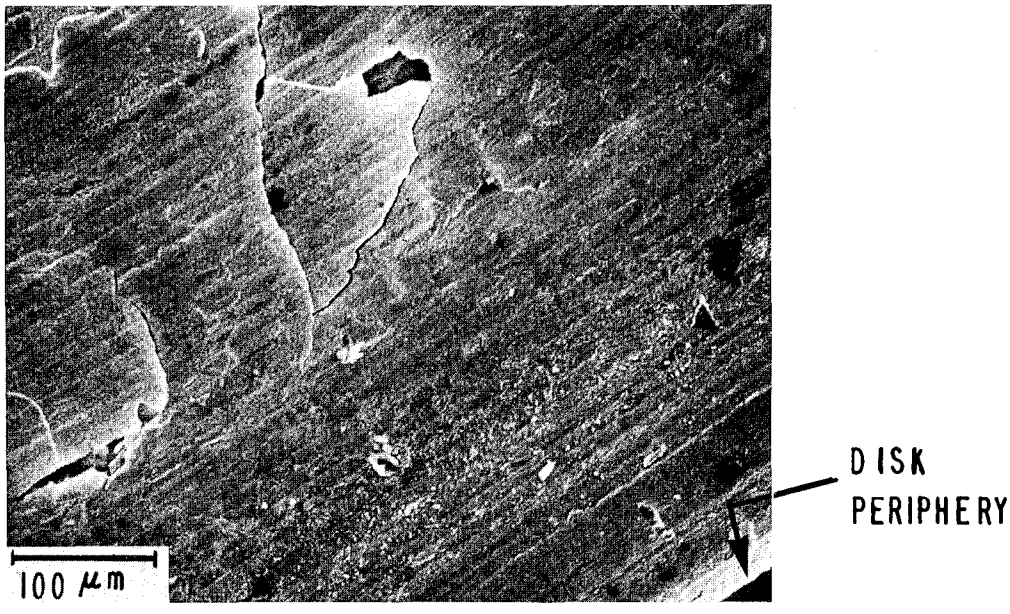

FIGURE 3-2 SEM MICROGRAPH OF THERMAL SHOCK SPECIMEN CYCLED 3 TIMES

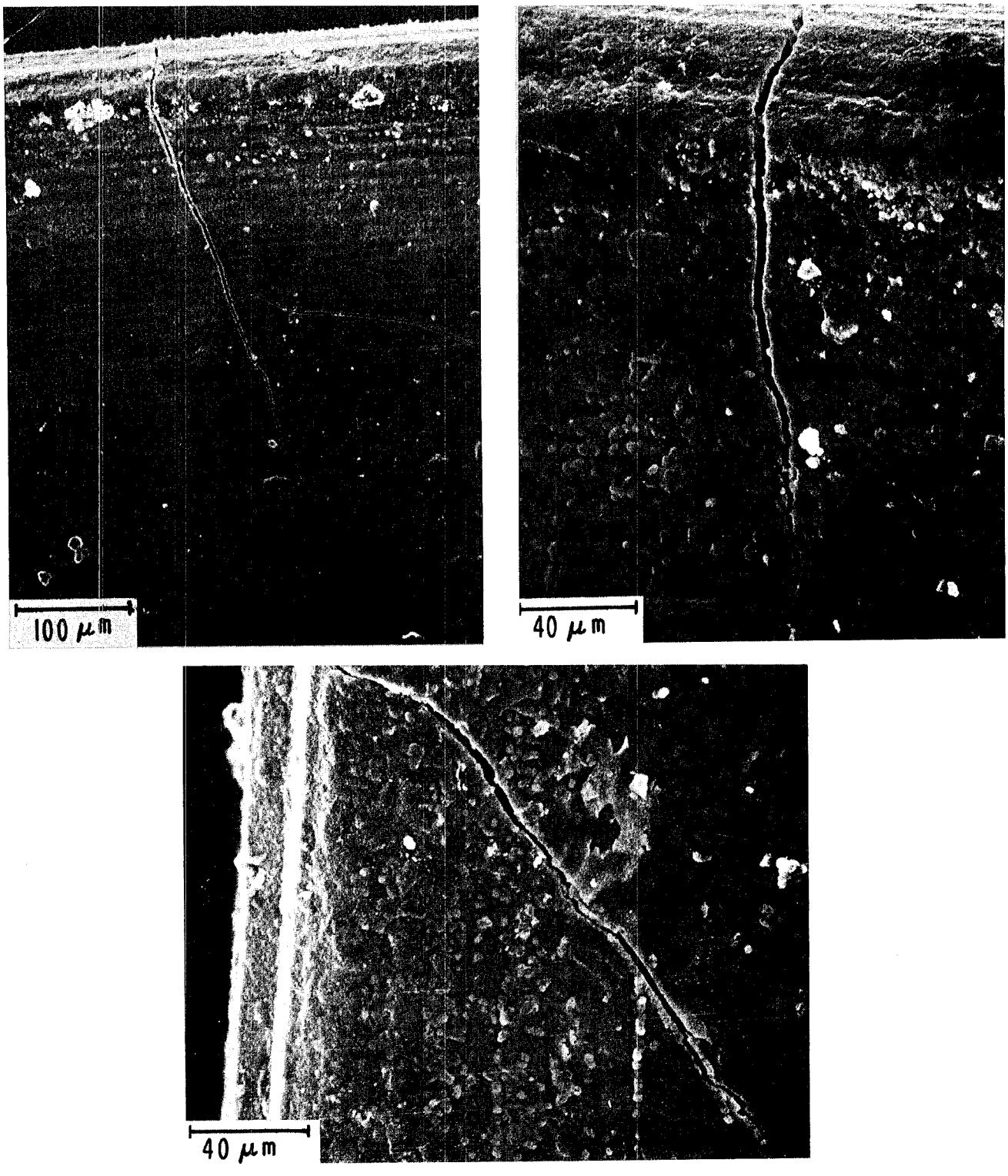

FIGURE 3.3 SEM MICROGRAPHS OF THERMAL SHOCK SPECIMEN CYCLED 10 TIMES

3.3.2 Discussion of Results

An order of magnitude estimate of the life to crack initiation based on the total strain range at the disk periphery suggests about 1000 cycles to failure even for the more extreme thermal cycle used in these experiments. This life calculation is based on (Ref. 12):

$$\Delta\varepsilon_T = \frac{3.5\sigma_u}{E} N_f^{0.12} + D^{0.6} N_f^{-0.6} \qquad (1)$$

where:

$\Delta\varepsilon_T$ = strain range = $\alpha_T \Delta T_{max}$

α_T = thermal coefficient of expansion

ΔT_{max} = maximum temperature differential for thermal strain

N_f = number of cycles to crack initiation

D = tensile ductility = $\ln\left(\frac{100}{100-RA}\right)$

RA = reduction in area

E = elastic modulus

σ_u = ultimate tensile strength

Room temperature properties are assumed to apply over the entire range and metallurgical stability prevails over the temperature range.

The observation of cracks after only a few thermal cycles implies that simple life prediction methods such as the one cited above may not be applicable in a situation involving complex thermal loading.

In interpreting the cause of cracking, several points should be kept in mind:

1. thermal strains, per se;
2. contractive strains accompanying the body-centered cubic to close-packed hexagonal crystallographic transformation upon cooling the alloy below about 1000°C;
3. the possible effect of grain size (and hence of holding time and temperature) on the susceptibility to cracking;
4. oxygen-induced embrittlement (nitrogen embrittlement seems unlikely).

The importance of thermal strain versus transformation strain could be determined through additional experiments in which quenching is done from just above and from just below the transformation temperature. The thermal

strain would be essentially the same in both cases, whereas the transformation strain would not. In the absence of experimental data, it is noted that thermal strains in these tests are estimated to be $\alpha\Delta T \cong 10^{-2}$, implying a tensile stress at the periphery of $\sigma < 10^{3}$ MPa (145,000 psi). This stress may be high enough to nucleate cracks in coarse-grained material. Transformation strains (axial) are of a similar magnitude, but, because they are imparted at high temperatures, are probably relaxed by plastic flow before stresses build up to levels as high as that suggested above. It would appear, therefore, that thermal strains are of greater concern than the other. Further testing is required before becoming firm on this point.

If thermal strains per se are the main cause of cracking, then the absence of cracks upon cycling from the lower temperature can be explained on the basis of lower induced strains. The question which arises, however, is why cracking did not occur after the first high-temperature cycle. One answer is that insufficient deformation damage was generated to nucleate cracks during one cycle, implying the operation of a more complicated process of thermal fatigue. In turn, this implies that cracking may occur upon quenching from the lower temperature if enough cycles are realized. However, as pointed out earlier, conventional life prediction correlations grossly overestimate the fatigue life in this instance. Another possible explanation is that cracking is caused by a combination of thermal strain and time-dependent microstructural changes (such as grain growth, hardening through oxygen dissolution, and thermal strain induced cracking of a hardened surface oxidation layer) which occur during the heating, holding and cooling parts of the cycle. If this synergistic process underlies cracking, then heating in air to dissolve more oxygen and/or holding for longer times at 1150°C before quenching into LN_2 should lead to crack formation in even fewer than three cycles.

Clearly, the exact origin of the cracks cannot be ascertained without further work.

3.4 Applicability of Test Results

These thermal shock tests show that cracking of the titanium alloy knife edge is possible under conditions of repeated cycles over an extreme temperature range. The effect of increased numbers of thermal cycles may also result in cracking even from the lower knife edge temperatures expected in HPFP rub interactions.

4 RUB INTERACTION EXPERIMENTAL PROGRAM

This section describes the rub interaction testing which was carried out on this project. Some background material is presented in order to establish the context for the design of the experimental hardware. Next, the test plan is described including the test facility and instrumentation design, materials selection and testing procedures. Results from the rub interaction tests are presented in the form of data measured during the tests, test observations and post-test examinations of the wear specimens.

4.1 Design Background

High speed sliding has been identified as the probable cause for cracking of the labyrinth seal knife edges in the SSME HPFP. The basic mechanism for failure is believed to be localized, thermally-induced stresses produced by a rub which combine with the centrifugal and pressure loads of normal pump operation to exceed the yield strength of the knife edge titanium alloy.

The basic assembly of the SSME HPFP and details of the labyrinth seal under investigation in this project are shown in Figure 4-1. The seal is designed to reduce leakage flow of high pressure fuel (liquid hydrogen) from the impeller discharge region back to the impeller inlet. The total pressure drop across the 4 stages of the labyrinth seal is approximately 11.8 MPa (1700 psi) and the fluid temperature is about 40K (-387°F) in the region of the seal. The design operating speed for the pump is about 37,000 rpm.

The labyrinth fingers in the seal are fabricated as an integral part of the impeller shroud which is made from Ti-5Al-2.5Sn in a fully annealed state. The wear ring is fabricated from 2024-T3 aluminum alloy and was selected to be sacrificially worn during a rub interaction with the adjacent labyrinth finger. In the static, no-load condition, the nominal clearance between the knife edges and seal ring is about 0.35 mm (0.014 inch). This clearance reduces to 0.18 mm (0.007 inch) during pump operation as a result of differential thermal contraction and pressure and centrifugal loads on the impeller and wear ring.

A labyrinth seal rub can be induced as a result of transient engine operation, an unbalance condition or from body forces on the engine due to vehicle maneuvers. The rub is usually just a momentary contact between the knife edge and sealing surface over just a portion of the wear ring periphery. However, even a short duration contact can result in locally high temperatures and stresses and metallurgical transformations can also take place.

High speed rubbing wear is a complex process which generally requires experimental verification of designs and materials compatability. Because in-service cracking of the labyrinth fingers has been observed (Reference 1), a testing program was undertaken to provide data on the wear process for the bill-of-materials (BOM) labyrinth seal system, and to examine the behavior of candidate replacement materials or treatments for the knife edge and wear ring.

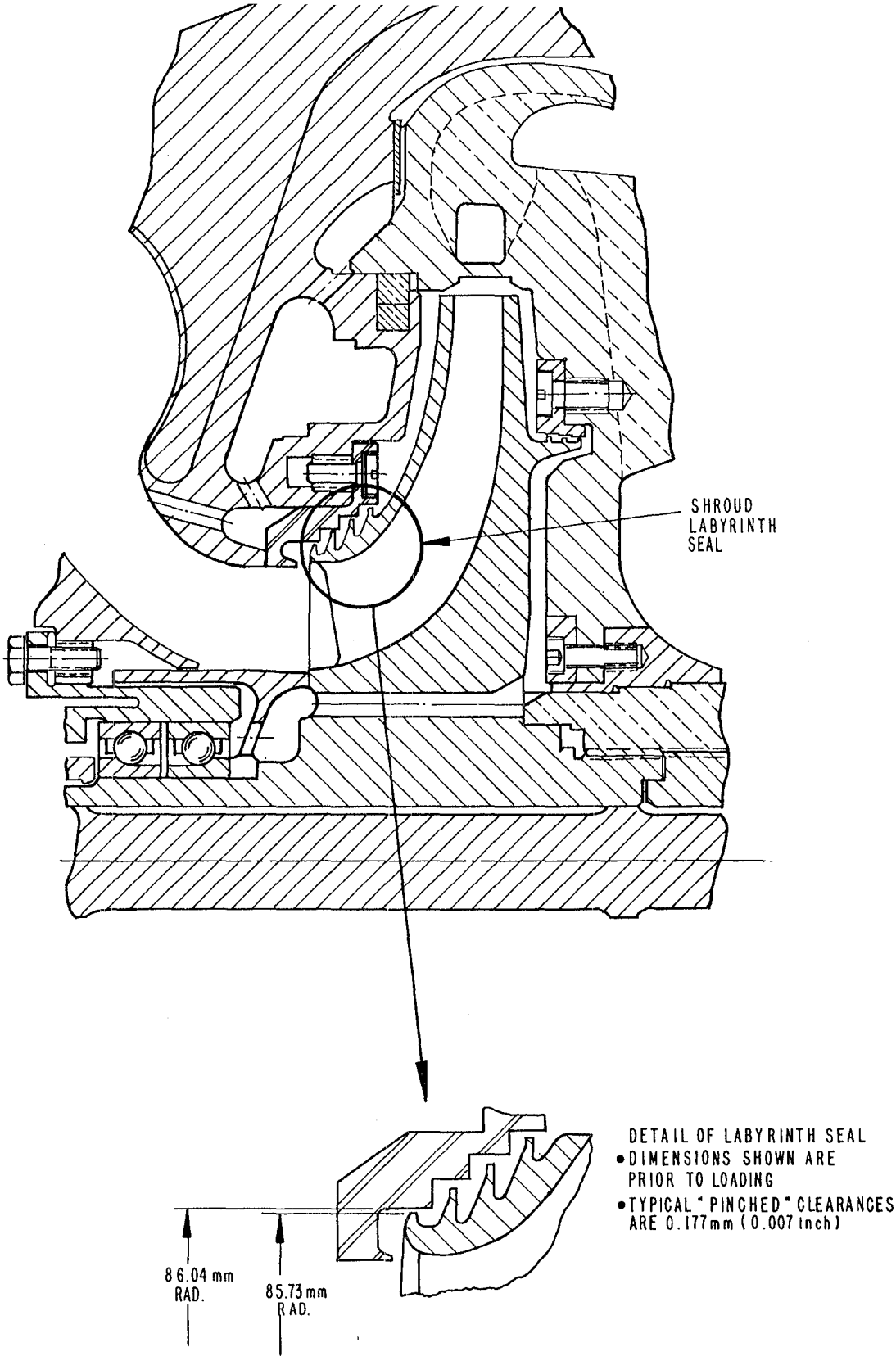

FIGURE 4-1. ASSEMBLY DETAIL (PARTIAL VIEW) FOR HIGH PRESSURE FUEL PUMP

4.2 Test Program

4.2.1 Test Facility Design

The basic test facility comprised a single knife edge rotating at high speed in an atmosphere of liquid and gaseous nitrogen, and a wear ring specimen which could be moved into contact with the knife edge at different rates of interaction and for a controlled interaction depth. In this section, the major components and assemblies which make up the rub testing hardware are described.

Knife Edge Disk

The knife edge disk is shown in Figure 4-2. It consists of a 1.59 mm (0.0625 inch) thick disk of Ti-5Al-2.5Sn alloy with its outer periphery machined to provide a knife edge configuration similar to that found on the labyrinth seals in the HPFP. The outer diameter of the disk (172.7 mm, 6.80 inch) is approximately the same as the diameter of the first labyrinth finger on the impeller shroud, and is the maximum disk diameter which could be conveniently accommodated in the test facility. The width of the knife edge (0.762 mm, 0.030 inch) exactly matches the labyrinth knife edge and the tapered sides preserve the overall thickness and thickness distribution of the labyrinth finger.

Surface treatments and coatings were applied to the knife edge for some tests in order to evaluate their resistance to wear in this rubbing environment. Section 4.3 describes these alternate materials and their selection.

Wear Ring Specimen

Figure 4-3 shows the details of the geometry for the wear ring specimens used in this experimental program. The wear ring "pad" has a radius of curvature of 86.49 mm (3.405 inch) and is 20.3 mm (0.78 inch) wide. The difference in radius between the wear ring pad and knife edge disk (0.127 mm, 0.005 inch) approximates the nominal "pinched" clearance in the HPFP at design operating conditions.

The pad was machined as an integral part of a mounting plate which was used to locate the pad relative to the knife edge disk. As shown in Figure 4-3, the wear ring specimen was instrumented with two thermocouples located below the surface of the pad and in the plane of disk interaction.

The majority of the rub interaction tests were conducted with a wear ring pad fabricated from 2024 T351 aluminum alloy duplicating the basic wear ring material in the SSME HPFP. For some tests the aluminum pads were coated with abradable materials, and for one test the complete wear ring specimen was fabricated from 99.99% pure, oxygen-free copper. More will be said about the selection of these alternate materials in Section 4.3.

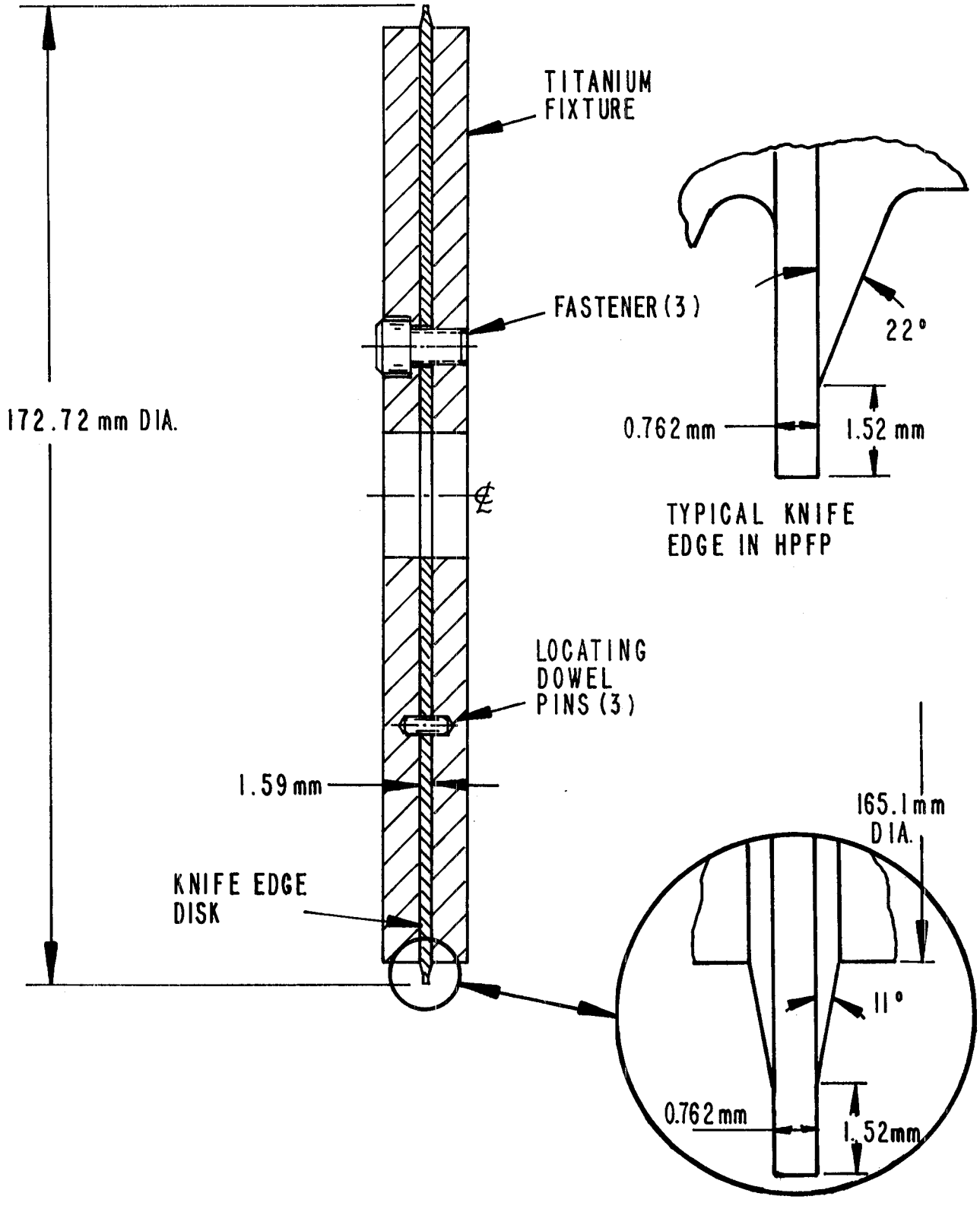

FIGURE 4-2. KNIFE EDGE TEST SPECIMEN

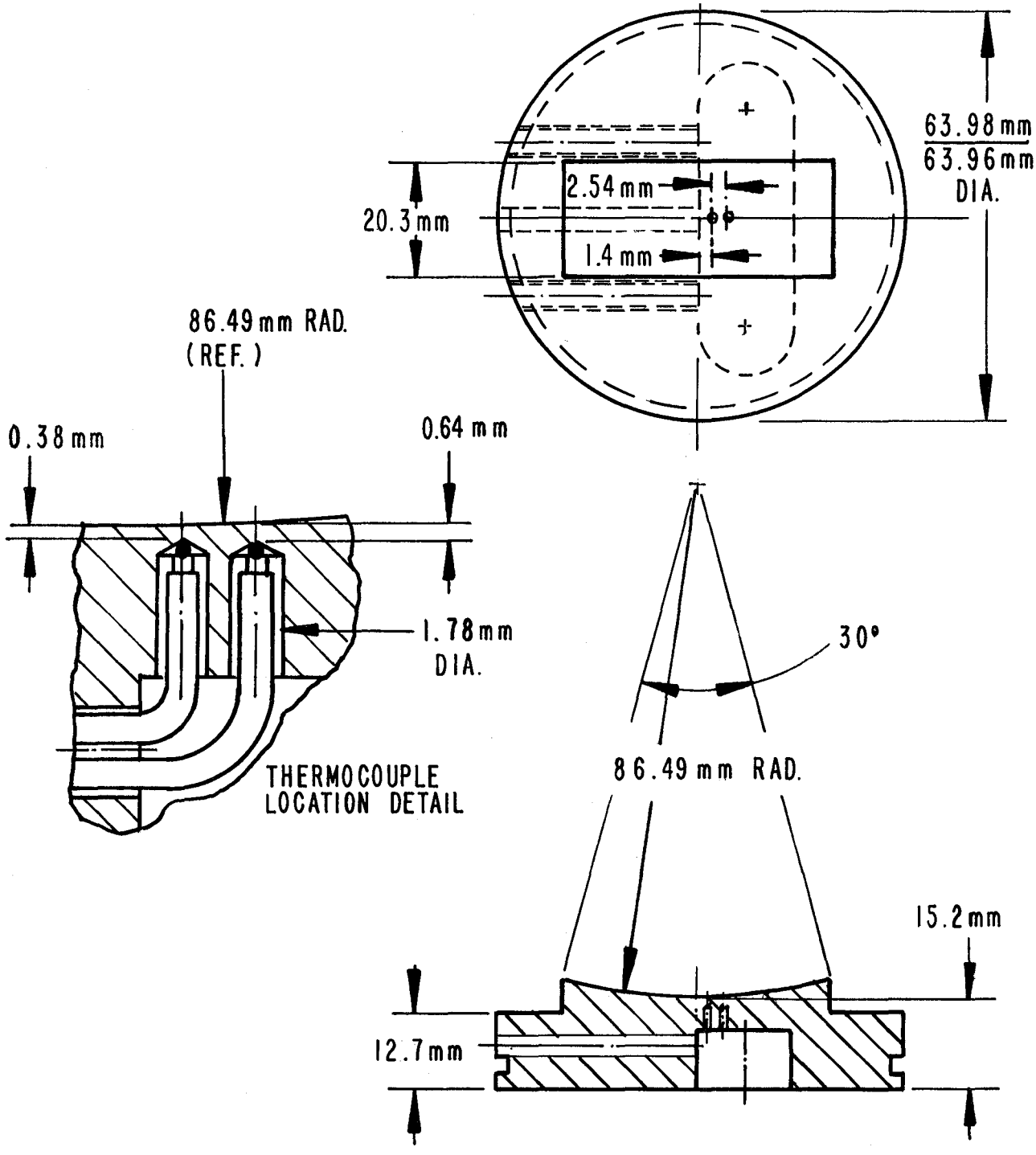

FIGURE 4-3. WEAR RING TEST SPECIMEN

Rub Interaction Hardware

A rub interaction test facility was assembled to provide high speed rotation of the knife edge disk and controllable interaction between wear ring specimen and a knife edge in a cryogenic environment. Figure 4-4 shows a section elevation view of the test facility and some details of the liquid nitrogen injection system.

In the setup of the test hardware, the knife edge disks were clamped between and pinned to Ti-6Al-4V side plates. The disks were concentrically aligned to the center of rotation of the assembly during the machining of the outer diameter of the knife edge and dowel pins were used to ensure repeatability of that alignment during setup of each test disk. This assembly was mounted on a drive shaft and was located against a shoulder on the shaft and held in place with a threaded nut which provided a clamping force of 13 kN (3000 lbf). The drive shaft was supported in two sets of angular contact ball bearings in a cartridge which was supported from the frame of the test fixture.

The knife edge disk shaft was connected with a splined coupling to the shaft of the drive turbine in Creare's Medium Aerodynamic Component (MAC) test facility. This turbine is part of a standard turbocharger package having its own radial and thrust bearings and lubrication system. The air supply for the drive turbine was provided from laboratory air compressors. Turbine speed was controlled by regulating the air flow rate to the turbine. With this drive system, rotational speeds of 35,000 rpm were achieved in the checkout tests, but test speeds were limited to 25,000 rpm (prior to the initiation of a rub) in order to minimize bearing loads and to accommodate changeover of knife edge disks without re-balancing of the rotating assembly. At 25,000 rpm the tip velocity of the knife edge was 225 m/s (742 ft/s).

Wear ring specimens were mounted in a collar assembly on the top of a column support (see Figure 4-4). The collar located the wear pad under the center of rotation of the knife edge and prevented lateral movement of the specimen during a rub interaction. The column could be raised and lowered with a hydraulic piston acting through wedge plates at the bottom of the column. A linear ball bushing provided lateral support for the column and guided its travel during a rub test. Both the rate of travel and the total extent of travel of the column were controlled, thereby providing a range of interaction rates between the wear specimen and the knife edge and a known total interaction depth.

The major components and subassemblies of the interaction control system are shown schematically in Figure 4-5. A brief description of the major components and their functions is given below:

1. A hydraulic piston actuator formed the core of the drive system used to force the wear specimen against the rotating knife edge. High pressure hydraulic fluid was supplied to the actuator at a controlled flow rate that established the rate of displacement of the actuator. The actuator was connected to a sliding wedge at the base of the column which translated the horizontal piston motion to vertical motion of the column. A range of displacement

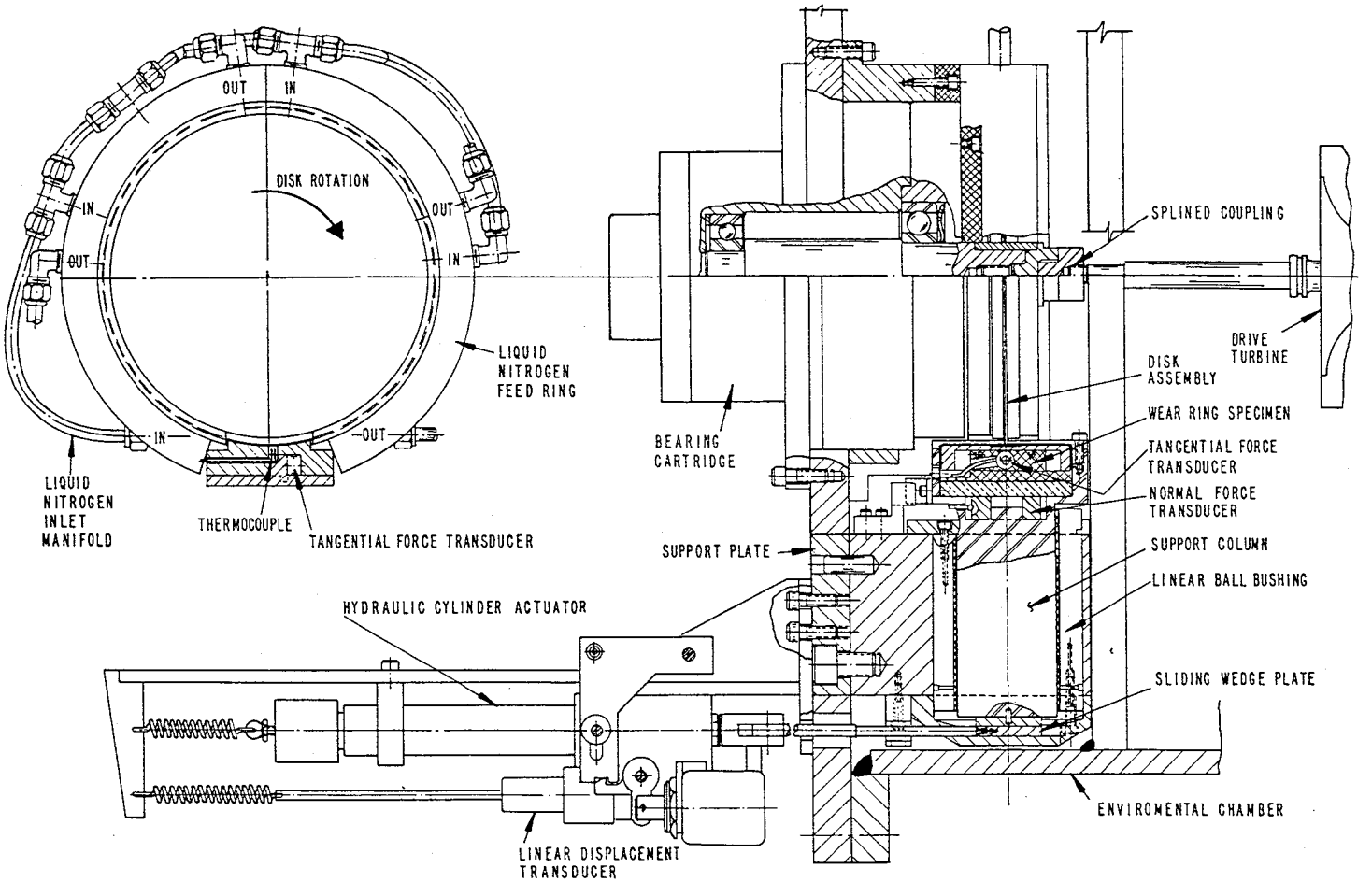

FIGURE 4-4. RUB INTERACTION TEST FACILITY ASSEMBLY DRAWING

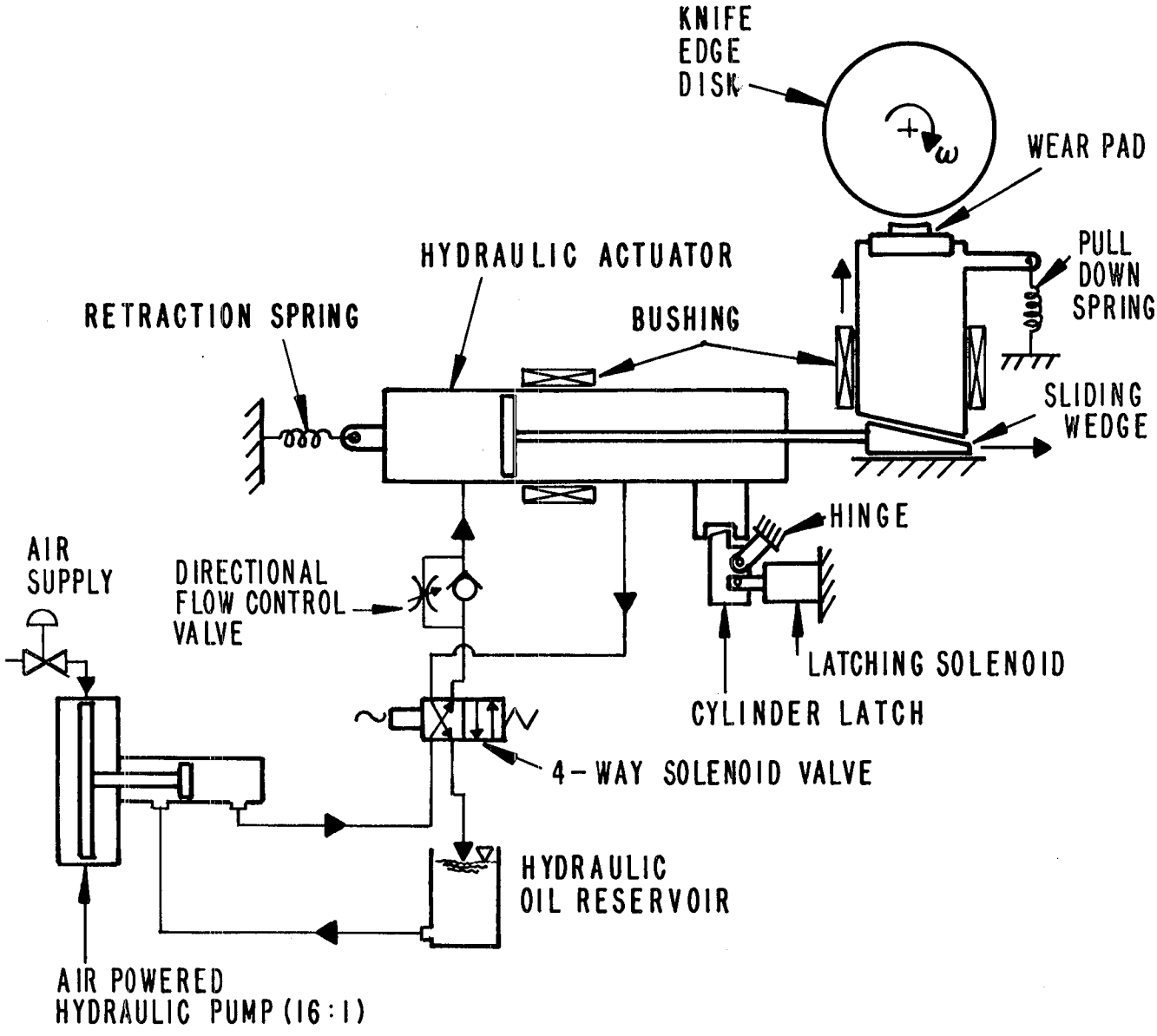

FIGURE 4-5. SCHEMATIC OF INTERACTION CONTROL SYSTEM

rates could be accommodated by using different wedge plate angles (ratio of vertical to horizontal motion), and by regulating the flow rate of hydraulic fluid to the actuator. For this test program a single wedge plate angle was used (4.435 degrees) and the oil flow rate was varied to provide interaction rates from 2.5×10^{-3} mm/s to 2.5×10^{-1} mm/s (10^{-4} inch/s to 10^{-2} inch/s).

2. The total depth of interaction was controlled by means of a pre-set limit switch. Prior to startup of a test, the wear specimen was placed in contact with the knife edge and the limit switch was adjusted to allow an additional 0.25 mm (0.010 inch) travel of the wear ring beyond the contact position. Actuation of the limit switch at the end-of-travel released a latch mechanism which caused the hydraulic cylinder to be rapidly retracted with the help of a spring, reversing the direction of travel of the piston and sliding wedge. Simultaneously, the column was pulled down with pre-loaded springs, breaking contact between the wear ring and the rotating knife edge.

3. A linear variable displacement transducer (LVDT) measured the rate and extent of interaction of the wear specimen. The body of the LVDT was fixed to the frame of the interaction device while the center core moved with the hydraulic piston. The wedge plate angle provided a fixed ratio of 12.8:1 between the measured displacement of the actuator rod and the vertical motion of the wear specimen.

Cryogenic Environment Control

In the HPFP the labyrinth seal on the first stage impeller operates in liquid hydrogen at about 47°K (-375°F) (Reference 9). For the rub tests this cryogenic environment was simulated by cooling the rotating knife edge and the wear ring specimen using liquid nitrogen having a temperature of 77°K (-321°F).

Liquid nitrogen (LN_2) was supplied from a pressurized tank through double-wall, insulated lines to a feed ring which surrounded the knife edge disk (Figure 4-4). The LN_2 was distributed in a manifold to four inlet ports located around the circumference of the feed ring. Four outlet ports were also located in the feed ring in order to drain away excess LN_2.

Figure 4-6 shows some of the details of the internal arrangement of the LN_2 feed ring and the means by which the knife edge disk was cooled. Each inlet port supplied the LN_2 to two jets which directed the fluid at opposite faces of the knife edge. The LN_2 filled the cavity surrounding the periphery of the disk, being held there and transported in the direction of rotation by the centrifugal "pumping" action of the disk in the small cavity.

The feed ring did not enclose the disk over the 30° arc where it interacted with the wear specimen (see Figure 4-4). At that location some of the LN_2 was allowed to escape from the feed ring cavity in order to cool the wear specimen pad.

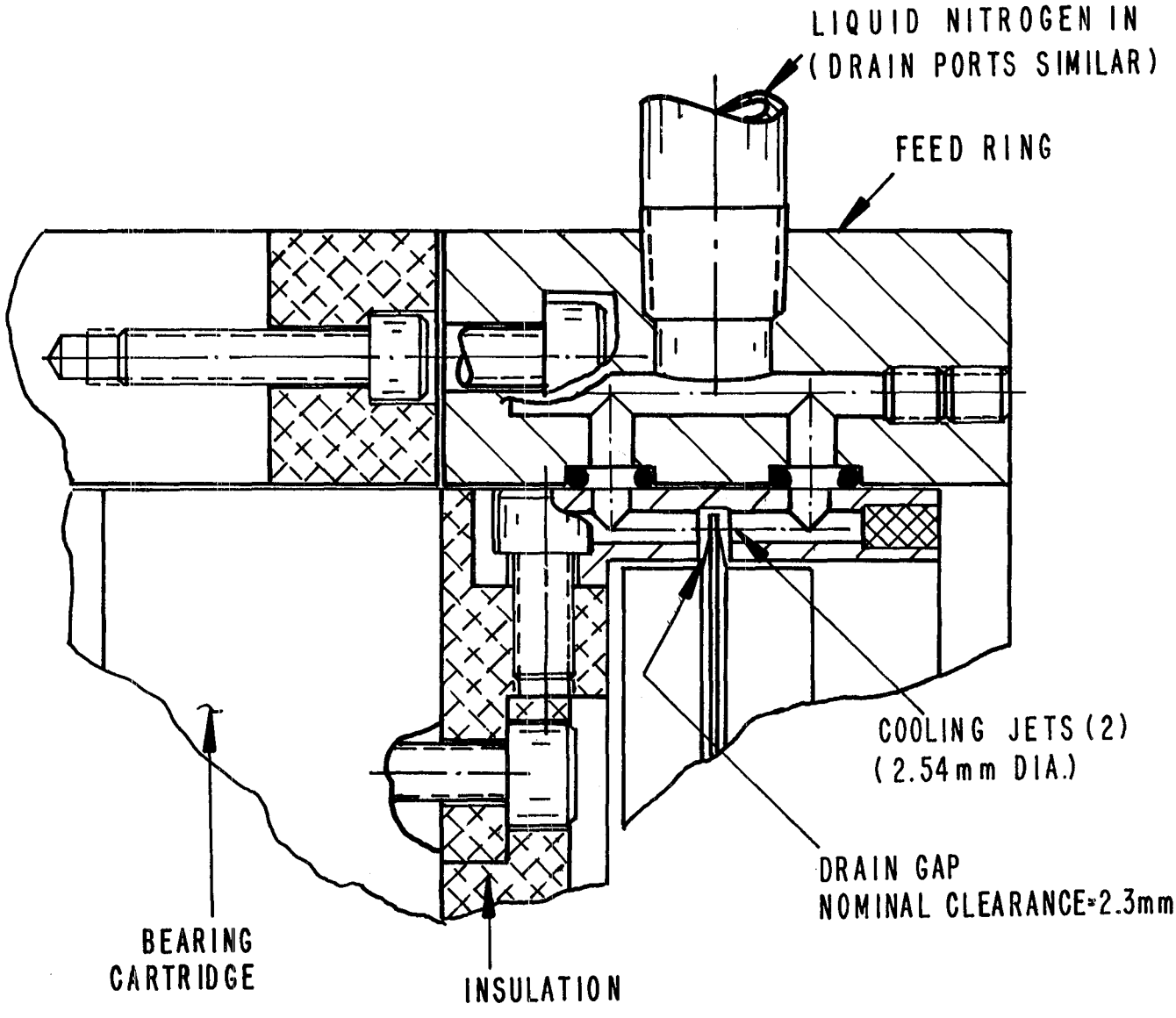

FIGURE 4-6. DETAIL OF LN_2 FEED RING ASSEMBLY

In operation, the LN_2 flow rate to the test hardware was manually controlled to meet two criteria:

1. the temperature of the wear pad was cold and stable,
2. excess liquid nitrogen was seen to be escaping from the four lines which were connected to the drain ports in the feed ring.

The design and operation of this system assured that the rub interaction tests were conducted in an environment which provided a realistic simulation of the conditions in the SSME HPFP.

Test Fixture

The interaction control device and the bearing cartridge were mounted on a heavy steel plate which was bolted to the MAC rig support fixture. This support fixture was very rigid and provided a convenient means for aligning the test hardware to the turbine drive.

4.2.2 Test Measurements and Data System

The measurements of major interest in these experiments were the forces and temperatures developed in the wear specimens as a function of the interaction rate and knife edge speed for the different materials systems investigated. Figure 4-7 shows a schematic representation of the instruments and signal conditioning used in these tests. Some additional information for each of the instruments is provided in Table 4-1.

Temperature

The wear ring specimen temperature was measured using two thermocouples located below the surface of the wear pad and in the plane of disk interaction (Figure 4-3). The thermocouples were made from 0.25 mm (0.010 inch) diameter wire and had a junction diameter of approximately 0.64 mm (0.025 inch). One thermocouple was installed 0.38 mm (0.015 inch) below the surface of the wear pad while the second was at a depth of 0.64 mm (0.025 inch). The thermocouple beads were firmly positioned at the ends of the drilled holes and were held in place by cementing the insulated wires where they exited from the installation holes. The small wires and intimate contact with the wear pad insured fast response and a temperature measurement which was representative of the local temperature beneath the wear scar.

The thermocouples were connected to a reference temperature zone block and their outputs were amplified to 5V full-scale prior to input to the data acquisition computer. A calibration system was used to record the zero offset and voltage gain for the thermocouple amplifiers before each test.

For some of the tests the thermocouple amplifier output exceeded 5V full-scale, which was beyond the input range of the analog-to-digital converter in the DAS computer.

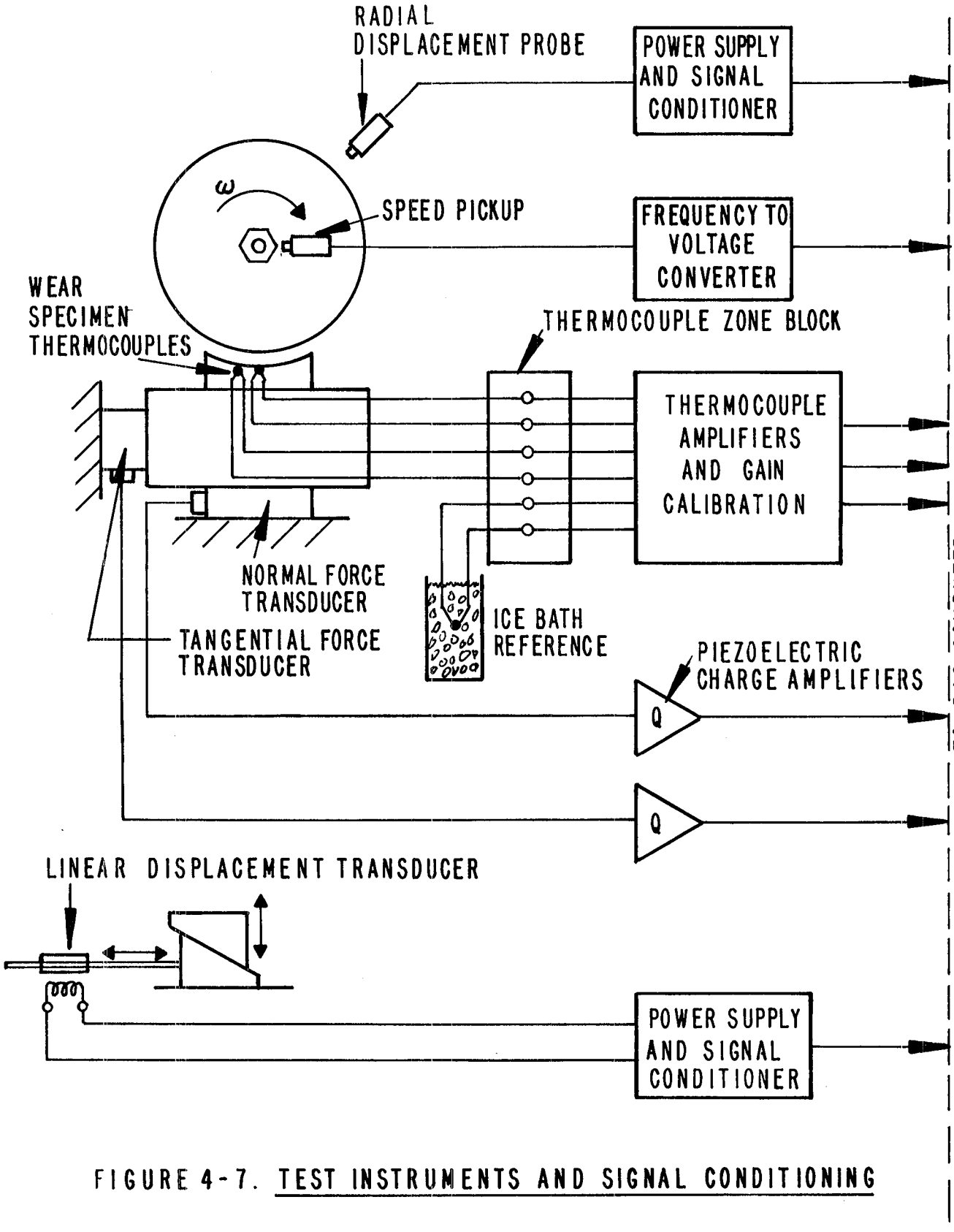

FIGURE 4-7. TEST INSTRUMENTS AND SIGNAL CONDITIONING

TABLE 4-1 MEASURING INSTRUMENTS FOR RUB INTERACTION TESTS

Test Measurement	Instrument	Description
Wear Specimen Temperatures (2)	Thermocouple	Bead-type grounded junction 0.25 mm wire diameter; Type K (Chromel-Alumel); Omega Engineering Catalog No. 5TC-GG-K
Tangential Rub Force	Load Cell	Piezoelectric force transducers; resonant frequency - 200 kHz; load range 7.5 kN; Kistler Model 9001
Normal Rub Force	Load Cell	Piezoelectric force transducer;resonant frequency - 65 kHz; load range 89 kN; Kistler Model 9041
Interaction Rate	Displacement Transducer	Linear, variable differential transformer; 12.7 mm range; Schaevitz Engineering Model 250 DC
Disk Speed	Tachometer	Magnetic pickup on hex nut; frequency-to-voltage converter
Disk Radial Displacement	Displacement Transducer	Eddy current probe; Bently-Nevada Series 190-3000

Force

Tangential and radial (shear and normal) forces were measured during the rub interaction tests using two piezoelectric load cells mounted below the wear ring specimen. The normal force transducer transmitted the vertical load component from the wear specimen to the support column, whereas the tangential force transducer formed the link between the wear pad and the support collar. Both transducers were connected to charge amplifiers which converted the charge sensitive output to a voltage proportional to the applied force.

The time constant of the force transducers and charge amplifiers was greater than 100 seconds during ambient operation and calibration of the force measuring system. However, the DC stability during actual rub tests does not appear to be that long. It is possible that the cryogenic environment affected the resistance of the transducer and cables, resulting in greater charge leakage during test operation.

Interaction Rate

The rate of interaction between the knife edge and the wear pad was measured with a linear variable differential transformer (LVDT) connected to the hydraulic actuator arm. The LVDT provided a DC voltage proportional to the change in position of the arm, which was translated to wear pad linear motion through the sliding wedge. The interaction rate was determined by calculating the rate of change of actuator position, divided by the wedge translation ratio.

Rotational Speed

The rotational speed of the knife edge disk was measured with a magnetic pickup which sensed the rotation of a hex nut on the end of the high speed shaft. The pulse output produced by the probe was monitored on a digital counter and was input to a frequency-to-voltage converter for recording by the data acquisition computer.

Disk Displacement

The radial displacement of the knife edge disk was measured to provide an indication of test rig balance and overall "health" for the test operator. An eddy current probe was aligned to measure the change in clearance gap between the probe face and one of the side plates used to clamp the disk specimens. That probe produced a voltage output proportional to the clearance gap which was linear for the small gap changes experienced.

Data Acquisition System

All of the instrument outputs were conditioned to 5V full-scale level and were connected to Creare's data acquisition computer. The computer is a Digital Equipment Corporation PDP 11/70 with a separate microprocessor for control of data acquisition using a built-in multiplexer and A/D

converter. This system was capable of recording data at an aggregate sampling rate (total number of A/D conversions) of 12 kHz. For these experiments the force, displacement and speed measurements were recorded at 1000 samples per second and the temperatures were recorded at 250 Hz each.

4.3 Materials and Coatings

As described earlier, the materials used in the HPFP are Ti-5Al-2.5Sn alloy for the impeller and 2024-T3 aluminum alloy for the wear ring.* The aluminum is expected to be abraded or worn away by the titanium labyrinth fingers during a rub interaction, but some cracking of the titanium has been observed during testing of the pump. Therefore, several alternate materials were considered as candidates for possible upgrades of the labyrinth seal to improve its performance in a rub event.

In considering a change of materials systems, emphasis was given to low wear rate of the labyrinth fingers and structural integrity of the labyrinth components, even following repeated interaction. Many materials were considered for this experimental evaluation and a preliminary thermal and stress analysis was used to screen candidate materials. The selection of the final materials was based largely on expected success in favorably impacting the wearability of the seal system and availability of the materials for this project.

Bill-of-Materials Knife Edge and Wear Ring

The knife edge disks were fabricated from titanium alloy sheets with 5% aluminum and 2.5% tin. A certificate of analysis for the material used on this project is included in Appendix C-1. All disks were made with this same material, even those which were later treated for wear resistance or with abrasive coatings.

The wear ring specimens used in the baseline tests and for testing with alternate knife edge treatments were made from 2024-T351 aluminum alloy. The material certification for the aluminum bar stock is also included in Appendix C-1.

Knife Edge Treatments

Three alternate treatments and coatings were used for the titanium knife edge disks as described in Table 4-2. One of the treatments involved nitrogen ion implantation (ion nitriding) of the knife edge. This surface modification procedure is known to improve the wear characteristics of components in sliding contact (Ref. 13). The process of ion nitriding involves injecting high energy nitrogen ions into a shallow layer of a substrate material to effect both physical and chemical modifications of

* One turbopump drawing provided to Creare----Rocketdyne Drawing No. RS007550 Sheet 2----shows the use of copper plating on the wear ring surfaces instead of aluminum. We are not certain of the in-service configuration of the HPFP seals, although the contract workscope specifies 2024-T3 aluminum for the BOM seal evaluation. These comments are recorded here because of the adverse wear characteristic of the copper wear ring observed during our rub tests as described in Section 4.6.1.

TABLE 4-2 KNIFE EDGE COATINGS

Treatment Code*	Vendor	Description
TN	Spire Corporation	nitrogen ion implantation on knife edge; ion flux of $2 \times 10^{17}/cm^2$ at 180 keV; see Appendix C-2.
AO	METCO Incorporated	flame-sprayed alumina-titania (METCO 101B-NS) to thickness of 0.2 mm on molydenum-nickel-aluminum bond coat (METCO 447) thickness 0.075 mm; see Appendix C-3; outer diameter finished by grinding to final 101B coating thickness of 0.076 mm.
TC	Union Carbide Corporation (Linde Division)	Detonation-Gun application of tungsten carbide-cobalt-chromium coating (UCAR LW-15) to thickness of 0.23 mm; see Appendix C-4; outer diameter finished by grinding to final LW-15 coating thickness of 0.076 mm.

*The Treatment Code is a mnemonic abbreviation which is used in the test number identification.

the substrate. For this specific application the nitrogen ion flux was $2x10^{17}/cm^2$ at an energy of 180 keV. Based on the calculated depth profiles in Appendix C-2, the peak ion concentration is estimated to be 10^{22} ions/cm^3 at a depth of about 0.2 μm. No post-treatment machining of the disks was necessary prior to their use in the rub tests.

The other two treatments shown in Table 4-2 involved the application of abrasive coatings to the knife edge in order to enhance its resistance to wear in a rub situation. The alumina-titania coating (METCO 101B-NS) has found applications on clearance control surfaces in air-breathing turbomachinery, whereas the tungsten-carbide coating (UCAR LW-15) has been used in cryogenic pump applications. More details of the properties and uses for these two coatings are provided in Appendices C-3 and C-4.

Wear Ring Alternate Materials

Two abradable coatings for the aluminum wear ring and a pure copper wear ring were evaluated in the experimental program. These alternate wear ring materials are briefly described in Table 4-3. The coatings, a aluminum-silicon-graphite composite (35% graphite, 7% porosity) and an yttria-stabilized zirconium oxide composite (YSZ) having 21.5% porosity were selected on the basis of being readily abraded or worn away during a rub interaction. Both of these materials have seen use as abradable components, although no prior cryogenic applications are known. Because these coatings are considered by the vendor (METCO) to be developmental, detailed product information is not available. Some processing data and photomicrographs of the applied coatings are provided in Appendices C-5 and C-6.

In addition to the coatings described above, a pure (99.99%), oxygen-free copper wear ring was evaluated as a possible replacement for the aluminum wear ring. The primary justification for selecting copper as a replacement seal is its increased thermal conductivity compared to 2024 aluminum (about a factor of 2 higher conductivity at cryogenic temperatures). The thermal analysis discussed in Section 2 showed that use of a copper wear ring substantially reduced the rub zone temperature for a model which assumed constant heat input at the rub interface.

TABLE 4-3 ALTERNATE MATERIALS FOR WEAR RINGS

Treatment Code*	Vendor	Description
AG	METCO Incorporated	flame sprayed aluminum-silicon-graphite composite; 35% graphite (METCO CE-2074A) to thickness of 0.51 mm on METCO 447 bond coat; see Appendix C-5; coating finished to 86.49 mm radius of curvature-final coating thickness 0.38 mm.
YZ	METCO Incorporated	flame-sprayed yttria stablized zirconia coating; 21.5% porosity (METCO CE-2198A) to thickness of 0.51 mm on bond coat of METCO 447; see Appendix C-6; coating finished to 86.49 mm radius of curvature-final coating thickness 0.38 mm.
CU	Creare R&D Inc.	99.99% pure, oxygen-free copper; machined to same configuration as BOM aluminum wear ring specimen.

*The Treatment Code is a mnemonic abbreviation which is used in the test number identification.

4.4 Rub Interaction Test Matrix

The rub interaction experimental phase was designed to meet two objectives:

1. Evaluation of the performance of the labyrinth seal configuration under realistic conditions of speed, interaction rate, and operating environment (cryogenic temperature).

2. Evaluation of alternative knife edge treatments and abradable wear ring coatings, for some test conditions.

A total of 15 tests were conducted in a matrix of three series as shown in Table 4-4. The Baseline Series of tests compares seal system behavior using the BOM knife edge and wear ring materials over a wide range of rub interaction rates. The second series of tests examined several alternate wear ring materials. Only a single test was carried out with the copper and YSZ coatings because of the adverse wear performance experienced at the interaction rate shown in Table 4-4. Tests at two interaction rates were carried out with the aluminum graphite wear ring coating. For the knife edge materials test series, the BOM aluminum wear ring was used. Each test used new wear components, i.e. no knife edge disks or wear pads were used for more than a single test.

Detailed descriptions and documentation of the alternate materials used in these tests are provided in Section 4.3 and in Appendix C.

Besides the materials variations, the only other test parameter employed was rub interaction rate, I. The interaction rate is defined as the rate, in units of radial distance, at which the knife edge and wear ring are forced together. For the baseline tests the interaction rate was varied over 2 orders of magnitude while for the alternate materials tests I covered a smaller range. The range of I selected for these tests has been used in other experimental investigations of wear (Reference 6), in which I has been shown to exert a major influence on the relative wear between the rotating and stationary components.

4.5 Test Procedures

All of the tests conducted in this program followed the same basic procedures for setting up the test hardware, preparing the specimens, carrying out the actual rub tests and examining the test specimen after the rub.

4.5.1 Instrument Calibration

The instruments and data system used for recording test data were calibrated during the experimental phase of this project.

1. The normal and tangential force transducers were calibrated, along with their respective charge amplifiers, by recording the amplifier voltage output with a known load (mass) applied to the load cells.

TABLE 4-4. LABYRINTH SEAL TEST MATRIX

Test Series	Knife Edge Material	Wear Ring Material	Interact Rates (mm/s)	No. of Tests
Baseline	BOM titanium[1]	BOM aluminum[2]	0.0016 to 0.13	5[3]
Wear Ring	BOM titanium	Copper	0.025	1
	BOM titanium	aluminum-graphite coating	0.018, 0.15	2
	BOM titanium	yttria-stabilized zirconia coating	0.022	1
Knife Edge	ion-nitrided titanium	BOM aluminum	0.021, 0.1	2
	alumina-titania coating	BOM aluminum	0.018, 0.11	2
	tungsten-carbide	BOM aluminum	0.011, 0.12	2
			Total No. of Tests	15

(1) Bill-of-Materials (BOM) knife edge material is Ti-5Al-2.5Sn.

(2) BOM wear ring material is 2024-T351 aluminum.

(3) Three tests at average interaction rate of 0.012 mm/s and one test each at 0.0016 and 0.13 mm/s.

2. Thermocouples for measuring the wear pad temperatures were standard commercial items with known temperature-to-emf characteristics. New thermocouples were used for each test specimen. The thermocouple amplifiers were calibrated for each test by voltage substitution.

3. The LVDT used for measuring displacement of the sliding wedge in the interaction controller was calibrated by recording its output voltage for a known displacement of its center core measured with precision laboratory verniers. Conversion of LVDT displacement to displacement of the wear specimen was directly related to the angle of the wedge plate (horizontal to vertical ratio of 12.8:1).

4. Calibration of the rotational speed signal involved comparison of the output voltage (proportional to speed) with the reading of a digital counter which was connected directly to the speed pickup. In addition, these speed signals were compared with the frequency of the vibration signal from the radial displacement probe, as displayed on a spectrum analyzer.

5. The disk radial displacement probe was calibrated by recording the output voltage from its signal conditioner at several values of clearance between the probe tip and the outer periphery of the side disks which support the knife edge. The calibration was undertaken at ambient temperature ($\cong$ 20°C) over the linear range of the probe.

6. Voltage meters and counters used for calibration and for recording test data were calibrated by Creare's Electronics Laboratory, which provides for annual calibration of primary measuring instruments by outside services, with calibrations traceable to NBS.

7. The analog to digital converter in the data acquisition computer is calibrated by Digital Equipment Corporation on a semi-annual schedule.

4.5.2 Test Preparation

Prior to initiation of a rub test, the test specimens were inspected to insure that they conformed to the design specifications and the test facility was checked for proper operation.

Other pre-test checkouts and verifications are listed below:

1. Thermocouples in the wear pad were checked for polarity and relative response rate prior to installing the wear pads in the test rig. The thermocouples were connected to the data system and the pad was quickly cooled using ice. The outputs were checked for consistency and new thermocouples were installed, if necessary.

2. The diameter of each knife edge disk was measured prior to installation in order to determine the extent of knife edge wear resulting from the rub interaction. The diameter was measured by comparison with a reference bar using a precision height gauge having an estimated accuracy of 1.3 μm.

3. Following inspection of the wear specimens, they were installed in the test rig, all nitrogen (gas and liquid) lines were connected, instruments were connected to the data system, and the air supply and lubricating oil systems for the drive turbine were brought on-line.

4. The balance of the assembled hardware was checked at this point by operating the disk up to test speed (25,000 rpm) and monitoring the radial displacement of the disk and the bearing temperatures. It was our experience that the as-built tolerances on the knife edge disks did not significantly affect overall rig balance, and rebalancing with each disk would have provided only marginal decreases in the disk radial displacement. The peak-to-peak radial displacement of the disk was less than about 0.04 mm (0.0015 inch) for most of the tests; rebalancing would have reduced this to about 0.025 mm (0.001 inch).

5. The interaction rate was checked before each test, and adjusted if necessary.

6. The depth of interaction was set prior to each test, after the rig had been cooled using liquid nitrogen. This was accomplished by manually traversing the wear specimen so that it just made contact with the periphery of the knife edge disk (not rotating) and then setting the limit switch to permit an additional 0.25 mm (0.010 inch) of travel of the specimen beyond that contact point. The traverse mechanisms and wear specimen were then retracted to provide approximately 0.13 mm (0.005 inch) clearance between the pad and disk prior to start of the test.

4.5.3 Test Operation

Initiation and operation of a test proceeded quickly once all preparations were satisfactorily completed.

1. Thermocouple amplifier gains and offsets were checked using the built-in gain calibration system and were recorded on the DAS computer.

2. The environmental chamber surrounding the test rig was purged with gaseous nitrogen to remove any moisture which could condense and form ice when the liquid nitrogen was introduced.

3. Test rig speed was increased to the desired pre-rub value (25,000 ± 500 rpm), and the rub specimens were cooled by injecting liquid nitrogen (LN_2) into the caliper assembly described in Section 4.2.1. The LN_2 flow rate was increased until excess liquid was observed to be issuing from the drain lines and the wear pad temperatures, monitored with digital volt meters, were stable.

4. When the temperature of the wear pad had stabilized and with the disk speed steady at the desired pre-rub value, the interaction device was actuated, causing the wear ring to move toward the knife edge disk. At that same time the data acquisition computer started recording signals from the test instruments. Some test data were also manually recorded in the test log book, e.g. initial speed, pad temperatures, LVDT reading, and disk peak-to-peak radial displacement.

5. The rub test proceeded until the limit switch reversed direction of travel of the interaction controller, breaking contact between the knife edge and wear pad and signaling end of test to the operator.

6. Shutdown of the rig involved closing the air supply to the turbine, securing LN_2 feed to the test section, terminating the computer data sweep and bringing other support equipment to the at-standby condition.

4.5.4 Post-Test Inspections

After shutdown, the test rig was allowed to warm back to ambient conditions before disassembly was initiated. The following describes the inspections which were routinely performed for the test specimens.

1. Both the wear ring and knife edge were examined in-place for evidence of failure or abnormal wear. The components were marked with an indelible pen to indicate rub direction and orientation to aid in interpretation of wear patterns.

2. The knife edge disk diameter was measured using the same method and apparatus as in the pre-test inspection. The depth of the scar in the wear pad was measured using a depth gauge. Other noteworthy observations of the condition of the wear specimens were recorded.

3. Following these inspections at Creare, the test pieces were packaged and transferred to Thayer School of Engineering (Dartmouth College) for detailed metallurgical evaluation. This work involved optical and scanning electron microscope (SEM) examination of the wear specimens, energy-dispersive X-ray spectroscopy (EDX) to identify material transfer resulting from the rubs and more detailed investigations for some test specimens.

4.5.5 Test Data Reduction

Immediately following completion of each test, the raw data acquired by the computer were plotted in the form of strip charts (parameter vs. time). The time interval for the plots included the duration of the rub interaction period, plus a precursor period of steady, no-rub data and a short postscript following retraction of the wear specimen. Thermocouple amplifier gains were calculated from the pre-test calibration data, and initial and peak temperatures of the wear pad recorded during the tests were calculated.

The duration of the interaction was determined by examination of the strip chart data plots. Initiation of the rub was assumed to occur at the time when the load cells first indicated a force signal above their baseline noise level. The termination of a rub was quite clearly marked by the step change in the output of the interaction position sensor (LVDT). The difference between these two times was taken to be the duration of the rub.

Interaction rate was determined from the indicated change in position of the interaction device during the time period of the rub. Because the rate is relatively constant throughout the interaction period, an average rate was calculated as the total displacement divided by rub duration.

The volume wear ratio (VWR) between the knife edge and wear pad was calculated for each pair of test materials based on the measured disk diameter reduction and depth of wear scar:

$$VWR = \frac{\text{volume loss of knife edge}}{\text{volume loss of wear pad}}$$

For the situation where the reduction in diameter and depth of wear scar are small relative to the radius of curvature, VWR can be approximated:

$$VWR = \frac{2\pi r_d \, w_d \, (\Delta r_d)}{1/6\pi r_p w_p (d)} \qquad (2)$$

where:
- r_d = disk radius of curvature
- r_p = pad radius of curvature
- w_d = width of knife edge
- w_p = width of wear scar
- Δr_d = reduction in disk radius due to wear
- d = depth of wear scar

This relationship can be somewhat simplified by setting $r_d = r_p$ and $w_d = w_p$, reasonable assumptions for the present situation. Then,

$$VWR = 6 \frac{\Delta D}{d} \qquad (3)$$

where ΔD = reduction in the disk diameter = $2(\Delta r_d)$.

4.6 Test Results

The data available from the rub interaction tests include the measurements of forces, temperatures, speed and interaction rate, total wear of the knife edge and wear ring, and the findings from the metallurgical examinations. This section provides a general overview of the test results, highlighting significant observations for specific tests and describes the "strip chart" and metallurgical data in detail for one test. Strip chart data for all of the tests are presented in Appendix D and the metallurgical data are found in Appendix F.

4.6.1 Data Summary

Fifteen rub interaction tests were undertaken, providing data on 7 materials systems (combinations of wear ring and knife edge materials) over a broad range of interaction rates, and including repeat tests for the baseline materials combination. A summary of results for these tests is presented in three parts:

Table 4-5a: Baseline Materials Tests
Table 4-5b: Evaluation of Wear Ring Materials
Table 4-5c: Evaluation of Knife Edge Materials

The Test Number used in these tables is a mnemonic description of the major test parameters--materials and interaction rate--and is used frequently in this report to identify the computer-plotted "strip chart" data and the SEM micrographs. Figure 4-8 provides a guide to the test numbering system.

The data tables show the average interaction rate, the depth of the scar in the wear pad, reduction in disk diameter and the calculated volume wear ratio (VWR). The estimated uncertainties in the measurements of wear scar depth and disk diameter reduction are 0.025 mm and 0.0013 mm, respectively. Assuming these measurement errors are random, i.e. not systematically biased high or low, the uncertainty in VWR can be calculated from:

$$(\Delta VWR)^2 = \left(\frac{\partial VWR}{\partial D}\right)^2 (\Delta(\Delta D))^2 + \left(\frac{\partial VWR}{\partial d}\right)^2 (\Delta d)^2 \qquad (4)$$

where ΔVWR = calculated uncertainty in volume wear ratio
$\Delta(\Delta D)$ = estimated uncertainty in measured disk wear = 0.0013 mm
Δd = estimated uncertainty in measured scar depth = 0.025 mm

The uncertainty in VWR is also included in Table 4-5 for those cases where VWR could be calculated.

Other tabulated data include the reduction in rotational speed during the rub (the air flow to the drive turbine was held constant throughout the interaction period of a test resulting in some change in speed due to the friction torque at the rub interface) and the total interaction time estimated from the strip-chart records. The column labeled "Test Observations" provides miscellaneous comments recorded by the test operators during the tests or during post-test examinations of the test specimens and data.

TABLE 4-5a SUMMARY OF TEST RESULTS - BASELINE MATERIALS SERIES

Test Number	Knife Edge Material	Wear Ring Material	Interaction Rate, mm/s (inch/s)	Wear Scar Depth mm (inch)	Disk Diameter Reduction mm (inch)	Volume Wear Ratio (uncertainty)	Disk Speed Reduction, rpm	Total Interaction Time, s	Test Observations
TIAL02	BOM Titanium	BOM Aluminum	13×10^{-2} (0.51×10^{-2})	0.33 (0.013)	0.13×10^{-2} (50×10^{-6})	0.023 (±0.02)	1,800	2.4	Peak temperatures reached at end of interaction
TIAL03	BOM Titanium	BOM Aluminum	16×10^{-3} (0.64×10^{-3})	0.25 (est) (0.010 est)	-	NA (1)	3,000	9.1	Double-peak temperature and force measurements; aluminum transferred to knife edge
TIAL13	BOM Titanium	BOM Aluminum	9.9×10^{-3} (0.39×10^{-3})	0.25 to 0.30 (0.010 to 0.012)	0.13×10^{-2} (50×10^{-6})	0.027 (±0.03)	9,000	34	Very high seal surface temperature; melting & cracking of aluminum in wear scar, smearing of aluminum
TIAL23	BOM Titanium	BOM Aluminum	10.9×10^{-3} (0.43×10^{-3})	0.25 to 0.30 (0.010 to 0.012)	8.89×10^{-3} (3.5×10^{-4})	0.19 (±0.1)	4,000	-	Test data terminated early due to computer failure; peak temperatures not as high as in Test TIAL13
TIAL04	BOM Titanium	BOM Aluminum	16.5×10^{-4} (0.65×10^{-4})	0.20 (0.008)	$+2.16 \times 10^{-2}$ ($+8.5 \times 10^{-4}$)	NA(2)	1,000	131	Cyclic temperatures and forces; small speed excursions; wear scar appears scuffed; build-up of aluminum on knife edge disk

(1) Disk diameter reduction not available so VWR not calculated.
(2) Disk diameter increased due to pickup, so VWR not calculated.

TABLE 4-5b SUMMARY OF TEST RESULTS - WEAR RING MATERIALS SERIES

Test Number	Knife Edge Material	Wear Ring Material	Interaction Rate, mm/s (inch/s)	Wear Scar Depth mm (inch)	Disk Diameter Reduction mm (inch)	Volume Wear Ratio (uncertainty)	Disk Speed Reduction rpm	Total Interaction Time, s	Test Observations
TICU03	BOM Titanium	Oxygen-free, 99.99% pure copper	25.4×10^{-3} (1.0×10^{-3})	<0.05 (est) (<0.002)	7.62×10^{-2} (3×10^{-3})	>9 (±2)	16,000	9.3	High temperature peaks recorded (>275°C); large reduction in speed; considerable reduction in disk diameter, material deposited in wear scar
TIAG02	BOM Titanium	Aluminum/ Silicon/ Graphite Coating (METCO CE2074A)	14.5×10^{-2} (0.57×10^{-2})	0.33 est (0.013 est)	0.13×10^{-2} (50×10^{-6})	0.023 (±0.02)	<500	1.6	Very small forces & temperature changes; only slight speed reduction
TIAG03	BOM Titanium	Aluminum/ Silicon Graphite Coating (METCO CE2074A)	18×10^{-3} (0.71×10^{-3})	0.25 (0.010)	3.2×10^{-3} (1.25×10^{-4})	0.075 (±0.09)	500	11.5(est)	Very small temperature changes; speed and force changes small
TIYZ03	BOM Titanium	Yttria-Stabilized Zirconia Coating (METCO CE-2198A)	22.4×10^{-3} (0.88×10^{-3})	nil	53.3×10^{-2} (21×10^{-3})	>>10	25,000	10 to 15	Large speed reduction ~2 sec into test, speed dropped to 0 at ~10 sec; sample retracted at ~15 sec; titanium deposited on wear pad; some YSZ adheres to disk

TABLE 4-5c SUMMARY OF TEST RESULTS - KNIFE EDGE MATERIALS SERIES

Test Number	Knife Edge Material	Wear Ring Material	Interaction Rate, mm/s (inch/s)	Wear Scar Depth mm (inch)	Disk Diameter Reduction mm (inch)	Volume Wear Ratio (uncer-tainty)	Disk Speed Reduction rpm	Total Interaction Time, s	Test Observations
TNAL02	Ion Nitrided Titanium	BOM Aluminum	10.4×10^{-2} (0.41×10^{-2})	0.25 (0.010)	$+4.7 \times 10^{-2}$ ($+1.85 \times 10^{-3}$)	NA(1)	2,500	2.6	Some aluminum buildup on disk periphery; very large surface temperature may be result of exposing of surface thermocouple during rub; T>320°C
TNAL03	Ion Nitrided Titanium	BOM Aluminum	21×10^{-3} (0.825×10^{-3})	0.25 (0.010)	nil	0 (±0.03)	3,400	15.3	Temperatures & forces cycled 3 times during rub; thin (0.025 mm) layer of aluminum deposited on segment of disk periphery
AOAL02	Alumina/ Titania Coating (METCO 101B-NS)	BOM Aluminum	10.6×10^{-2} (0.417×10^{-2})	0.305 (0.012)	0.13×10^{-2} (50×10^{-6})	0.025 (±0.02)	700	2.45	Peak temperatures occur at end of interaction
AOAL03	Alumina/ Titania Coating (METCO 101B-NS)	BOM Aluminum	17.5×10^{-3} (0.69×19^{-3})	0.25 (0.010)	3×10^{-2} (1.2×10^{-3})	0.72 (±0.08)	4,000	13.7	Disk coated with aluminum from wear pad; speed, temperature & normal force cycled during rub period
TCAL02	Tungsten Carbide Coating (UCAR LW-15)	BOM Aluminum	12.1×10^{-2} (0.477×10^{-2})	0.33 (0.013)	$+6.47 \times 10^{-2}$ ($+2.55 \times 10^{-3}$)	NA(1)	1,000	2.6	Peak temperatures occur at end of interaction; buildup of aluminum on disk periphery
TCAL03	Tungsten Carbide Coating (UCAR LW-15)	BOM Aluminum	11×10^{-3} (0.435×10^{-3})	0.25 (0.010)	1.1×10^{-2} (4×10^{-4})	0.24 (±0.04)	2,400	25.5	Temperatures & normal force cycle during rub period

(1) Disk diameter increased due to transfer so VWR not calculated.

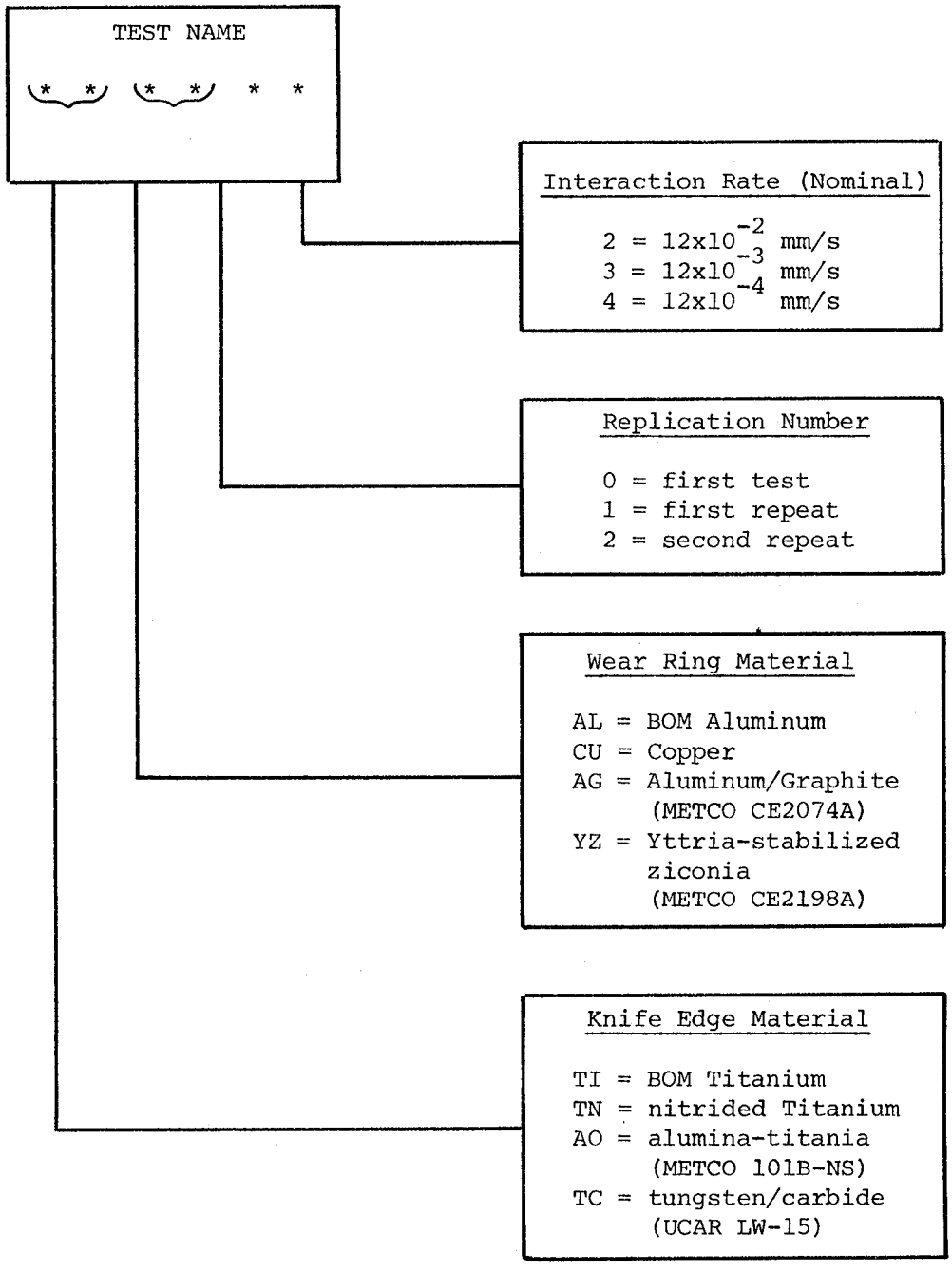

Figure 4-8. Test Number Code Nomenclature

Baseline Materials Tests

A total of 5 tests were conducted using the BOM materials for the knife edge and wear ring covering interaction rates ranging from 16.5×10^{-4} mm/s to 13×10^{-2} mm/s. Three of the tests were run at an intermediate rate ($\sim 10^{-2}$ mm/s).

At the high interaction rate (Test TIAL02) there was only slight wear of the knife edge (VWR $\cong$ 0.02), whereas the test at the lowest interaction rate (TIAL04) resulted in a slight increase in disk diameter due to pickup of aluminum from the wear scar. The tests at the intermediate rate (TIAL03, TIAL13, TIAL23) showed a range of VWR from slight (VWR $\cong$0.03) to moderate (VWR $\cong$0.2).

Cyclic temperature and force measurements were observed for some of these tests, i.e. for tests at the lower incursion rates, I <0.02 mm/s. As a rub progressed, the wear ring temperatures would rise to a maximum, followed by a rapid drop back to or near the starting (cold) temperature, followed by one or more repetitions of this cycle. The normal and tangential force signals exhibited the same cyclic behavior and in phase with the temperature cycles. Although not as clearly defined, the rotational speed also tended to cycle synchronously with the temperature and force measurements. The strip chart plots discussed in Section 4.6.2 illustrate this periodic nature of the rub interaction between the knife edge and wear ring.

The observed cyclic behavior might be related to a process of wear which involves plastic deformation of the wear pad accompanied by increasing pad temperature, followed by "tearing away" of wear pad material, perhaps due to plastic flow, fracture, melting or a combination of these. As material is removed, the interference between disk and wear ring is momentarily eliminated, reducing the rub forces and heat input to the pad, allowing the pad to cool down. The continued incursion of the wear ring specimen sets the cycle into motion again.

At the high interaction rate, the pad temperature and force measurements did not cycle in the shorter time of incursion, suggesting that the wear proceeded more uniformly than in the tests at lower interaction rates.

Wear Ring Materials Tests

Four tests were conducted in the series to evaluate alternate wear pad materials and coatings. In two of the tests the knife edge suffered extensive wear (VWR >> 1) when rubbed against a wear pad of copper (TICU03) and a wear pad coated with yttria-stabilized zirconia (TIYZ03). In the other two tests (TIAG02 and TIAG03) the relative wear rates were low (VWR < 0.1) and other test measurements (forces, temperatures, rotational speed) indicated that the aluminum/graphite coating has good abradability in this knife edge rub situation.

Copper was proposed as a candidate seal material (and shows up as an alternate in some HPFP drawings-see Section 4.3) based on the preliminary thermal analyses, which predicted lower rub interface temperatures because of the higher thermal conductivity of copper when compared to aluminum. In spite of this better "heat-sinking" capability, the copper/titanium system

apparently is not compatible in a sliding wear situation. For the test reported here, the disk underwent a substantial diameter reduction (0.076 mm) with some of the disk material being deposited in the wear scar. Also, the wear pad temperatures exceeded 275°C even with the larger thermal conductivity of the copper. (The maximum values could not be measured due to the limited range of the thermocouple amplifier for that test.)

In the test with the YSZ coating, the wear rate of the disk was quite high. Nearly all of the interaction involved reduction in the disk diameter (0.53 mm), leaving a slight build-up of material on the wear pad surface. The rubbing loads caused the disk to cease rotating within about 10 seconds after initiation of the rub. During disassembly of the test components, some material presumably YSZ, was found to be fused to the knife edge (Figure 4-9). Further evidence of the aggressive wear on the knife edge is seen in Figure 4-10 which shows several small cracks at the corner of the knife edge.

Because of the adverse behavior of the copper and YSZ wear surface materials only a single test was undertaken with each. Even though the Al/Si/C wear pad produced a favorable rub situation, there was still some loss of knife edge material in the two tests. At the higher interaction rate the change in disk diameter was only barely perceptible, but examination of the wear pad using SEM/EDX turned up evidence of titanium in the wear scar which had transferred from the knife edge during the rub. The lower interaction rate test produced a measurable diameter change with an estimated VWR of 0.075. The wear rates with the aluminum/graphite coating are comparable to those in which the titanium knife edge was rubbed against the BOM aluminum.

Knife Edge Materials Tests

The tests to evaluate alternate knife edge materials followed the original test plan, incorporating 3 different knife edge treatments, each at two interaction rates for a total of 6 tests. All of the treatments showed VWR < 1 with the minimum VWR, or pickup, occurring at the higher interaction rate for each material. The wear rate for each of these alternates is comparable to the untreated titanium disk when rubbed against aluminum at the high interaction rate. The nitrided titanium disk showed the lowest overall wear of the three alternate materials tested, and had even lower wear than the BOM titanium.

Even though the two abrasive knife edge coatings (alumina/titania and tungsten/carbide) had favorable wear in the tests at high interaction rate, there is evidence of cracking of the coatings (see Figure 4-11) near the outer edge of the disk. These cracks were probably raised by combinations of thermal and mechanical stresses during the rub interaction tests. The presence of cracks calls into question the long-term structural integrity of knife edge coatings in this application.

These tests showed the same cyclic behavior of pad temperatures and rub forces at the lower interaction rate as described earlier for the Baseline tests. At the higher interaction rate, the pad temperatures increased monotonically throughout the interaction period reaching a maximum value at the end of interaction. The maximum temperatures were higher than the peak temperatures measured for the same material at the lower interaction rate.

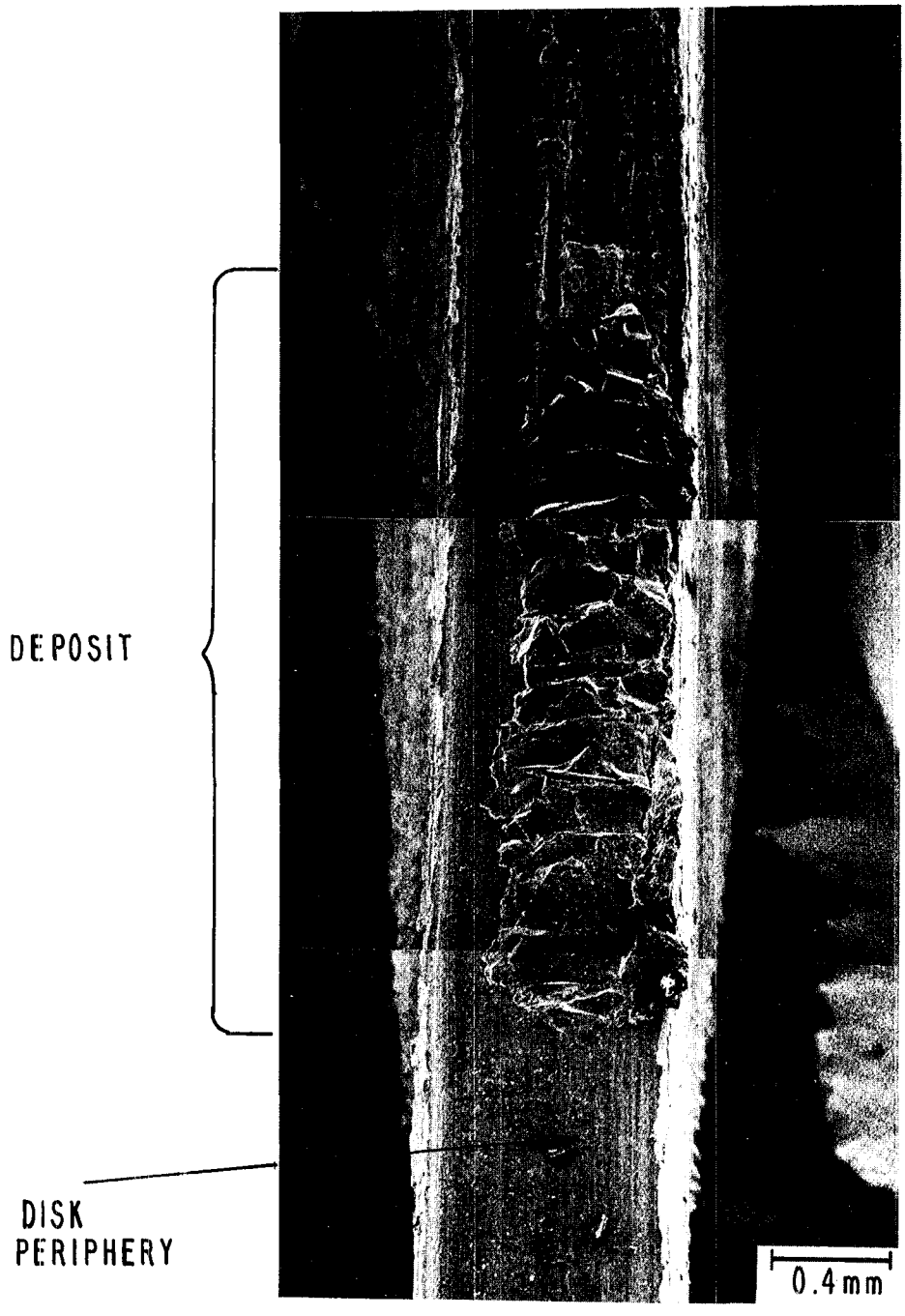

FIGURE 4-9. PHOTOGRAPH OF PERIPHERY OF DISK SHOWING DEPOSIT OF YSZ (TEST TIYZ03)

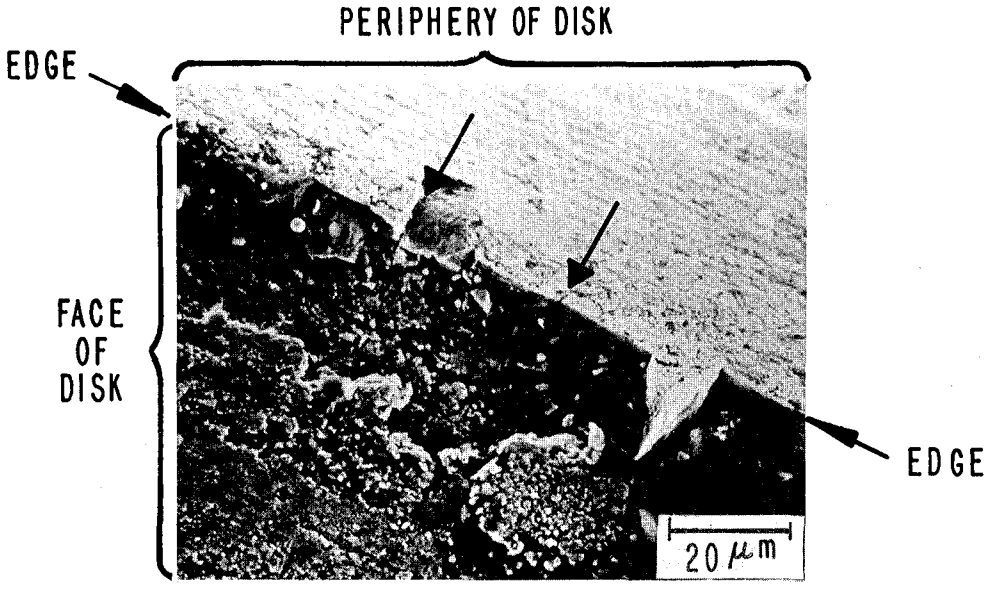

FIGURE 4-10. SEM MICROGRAPH OF KNIFE EDGE TEST TIYZ03

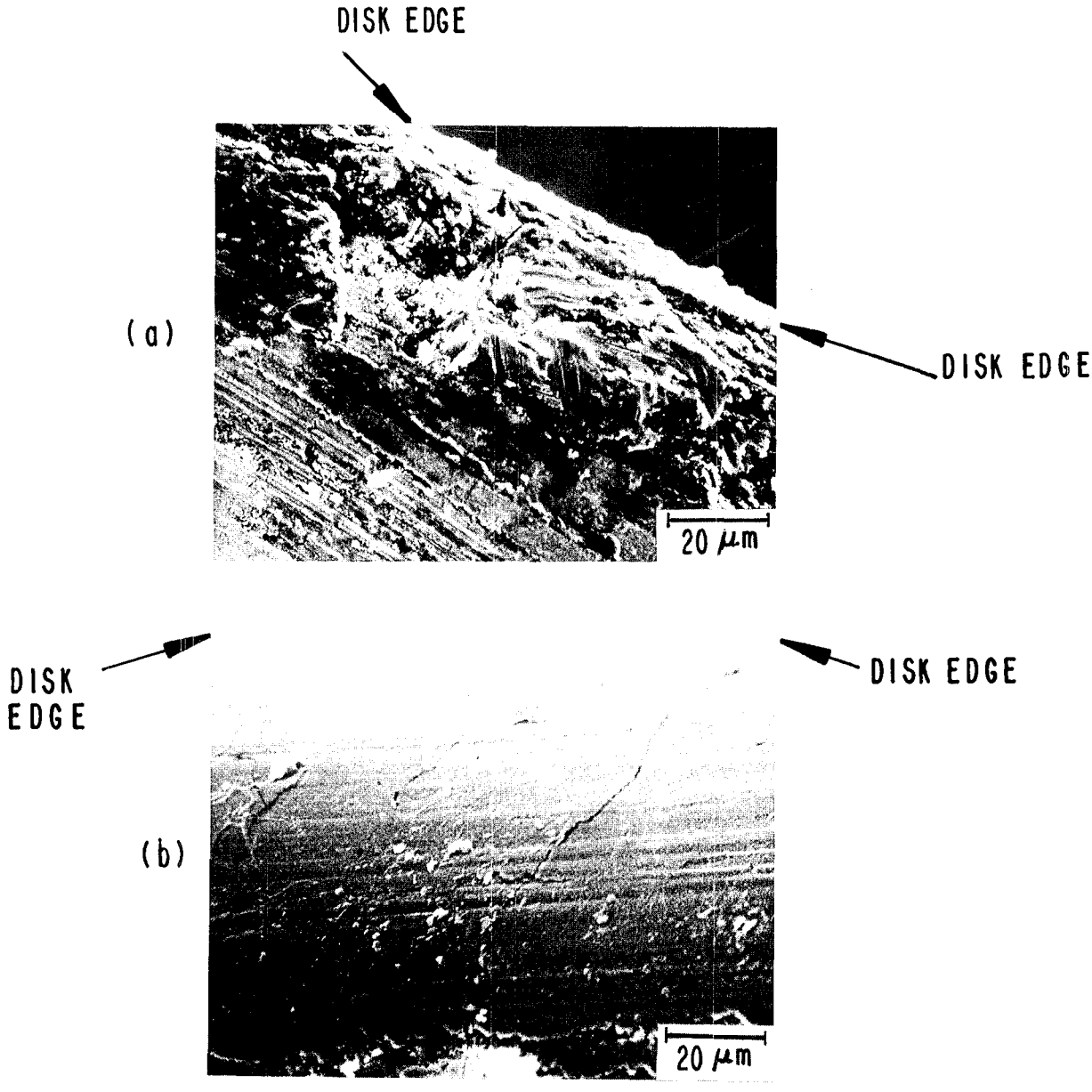

(a) TUNGSTEN CARBIDE COATING - TEST TCAL02

(b) ALUMINA/TITANIA COATING - TEST AOAL02

FIGURE 4-11. SEM MICROGRAPHS OF ABRASIVE COATINGS ON KNIFE EDGE DISKS SHOWING CRACKS

4.6.2 Strip Chart Records

Time-dependent data from the rub interaction tests were recorded by the Creare data acquisition computer as described in Section 4.2.2. Following each test, these data were plotted in the form of "strip charts", i.e. plots of measured parameter as a function of time, for the duration of the rub interval. Some of the general observations from these records were discussed in Section 4.6.1. In this section, the results from one test (TIAL03) are presented and described in greater detail, providing a guide to interpretation of these data. Strip charts for all 15 rub interaction tests are available in Appendix D.

Force, speed and displacement data from test TIAL03 are shown in Figure 4-12a, and the temperatures are displayed in Figure 4-12b. All of the test data are plotted in units of volts (measured at the computer) versus time in seconds. (Time = 0 at the start of the computer data sweep.) The strip plots are labeled with a data system channel number and an abbreviated instrument name. Table 4-6 identifies the measurements with their respective data system channels and provides conversion factors from volts to engineering units. Note that the temperature measurements in Figure 4-12b do not have a simple conversion factor due to the non-linear output of the thermocouples, especially at the cryogenic temperature. Instead, the strip plots have been annotated with the pre-rub temperature and the peak temperature observed during the rub.

Both sets of plots are marked with vertical arrows noting the beginning and ending of the rub (12.1 sec and 19.2 sec, respectively). The start of the rub was deduced from the response of the normal force transducer (Channel 100) wherein its signal level rapidly increased above the background "noise" level at the time the wear pad first contacted the rotating knife edge. The end of the rub is clearly marked by the step change in the output of the interaction device position indicator (Channel 103). This step change accompanies the retraction of the hydraulic actuator which allows the wear pad to be pulled away from the disk.

Several features of the data in these plots were common to many of the tests. For example, the force transducer (Channel 100) shows periodic "bursts" of high frequency oscillation over the interval of the rub. The disk speed also has a cyclic behavior--initially decreasing during the early rub time, then stabilizing, followed by another speed decrease during the second period of oscillatory rub forces. Wear pad temperatures (Figure 4-12b) are also cyclic in many of the tests. The temperatures begin to increase shortly after the rub starts, reaching a peak just as the rub forces cease, followed by a period of cooling and then reheating as the rub continues.

This cyclic behavior was described earlier with the suggestion that it may be caused by a process involving thermal softening and material loss due to plastic flow, fracture, or melting, which briefly relieves the interaction forces, allowing the pad to cool down. Another possible explanation for the thermal cycling is a thermoelastic instability in which the interaction between thermal expansion and wear causes non-uniform contact between the knife edge and wear pad, resulting in localized "hot spots" which can move along the line of contact. Thermoelastic instability

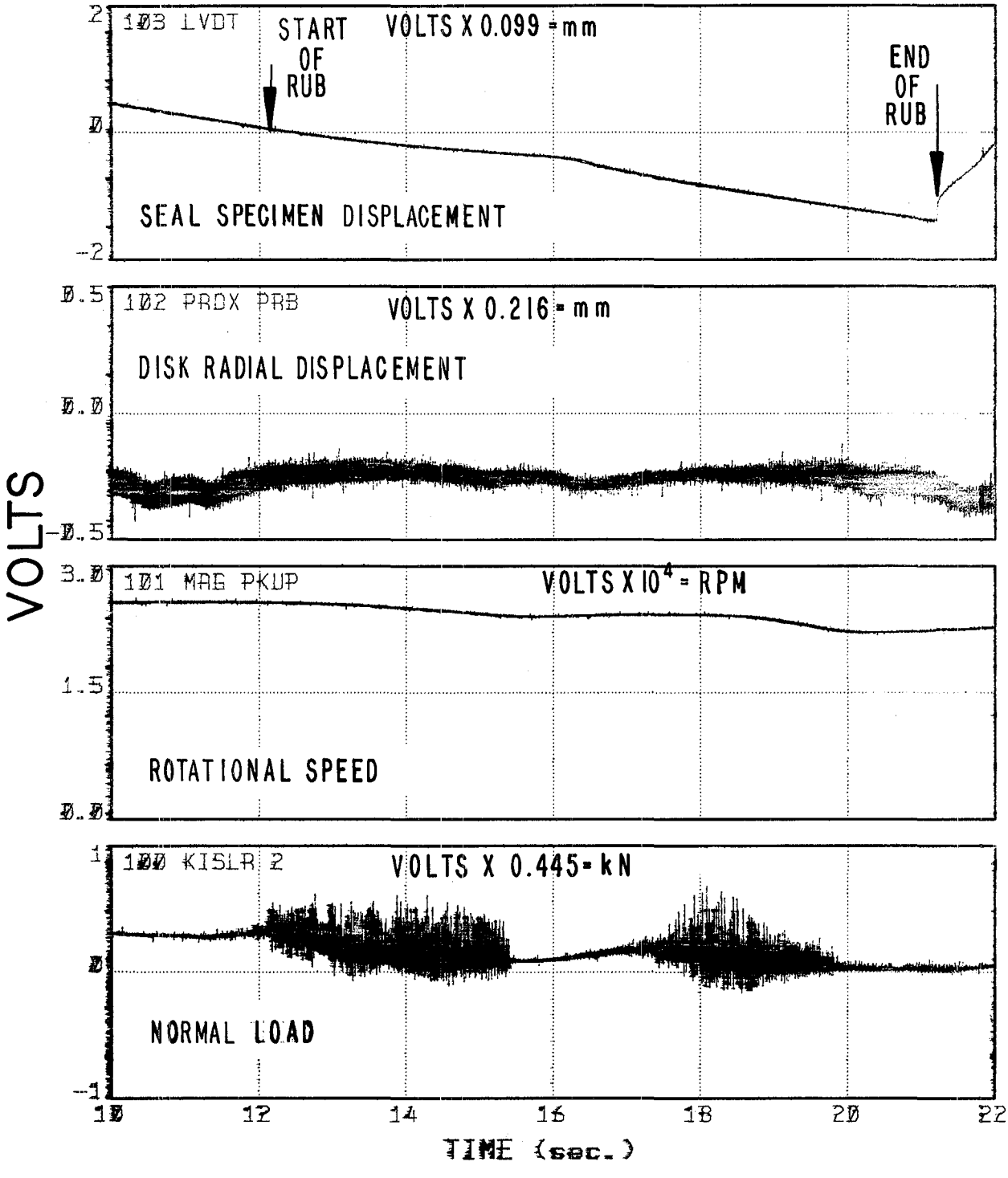

FIGURE 4-12a. STRIP CHART DATA FOR TEST TIAL03

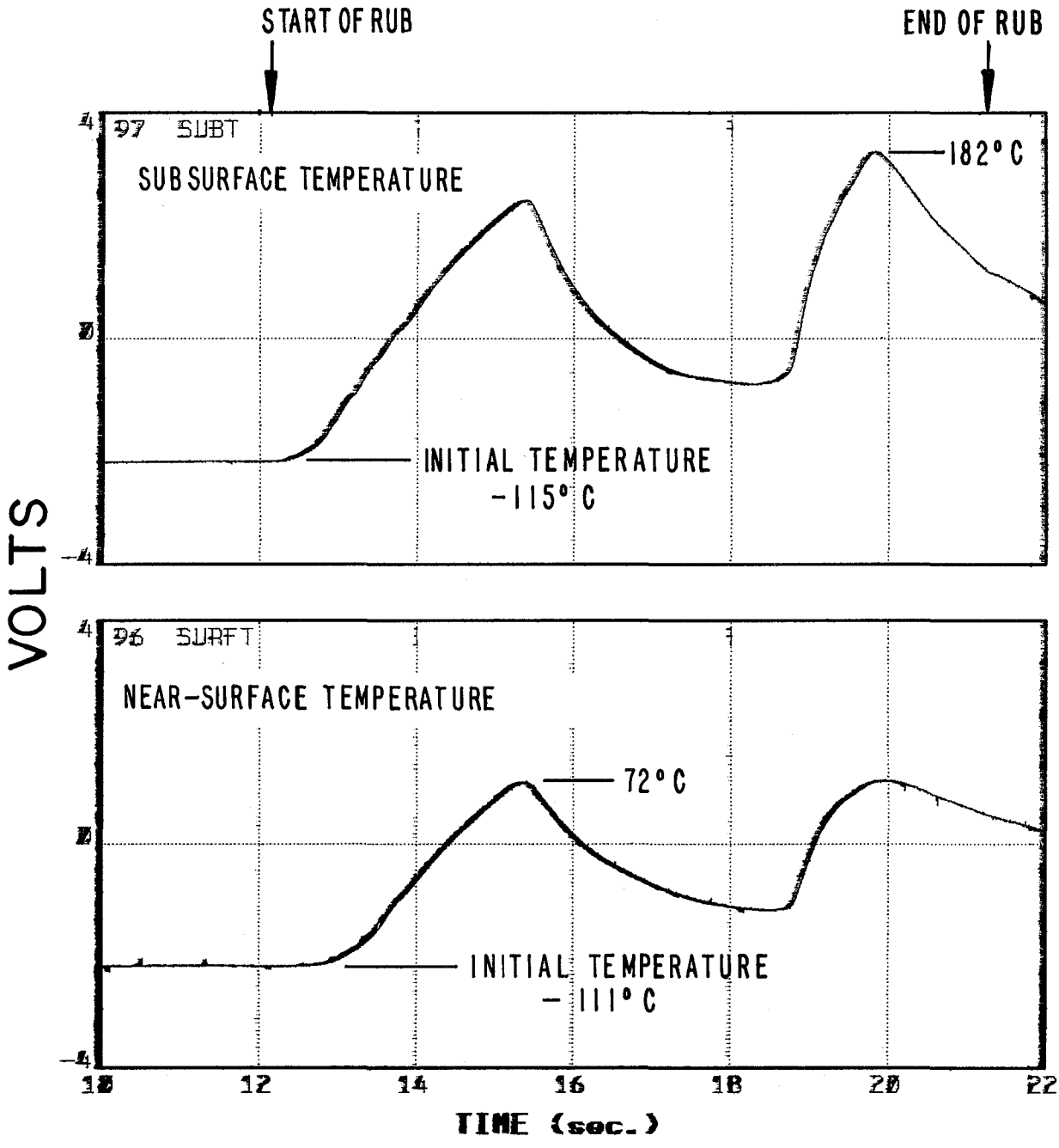

FIGURE 4-12b. STRIP CHART DATA FOR TEST TIAL03

TABLE 4-6 STRIP CHART DATA CHANNEL IDENTIFICATION

Data Channel and Name	Measurement	Conversion to Engineering Units (1)
96 SURFT	Wear pad near-surface temperature	(2)
97 SUBT	Wear pad subsurface temperature	(2)
99 KISLR1	Wear pad tangential force	kN = volts x 0.4448
100 KISLR2	Wear pad normal force	kN = volts x 0.4448
101 MAG PKUP	Disk rotational speed	RPM = volts x 10^4
102 PROX PRB	Disk radial displacement	mm = volts x 0.216
103 LVDT	Seal specimen displacement	mm = volts x 0.099

(1) The conversion factors apply to the voltage scales on the data plots in Figure 4-12 and in Appendix D.

(2) There is no single conversion factor for the temperature scales. The amplifier gain and offset must be accounted for, as well as the non-linear thermocouple outputs in order to convert volts to °C. In order to simplify data interpretation, the initial and peak temperatures for test TIAL03 are noted on Figure 4-12b and on the temperature plots in Appendix D.

has been analytically examined in combination with surface wear for disk brake systems (Reference 15) and the existence of transient temperature patterns has been observed in other experimental investigations involving sliding contact wear (References 16, 17).

In the 5 tests at the high interaction rate (I > 0.1 mm/s), thermal and force cycling were not observed. The strip plots for these tests (Appendix D) show that rub forces (peak-to-peak) remained relatively constant during the incursion period and wear pad temperatures continuously increased until the incursion was ended by retraction of the wear specimen. Apparently in these tests the wear proceeded as a more or less steady process, compared with the tests at lower interaction rates.

4.6.3 Metallurgical Inspection Results

The wear pad and knife edge specimens were inspected following the tests using optical and scanning electron microscopes to locate and document, if any, cracks in the rub surfaces. The SEM was also used to record topographic features of the wear specimens. Energy-dispersive X-ray spectroscopy (EDS) was used in conjunction with the SEM to find evidence of suspected material transfers occurring during the rub interactions.

The specimens from the first interaction test (TIAL03) received close scrutiny, particularly the disk, because of the concern for possible cracking of the titanium knife edges. Reports on the as-found conditions of these specimens clearly describing and illustrating the transfer of aluminum to the knife edge, are included as Appendix E. Although numerous cracks were observed in the transferred material, detailed examination of the disk periphery produced no evidence of cracks in the titanium knife edge itself.

Appendix F contains sets of SEM photomicrographs of the wear specimens from the remaining 14 rub tests. Each set includes several photographs covering a range of magnifications for both the wear pad and knife edge from a single test. The dominant feature seen in the metallurgical examination of the wear specimens was the transfer of materials between the rubbing surfaces. Except for the abrasive coatings discussed in Section 4.6.1, no cracks were observed in the knife edge disks.

4.6.4 Comparison with Other Test Results

Although the test results presented here are the only known published data from rub tests at cryogenic temperatures, most of the materials tested here had previously been studied by other investigators in rub tests at higher temperatures. Most of the results of this study were, in fact, similar to those of earlier, higher temperature tests.

The poor rub performance of copper relative to aluminum in these cryogenic tests was similar to that found in room temperature and 900°F tests of seal specimens against Ti-6Al-4V alloy blade tips (Refs. 3 and 18). As was the case in our cryogenic knife edge tests, the copper rub specimens caused much more blade tip wear than did aluminum rub specimens (Ref. 18). After some of those tests a copper-titanium eutectic was found in the rub zone (Ref. 3); evidence that localized surface temperatures had reached at least 885°C. Although we have been unable to definitely confirm the presence of an eutectic on our copper rub specimen (test TICU03), there was some indication that such melting may have occurred (Figures F-5, Appendix F). In any event, the metallurgical compatability between copper and titanium could have been responsible for the large frictional energy loss and knife edge wear in the rub test of copper.

It might be noted that single-pass abrasion tests, in which a sharp abrader was rubbed once past a rub specimen, showed that copper abraded more easily than aluminum at both room and cryogenic temperatures (Appendix A). The difference between those results and our rub test results can be attributed to the difference in wear mechanism. In a knife edge/rub strip interaction the primary mechanism for wear particle removal is one of plastic deformation due to shear tractions at the rub interface. In a true abrasion situation, as in the single pass tests of Appendix A, chip formation is the primary wear particle removal mechanism. This latter mechanism is less influenced by adhesive interactions than is the former. It appears that copper would fare well as a rub strip material only in cases where it saw chip-forming abrasive interaction with sharp abraders and such interactions would not be expected in labyrinth seals.

The relatively mild rub behavior with the aluminum/graphite composite was similar to results of higher temperature tests by other investigators. It was shown in Reference 4 that plasma-sprayed aluminum graphite rub strips yielded considerable reductions in normal and friction forces compared with aluminum rub strips in knife edge tests at room temperature. The beneficial presence of graphite in the aluminum silicon graphite material may have facilitated near-surface deformation during a rub and, therefore, made wear particle removal easier. Some wear of the titanium knife edge still occurs however (Ref. 4).

The yttria-stabilized zirconia material used in test TIYZ03 is similar to that developed for use in the high temperature environment seen by high pressure turbine gas path seals (Ref. 6). Although they have better rub behavior than most other materials at those high temperatures, their room temperature abradability is known to be worse than that of low shear strength metals or porous metals (Ref. 2). Our tests show that their cryogenic temperature abradability is also relatively poor.

Room temperature tests of abrasive coatings for seal applications have shown that alumina and tungsten carbide coatings can result in small reductions in rub surface temperatures and rub forces over those obtained with uncoated rotors (Ref. 7). Such was also the case in our cryogenic tests. It was also noted by others (Ref. 7) that cyclic or intermittent rub behavior occurs with some of the coated disks, similar to that observed in many of our tests with coated knife edges. One potential difficulty with abrasive treatments is that they lose their effectiveness with time. As we found in our tests, transfer of rub strip material can load up the coating, much as happens with grinding wheels (Ref. 8), and that the sharp abrasive grits (of the alumina coatings) can be worn with time, making them less effective as abraders.

Implantation of nitrogen ions has proven to be effective in reducing the wear of a variety of metallic surfaces (Ref. 13). In our tests it appeared to reduce knife edge wear quite effectively. There is some question about long term benefits, though, because of the very thin implanted layer (Appendix C-2) and the tendency of some aluminum transfer to occur. These questions could best be addressed by further rub tests, perhaps using other rub strip materials, such as aluminum-silicon-graphite, against ion nitrided disks.

5 CONCLUSIONS AND RECOMMENDATIONS

This project has produced several important results in connection with the observed cracking of labyrinth seal knife edges in the liquid hydrogen turbopump and has identified a material which might be a candidate coating for the wear ring seal surface for improved wear performance.

Major conclusions drawn from analysis of the finite element modeling and from the results of the experimental phases are:

1. An aluminum/silicon/graphite wear surface coating exhibited the most favorable behavior in the rub interaction tests and should be considered as a possible alternate material for this application.

2. Nitrogen ion implantation of the titanium knife edge improved the wear performance when rubbed against an aluminum seal.

3. Finite element modeling of the heat conduction in the mating labyrinth finger and wear ring coupled with realistic heat input assumptions or with interactive models of the wear process can be useful to help screen materials for wear surface applications.

4. Cracking of the titanium knife edge is possible in a situation involving multiple thermal cycles between an elevated temperature and the temperature of a cryogenic fluid.

5. Rub interaction tests over a broad range of interaction rates did not produce cracking in the titanium knife edge, although cracks were observed in the layer of aluminum transferred to the knife edge.

6. The cryogenic rub test results were similar in most respects to those compiled by other investigators in rub tests at higher temperatures for the various test materials.

Several recommendations can be made for additional work in this area to apply the results for improving labyrinth seal wear behavior.

1. Thermal analysis methods should be used to screen candidate wear surface materials prior to their first use in seal systems.

2. Presently available data from different wear situations--geometries, speeds, environmental conditions, incursion rates--should be correlated with existing wear models or should be used to improve models in order to provide appropriate inputs to the thermal analysis.

3. Additional rub interaction testing of the ion-nitrided knife edge and the aluminum/graphite wear coating should be undertaken with an expanded range of application parameters. Tests might be run with these two materials in combination, or with either one in combination with other seal materials. Other tests might be run in which the concentration of ions is broadened relative to the distribution in the specimens tested here (Appendix C). These tests are expected to provide data to design an improved labyrinth seal for the HPFP.

6 REFERENCES

1. NASA; SPACE SHUTTLE MAIN ENGINE (SSME) LIQUID HYDROGEN TURBOPUMP IMPELLER SEAL PROGRAM; RFP3-365665, NASA Lewis Research Center, June 29, 1981.

2. Ludwig, L.P. and Bill, R.C.; GAS PATH SEALING IN TURBINE ENGINES; ASLE Trans., Vol. 23, Jan. 1980, pp. 12-22.

3. Schell, J.D. and Schwab, R.C.; PROGRAM TO DEVELOP SPRAYED, PLASTICALLY DEFORMABLE COMPRESSOR SHROUD SEAL MATERIALS; NASA CR-165237, General Electric Co., Jan. 1980.

4. Bill, R.C. and Wisander, D.W.; FRICTION AND WEAR OF SEVERAL COMPRESSOR GAS-PATH SEAL MATERIALS; NASA TP-1128, Jan. 1978.

5. Bill, R.C. and Shiembob, L.T.; FRICTION AND WEAR OF SINTERED FIBERMETAL ABRADABLE SEAL MATERIALS; J. Lubrication Tech., Trans. ASME, Vol. 99, 1977, pp. 421-427.

6. Shiembob, L.T., Stewart, O.L., and Bill, R.C.; DEVELOPMENT OF SPRAYED CERAMIC SEAL SYSTEM FOR TURBINE GAS PATH SEALING; J. Engrg. for Power, Trans. ASME, Vol. 101, Oct. 1979, pp. 549-555.

7. Vogan, J.W. and Stetson, A.R.; APPLICATION OF ABRASIVE COATINGS TO CLEARANCE CONTROL IN THE GAS TURBINE; J. Engrg. for Power, Trans. ASME, Vol. 102, 1980, pp. 113-119.

8. Hermanek, F.J., Jr.; COATINGS LENGTHEN JET ENGINE LIFE; Source Book on Wear Control Technology, Metals Park, OH: ASM, 1978, pp. 368-370.

9. Lockheed-Huntsville Res. & Engrg. Center; HPFTP FIRST STAGE IMPELLER AND PUMP BEARING FLOW ANALYSIS; LMSC-HREC TR D697954, Section 3.

10. Marscher, W.D.; A PHENOMENOLOGICAL MODEL OF ABRADABLE WEAR IN HIGH PERFORMANCE TURBOMACHINERY; Wear, Vol. 59, 1980, pp. 191-211.

11. Williams, D.N. and Wood, R.A.; INVESTIGATION OF THE REACTION OF 5Al-2.5Sn TITANIUM WITH HYDROGEN AT SUBZERO TEMPERATURE; NASA CR-128496, May 15, 1972.

12. Manson, S.S.; FATIGUE: A COMPLEX SUBJECT - SOME SIMPLE APPROXIMATIONS; Experimental Mechanics, 5(7), 1965, pp. 193-226.

13. Dearnaley, G.; THE ION IMPLANTATION OF METALS AND ENGINEERING MATERIALS; Trans. Inst. Metal Finish, Vol. 56, 1978, pp. 25-31.

14. Mozolic, J.A., Engineering Products Div., Union Carbide Corp.; Letter to F. Dolan, Creare R&D Inc., [INFORMATION ON UNION CARBIDE COATINGS LW-1n20 AND LW-15]; Sept. 8, 1982.

15. Kennedy, F.E. and Ling, F.F.; A THERMAL, THERMOELASTIC AND WEAR SIMULATION OF A HIGH ENERGY SLIDING CONTACT PROBLEM; J. Lubrication Tech., Trans. ASME, Vol. 96, 1974, pp. 457-508.

16. Santini, J.J. and Kennedy, F.E.; AN EXPERIMENTAL INVESTIGATION OF SURFACE TEMPERATURES AND WEAR IN DISK BRAKES; ASLE Preprint No. 74-LC-IB-3, ASME/ASLE Lubrication Conf., Oct. 1974.

17. Dow, T.A. and Stockwell, R.D.; EXPERIMENTAL VERIFICATION OF THERMOELASTIC INSTABILITIES IN SLIDING CONTACT; ASME Paper No. 76-Lub-21, ASME Joint Lubrication Conf., Oct. 1976.

18. Bill, R.C. and Ludwig, L.P.; WEAR OF SEAL MATERIALS USED IN AIRCRAFT PROPULSION SYSTEMS; Wear, Vol. 59, 1980, pp. 165-189.

This Page Intentionally Left Blank

APPENDIX A

THERMAL ANALYSIS OF SEAL RUBS AND RESULTS OF LOW SPEED AND SINGLE-PASS RUBBING TESTS

by

Francis E. Kennedy

APPENDIX A
THERMAL ANALYSIS OF SEAL RUBS AND RESULTS OF LOW SPEED AND SINGLE-PASS RUBBING TESTS

ABSTRACT

This report describes the results of analysis and testing carried out at Thayer School of Engineering, Dartmouth College, in support of the effort at Creare R&D Inc. to evaluate the wear processes in labyrinth seals in the high pressure fuel pumps of the Space Shuttle main engines.

A.1 THERMAL ANALYSIS OF SEAL RUBS

An analysis was conducted of temperatures in the components of the labyrinth seal in the second stage impeller of the NASA space shuttle fuel pump. The analysis modeled the second finger of that labyrinth seal and used Dartmouth's THERMAP (Reference A-1) finite element thermal analysis program. The geometry for the model was based on engineering drawings of the seal provided by Creare.

Two seal rub cases were studied: a 360° rub and a 30° rub (see Appendix B for discussion of contact angle). For both cases the rotor including knife edge was assumed to be made of titanium alloy with 5% aluminum and 2½% tin. Two shroud materials were investigated for each case, the baseline 2024-T4 aluminum alloy, and a possible substitute, nearly pure copper. Temperature-dependent thermal properties for each of the materials were obtained from Creare.

Finite element meshes for the two cases were created and are shown in Figures A-1 and A-2. For the 360° rub case an axisymmetric model was chosen (Figure A-1). A modified two-dimensional model (Figure A-2) was used for the 30° case. Although the equations for that model were the two-dimensional heat conduction equations, the various elements were given thicknesses which depended on their location. If a cross-section of those elements could be shown, it would look like the cross-section in Figure A-1.

Boundary conditions for the analyses were based on information given by Reference 9 and by Creare personnel. The inside diameter of the rotor and the outside diameter of the shroud (3.17 in. radius and 3.767 in. radius respectively) were assumed to be held constant at -400°F. It was assumed that all of the free surfaces - the free edges in the 360° model in Figure A-1 and all the element faces (areas) in the 30° model in Figure A-2 - were transferring heat by convection to liquid hydrogen at -375°F. The convection coefficient was estimated, based on known fluid velocities and properties, to be approximately 0.004 BTU/in^{2}sec°F. Since Creare personnel had determined a convection coefficient of 0.04 BTU/in^{2}sec °F for the same surfaces, it was decided to try a variety of convection coefficients in order to investigate the influence of that parameter on the results.

Heat flux was assumed to be input to the model uniformly along the contact interface. The magnitude of the heat flux, and of the total rate of frictional heat generation, is not really known. The total heat generation rate is:

$$Q = F_f \times V \qquad \text{(A1)}$$

where F_f is the friction force and
V is the rub velocity

It is known that V = 1135 feet per second at operating conditions. The friction force, F_f can be estimated using the results of our room temperature, slow speed rub tests (see Section A.2). This would give, for the 360° rub case, 72 lbf at an interaction rate of 10^{-4} in/sec and 720 lbf at the rate of 10^{-3} in/sec. These values are quite likely high, however, especially the 10^{-3} in/sec number. A quick analysis shows that if no material were removed at all during a 360° incursion, resulting in a shrink fit situation, the maximum friction force would be only 200 lbf with a friction coefficient of 0.2. The force should be lower if material has been removed by wear. Because of the uncertainty in this heat flux value, a range of heat flux values were investigated for the 360° rub case.

It should be noted that the heat conduction equations are different in the two cases, 360° and 30°. In the 30° case, one of the bodies is moving in its plane relative to the source of heat. This requires a solution of the heat conduction equation including a convective diffusion term for that body. In the 360° case, both bodies can be considered stationary relative to the heat source, so that the convective diffusion term is zero.

A.1.1 Results for 360° Rub Case

For any heat flux at the contact interface, the maximum temperature occurs in the middle of the contact surface. If the heat flux was constant throughout the rub (i.e. a constant incursion rate yielding a constant wear rate yielding a constant friction force), the temperatures were found to reach their steady state value < 2 seconds after the beginning of a 30 second rub. Thus, a transient analysis of the temperature distribution is unnecessary since the steady state analysis accurately predicts the maximum temperature values.

The magnitude of the maximum surface temperature is approximately proportional to the heat flux as can be seen in Table A-1. The range of heat flux values in Table A-1 covers the range of friction forces which may occur in a rub. For example, a flux of 1,000 BTU/in^2 corresponds to a friction force of 450 lbf, while 125 BTU/in^2 corresponds to 56 lbf. It can be seen from the results that some melting of the aluminum surface can be expected for most of these rub conditions. An accurate analysis of surface temperature does require, however, a good knowledge of actual rub forces; a parameter which remains unknown. The influence of convection coefficient on the maximum surface temperature is shown in Table A-2. It can be seen that the better the convective cooling (higher h) the lower the surface temperature. There is a substantial difference between the temperature predictions at h = 0.004 and h = 0.04, the range of values of h determined for this configuration.

A.1.2 30° Rub Case

Solutions for the 30°rub case were less satisfactory than those for the 360° case. Two problems were encountered:

1. the rub velocity was so high, and the resulting Peclet number was so high, that numerical instabilities resulted in the solution of the finite element equations (convective diffusion).

2. The number of nodes was large, necessitating large computer storage requirements, therefore limiting the number of runs.

The temperatures predicted for this case were approximately 55% higher than those predicted for the 360° case under similar conditions (same heat flux, same velocity, same boundary conditions). There is some question about the validity of that number, however, because of some numerical oscillations which appeared in all results for the 30° case due to the high Peclet number.

A.1.3 Influence of Material

Analysis of both 30° and 360° cases were done in which the shroud material was copper instead of aluminum. Properties of a nearly pure, wrought copper alloy were used in the analysis. Results of the analysis showed that the maximum surface temperatures with the copper shroud are approximately 60% less than those with the aluminum alloy shroud. This 60% value was true of both 360° and 30° cases, and is primarily due to the 50% or more difference in thermal conductivity between copper and aluminum 2024.

A.2 KNIFE EDGE RUB TESTS

Tests were run on three specimens of 2024-T4 aluminum on a knife edge rub tester. Flat specimens, approximately 2.5 cm x 2.5 cm x 1 cm, were rubbed against the outer diameter of a thin rotating disk (knife edge) of 6.25 inch diameter. Two different disk materials were used, 304 stainless steel and Ti-5Al-2.5Sn. All tests were run in air at a constant applied normal force of 5 lb_f and a constant rotor speed. Measurements were made of friction force and incursion during the tests, which had durations ranging from 10 to 60 seconds. The test configuration is shown in Figure A-3.

Test results are given in Table A-3, for the stainless steel disk tests and in Table A-4 for tests with the titanium knife edge. It can be seen that the tests with the stainless steel rotor showed that an incursion rate of 10^{-4} sec required a friction force of about 1.5 lb_f. Friction forces with the titanium disk were slightly larger, while incursion rates were slightly smaller. The friction force values with the titanium disk should be used with caution, however, since the force calibration for those tests may be in error. It was found that higher rub speeds resulted in slightly lower friction forces, probably because of frictional heating effects. Sparking was noted in all tests with the titanium rotor and in

longer and/or higher speed tests with the stainless steel rotor. Surface temperatures in those tests must have, therefore, been close to the melting temperatures of the materials.

A.3 INCURSION RATE - RUB FORCE RELATION

The rub tests (aluminum flat vs stainless steel rotor) showed that an incursion rate of 10^{-4} in/sec resulted in a friction force of about 1.5 lb_f. Use of the incursion-contact angle analysis program (see Appendix B) showed that the contact angle on these tests was approximately 5° at the end of a 30 second test and that the wear rate of the aluminum was approximately 1.35×10^{-6} in^3/sec.

If it is assumed that wear rate is proportional to the friction force for this material combination (a valid assumption under certain conditions for many materials); then for an incursion rate of 10^{-4} in/sec, the friction force-to-wear rate ratio is about 1.1×10^{6} lb_f/in^3/sec. A 360° rub in the NASA seal for this combination would have a wear rate of:

$$\dot{V} = 2\pi r w \dot{I} = 2\pi(3.5)(0.03)(10^{-4}) = 6.6 \times 10^{-5} \text{ in}^3/\text{sec} \qquad \text{(A2)}$$

This would require a rub force of about 72 lb_f. A 30° rub at the same incursion rate would have a volume wear rate of 5.43×10^{-6} in^3/sec (from the incursion rate-angle program) and this would require a friction force of about 6 lb_f (at an incursion rate of 10^{-4} in/sec).

Following the same line of reasoning, it would appear that an incursion rate of 10^{-3} in/sec (10 times the above value) would require wear rates of 10 times the above value in order to remove the required amount of material. This would result in friction force requirements 10 times larger than the above values for the same rub angle, assuming the rub force-to-wear rate relation remains valid. This assumption is probably faulty, however, since our rub tests show that different rub conditions seem to have different rub force requirements. Insufficient data are available to determine the influence of various rub parameters (velocity, incursion rate, materials) on the rub force-to-wear rate relationship.

A.4 SINGLE PASS RUB TESTS

A series of abradability tests was run on a pendulum type single pass test apparatus recently built in the Thayer School laboratory (Reference A-2). The apparatus has a hard triangular abrader (a carbide cutting tool insert) attached to the end of a swinging pendulum, with a specimen to be abraded being fixed to the stationary bed of the tester. A given incursion (or interference) is set between abrader and specimen before the pendulum is released. Energy lost during a single abrasion event is monitored and weight loss measurements are made to determine wear. The temperature of the test material can be varied over a range of -196°C (liquid nitrogen) to +500°C. This type of test had previously been shown to give a good measure of a material's abradability in tests of a wide variety of materials. For these tests, a constant incursion of 0.1 mm was set. Two different materials were tested, 2024 T4 aluminum, and a free machining copper (99.5%

copper, 0.5% tellurium). Tests were run on both materials at -196°C and 21°C. Test results are shown in Table A-5. Each of the results is the average of 7 to 10 tests run at each condition during July 1982.

Past work with the test device has shown that the specific energy (energy loss per unit mass of material removed) is a good measure of abradability. Here it can be seen that each material is more abradable at room temperature than at cryogenic temperatures. This is probably related to the increased resistance to plastic deformation at low temperatures. Thus, rub tests performed at room temperature (or higher) do not necessarily give an accurate prediction of rub behavior at cyrogenic temperatures.

It can also be seen from the results in Table A-5 that the copper material is more abradable than the aluminum alloy at both room and cryogenic temperatures. This conclusion holds even when translating the specific energy values from energy per unit mass to energy per unit volume (using the densities of the two materials).

TABLE A-1 INFLUENCE OF HEAT FLUX ON SURFACE TEMPERATURE FOR 360° CONTACT

Heat Flux[1] (BTU/in²-sec)	T_{max} (°F)	Comments
1000[2]	7923	$T > T_{melt}$ to 0.1 inch deep in aluminum
500	3927	$T > T_{melt}$ to 0.04 inch deep in aluminum
250	1993	$T > T_{melt}$ to 0.012 inch deep in aluminum
125	981	$T < T_{melt}$ everywhere

[1] Heat Flux = Contact Pressure x Rub Velocity

[2] For 360° contact, 1000 BTU/in²-sec corresponds to a rub force of 452 lb_f acting on an area of 0.66 in² (Area = π x 7 inch x 0.03 inch) and at a rub velocity of 1135 ft/s.

TABLE A-2 INFLUENCE OF THERMAL CONVECTION COEFFICIENT ON SURFACE TEMPERATURE FOR 360° RUB (1)

Convection Coefficient (BTU/in^2-sec-°F)	T_{max} (2) (°F)
4.0	2417
0.4	2784
0.04	3927
0.004	7551
0	13829

(1) Heat Flux = 500 BTU/in^2-sec

(2) Properties of the rub materials above their melt temperatures were assumed to be the same as at slightly below T_{melt}. No change of phase was considered.

TABLE A-3 RESULTS OF INCURSION TESTS - FLAT SPECIMEN VS ROTATING STAINLESS STEEL KNIFE EDGE

- 2024-T4 aluminum specimen
- 304 stainless steel knife edge disk, 6.25 inch diameter x 0.05 inch thick
- 5 lb_f normal load
- Room temperature

Test No.	Duration (sec)	Rotational Speed (rpm)	Friction Force (lb_f)	Incursion Rate (10^{-4} inch/sec)
1	10	1000	1.5	-
2	10	975	1.2	-
3	60	1025	1.5 to 1.2	0.5
4	60	1000	1.25	0.375 to 0.875
5	30	1850	0.86 to 1.2	0.35 to 1.65
6	15	910	1.45	1
7	15	900	1.6	1.1
8	30	900	1.0 to 1.5	0.4

Notes: At lower speed (900 to 1000 rpm), an incursion rate of 10^{-4} inch/sec required a friction force of $\cong$ 1.5 lb_f.

At higher speed (1850 rpm), an incursion rate of 10^{-4} inch/sec required a friction force of $\cong$ 1 lb_f.

Sparking noticed after 25-30 seconds for tests 3, 4, 5.

TABLE A-4 RESULTS OF INCURSION TESTS - FLAT SPECIMEN VS ROTATING TITANIUM STEEL KNIFE EDGE

- 2024-T4 aluminum specimen
- Titanium 5Al-2.5 Sn knife edge disk, 6.25 inch diameter x 0.05 inch thick
- 5 lb_f normal load
- Room temperature

Test No.	Duration (sec)	Rotational Speed (rpm)	Friction Force[1] (lb_f)	Incursion Rate (10^{-4} inch/sec)
9	20	950	2.1	0.3
10	30	950	1.7 to 2.	0.4
11	30	950	2	0.6

(1) Friction force may be in error due to questionable calibration.

Notes: Sparking of titanium (typical white titanium sparks as in grinding) was noted in all tests.

Rub forces appear to be slightly larger than with stainless steel.

TABLE A-5 RESULTS OF SINGLE-PASS ABRASION TESTS OF COPPER AND ALUMINUM

Material	Test Temperature (°C)	Average Energy Loss (N-m)	Average Wear (mgram)	Average Energy Loss/Wear $(\frac{N-m}{gram})$	$(\frac{N-m}{cm_3})$
Al 2024	-195°C	1.35	1.14	1190	3300
Al 2024	21°C	1.77	3.35	530	1460
Copper	-195°C	2.24	16.3	137	1225
Copper	21°C	1.65	15.0	110	985

Notes: All tests run at a rub velocity of 5 m/s.

All tests run with incursion depth of 0.1 mm (0.004 inch).

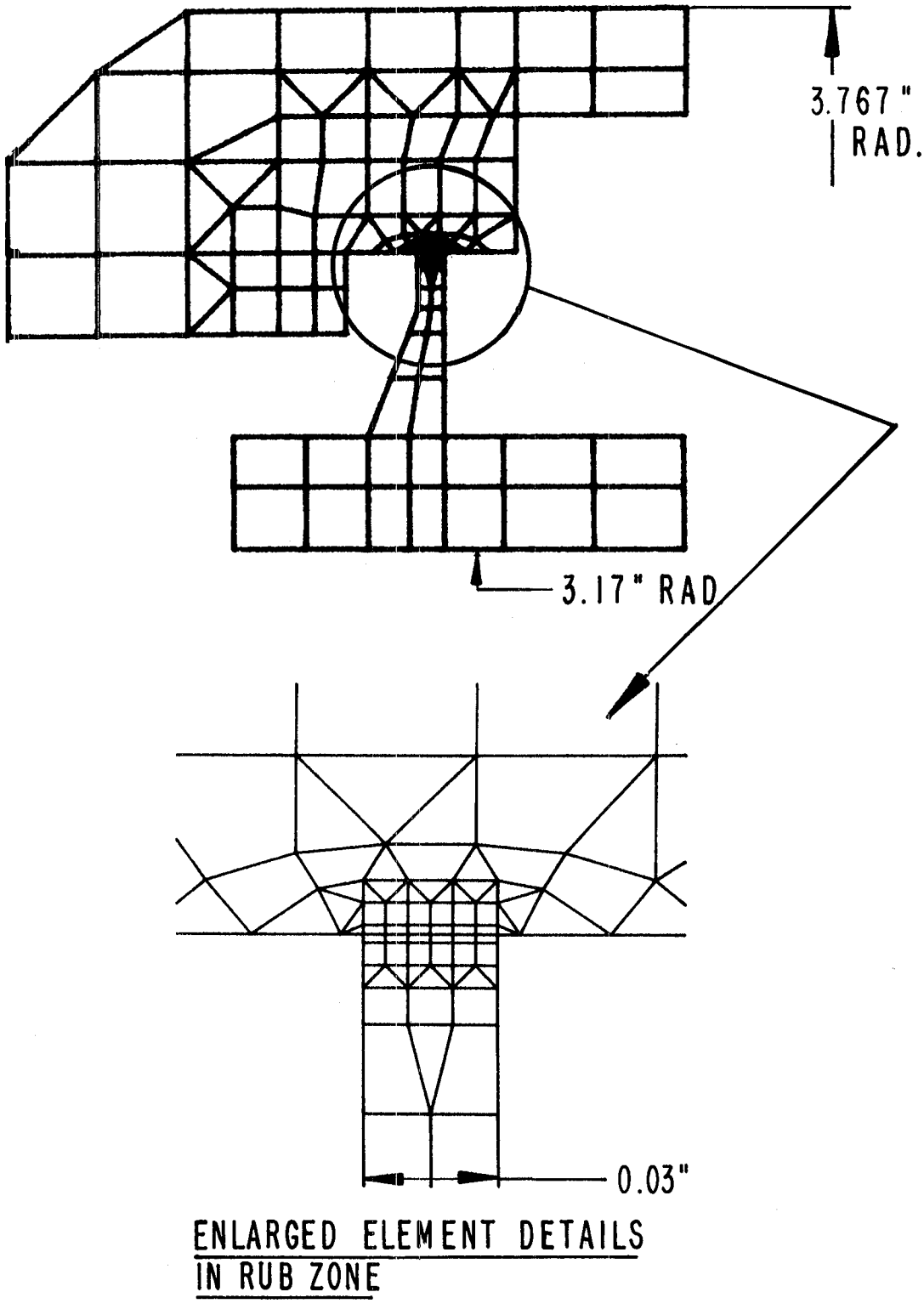

Figure A-1. Finite Element Mesh for 360° Rub Case (158 nodes; 152 elements; axisymmetric)

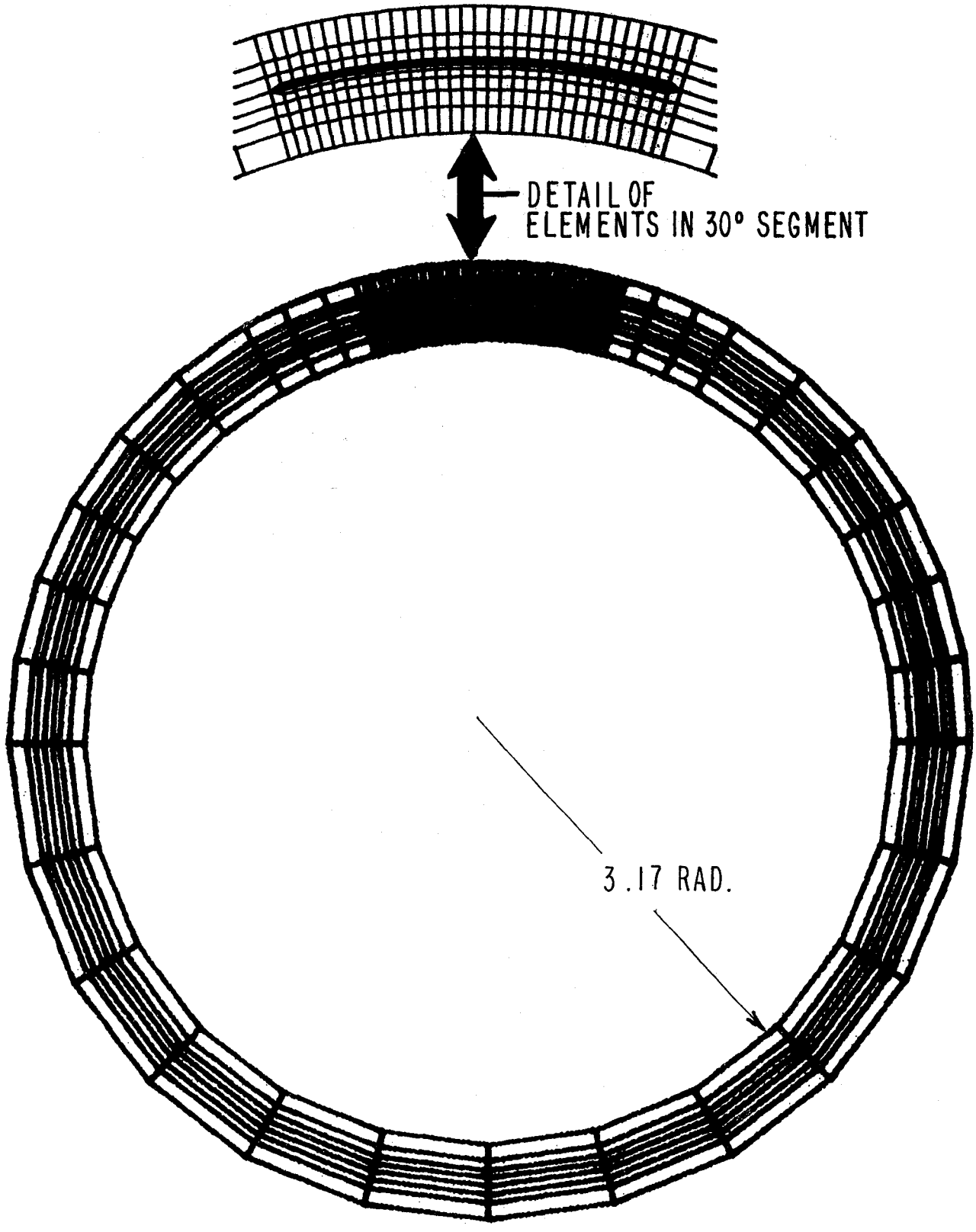

Figure A-2. Finite Element Mesh for 30° Rub Case (651 nodes; 562 elements; modified 2-dimensional)

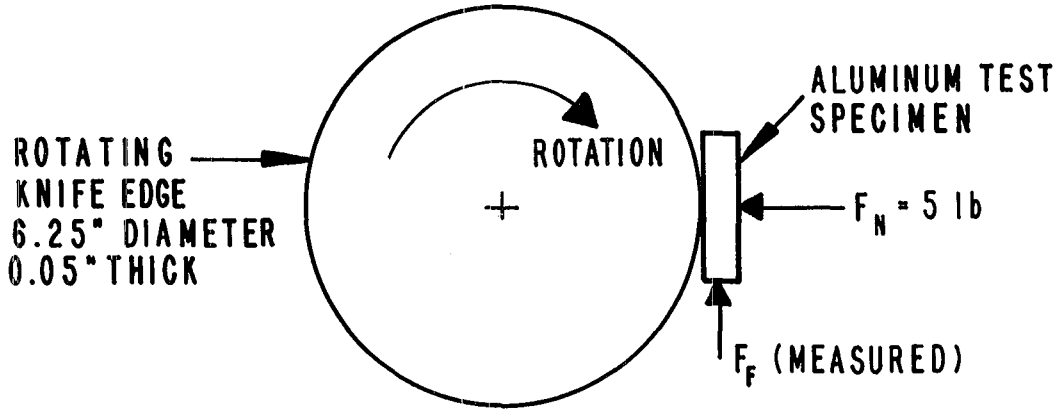

Figure A-3. Low-Speed Knife Edge Test Setup

REFERENCES

A-1. Kennedy, F. E., Jr.; SURFACE TEMPERATURES IN SLIDING SYSTEMS - A FINITE ELEMENT ANALYSIS; ASME Journal of Lubrication Technology, Vol. 103 (1981), pp. 90-96.

A-2. Santini, J. J. and Kennedy, F. E, Jr.; AN EXPERIMENTAL INVESTIGATION OF SURFACE TEMPERATURES AND WEAR IN DISK BRAKES; Lubrication Engineering, Vol. 31, 1975, pp. 402-417.

APPENDIX B

INCURSION CONTACT ANGLE ANALYSIS

APPENDIX B

INCURSION CONTACT ANGLE ANALYSIS

INCURSION-CONTACT ANGLE ANALYSIS

The incursion of a rotating labyrinth finger with the stationary wear ring results in loss of material from both of the seal elements. The extent and rate of this wear are of concern in the analysis of seal designs. For instance, the energy dissipation in the rub will be related to the total volume of material worn away and the relative volume loss (called the volume wear ratio, VWR) between the finger and the wear ring. Also, the area for heat removal in the wear ring is directly related to the length of the arc of contact between the labyrinth finger and the wear ring. Figure B-1 illustrates the geometry of the incursion, and defines nomenclature for the analysis of contact angle θ_1, and VWR.

The contact angle θ_1 was calculated for the labyrinth seal configuration in the HPFP for a case where all the material loss occurs in the wear ring (VWR = 0) and for a case where the wear is equally split between knife edge and wear ring (VWR = 1). Figure B-2 shows that the contact angle rapidly increases with incursion and for a rub depth of 0.25 mm reaches a value of $\sim$ 130°.

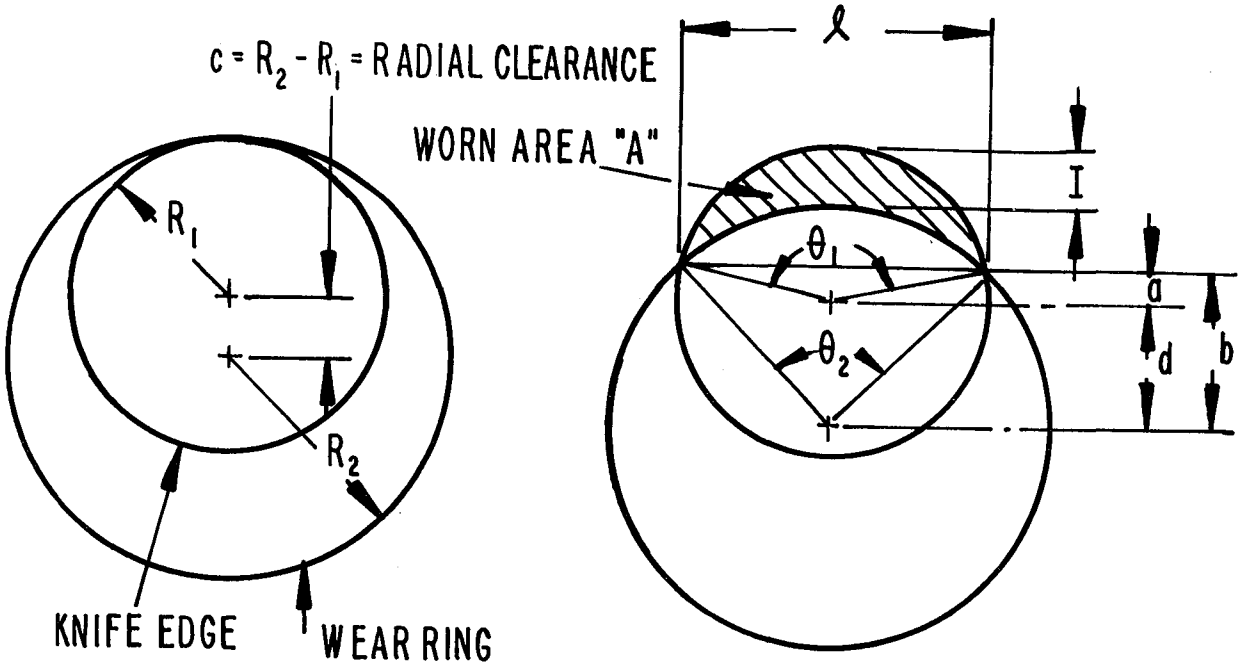

Figure B-1. Geometry and Nomenclature for Rub Interaction

Incursion: $I = d-c$

Worn Area: $A = \frac{1}{2}[R_1^2\theta_1 - R_2^2\theta_2 + \ell(b-a)]$

Worn Volume: $V = Aw$ (w = thickness of knife edge)

Wear Rate: $\frac{dV}{dt} = w\frac{dA}{dt}$

$$\frac{dV}{dt} = 2w\dot{I}\sqrt{R_1^2 - \left[\frac{R_2^2 - R_1^2 - d^2}{2d}\right]^2}$$

($\dot{I}$ = interaction rate)

Contact Angle: $\theta_1 = 2\cos^{-1}\left(\frac{a}{R_1}\right)$

$$= 2\cos^{-1}\left[\frac{R_2^2 - R_1^2 - d^2}{2R_1 d}\right]$$

Volume Wear Ratio: $VWR = \frac{\text{volume removed from knife edge}}{\text{volume removed from wear ring}}$

$$VWR = \frac{2\pi R_1 \Delta R_1}{A}$$

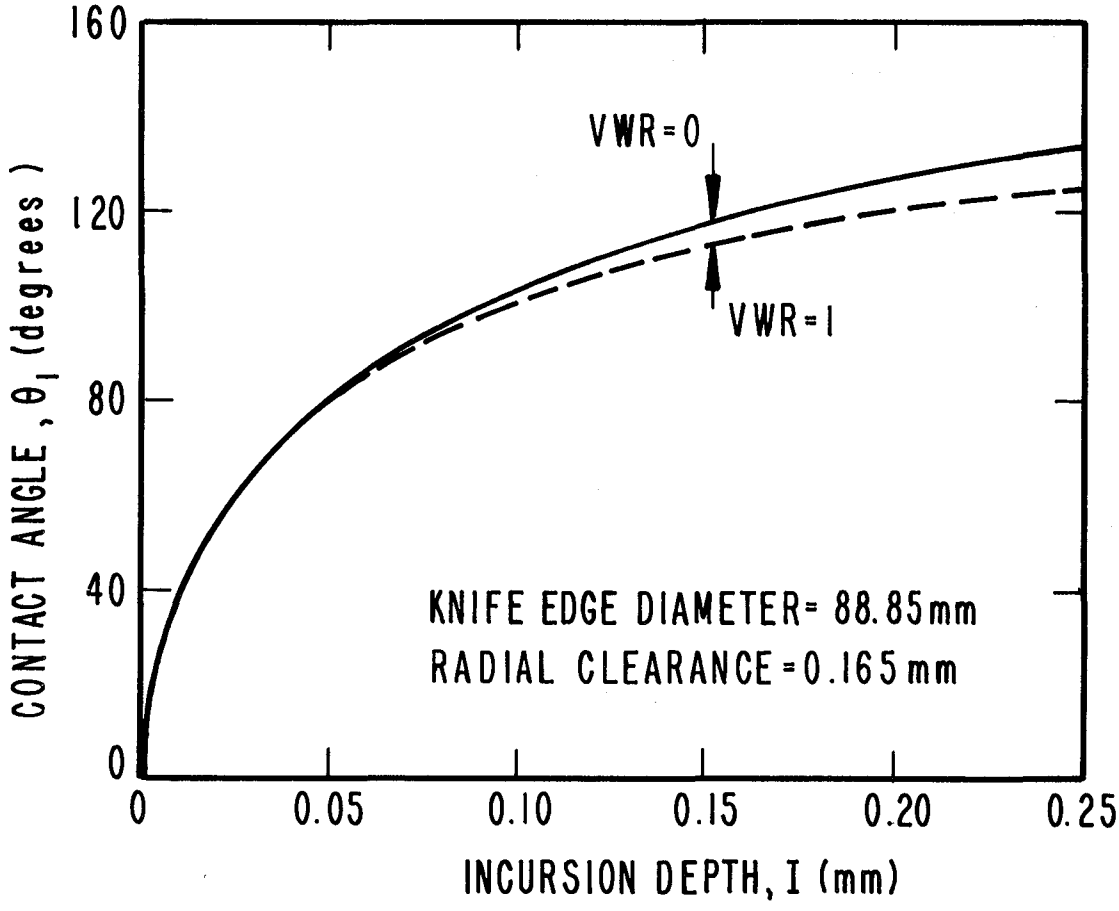

Figure B-2. Incursion Contact Angle

APPENDIX C

CERTIFICATIONS AND SPECIFICATIONS FOR MATERIALS USED IN EXPERIMENTAL INVESTIGATIONS OF LABYRINTH SEAL WEAR

APPENDIX C-1

MATERIALS CERTIFICATION

- Thermal Shock Specimens
- BOM Knife Edge
- BOM Wear Ring

Titanium Metals Corporation of America

CERTIFICATE OF TEST

CHEMICAL ANALYSIS

HEAT NO.	C	Fe	N	Al	Va	Cr	Mo	H	Zr	Sn	Mn	O
CS 04	.026	.36	.010	4.85				.0065		2.4		.14
CS 93	.023	.36	.014	4.93				.0107		2.3		.14

YTTRIUM LESS THAN 10 PPM

BALANCE TITANIUM

MECHANICAL PROPERTIES

HEAT NO.	TEST NO.	SIZE OR GAUGE	YIELD STRENGTH	TENSILE STRENGTH	ELONG.	R. A. %	HARDNESS	BEND TEST
			KSI	KSI	%			BETA TRANS'S
		ANNEALED 2 HRS @ 1500°F AC						
CS 04		CL	114	126	17	47		1855°F
CS 93		CL	120	130	18	41		1835°F

NOTCHED STRESS RUPTURE OK 5 HRS @ 150 PSI

MICROSTRUCTURE & MACROSTRUCTURE EXAMINED AND ACCEPTABLE

IMMERSION ULTRASONICALLY INSPECTED TO A #2 FBH

SURFACE CONTAMINATION FREE

SUBSCRIBED AND SWORN TO BEFORE ME
THIS DATE May 7, 1982

RESULTS AS ABOVE CERTIFIED
TITANIUM METALS CORPORATION OF AMERICA
Susan R. Picard

Material Certification for Titanium Thermal Shock Specimens

Ti 5AL-2.5SN Sheet to AMS 4910D & PWA S 4910-C
P.O. #3359-3307

Titanium Metals Corporation of America

CERTIFICATE OF TEST

CHEMICAL ANALYSIS

HEAT NO.	C	FE	N	AL	VA	CR	MO	H	ZR	SN	MN	O
S2836	.015	.30	.019	5.4				.010		2.4		.15

YTTRIUM LESS THAN 10 PPM

BALANCE TITANIUM

MECHANICAL PROPERTIES

HEAT NO.	TEST NO.	SIZE OR GAUGE	YIELD STRENGTH	TENSILE STRENGTH	ELONG.	R. A. %	HARDNESS	BEND TEST
			KSI	KSI	%			R/T @ 20X
		ANNEALED 2 MIN @ 1500°F AC						
S2836	J0418	L	131	140	17			
		T	131	140	16			4.0
		L	129	139	19			
		T	131	141	16			4.0

SURFACE CONTAMINATION FREE.

SUBSCRIBED AND SWORN TO BEFORE ME

THIS DATE 3/26/82

RESULTS AS ABOVE CERTIFIED
TITANIUM METALS CORPORATION OF AMERICA

Susan R. Picard

Material Certification for Titanium
Knife Edge Disk Specimens

NORTHSTAR Steel & Aluminum Inc.

205 BOUCHARD STREET • P.O. BOX 4886 • MANCHESTER, N. H. 03108

TO

CREARE, INC.
Great Hollow Rd.
P.O. Box 71
Hanover, NH 03755
Attn: Marilyn Lyons

DATE March 11, 1982

CERTIFICATE OF ANALYSIS

YOUR ORDER NO.	OUR INVOICE NO.	DATE SHIPPED	SHIPPED FROM
3286-3307	226-75	3/8	MANCHESTER, N. H.

MATERIAL - SPECIFICATION:

2024T351 Aluminum Bar

1 pc 3" rd x 24" CTL

I hereby certify that the following figures are correct as contained in the records of this corporation.

2024T351 Aluminum Bar

Copper	4.4
Manganese	0.6
Magnesium	1.5

Aluminum and Normal Impurities Constitute Remainder

Very truly yours
NORTHSTAR STEEL AND ALUMINUM, INC.

By Thomas D. Sirois

Material Certification for Aluminum
Wear Ring Specimens

APPENDIX C-2

APPLICATION DATA FOR NITROGEN ION IMPLANTATION TREATMENT OF KNIFE EDGE DISK

(Calculated density profiles at 150 and 200 keV. Actual implant performed at 180 keV at dose of $2X10^{17}$ ions/cm^2.)

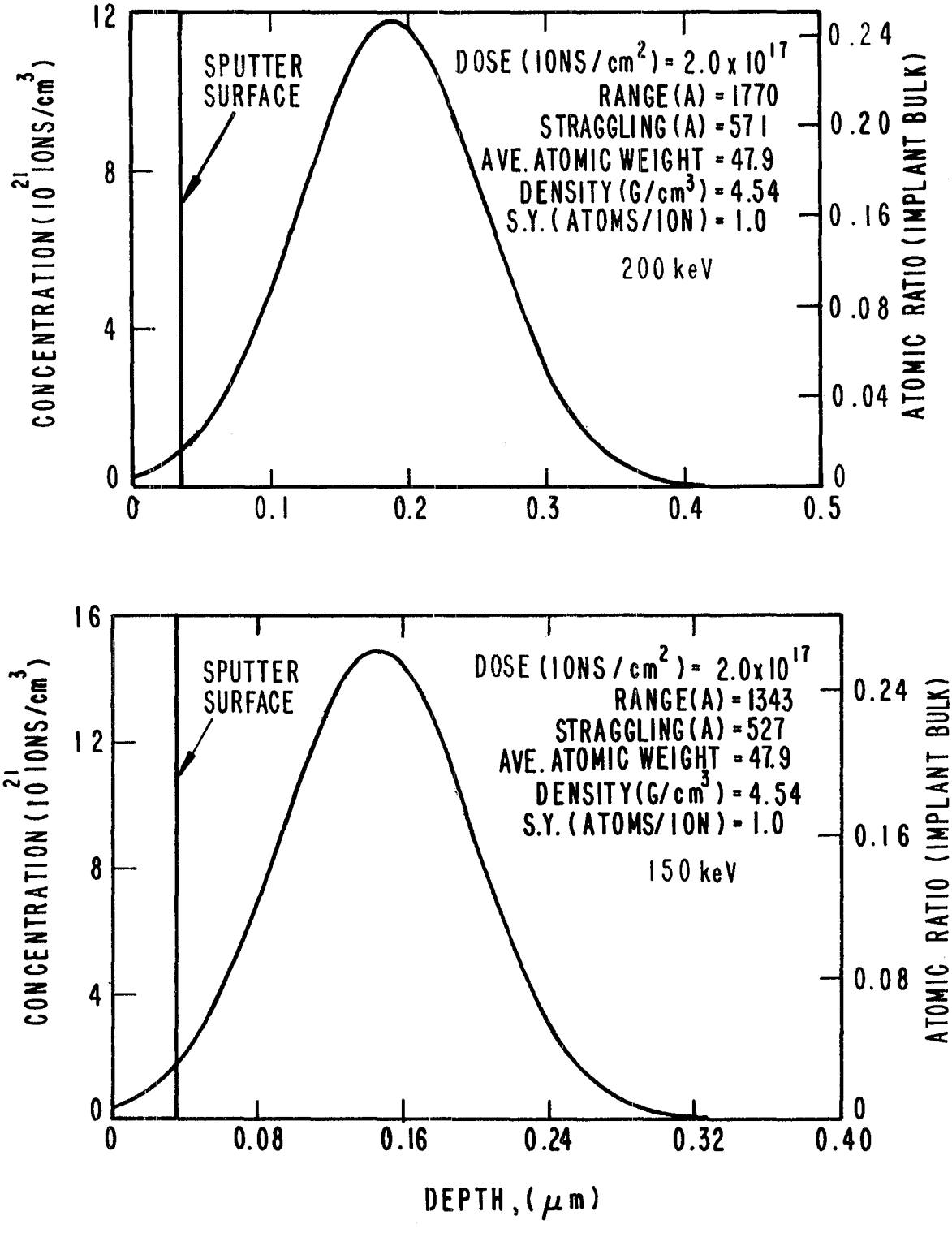

Figure C-1. Calculated Implant Profiles at Energy Levels of 150 and 200 keV

APPENDIX C-3

TECHNICAL INFORMATION FOR ALUMINA COATING OF KNIFE EDGE DISK

- Descriptive Literature - METCO 447 and 101B-NS
- Spray Parameters
- Photomicrograph of Applied Coating

METCO
Flame Spray Equipment and Supplies

TECHNICAL BULLETIN

METCO INC. 1101 Prospect Avenue, Westbury, L.I., N.Y. 11590

SUPPLIES
POWDER

ISSUED: 1 Mar 82
SUPERSEDES: 1 Apr 81
FILE: Section 1b

METCO 447 AND METCO 447NS
SELF-BONDING MOLYBDENUM-NICKEL-ALUMINUM COMPOSITE POWDER

NOTE: METCO 447 and METCO 447NS are identical materials. For the sake of simplicity, this bulletin will refer only to METCO 447. The information it contains applies equally to METCO 447NS.

Summary: METCO 447 is a Molybdenum-Nickel-Aluminum composite powder. It was especially developed as a General Purpose material for producing medium hard coatings for hard bearing and wear resistance applications. This material offers two major advantages: "One-Step" spraying and High-Integrity coatings.

"One-Step" coatings offer these benefits:

Eliminate the need for a separate bond coat.

Less undercutting required. The allowance for bond coat thickness is eliminated.

Less technique dependence. Reducing the number of steps required to produce the coating, also reduces the chance of error.

More convenience. One-step coatings eliminate having to change materials and spraying parameters.

METCO 447 was designed to produce moderately hard, low-shrink, high-strength coatings which are recommended for wear resistance, resistance to particle erosion, and for the salvage and build-up of both machinable and grindable carbon steels.

Coatings of METCO 447 are extremely tough, and exhibit good erosion resistance. They can withstand impact without cracking. Flaking and chipping are minimized.

METCO 447 coatings can be ground to very fine finishes. Also, good machined finishes can be obtained with conditional technique.

This revision includes a change in the argon/hydrogen plasma system parameter Set #4, which has been revised to ensure a more consistent, high deposition rate coating.

SPECIFICATION CONFORMANCE:

METCO 447NS meets the AiResearch Specification FP5045, Type XVI, General Electric Company Specification B50TF166, Avco Lycoming Division Specification M 3961, Perfect Circle Specification 110-265, and Rolls Royce Specification MSRR 9507/35.

- Continued -

FEATURES:

METCO 447 can be sprayed with minimum dependence on technique or need for temperature control. This allows for continuous spraying, and reduces chances of lamination occurring due to interruptions.

Thick coatings can be applied without cracking. Thin coatings can also be applied with minimum surface preparation requirements.

The properties of the coatings produced with METCO 447 provide a number of additional benefits:

High Bond Strength - Tensile bond strengths of 6,000 psi (4140 N/cm^2) for ThermoSpray coatings, and 7,000 psi (4825 N/cm^2) for Plasma Sprayed coatings are typical.

Good Wear Resistance - Resistance to abrasive wear is better than coatings of METCO 450, METCOLOY 5 and combustion sprayed SPRASTEEL 80, and less than coatings of METCOLOY 2 and SPRABOND.

Low Shrink - Coatings of unlimited thickness can be applied without cracking, which makes METCO 447 ideally suitable for machine element applications.

High Interparticle Cohesion - Coatings exhibit excellent internal strength which provides high tensile strength over 15,000 psi (10,350 N/cm^2), and good edge retention after machining.

Toughness - Coatings exhibit high toughness and good erosion resistance. They can withstand impact without cracking. Flaking and chipping are minimized.

Moderate Hardness - Coating macrohardness ranges from R_b75 to R_b80, as compared with R_b65 for METCO 450 coatings.

Good Finishing Capability - Coatings can be ground to a very fine finish. Also, machining with conditional technique will produce good finishes. METCO 447 coatings are more machinable than coatings of METCO 450. Ground finishes are better than ground finishes of METCOLOY 2 or SPRABOND.

Good Bond Coat Material - In addition to its capabilities as a single coat material, METCO 447 is equivalent to METCO 450 as a bond coat material.

METCO 447 can be sprayed with either the METCO Type 5P or 6P ThermoSpray Guns, and with the METCO Plasma Flame Spray Systems.

- Continued -

METCO
Flame Spray Equipment and Supplies

TECHNICAL BULLETIN

METCO INC. 1101 Prospect Avenue, Westbury, L.I., N.Y. 11590

SUPPLIES
POWDER

ISSUED: 2 SEPT 77
SUPERSEDES: 30 APR 74
FILE: Section 1b

METCO 101B-NS GREY ALUMINA POWDER

Summary: METCO 101B-NS is a grey alumina powder. It is identical in chemical composition to METCO 101NS, but it is coarser and can be used in thicker coatings.

Coating P101B-10 is recommended as an abrasive coating for clearance control applications in jet engines. Considerable heat is generated in the first start of the engine after spraying. Coating P101B-10 resists heat to 2000°F (1095°C). It is used on the compressor casing. It will not scratch, chip or roughen the revolving titanium compressor blades, nor permit transfer of material between the mating surfaces. For further information, see the METCO Technical Bulletin on "Abradable and Abrasive Coatings", and also Sections F1 and F2 of the METCO Handbook of Coating Recommendations.

****

This revision of the bulletin has been issued to add 7M System parameters.

METCO 101B-NS can be sprayed only with METCO Plasma Flame Spray Equipment. It cannot be sprayed with standard ThermoSpray Equipment.

SPECIFICATION CONFORMANCE:

METCO 101B-NS meets the requirements of Pratt & Whitney Aircraft Corporation specification PWA 1311, and General Electric Company specification A50TF87.

APPLICATIONS:

METCO 101B-NS is being used in jet engines for producing abrasive machine element clearance control coatings.

Use METCO 101B-NS wherever a GE A50TF87 or PWA 1311 material is required.

METCO 101B-NS is recommended for the following applications:

Coating No.	Coating Function	Typical Application
P101B-10	Abrasive coating to 2000°F (1095°C)	Jet Engine Compressor Casing

METCO 101B-NS should also be considered and tested for applications on foundry equipment and the like, for thermal barriers, and for resistance to molten zinc, molten aluminum and molten copper. METCO 101B-NS has been applied in coatings more than .120" (3mm) thick with no evidence of spalling or laminating.

- Continued -

POWDER CHARACTERISTICS:

Typical Composition:	Aluminum Oxide	94.0%
	Titanium Dioxide	2.5%
	Silicon Dioxide	2.0%
	Iron (Ferric) Oxide	1.0%
	Other Oxides	Balance
Typical Size Range:	-200 mesh +30 microns	
	-75 +30 microns	
Melting Point:	3625°F (1995°C)	

TYPICAL PHYSICAL PROPERTIES OF THE COATING:

	Coating P101B-10
Texture, as-sprayed (microinches aa):	700+
Finish, as-ground (diamond wheels) (microinches aa):	40-70
Macrohardness:	$R_C 50$
Cross Sectional Hardness:	$DPH_{300} 760$
Density (g/cc):	3.3
Weight ($lb/ft^2/.001"$):	.017
($kg/m^2/0.1mm$):	.33

FINISHING:

Coatings of METCO 101B-NS can be ground to good-to-excellent finishes. Use the parameters listed in the METCO Flame Spray Handbook, Volume III, for grinding coatings of METCO 101 Alumina Powder.

SAFETY MEASURES:

Flame spraying is a completely safe process when performed in accordance with "METCO's Safety Measures". Familiarize yourself with local safety regulations before starting spraying operations. DO NOT operate your spraying equipment or use the spray material supplied before you have thoroughly read the METCO Instruction Manual.

DISREGARDING THESE INSTRUCTIONS MAY BE DANGEROUS TO YOUR HEALTH.

W.O.# _____ Sales Sample Report

Completed _____ Field Engineer _____

Customer CREMAC INC Appvd. for shipment J. Ramsey

PARAMETERS

GUN	MAT'L.	P. PORT MTRV AIR CAP	NO.2	WHEEL RPM	CLICKS AMPS VOLTS	SPRAY DIST	CARRIER FLOW	PRESSURE			FLOW			SPRAY RATE	PSA	VIBRATOR
								HC	H2		AV	H2				
7MB	METCO 447	#1	GH	4/30	500/65-75	6	37	100	50		100	15		25 lbs/hr		
7MB	METCO 101B-NS	#2	GH	5/50	500/70-90	3-5	37	100	50		90	25		7 lbs/hr		

Preparation and Spraying

1. Coating thickness 0.012 ± .002
2. Degrease Vapor Degrease - trichorethylene
3. Mask — Blast 54 GRIT Al_2O_3
4. Preheat temp. 200 Max. Spraying temp. _____ Cooling _____
5. Sealed —
6. Undercoat METCO 447 Thickness 0.003 ± .001
7. Finish Coat METCO 101B-NS Thickness 0.004 ± .001
8. Number of pieces completed 3
9. Work Handling Equipt. None
10. Traverse speed _____ RPM _____ No. passes _____

SPRAY PARAMETERS FOR ALUMINA KNIFE EDGE COATING

METCO INC. PHOTO RECORD MD DATE 11-11-82

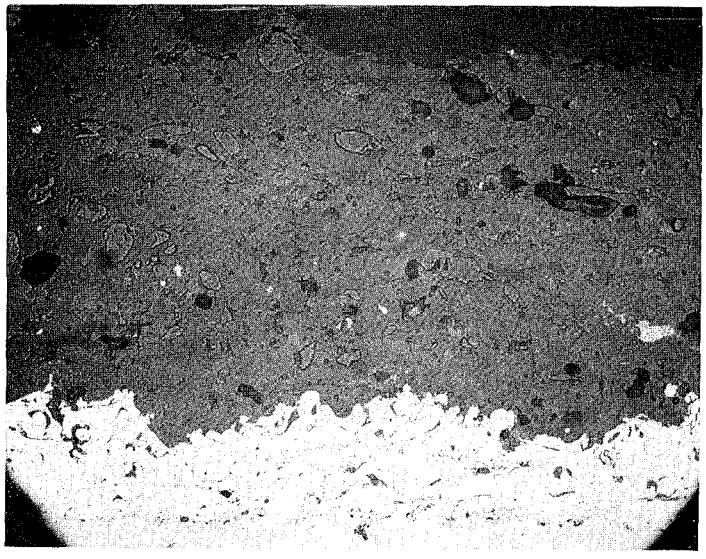

SPEC. NO. 5529A MAG. 200 X

ETCHANT

PROJECT NO. W 702

SAMPLE DESCRIPTION

101 B-NS

POROSITY = ~ 2-3 %

Micrograph of Alumina Coating Surface

APPENDIX C-4

TECHNICAL INFORMATION FOR TUNGSTEN CARBIDE COATING OF KNIFE EDGE DISK

- Union Carbide Letter and Specifications for LW-15 Coating

UNION CARBIDE CORPORATION 441 SACKETT POINT ROAD, NORTH HAVEN, CT 06473
Coatings Service TELEPHONE: (203) 288-3331
LINDE DIVISION

September 8, 1982

Creare
P.O. Box 71
Hanover, NH 03755

Attention: Mr. Frank Dolan

Gentlemen:

Enclosed is the information you requested on two Union Carbide coatings: LW-1N40 and LW-15. Also enclosed is a quotation for applying these two coatings on your cryogenic pump disc. As we discussed, the as-coated thickness for either coating will be .008"/.010" per side to allow you to finish to .003"/.005" per side. Based on this finished thickness, we suggest you undercut the parts to the nominal .004" per side or .008" on the diameter. Because of the geometry of these parts, there is no effective way to mask the 11° bevel or either side of the knife edge. Full coating thickness will be present on these areas after processing. Any areas that are parallel to the coating flow will at most have smoke on them that can be easily cleaned by you when finishing these parts.

As I indicated, the bond strength of these coatings is too high to be measured by ASTM method C633-69. However, special laboratory tests for these coatings estimates values in excess of 25,000 psi. Of the two coatings, LW-15 is the only one that has been used in a cryogenic pump application. The CTE of LW-15 at 139° R is 3.68×10^{-6} in/in/°C or 2.04×10^{-6} in/in/°F which is lower than the CTE of your base material. LW-1N40 is also recommended because we have had good experience with this coating on knife edge applications even though we have not had cryogenic experience with it. Because of the temperature excursions this part is going to experience, we strongly recommend that you test both coatings to determine if either one will work in your application. If after reviewing the technical data on both coatings you have additional questions, please call.

Very truly yours,

UNION CARBIDE CORPORATION
Engineering Products Division

Jean A. Mozolic

Jean A. Mozolic
Field Representative

JAM/cmc
Enclosure

UCAR COATING: LW-15

CUSTOMER SPECIFICATION: None

TYPE: D-Gun, Tungsten Carbide + Cobalt-Chromium

COMPOSITION: 86 WC-10 Co - 4 Cr

CROSS-SECTIONAL HARDNESS: 1000 minimum VPN_{300}

BOND-STRENGTH: > 10,000 psi

POROSITY: 1.5% Max.

MAXIMUM OPERATING TEMPERATURE: Not Available

MODULUS OF RUPTURE: Not Available

MODULUS OF ELASTICITY: Not Available

DENSITY: 14.0 gm/cm^3

COEFF. OF THERMAL EXPANSION: 2.04×10^{-6} in/in/°F @ 139 °R

ELECTRICAL RESISTIVITY: Not Available

SURFACE ROUGHNESS: AS-COATED: 125-150 MU IN. RMS (RMS ≐ 1.1 AA)

LAPPED: 1-10 MU IN. RMS (Depending on part geometry).

OTHER: Not Available

EXTRA GRINDING STOCK REQUIRED: .003"-.004"

APPLICATIONS AND MAIN FEATURES: LW-15 applications include impellers and wear rings for centrifugal pumps, plungers and rods for reciprocating pumps and compressors, gates and seats for valves used in the petroleum industry and foils for paper-making machines. It is recommended for applications in the chemical processing industry where better corrosion resistance than the LW-1 series is required. LW-15 has intermediate wear resistance to LW-5 and LW-1 (best) in a laboratory sand abrasion test.

Preliminary tests indicate that the modulus of rupture and modulus of elasticity are intermediate to LW-5 and LW-1, but additional tests are required for confirmation. LW-15 has been used on water blaster pump plungers operating at 7500 psi and on ammonia compressors operating at 6000 psi.

CORROSION RESISTANCE (Speedway Laboratory Data)

Environment	Temp. °F*	Corrosion Rate Mil/Year	Rating**
50% Sodium Hydroxide	RT	GAIN	I
" " "	294	10	G
5% Nitric Acid	RT	GAIN	I
" " "	213	10	G
20% Hydrochloric Acid	RT	0.9	E
" " "	226	22	U
5% Sulphuric Acid	RT	1.8	E
" " "	215	13	M

Relative Corrosion Resistance of D-Gun Carbide Coatings

			CORROSION RESISTANCE RATING**							
	COMPOSITION		50% NaOH		5% HNO_3		20% H Cl		5% H_2SO_4	
COATING	CARBIDE	BINDER	R.T.	294°F*	R.T.	213°F	R.T.	226°F	R.T.	215°F
LW-1N30	WC	Co	I	U	I	I	E	M	E	G
LW-15	WC	Co-Cr	I	G	I	G	E	U	E	M
LW-16	WC	Co-Cr	E	U	I	I	E	M	E	G
LW-16N30	WC	Co-Cr	E	U	I	E	G	U	E	G
LW-5	$(W,Cr)C$	Ni	E	G	G	G	M	U	G	U
WT-1	$(W,Ti)C$	Ni	E	E	U	U	U	U	G	U
LC-1C	Cr_3C_2	Ni-Cr	E	E	G	U	U	U	U	U

*Elevated temperature tests are at the boiling point of the solution.

**Rating system for UCAR coatings

Excellent (E): $\leq$ 2 mil penetration/year

Good (G): $>2, \leq 10$

Marginal (M): $>10, \leq 20$

Unsatisfactory (U): >20

Indeterminant (I): weight gain during corrosion test

APPENDIX C-5

TECHNICAL INFORMATION FOR ALUMINUM/GRAPHITE COATING OF WEAR RING

- Spray parameters for METCO CE-2074A
- Photomicrograph of Applied Surface
- Finishing Instructions

W.O.#_____ Sales Sample Report

Completed_____ Field Engineer_____

Customer Crane Inc Appvd. for shipment D. Kosanke

PARAMETERS

GUN	MAT'L.	P. PORT MTRV AIR CAP	NO.2	WHEEL RPM	CLICKS AMPS VOLTS	SPRAY DIST	CARRIER FLOW	PRESSURE N_2	PRESSURE H_2		FLOW Ar	FLOW H_2		SPRAY RATE	PSA	VIBRATOR
7MB	METCO 447	#4	GH	H/30	500/65-75	6	37	100	50	—	100	15	—	25	—	—
7MB	METCO 313 CE 2074A	#1	GH	H/27	400/75-85	5	37	100	50	-	190	8	-	9	—	—

Preparation and Spraying

1. Coating thickness 0.023 ± .002
2. Degrease Vapor degrease - Trichoretylene
3. Mask — Blast 54 Grit Al_2O_3
4. Preheat temp. 200 Max. Spraying temp._____ Cooling_____
5. Sealed —
6. Undercoat METCO 447 Thickness 0.003 ± .001
7. Finish Coat METCO CE 2074 A Thickness 0.020 ± .001
8. Number of pieces completed 3
9. Work Handling Equipt. None
10. Traverse speed_____ RPM_____ No. passes_____

SPRAY PARAMETERS FOR ALUMINUM/GRAPHITE WEAR RING COATING

METCO INC. PHOTO RECORD MD DATE 11-11-82

SPEC. NO. 5530A MAG. 200x

ETCHANT

PROJECT NO. W 702

SAMPLE DESCRIPTION

CE 2074 A

GRAPHITE = ~ 34-36 %

POROSITY = ~ 6-8 %

Micrograph of Aluminum/Graphite Coating Surface

GENERAL RECOMMENDED FINISHING INSTRUCTIONS

CE-2074A (Aluminum-Silicon-Graphite Composite)

Procedure: Machine

Tool: 5/16" carboloy AR5 Grade 78
Set approximately .010" (0.25 mm)above center

Work Speed: 390 SFPM (120 m/min)

Traverse Speed: .0025"/Rev (0.06 mm)

Infeed: .010" (0.25 mm)

Condition: Dry

APPENDIX C-6

TECHNICAL INFORMATION FOR YTTRIA STABILIZED ZICONIA COATING OF WEAR RING

- Spray Parameters for METCO CE-2198A
- Photomicrograph of Applied Coating
- Finishing Instructions

W.O.#_____ Sales Sample Report

Completed_____ Field Engineer BILL RUSCH

Customer CREPEC INC Appvd. for shipment J. Rusch

PARAMETERS

GUN	MAT'L.	P. PORT MTRV AIR CAP	NO.2	WHEEL RPM	CLICKS AMPS VOLTS	SPRAY DIST	CARRIER FLOW	PRESSURE N_2	PRESSURE H_2		FLOW N_2	FLOW H_2		SPRAY RATE	PSA	VIBRATOR
7M	METCO 447	#2 PP	G	S/15	500/70-80	5"	37	50	50		150	10		9#/Hr.	—	—
7M	METCO CE 2198A	#4PP	G	H/30	400/77	6.5"	37	50	50		75	15		15#/Hr.	—	—

Preparation and Spraying

1. Coating thickness .030" ± .005"
2. Degrease 1 MIN. IN TRICHLORO TRIFLUORO ETHANE
3. Mask STEEL 1/8" THICK Blast C-16 @ 50 PSIG
4. Preheat temp. 120°F Max. Spraying temp. 320°F Cooling
5. Sealed
6. Undercoat METCO 447 Thickness .003" ± .002" .000"
7. Finish Coat METCO CE 2198 A Thickness .020" ± .010" .000"
8. Number of pieces completed 3
9. Work Handling Equipt. NONE
10. Traverse speed SLOW RPM — No. passes

Remarks

D.E. DROPS OFF ABRUPTLY IF S.D. GREATER THAN 6.5" IS USED.

SPRAY PARAMETERS FOR YSZ WEAR RING COATING

METCO INC. PHOTO RECORD MD DATE 11-11-82

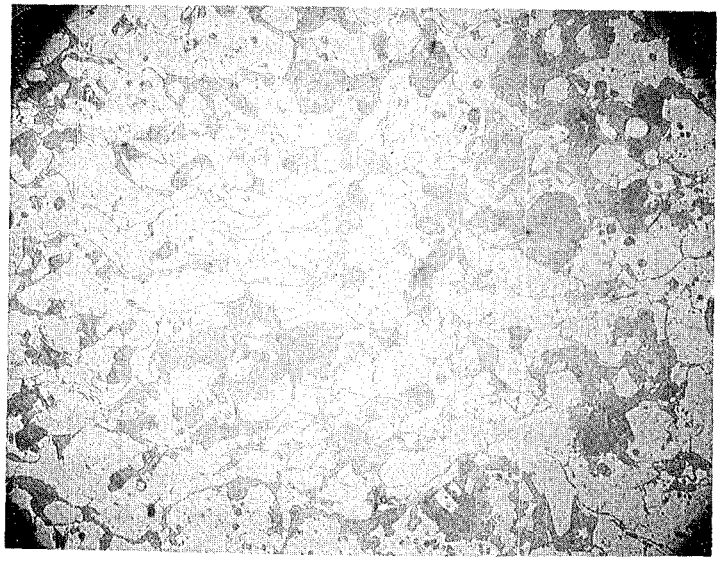

SPEC. NO. 5531A MAG. 200 X

ETCHANT

PROJECT NO. W 702

SAMPLE DESCRIPTION

© CE 2198 A

POROSITY = ~ 21.5 %

Micrograph of YSZ Coating Surface

GENERAL RECOMMENDED FINISHING INSTRUCTIONS

CE-2198A (6-8 wt. % Yttria Stabilized Zirconia Powder)

Procedure: Grind

Wheel: Silicon carbide wheel (GC 100-G11 VGE or similar type wheel) or Diamond Wheel D120-N100-87 or similar type wheel.

Wheel Speed: 5500 - 6500 SFPM (1700 - 2000 m/min)

Infeed: .002" (.050 mm) rough cut
.0005" (.013 mm) finish cut

Work Speed: Cylindrical - 70 - 100 SFPM(20-30 m/min)
Flat -30-50 SFPM (8-15 m/min)

Cross Feed: Flat - .030" per pass (.75 mm) rough cut
.010" per pass (.25 mm) finish cut

Traverse Speed*: Cylindrical - 12"/min (305 mm/min) rough cut
6"/min (150 mm/min) finish cut

*Amount of wheel width advance per revolution of work

Roughing = 1/4" - 1/2" (6-13 mm)
Finishing =1/2" - 1/6" (2-4 mm)

APPENDIX D

STRIP CHART RECORDS FROM RUB INTERACTION TESTS

APPENDIX D

Strip Chart Records from Rub Interaction Tests

This appendix contains the computer plotted strip chart records from the 15 rub interaction tests. Each set of data displays the temperatures on one page and the 5 high response rate instruments on a second page. The data are plotted vs. time into the test, as in the sample data discussed in Section 4.6.2.

The thermocouple amplifier gains and offsets were adjusted several times during the course of the experimental phase in order to increase the temperature measuring range and still maintain adequate measurement sensitivity. Table D-1 provides a listing of the pre-rub wear pad temperatures and the peak temperatures indicated by each thermocouple during each incursion test. Other intermediate temperatures can be calculated using the tabulated amplifier gains and a table of thermocouple emf values for the Type K thermocouples used in the wear pads.

TABLE D-1 WEAR PAD TEMPERATURE DATA

Test Name	Near-Surface Thermocouple			SubSurface Thermocouple		
	Pre-Rub Temp. (°C)	Maximum Temp. (°C)	Amplifier Gain (volts/volt)	Pre-Rub Temp. (°C)	Maximum Temp. (°C)	Amplifier Gain (volts/volt)
TIAL02	-151	314	483.7	-147	213	479.4
TIAL03	-111	72	480.0	-115	182	480.0
TIAL13	-179	560(1)	240.4	-176	437	240.4
TIAL23	-187	265	241.5	-187	283	239.6
TIAL04	-190	87	240.3	-187	82	239.1
TICU03	-103	274(1)	481.5	-103	269	482.2
TIAG02	-175	- 29	483.7	-176	- 79	479.6
TIAG03	-158	-146	483.0	-155	-151	480.0
TIYZ03	- 99	126	484.4	- 98	23	479.8
TNAL02	-167	313(1)	483.7	-173	123	478.7
TNAL03	- 82	267	484.4	- 82	197	479.6
AOAL02	-186	234	240.2	-184	119	240.0
AOAL03	-124	197	483.9	-125	212	478.9
TCAL02	-134	317	239.8	-132	134	239.8
TCAL03	-124	182	483.3	-124	181	478.9

(1) These temperatures correspond to the maximum full-scale voltage (5V) input to the computer. Wear pad temperatures were actually higher, but the peak values cannot be determined from the data.

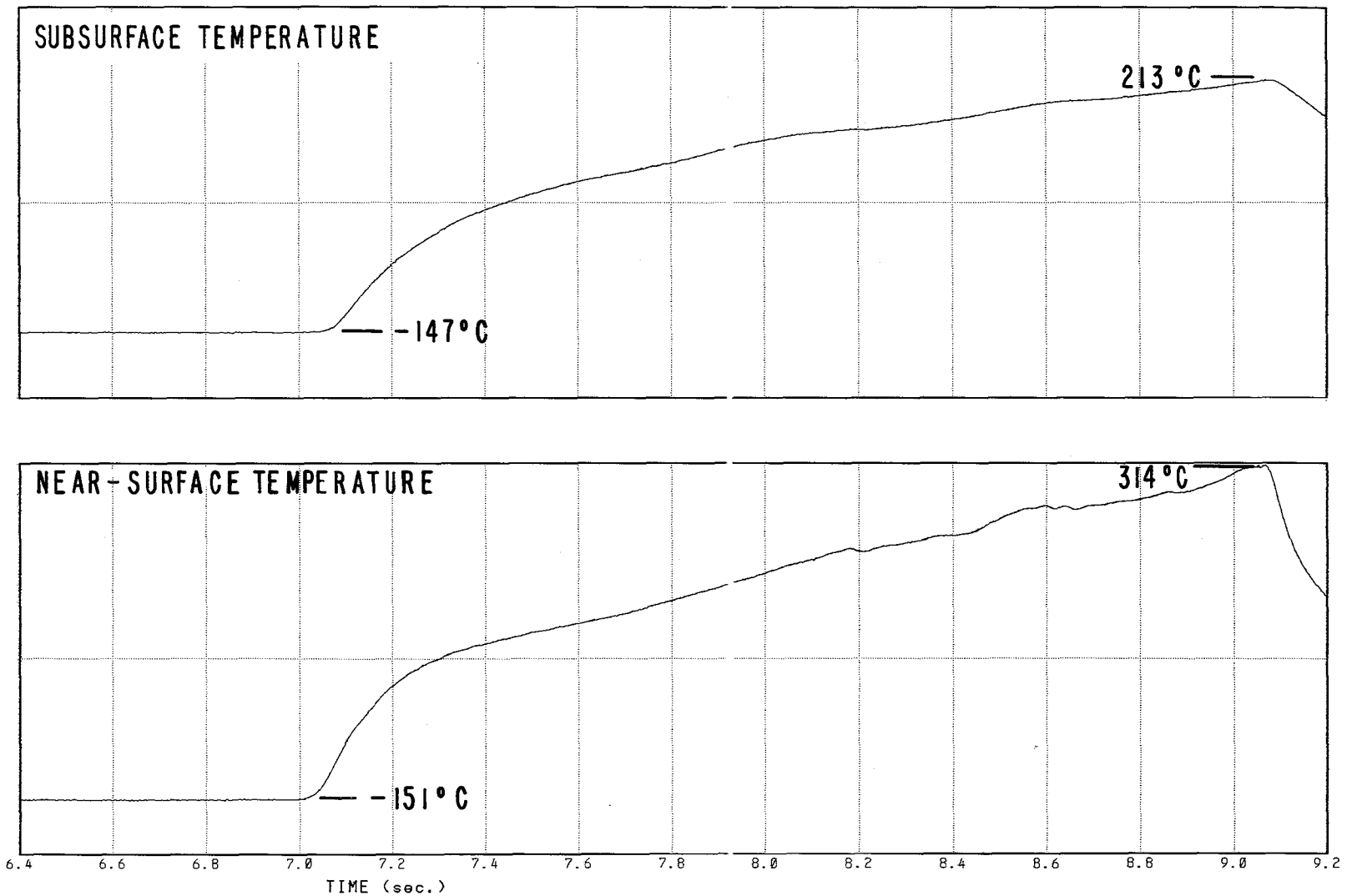

RUB Test : TIAL02

Reduction Date: 30-AUG-84
Test Date: 22-FEB-83

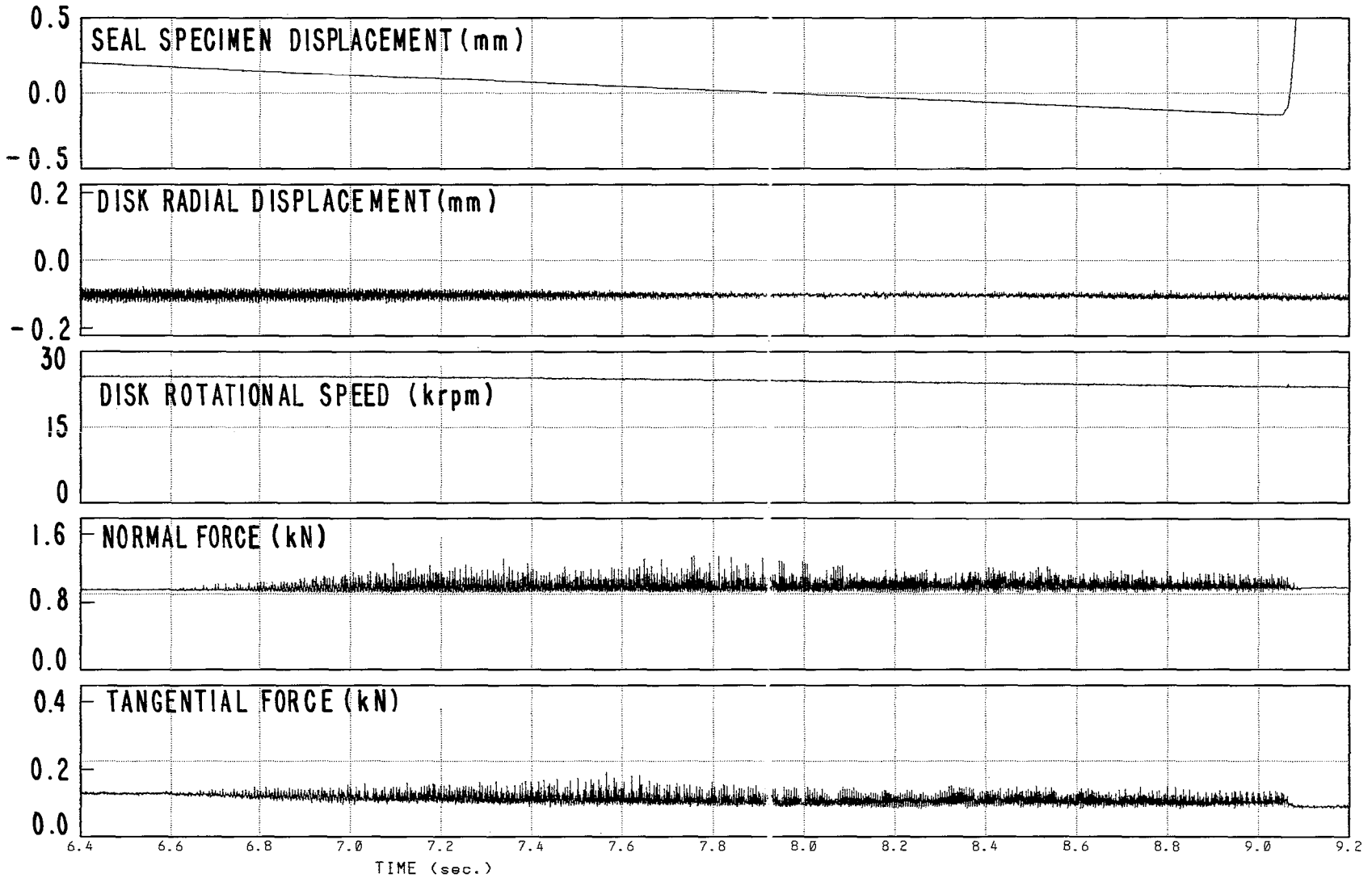

RUB Test : TIAL02

Reduction Date: 30-AUG-84
Test Date: 22-FEB-83

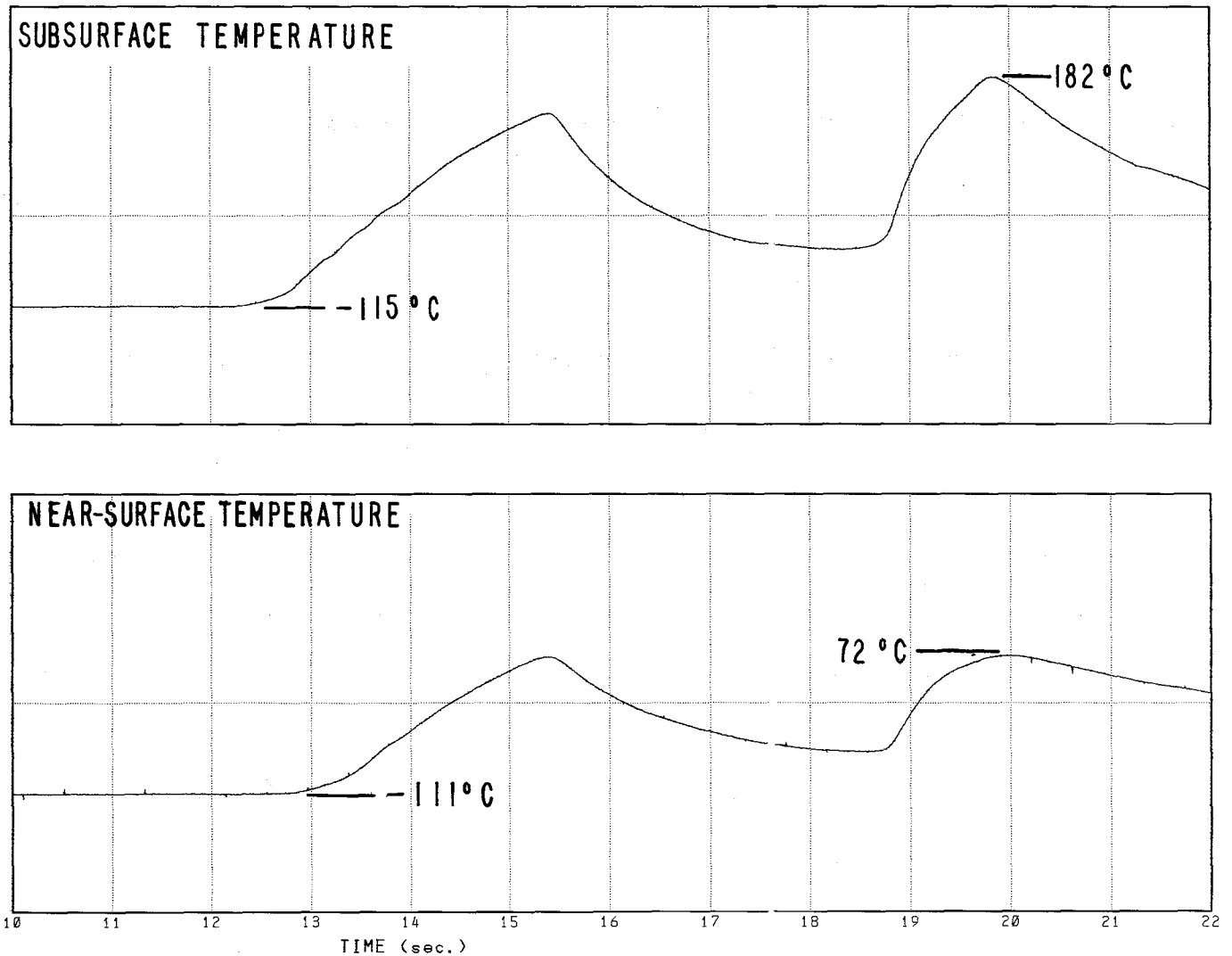

RUB Test : TIAL03

Reduction Date: 30-AUG-84
Test Date: 21-OCT-82

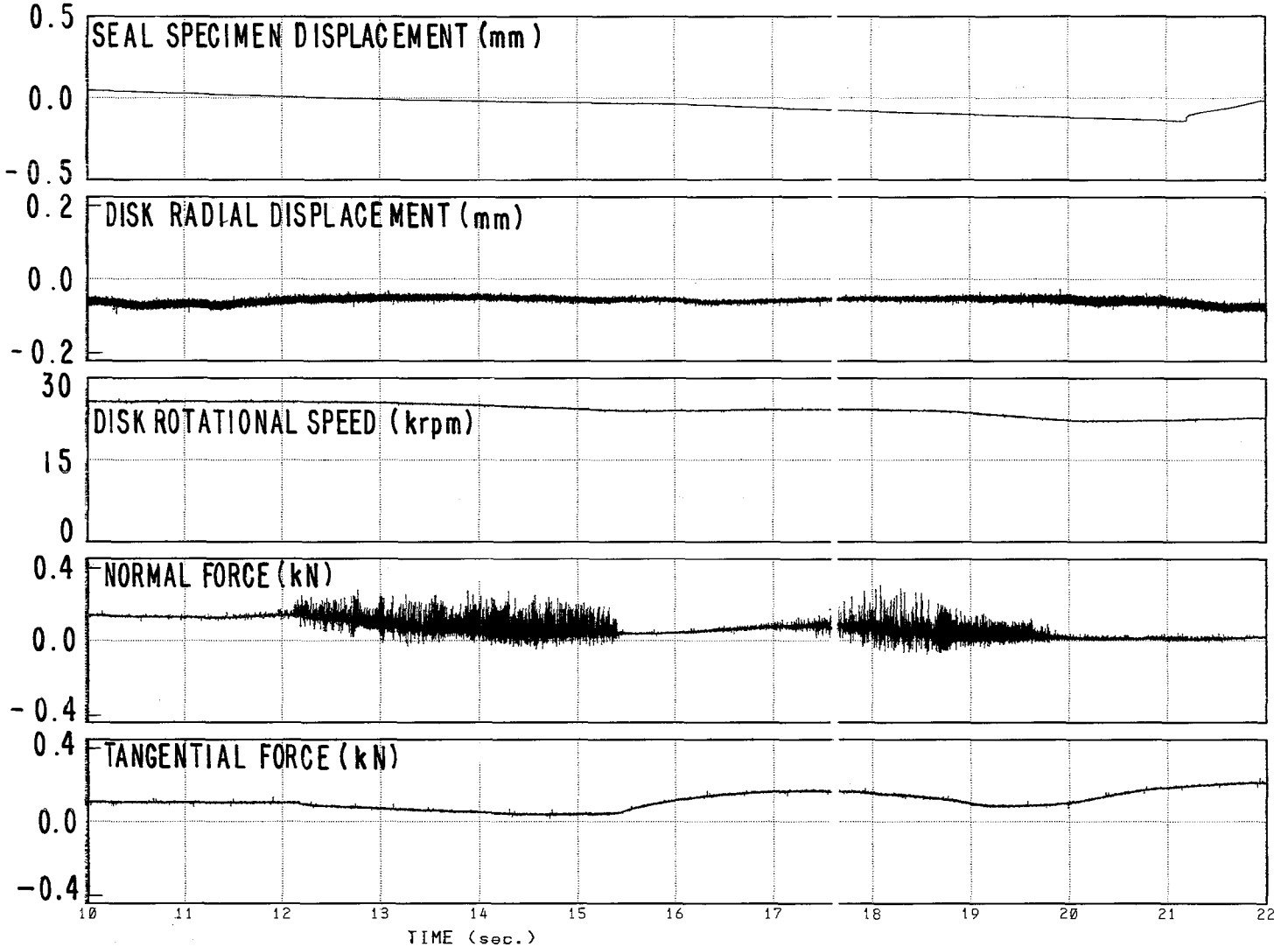

RUB Test : TIAL03

Reduction Date: 30-AUG-84
Test Date: 21-OCT-82

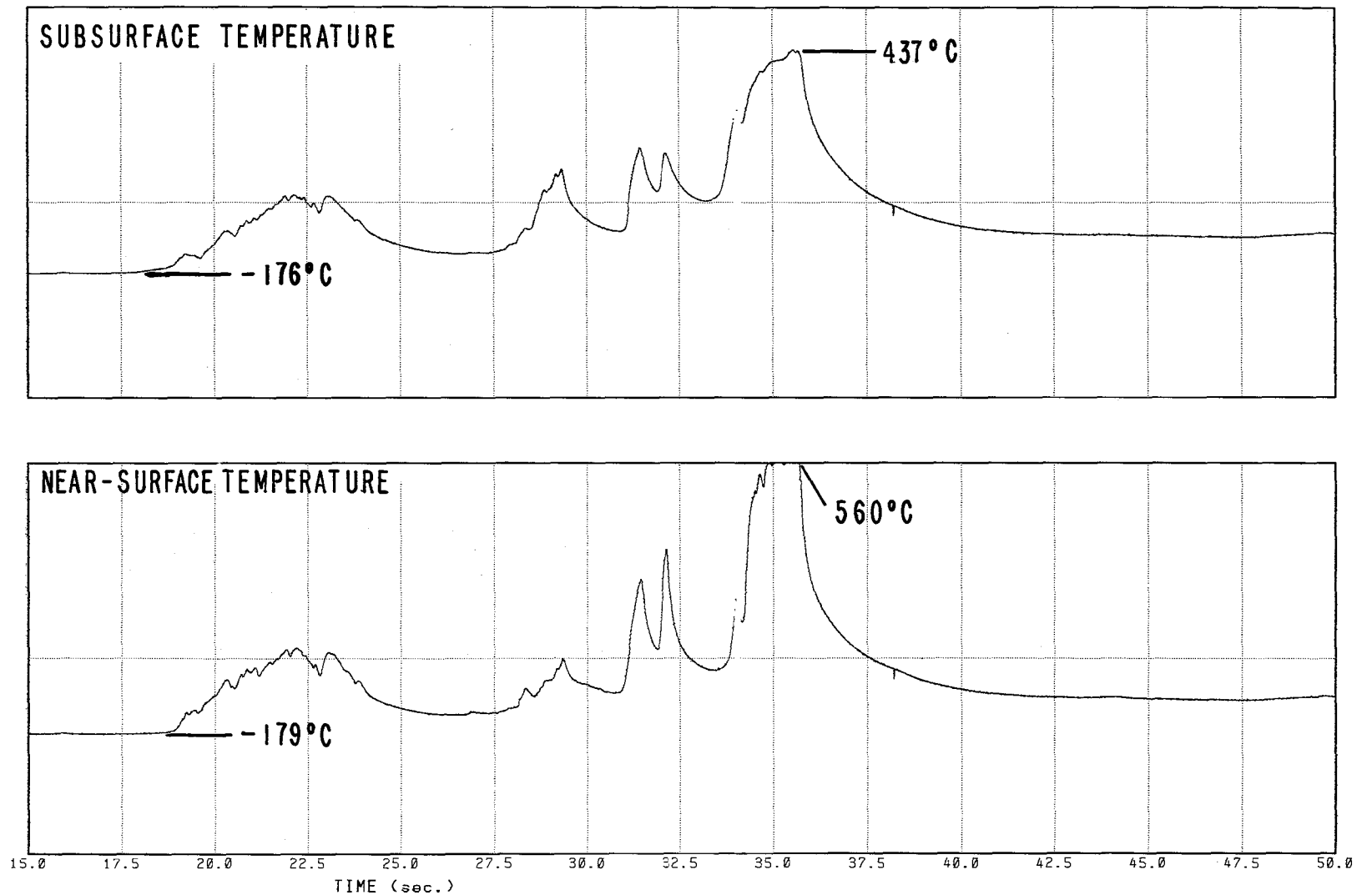

RUB Test : TIAL13

Reduction Date: 30-AUG-84
Test Date: 24-FEB-83

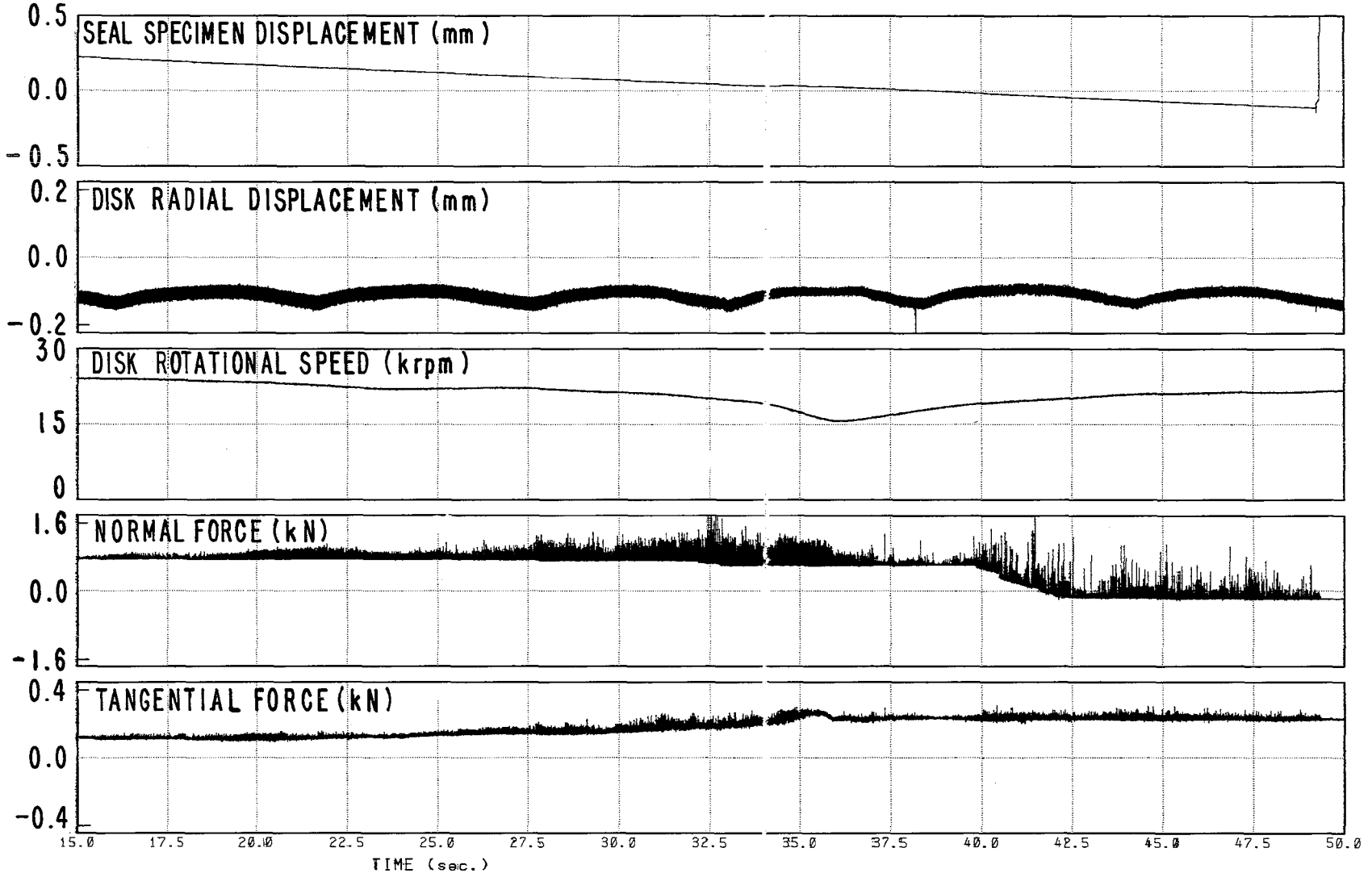

RUB Test :TIAL13

Reduction Date: 30-AUG-84
Test Date: 24-FEB-83

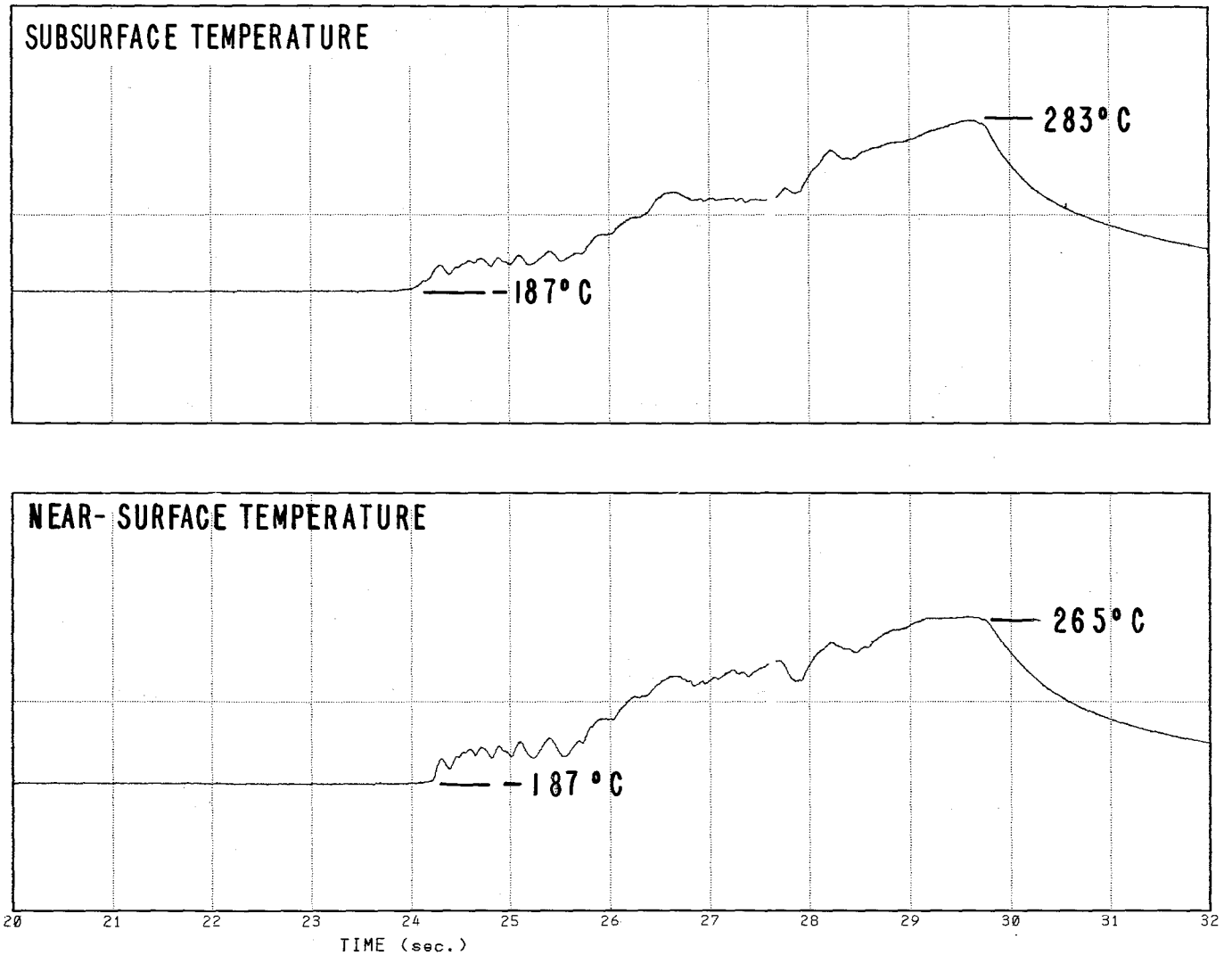

RUB Test : TIAL23

Reduction Date: 30-AUG-84
Test Date: 25-FEB-83

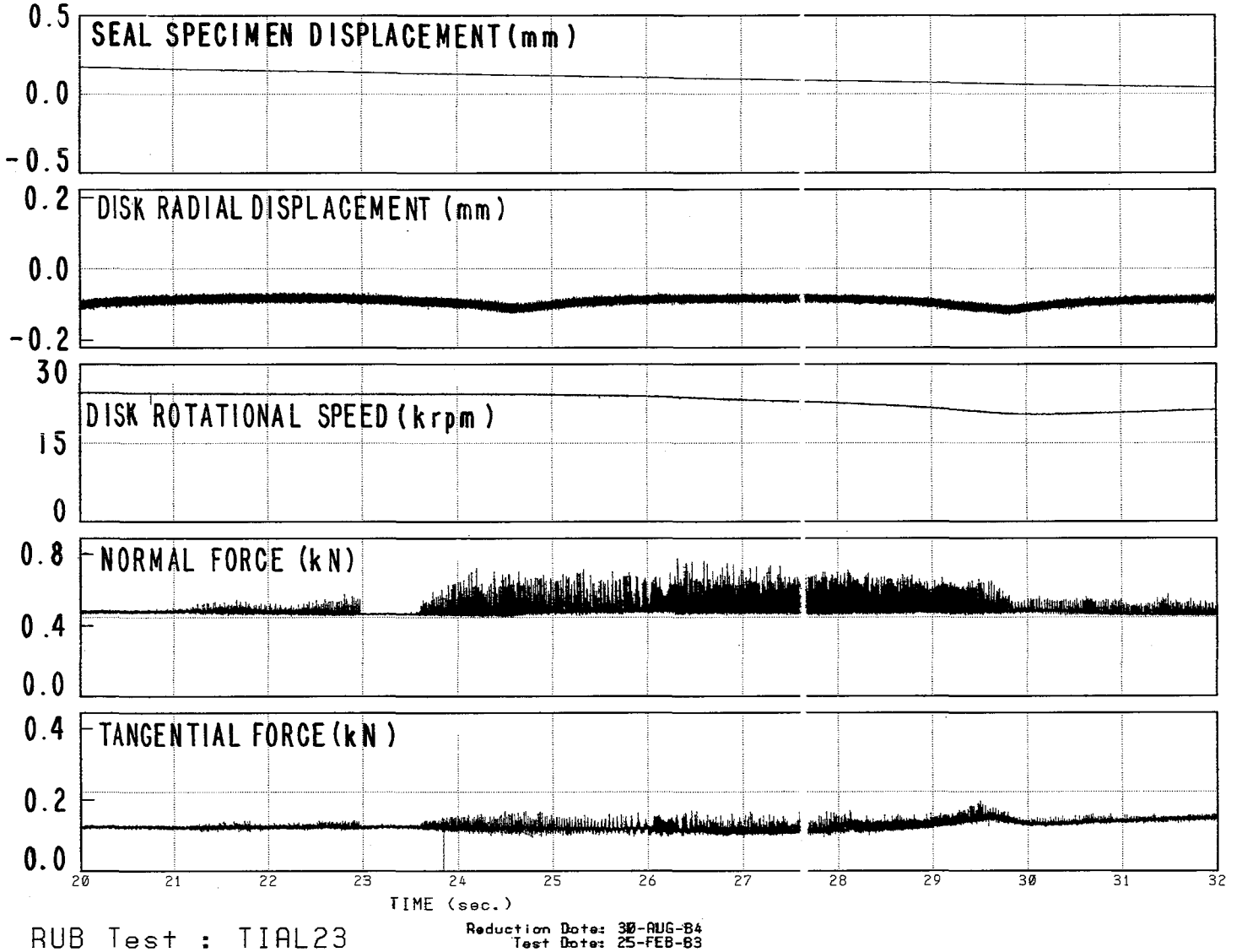
0.5
SEAL SPECIMEN DISPLACEMENT(mm)
0.0
-0.5
0.2
DISK RADIAL DISPLACEMENT (mm)
0.0
-0.2
30
DISK ROTATIONAL SPEED(krpm)
15
0
0.8
NORMAL FORCE (kN)
0.4
0.0
0.4
TANGENTIAL FORCE(kN)
0.2
0.0
20
21
22
23
24
25
26
27
28
29
30
31
32
TIME (sec.)
RUB Test : TIAL23
Reduction Date: 30-AUG-84
Test Date: 25-FEB-83

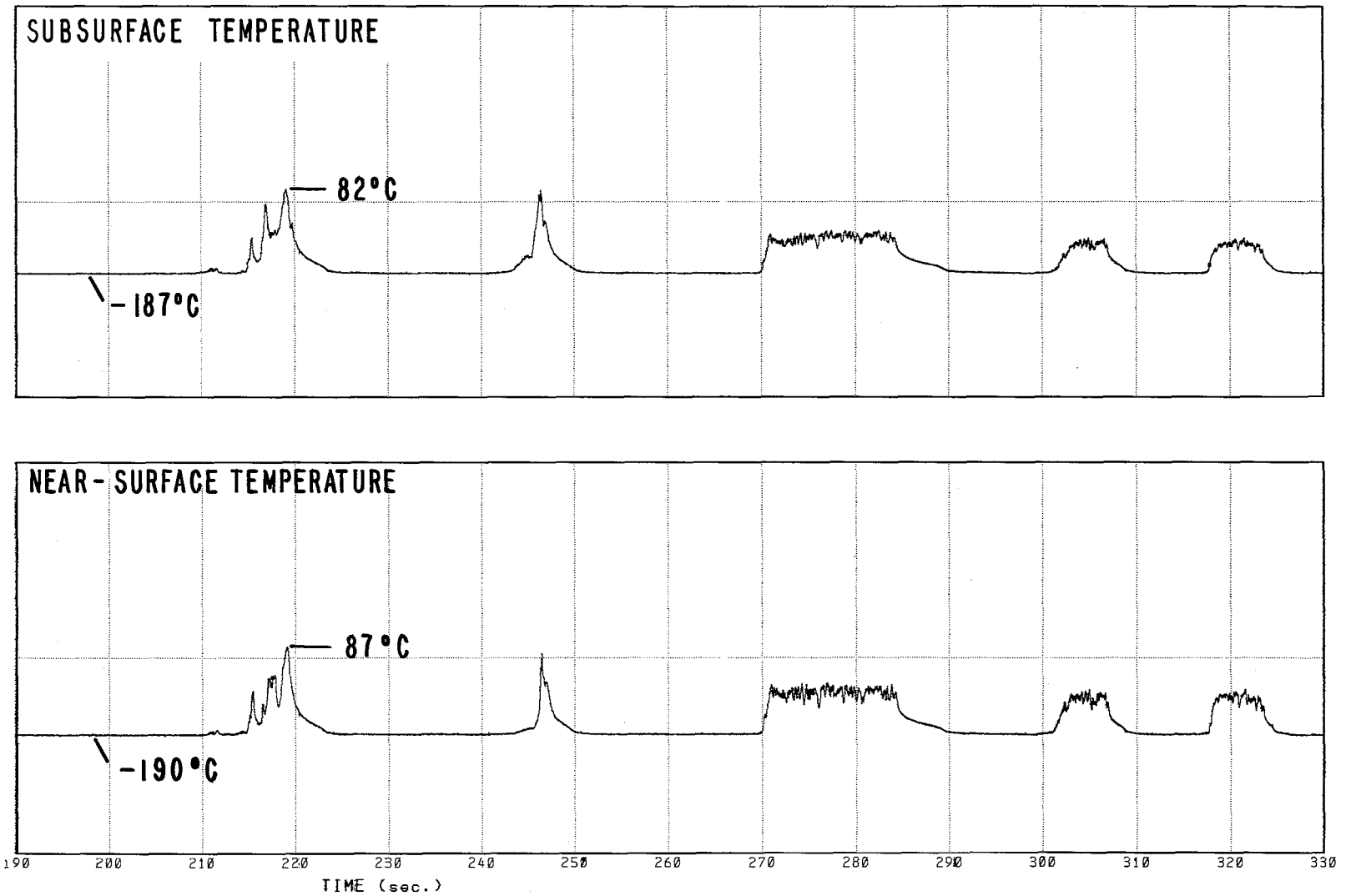

RUB Test : TIAL04

Reduction Date: 30-AUG-84
Test Date: 01-MAR-83

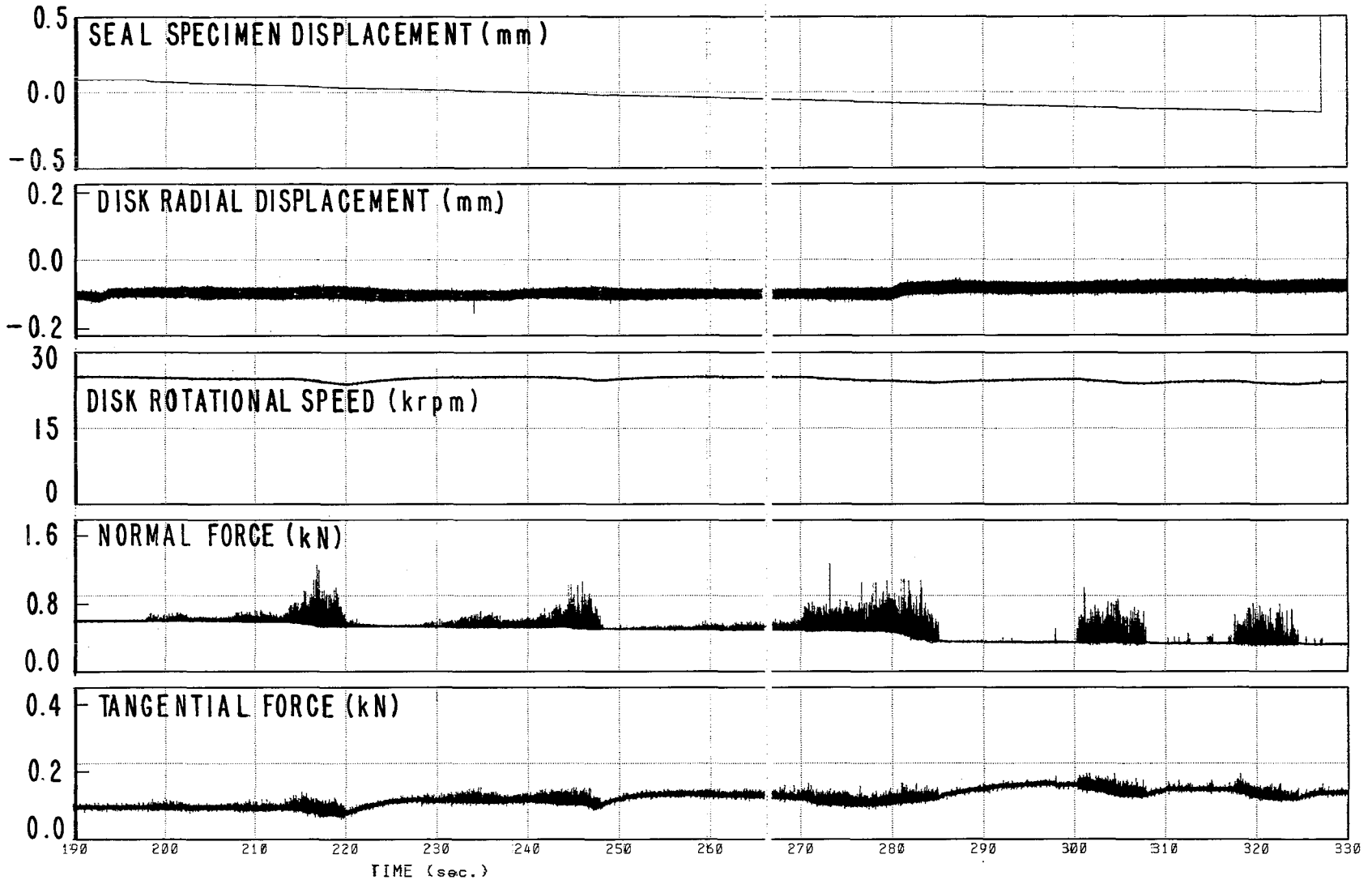

RUB Test : TIAL04

Reduction Date: 31-AUG-84
Test Date: 01-MAR-83

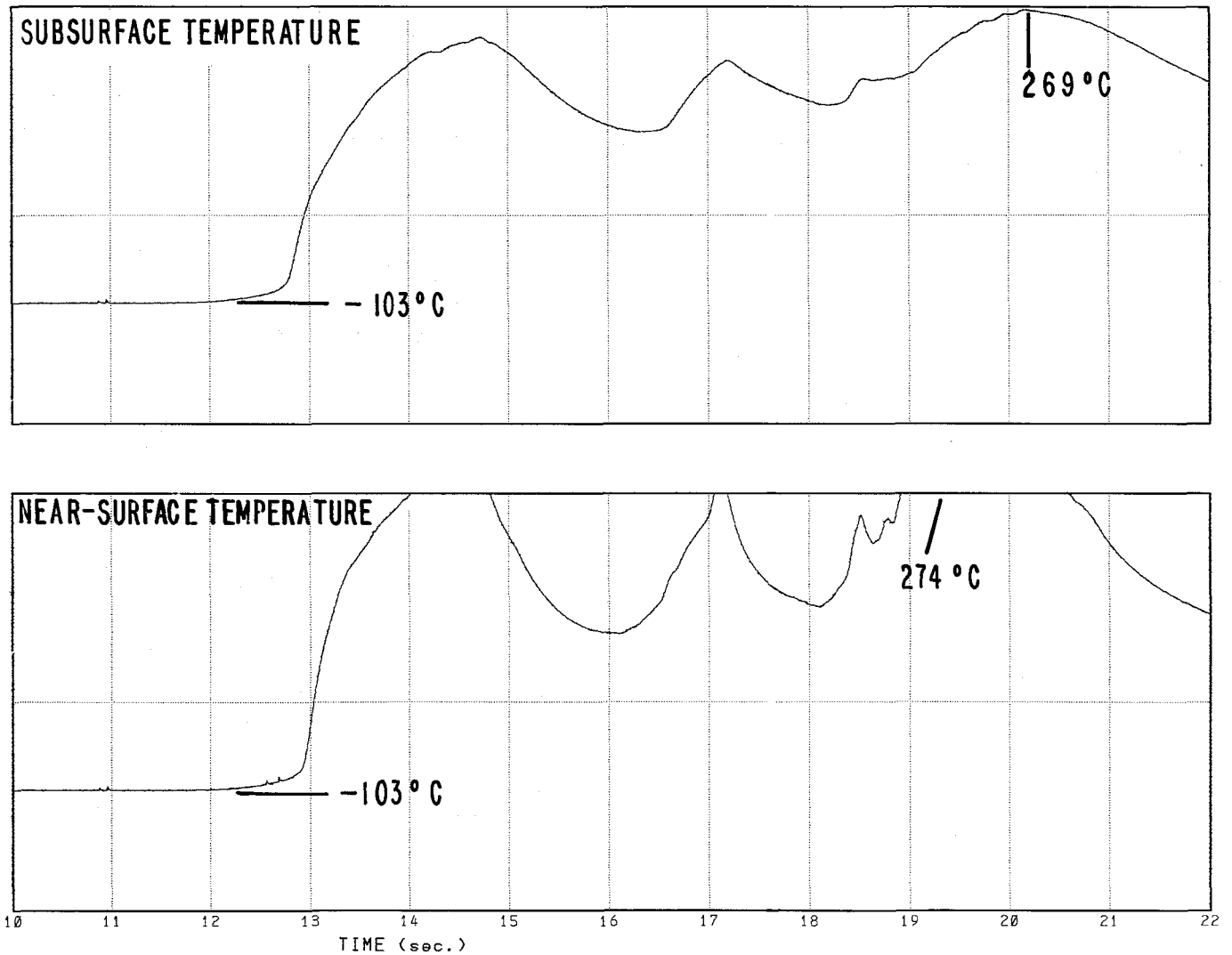

RUB Test : TICU03

Reduction Date: 30-AUG-84
Test Date: 03-FEB-83

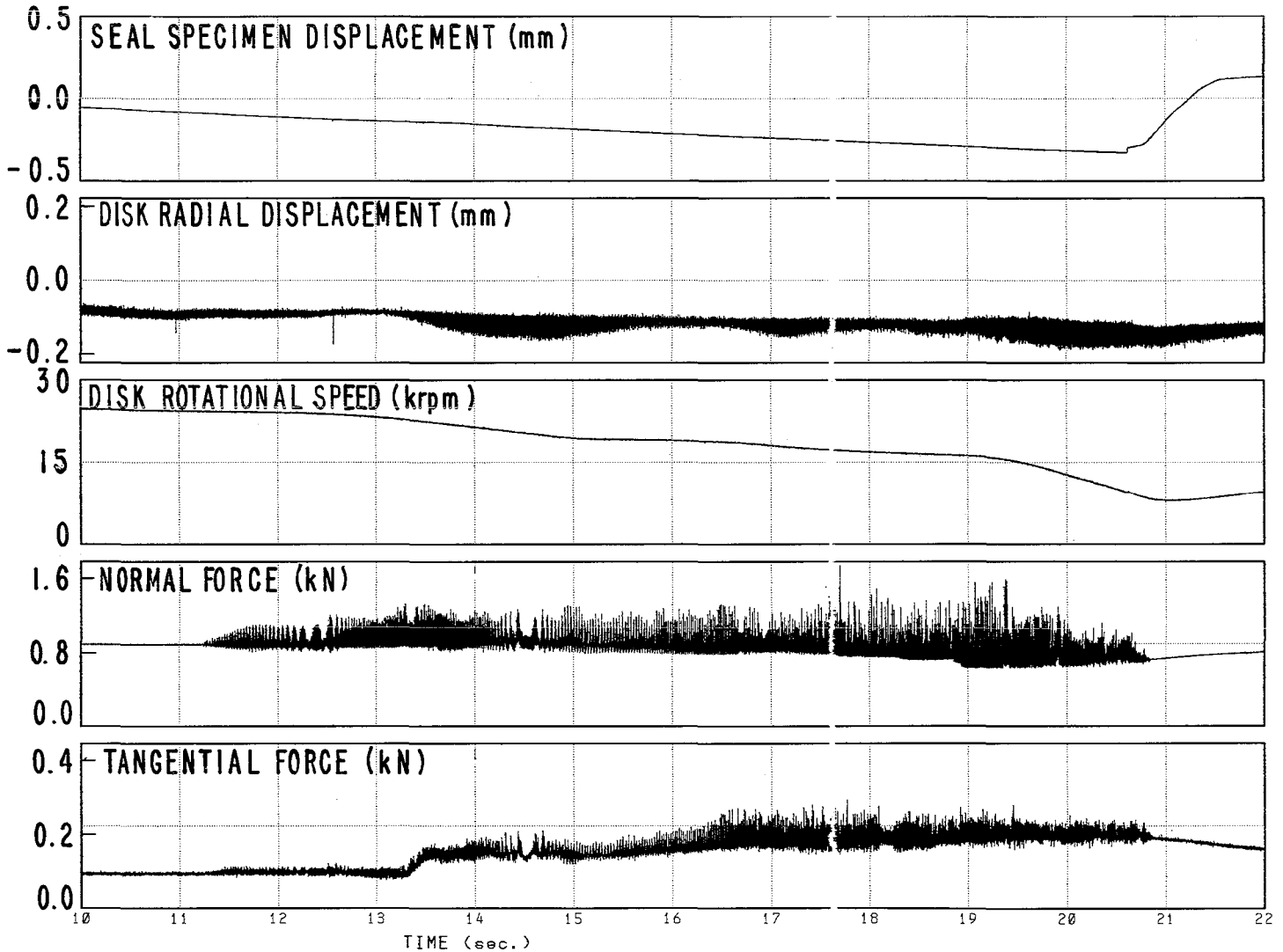

RUB Test : TIEU03

Reduction Date: 30-AUG-84
Test Date: 03-FEB-83

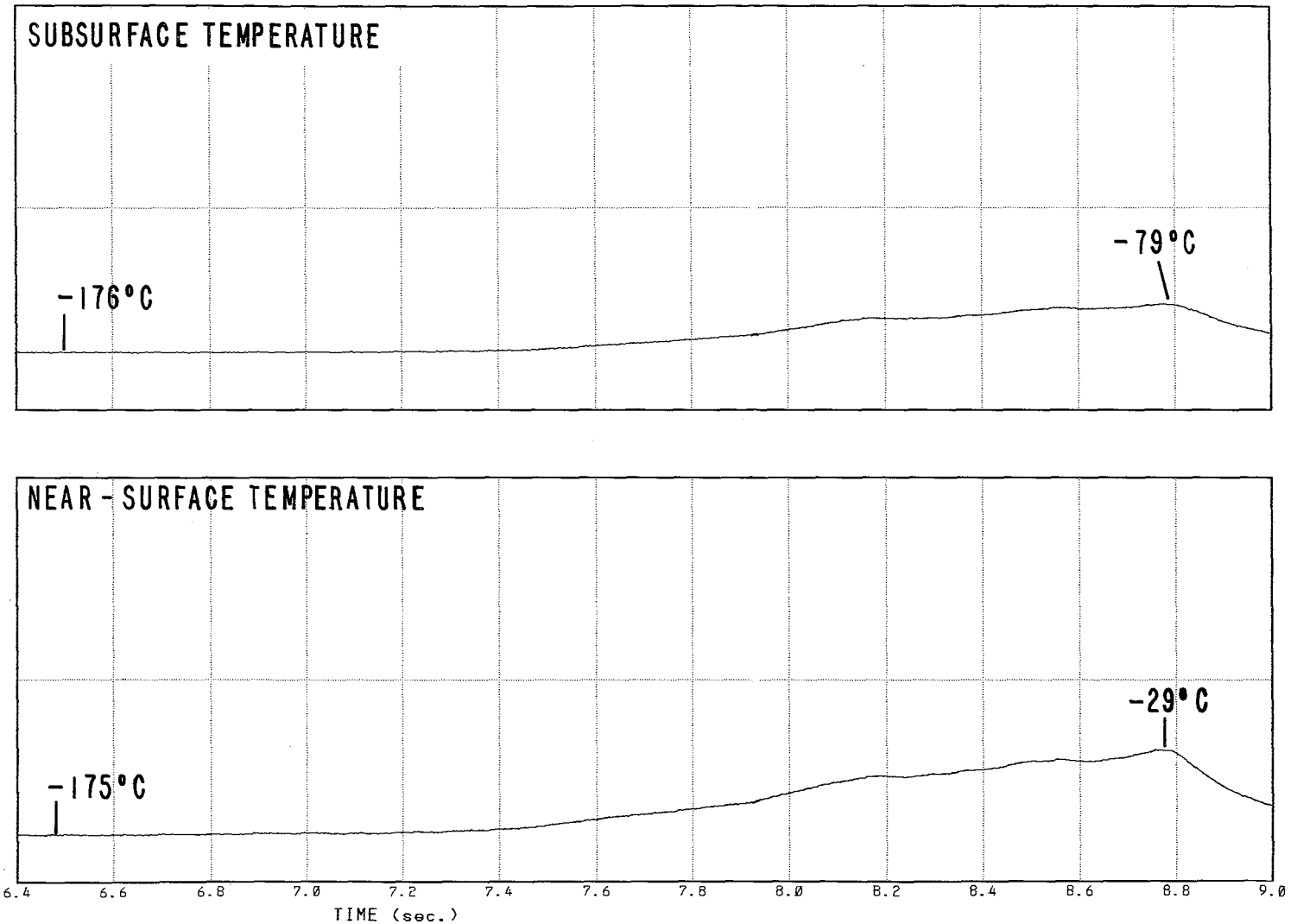

RUB Test : TIAG02

Reduction Date: 30-AUG-84
Test Date: 22-FEB-83

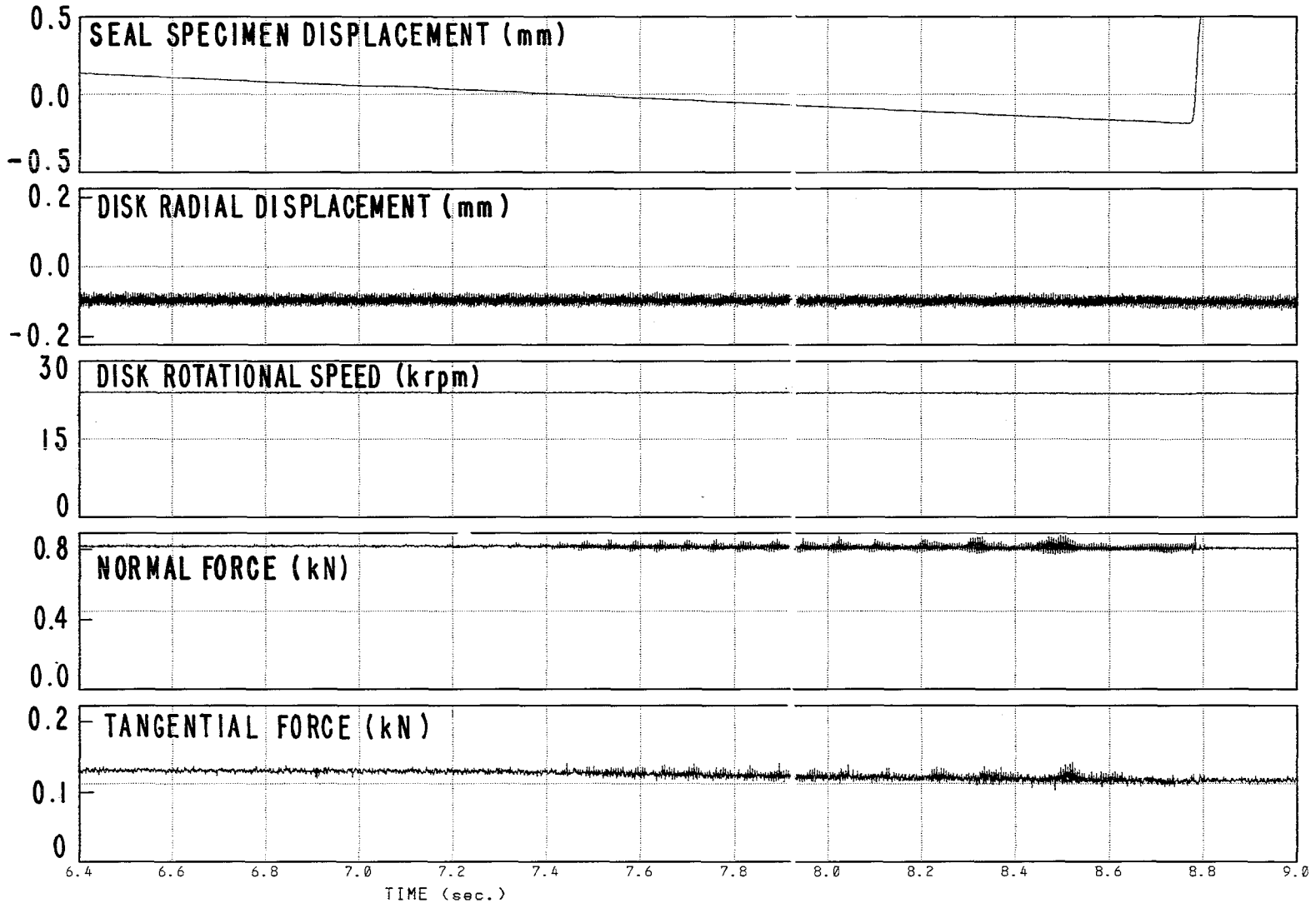

RUB Test : TIAG02

Reduction Date: 30-AUG-84
Test Date: 22-FEB-83

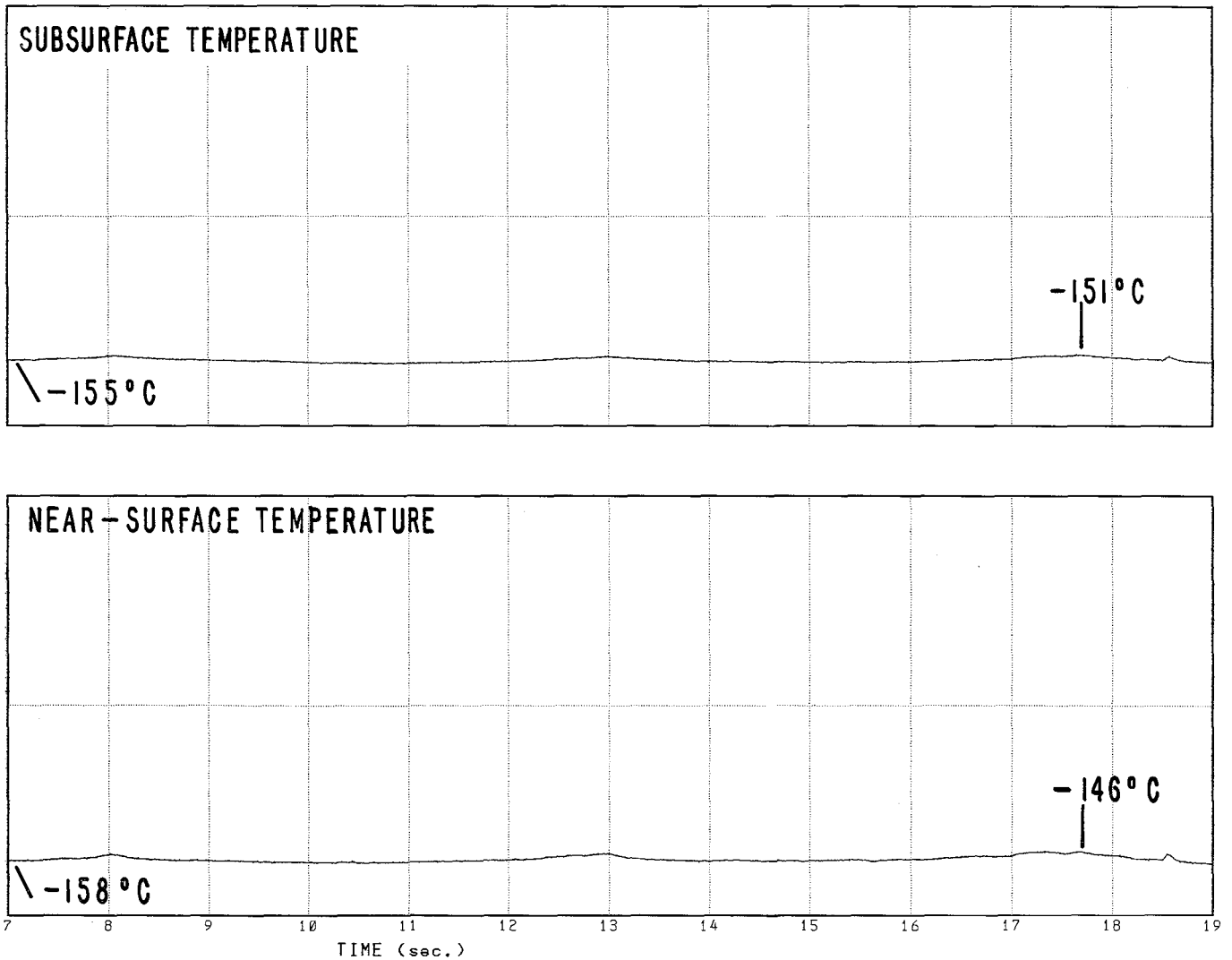

RUB Test : TIAGØ3

Reduction Date: 30-AUG-84
Test Date: 10-FEB-83

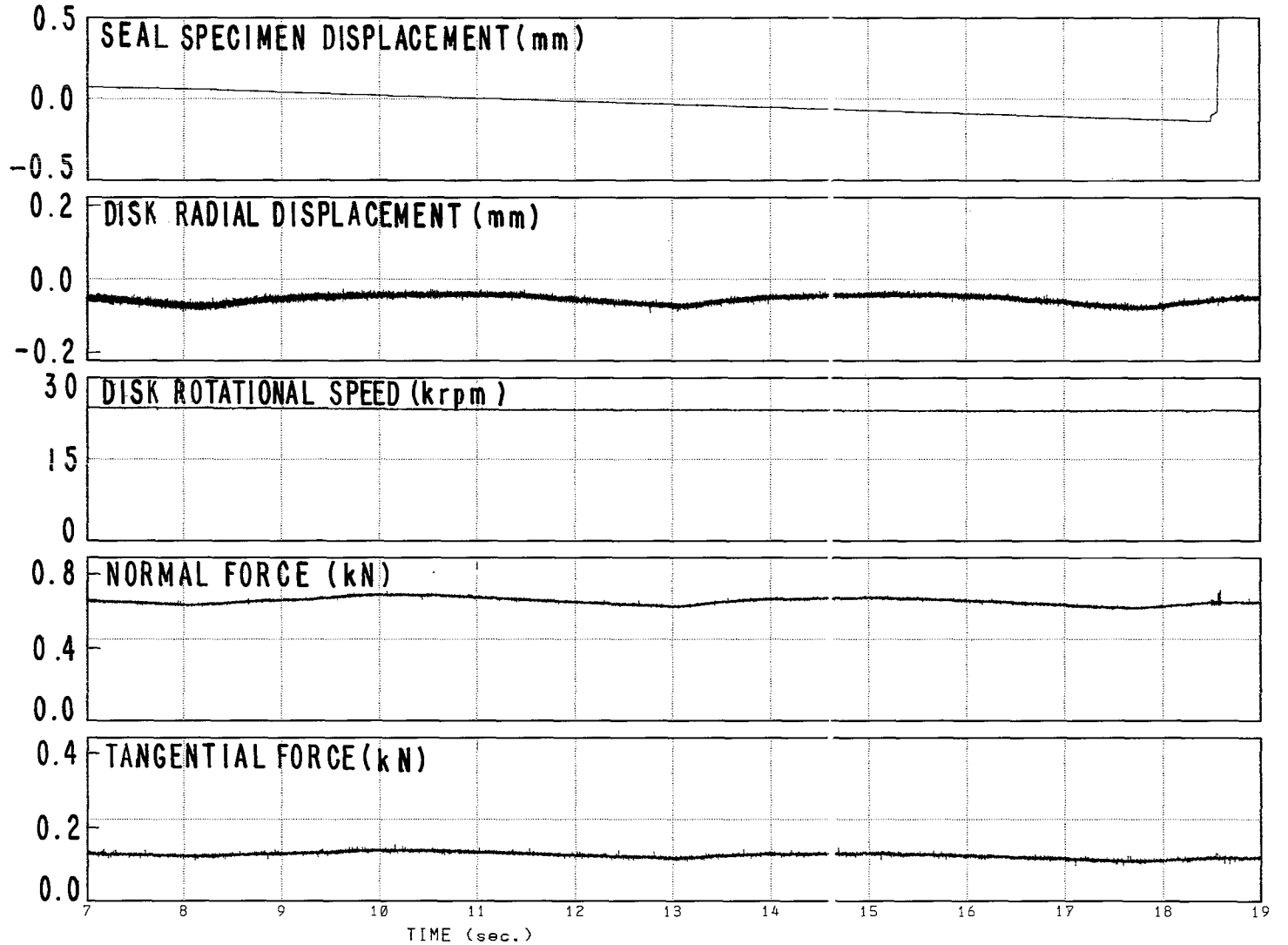

RUB Test : TIAGØ3

Reduction Date: 30-AUG-84
Test Date: 10-FEB-83

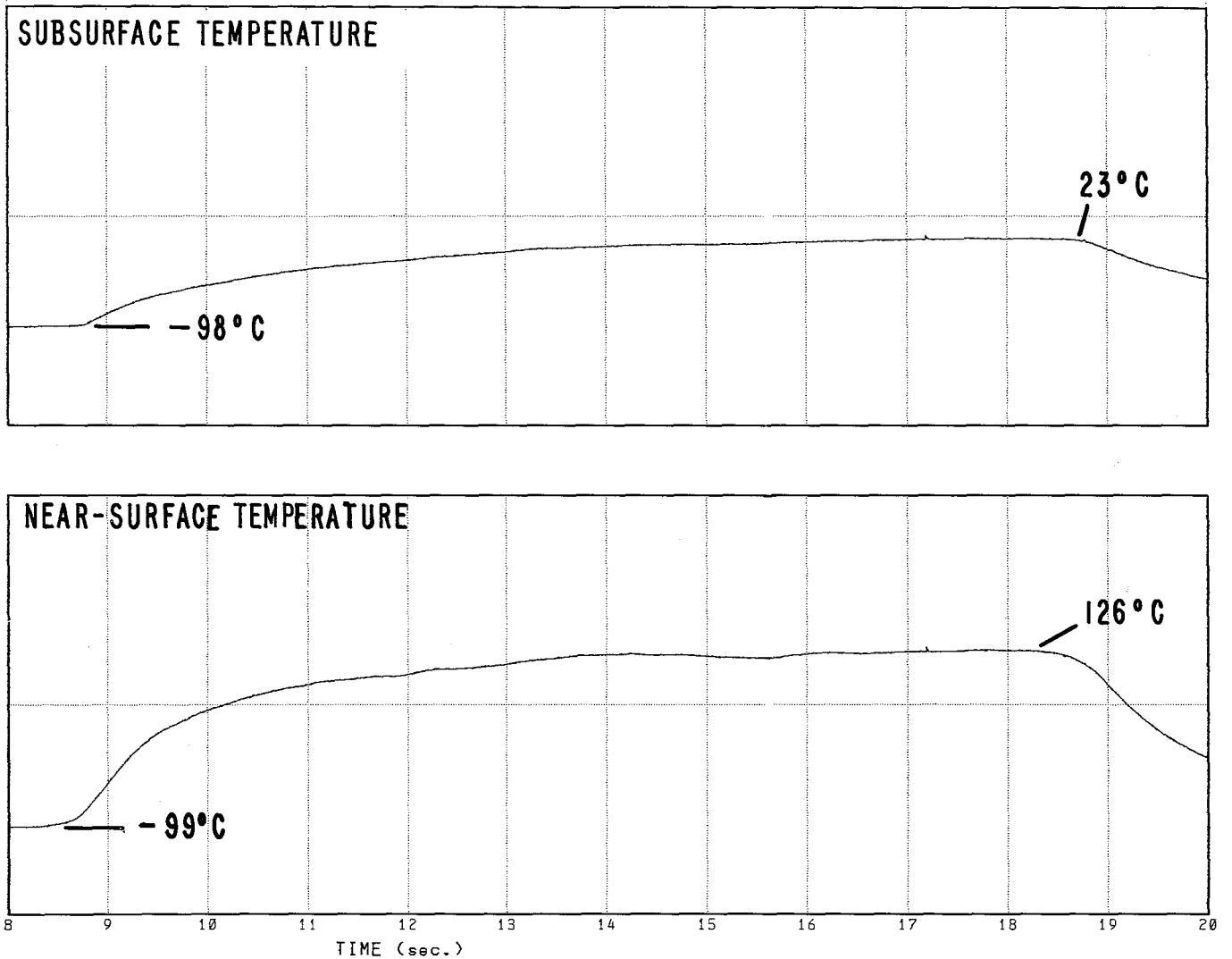

RUB Test : TIYZØ3

Reduction Date: 30-AUG-84
Test Date: 11-FEB-83

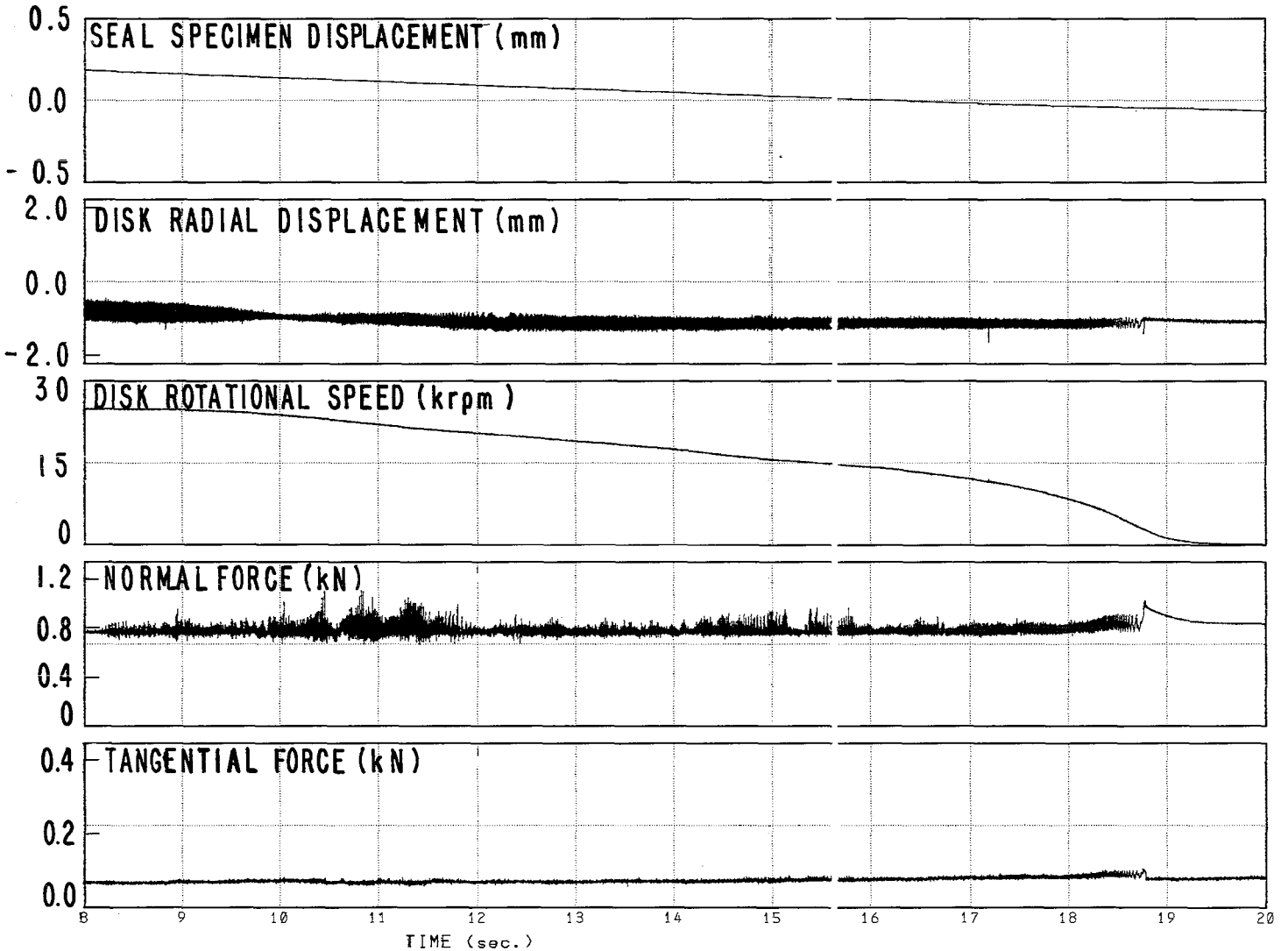

RUB Test : TIYZØ3

Reduction Date: 30-AUG-84
Test Date: 11-FEB-83

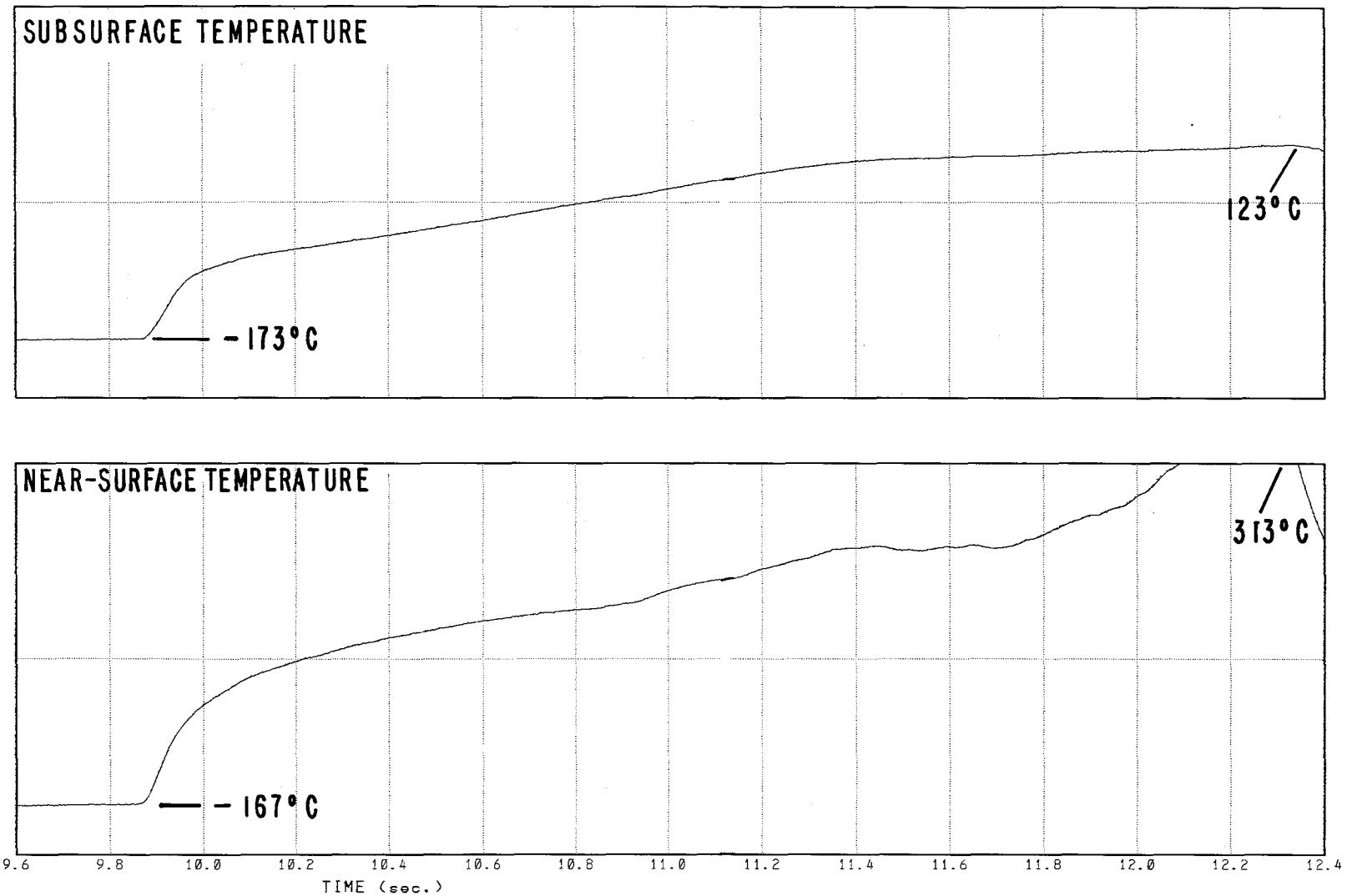

RUB Test : TNAL02

Reduction Date: 31-AUG-84
Test Date: 23-FEB-83

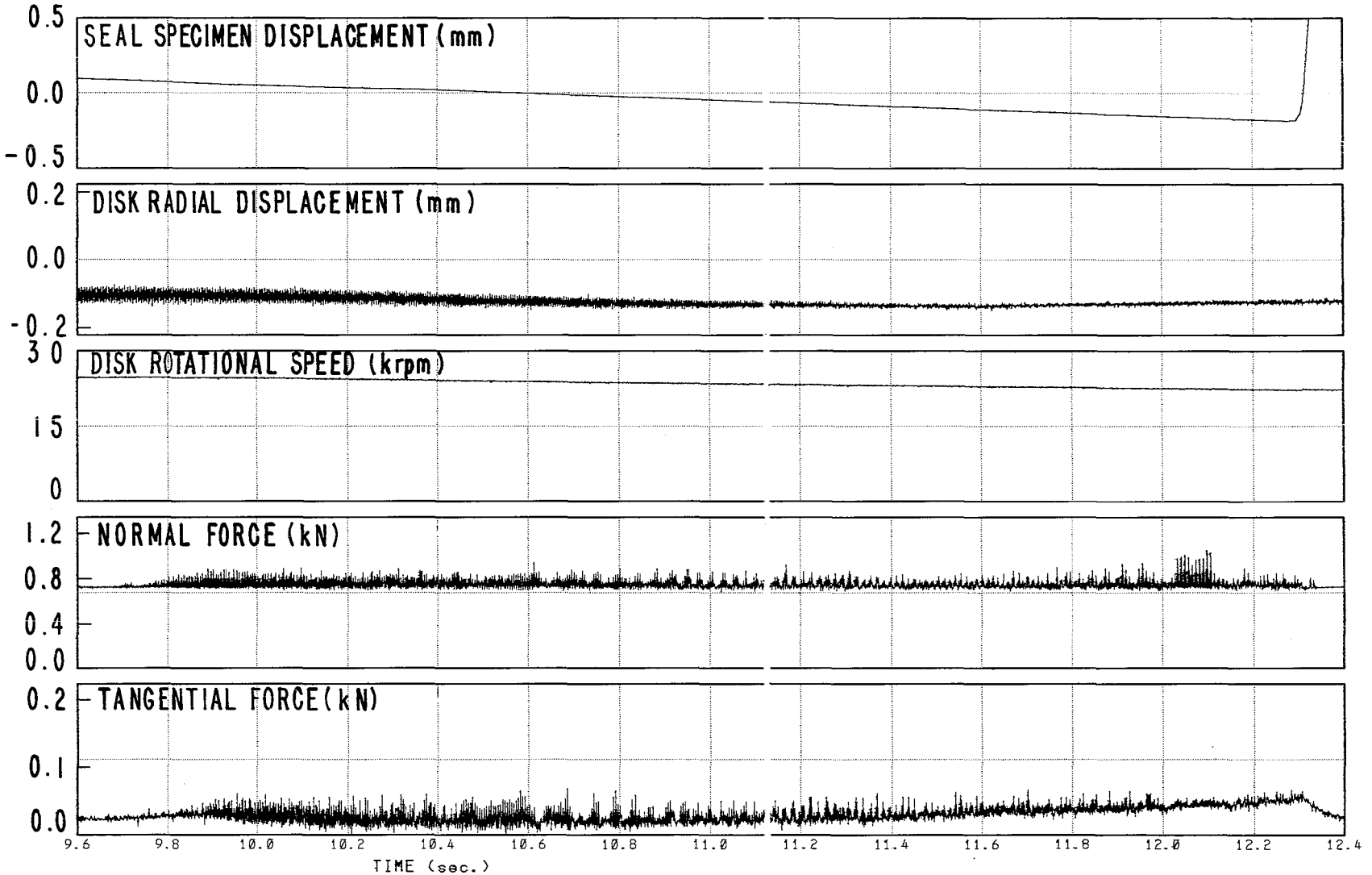

RUB Test : TNAL02

Reduction Date: 30-AUG-84
Test Date: 23-FEB-83

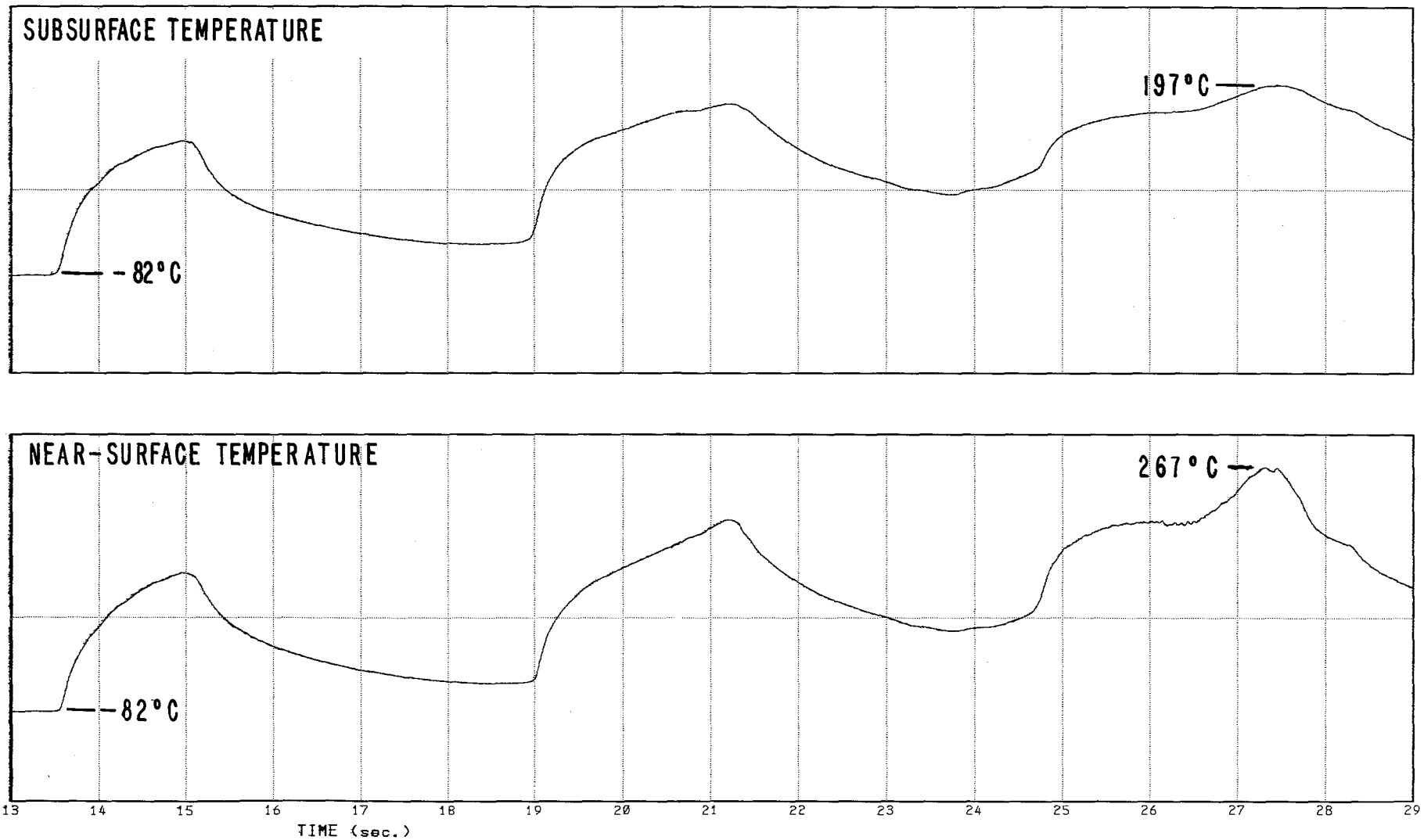

RUB Test : TNAL03

Reduction Date: 30-AUG-84
Test Date: 04-FEB-83

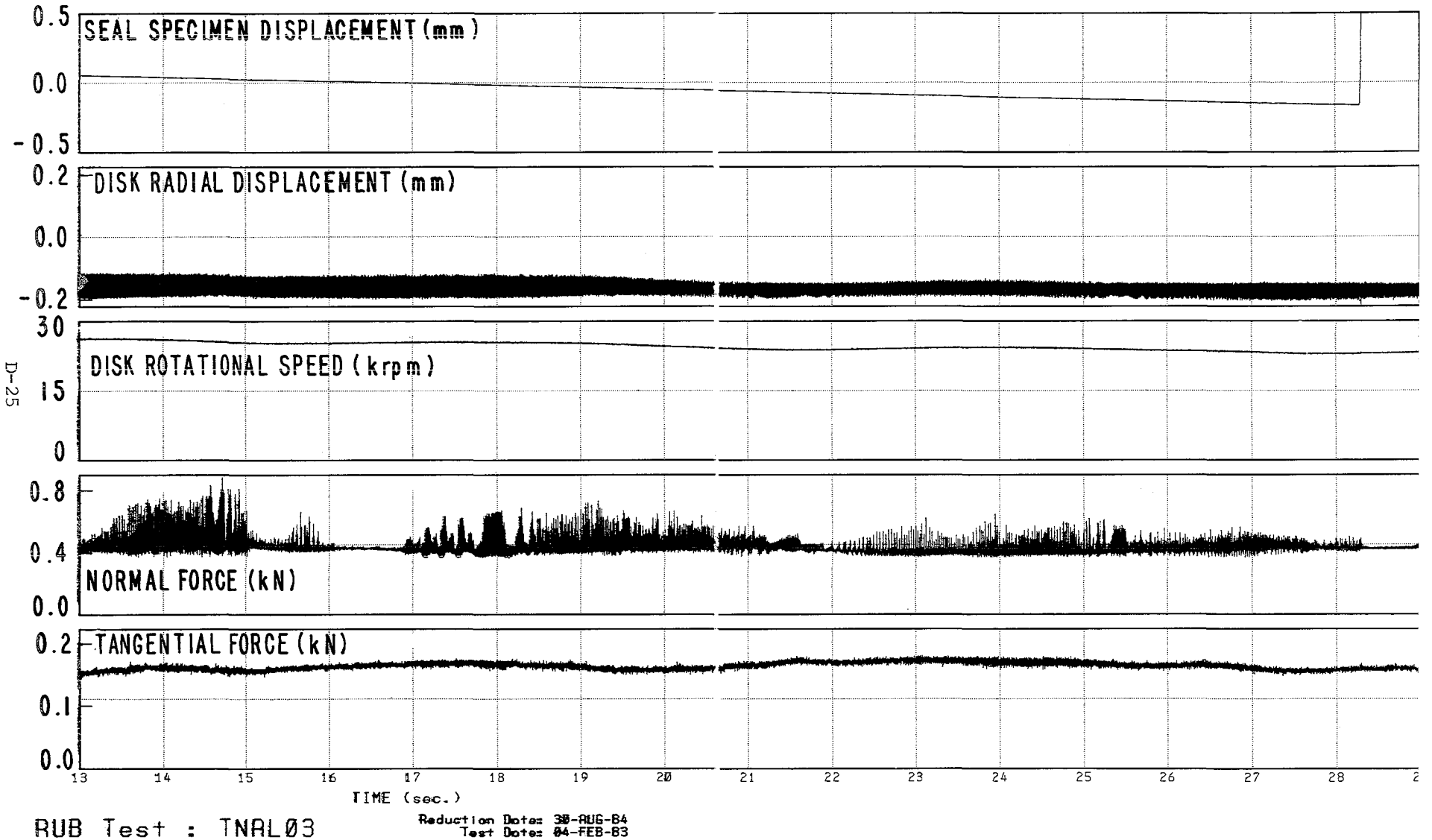

RUB Test : TNRL03

Reduction Date: 30-AUG-84
Test Date: 04-FEB-83

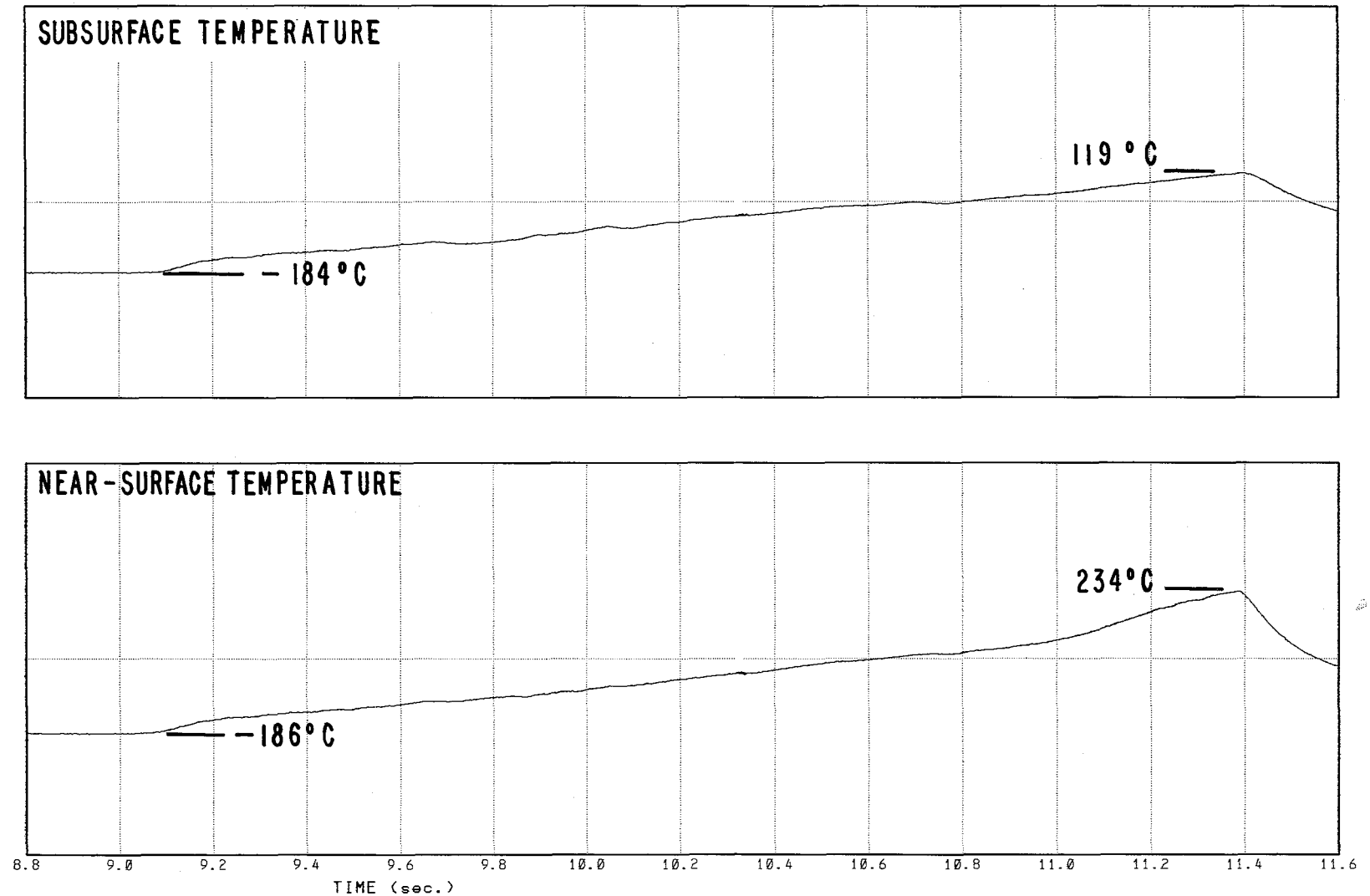

RUB Test : AOAL02

Reduction Date: 30-AUG-84
Test Date: 23-FEB-83

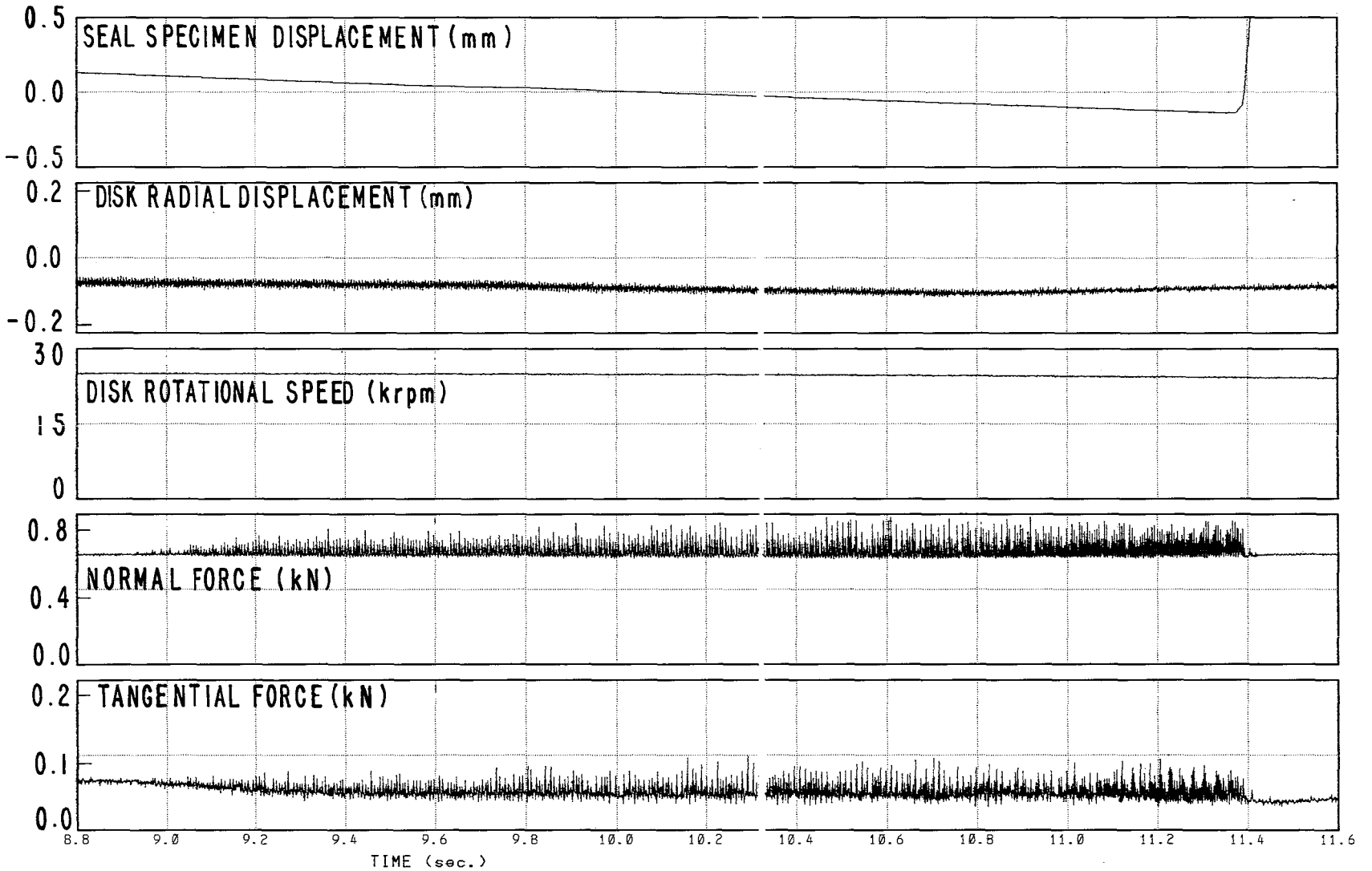

RUB Test : AOAL02

Reduction Date: 30-AUG-84
Test Date: 23-FEB-83

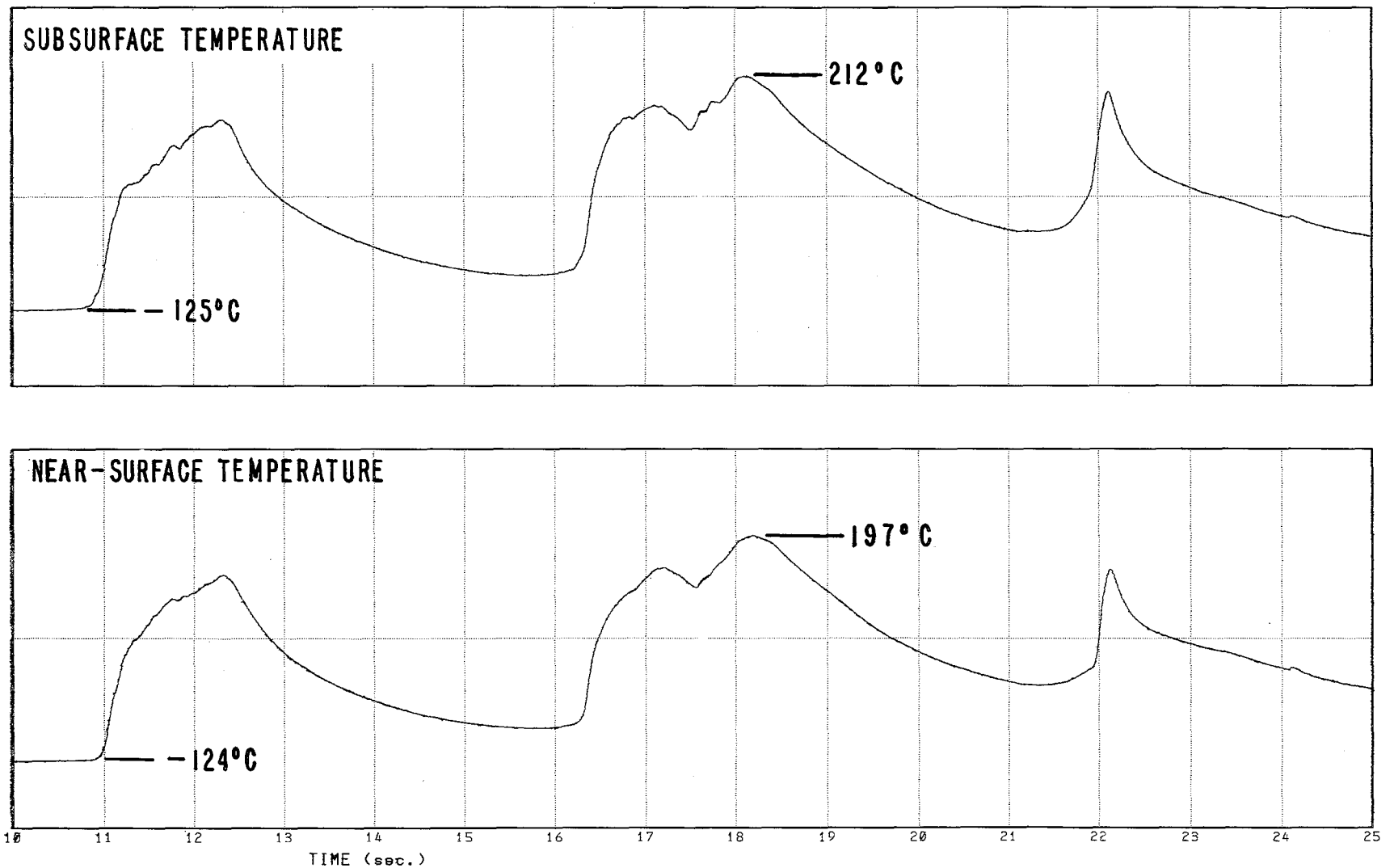

RUB Test : AOAL03

Reduction Date: 30-AUG-84
Test Date: 14-FEB-83

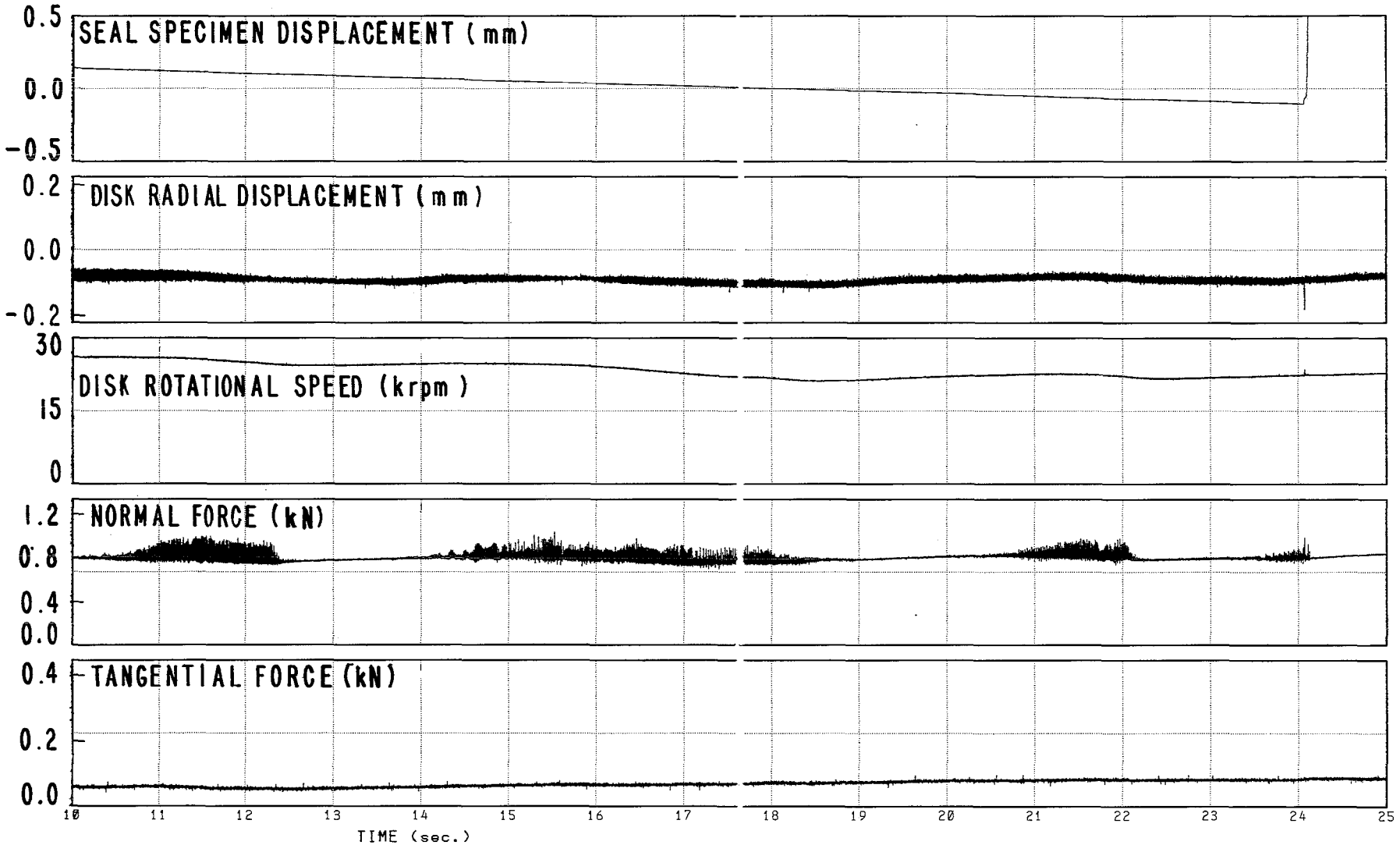

RUB Test : A0AL03

Reduction Date: 30-AUG-84
Test Date: 14-FEB-83

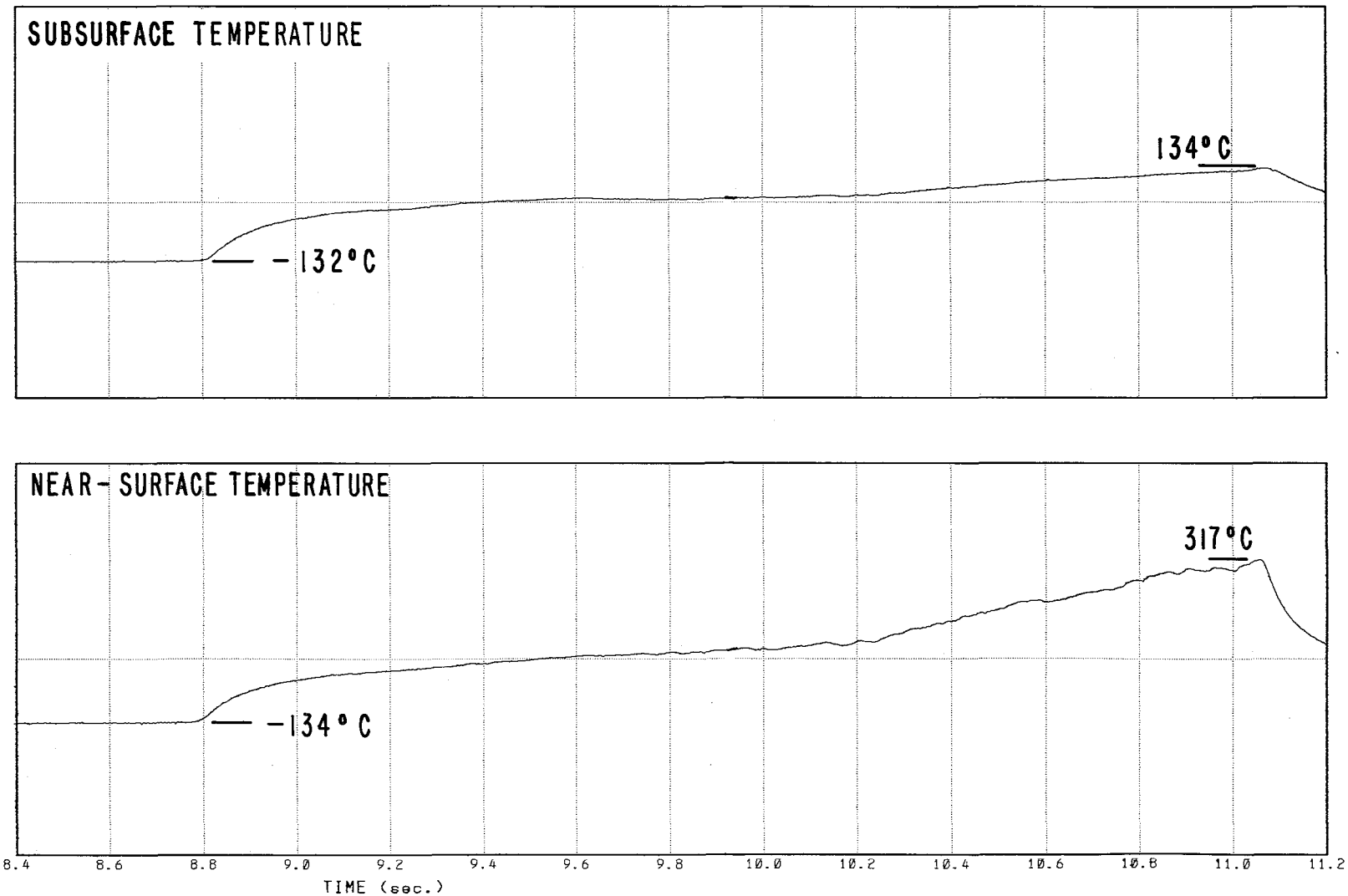

RUB Test : TCAL02

Reduction Date: 30-AUG-84
Test Date: 24-FEB-83

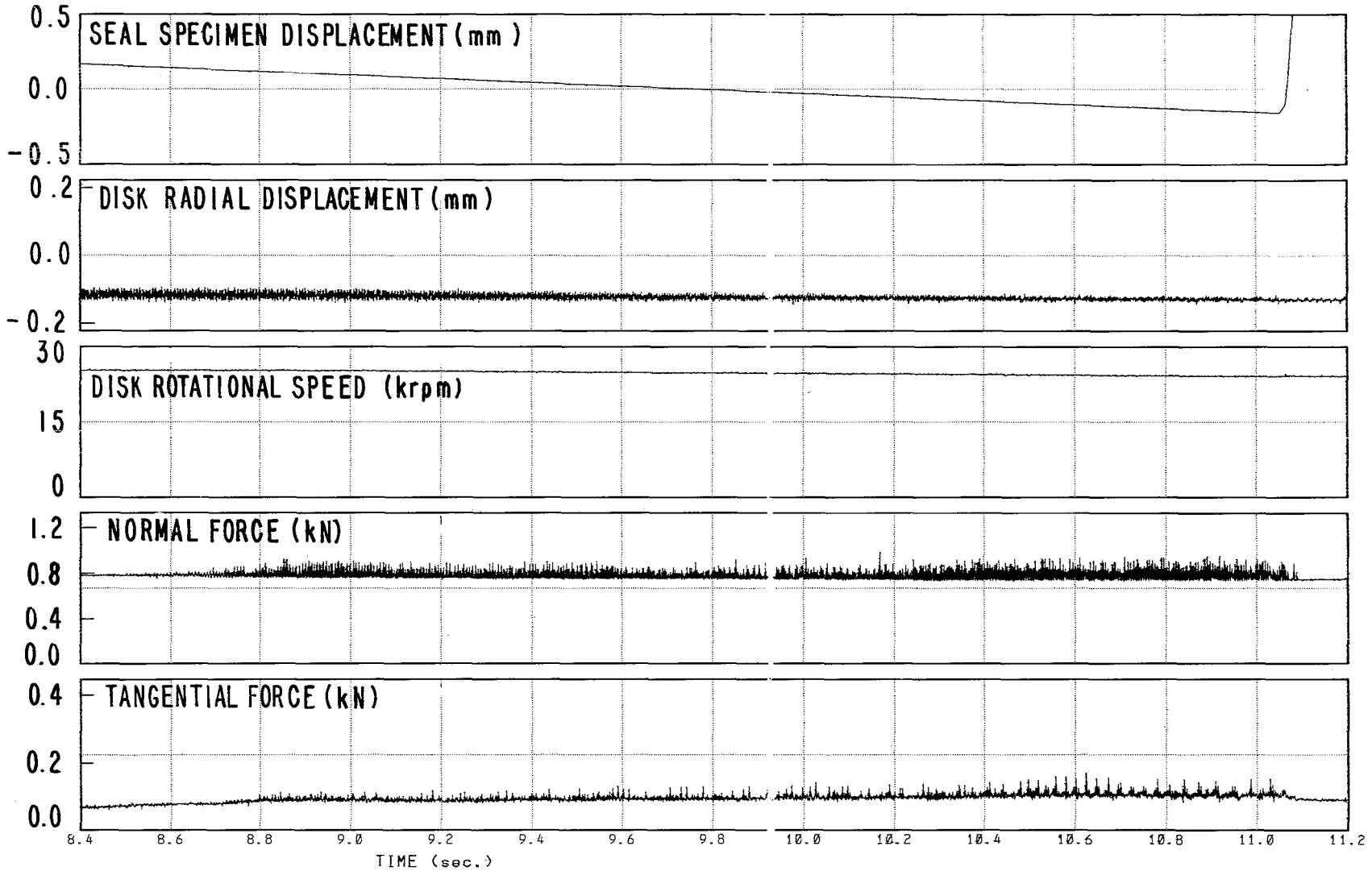

RUB Test : TCAL02

Reduction Date: 30-AUG-84
Test Date: 24-FEB-83

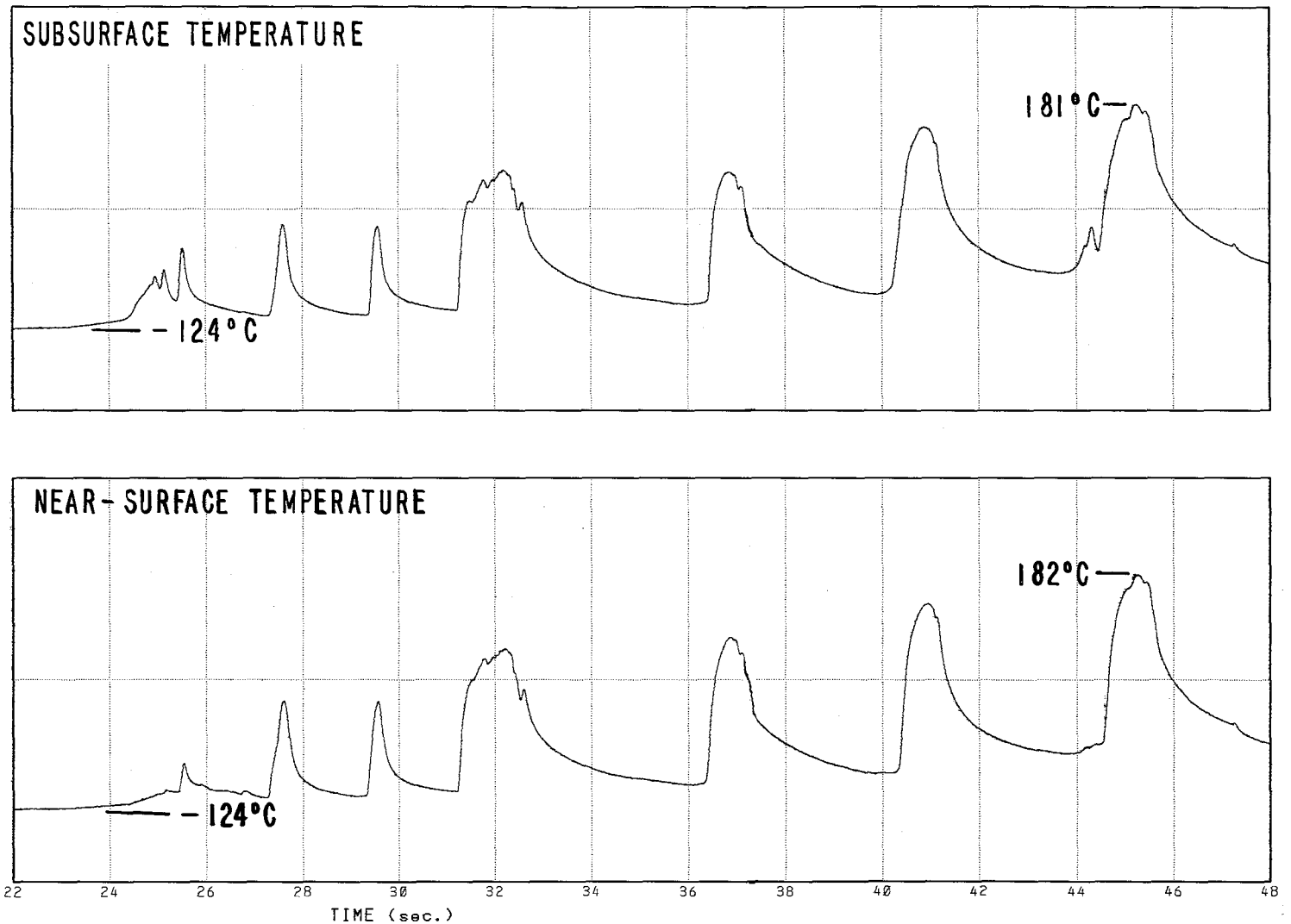

RUB Test : TCALØ3

Reduction Date: 30-AUG-84
Test Date: 14-FEB-83

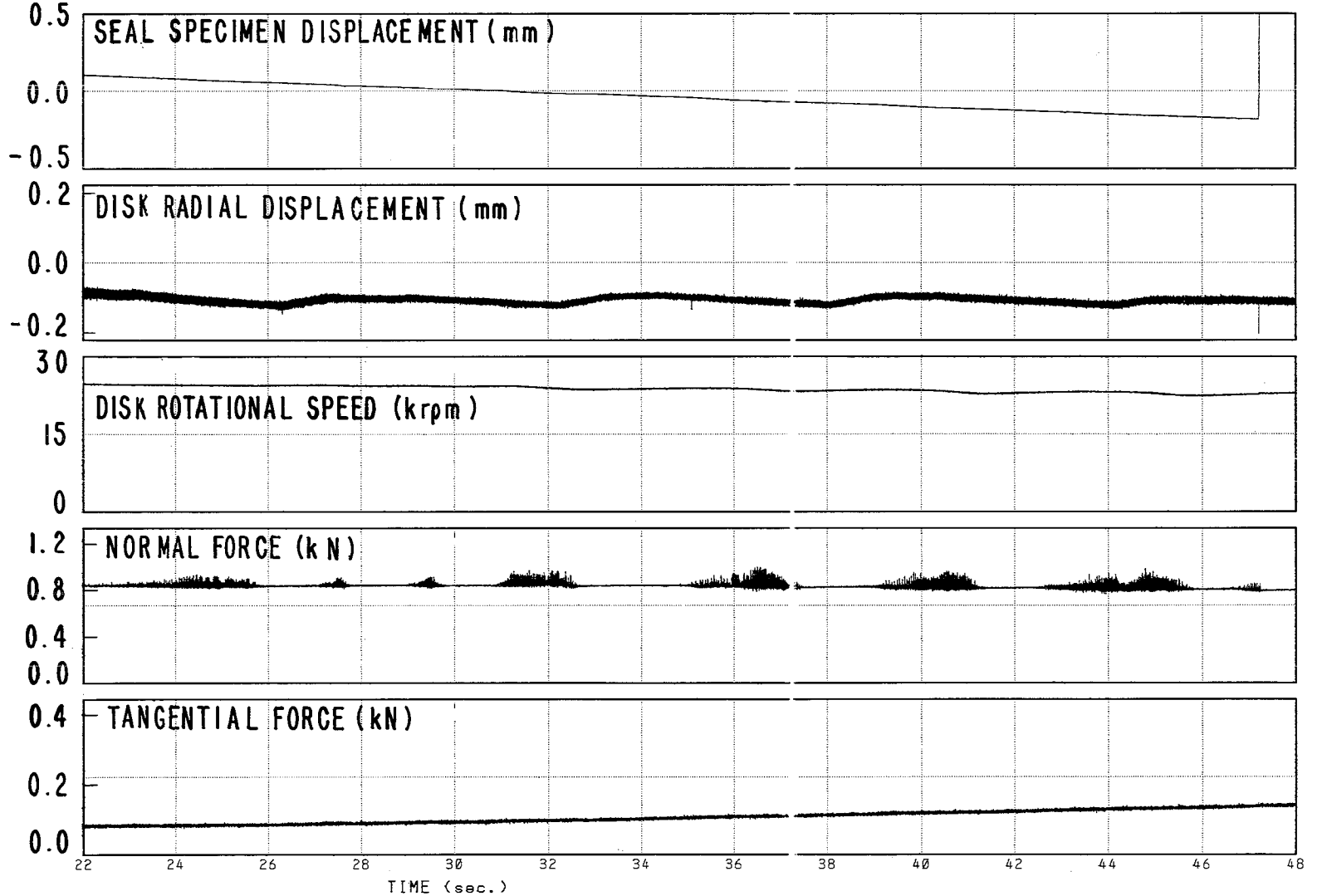

RUB Test : TCAL03

Reduction Date: 30-AUG-84
Test Date: 14-FEB-83

This Page Intentionally Left Blank

APPENDIX E

A METALLURGICAL EXAMINATION OF A Ti-5Al-2.5Sn DISK RUBBED AT -196°C AGAINST AN ALUMINUM PAD

FURTHER OBSERVATIONS OF A Ti-5Al-2.5Sn DISK RUBBED AT -196°C AGAINST AN ALUMINUM PAD

by

E. M. Schulson

A METALLURGICAL EXAMINATION OF A Ti-5Al-2.5Sn DISK RUBBED AT -196°C AGAINST AN ALUMINUM PAD

ABSTRACT

Scanning electron microscopy revealed extensive transfer of aluminum to titanium during the rubbing of a Ti-5Al-2.5 Sn disk at -196°C against a cooled 2024 (T351) aluminum pad. The examination also revealed that the transfer was greater on one side of the disk than on the other. The transfer layer was cracked.

E.1 INTRODUCTION

The purpose of this report is to summarize some observations of rubbing damage incurred by a Ti-5Al-2.5 Sn disk (No. 1) when rubbed at 25,000 rpm at -196°C (-320°F) against a 2024 (T351) aluminum pad cooled to around -112°C (-170°F). The disk and pad were rubbed at Creare (at an interaction rate of 0.025 mm/sec (0.001 in./sec) and were submitted by F. Dolan for examination.

E.2 EXAMINATION PROCEDURE

Observations at magnifications up to 30X were make using a binocular microscope. Observations at higher magnifications (up to 3300X) were made on the disk only, using a scanning electron microscope (SEM) equipped with energy dispersive and wavelength dispersive spectrometers (EDS and WDS). SEM/EDS analyses were performed to estimate chemical compositions and, thus, to determine whether material was transferred from the pad to the disk during the rub.

To facilitate the SEM examinations, four pieces (≅ 1 cm in length) were cut from the peripheral region of the disk at 90°, 180°, 270° and 360° (arbitrary co-ordinate system). One piece was cut from an un-rubbed disk, for reference.

E.3 OBSERVATIONS

E.3.1 Pad

Examination of the pad at 30X revealed extensive ridging (i.e. aluminum build-up) on the non-turbine side of the wear scar, along the full length of the track. On the turbine side, ridging occurred only at the entrance, over a distance of approximately one-quarter of the length of the scar. Curiously, a thin (≅ 0.1 mm) tongue of material (presumed to be aluminum) ≅ 0.3 mm in length, formed at the base of the scar at its entrance. These observations are illustrated in Figure E-1. When coupled with those by Dolan, who noted that the depth of the scar is deeper at the entrance than at the exit, they suggest that the rubbing occurred unevenly.

E.3.2 Disk

Examination of the disk at low magnification (30X) revealed that material transfer had occurred all along the periphery on the turbine side

of the blade near its periphery. Examination at higher magnification, made with the SEM, clearly revealed the transfer layer, Figure E-2. Moreover, they showed that in many places the layer was cracked, mainly in a radial direction, Figure E-3. Furthermore, these observations indicated that part of the transfer layer furthest from the periphery of the disk may have broken off, as suggested by the rough edge parallel to the periphery (heavy arrows, Figure E-3) and by the hairline cracks within the layer and parallel to the rough edge (fine arrows).

On the opposite side of the disk (i.e. opposite the turbine side) clear evidence of material build-up was not seen. Instead, the peripheral region on this side contained dark patches within which superficial cracks appeared, Figure E-4. Unlike the cracks within the transfer layer on the turbine side of the disk, those on the opposite side had the appearance of an incision (Figure E-4b). Moreover, they appeared to have formed within a very thin surface skin of material, so thin that topographical features of the underlying disk were imaged through the "skin", Figure E-5. The last point, when combined with SEM contrast theory, suggests that the skin was less than a fraction of a micron in thickness. As suggested below (Section E.4) the skin is most probably a thin film of aluminum which transferred to the disk during an early stage of the rub.

SEM/EDS analyses revealed that the transfer layer on the turbine side of the disk was rich in aluminum. Titanium was also detected, indicating either that the layer was sufficiently thin ($\cong$ 1 μm) to allow the transmission of X-rays, generated within the underlying disk by the incident electron beam (25 kV), or that the layer was an alloy of titanium and aluminum. Analysis of the thin, dark, cracked regions on the opposite side of the disk revealed titanium and a small amount of aluminum; in this case, the respective X-rays were most probably generated within the underlying disk, and are thus of little use in identifying the film.

Concerning the periphery of the disk per se, striated features running in the direction of the rub were observed, all along the specimens examined, Figure E-6. In addition, pock marks (arrow, Figure F-6a) were noted. Striated features were evident on the periphery of an unrubbed blade, Figure E-6b, due to machining, but pock marks were not. Again, SEM/EDS analysis revealed strong X-ray peaks from aluminum and from titanium, indicating that the transfer of aluminum had occurred and either that this layer, too, was thin enough to allow the penetration of Ti X-rays generated within the disk below, or that alloying had occurred.

E.4 DISCUSSION

A number of questions arise from these observations. Do the cracks within the transfer layer on the turbine side of the disk extend through the layer and into the disk? Is the transfer layer alloyed with titanium? If not, does alloying occur at the layer/disk interface? What is the thickness of the layer? What is the nature of the very thin film on the side of the disk opposite the turbine? How do the cracks arise, and what is the structure (elongated grains? recrystallized grains?) of the transfer layer? And, does material transfer occur all along the periphery of the disk?

Concerning the first question, conclusions cannot be drawn until additional metallography has been performed (now under way) on sections perpendicular to the plane of the disk and the plane of the cracks. Tentatively, however, it appears as though the cracks do not enter the disk. This point is deduced from the fact that the radial cracks terminate where the transfer layer appears to have broken off (Figure E-3). It is also in keeping with the incision-like appearance of the cracks on the opposite side of the disk, if one assumes that the skin is really comprised of aluminum or of an aluminum/aluminum oxide composite.

Regarding the chemistry of the transfer layer and of the layer/disk interfacial region, meaningful comments are not possible until the sections noted in the foregoing paragraph have been prepared and subjected to SEM/EDS analysis. Similarly, good judgements about the thickness of the transfer layer must await such sectioning.

Concerning the thin film, the only possibility that makes any sense is that it is comprised either of aluminum or of an aluminum/Al_2O_3 composite, as alluded to above. The oxide of titanium, formed under ambient conditions prior to rubbing, is relatively thin (< 150 A) and uniform; not patchy as is the skin observed here. Unambiguous identification, however, is not possible at this stage. If ambiguity is unacceptable, then an examination by Auger electron spectroscopy is recommended, preferably using a system which is equipped with an ion gun which can sputter away the first few atomic layers of "dirty" surface material.

That cracks form in the aluminum-rich transfer layer and in the (assumed) aluminum skin may indicate either severe thermal shocks, a rather brittle aluminum-titanium alloy, or both. The globular character of parts of the transfer layers, evident in Figures E-2b and E-3b, suggests that the aluminum may have been molten when undergoing transfer onto the cold disk. If so, then the cracks could have arisen during the sharp quench which followed. To test for this possibility is not easy: examinations of the structure of the layer using transmission electron microscopy would be informative, but, because the layer was probably subsequently rubbed after being deposited, may not provide unambiguous evidence concerning the process of build-up.

Finally, concerning the periphery, there is no reason to suspect that the transfer of aluminum is restricted to localized regions, for it was quite uniform along the sample (albeit small in relation to the circumference of the disk, ≅ 1 cm vs. ≅ 75 cm). Certainty, however, would require examination of the complete periphery; an easy but time-consuming exercise.

E.5 CONCLUSIONS

It is concluded that:

a. During the first trial at -196°C, rubbing occurred more heavily on the turbine side of the disk.
b. During rubbing, aluminum was transferred to the periphery and to the peripheral edges of the disk. Owing to (a), more material transferred to the turbine side of the disk.
c. Cracks formed at localized sites within the transferred material.

FURTHER OBSERVATIONS OF A Ti-5Al-2.5Sn DISK RUBBED AT -196°C AGAINST AN ALUMINUM PAD

This note summarizes some additional observations concerning the transfer of material from the Al pad to the Ti disk. The observations were made to determine whether the radial cracking noted in the transferred layer enters the Ti disk.

The specimen examined was one of the four pieces mentioned earlier. It was mounted on end in epoxy (cold-mounted), and then mechanically polished (to the level of 0.3 μm Al_2O_3) to reveal the Al/Ti interface. To prevent tensile stresses from developing normal to the interface, all polishing was performed in a direction parallel to this interface. Metallographic examination was performed using a Reichert MeF2 metallograph at magnifications up to 1500 times.

Clear views of the transferred layer and disk, together in focus, were not possible, owing to a rounding of the softer transfer material. However, by focusing on the disk and then on the layer the following observations were made:

1. Cracks were not detected within the Ti disk, neither at any point along the Al/Ti interface (approximately 5 mm examined) nor away from the interface. They were seen in the Al transfer layer, Figure E-7.

2. At several points along the interface, the layer had separated from the disk, Figure E-8.

3. The transfer layer is approximately 3 to 4 μm in thickness.

That cracks could not be seen within the disk, but could be detected within the transfer layer, strongly indicates that crack propagation from the layer to the disk did not occur. This point supports the earlier deduction which was based upon the observation that the radial cracks within the transfer layer terminated at points where this layer broke free from the disk.

It is not clear whether the separation at the layer/disk interface occurred during the rub (or immediately afterwards) or during the preparation of the specimen (even though care was taken to avoid such effects). The significant point is that the interface appears to be relatively weak. This point implies that tensile stresses which are induced within the transfer layer ahead of or in the plane of the crack are probably sufficient to promote decohesion. In turn, the decohesion acts as a crack stopping mechanism. Why decohesion occurs so easily cannot be determined without additional work.

In conclusion, the evidence strongly suggests that the cracks which form within a layer of Al transferred from an Al pad to a Ti disk during cold rubbing at -196°C do not propagate into the disk.

(a)

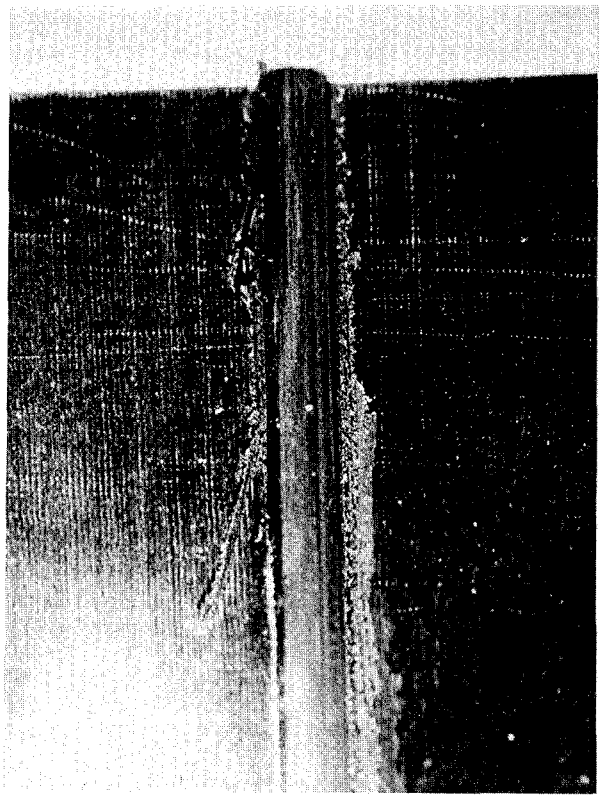

(b)

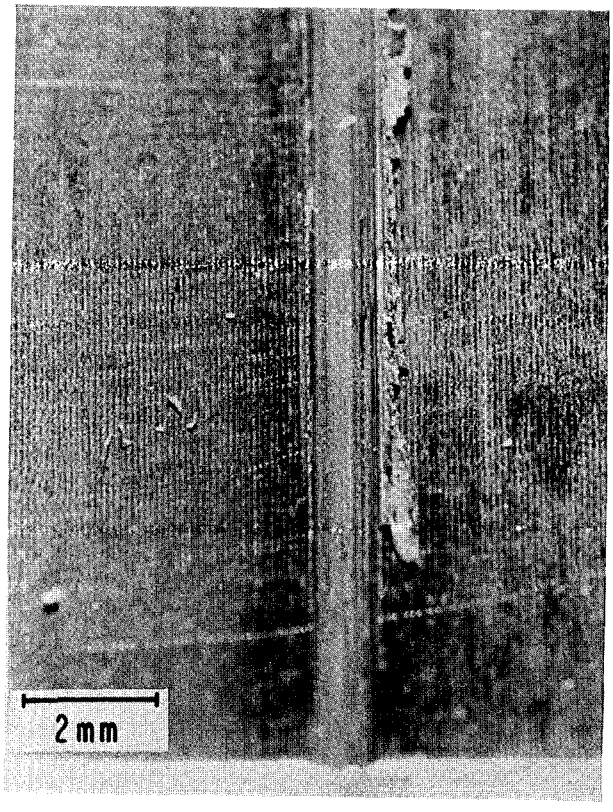

Figure E.1 Optical Macrographs Showing the Wear Scar in an Aluminum (2024 T351) Pad. (a) the entrance to the pad, and (b) the exit.

(a)

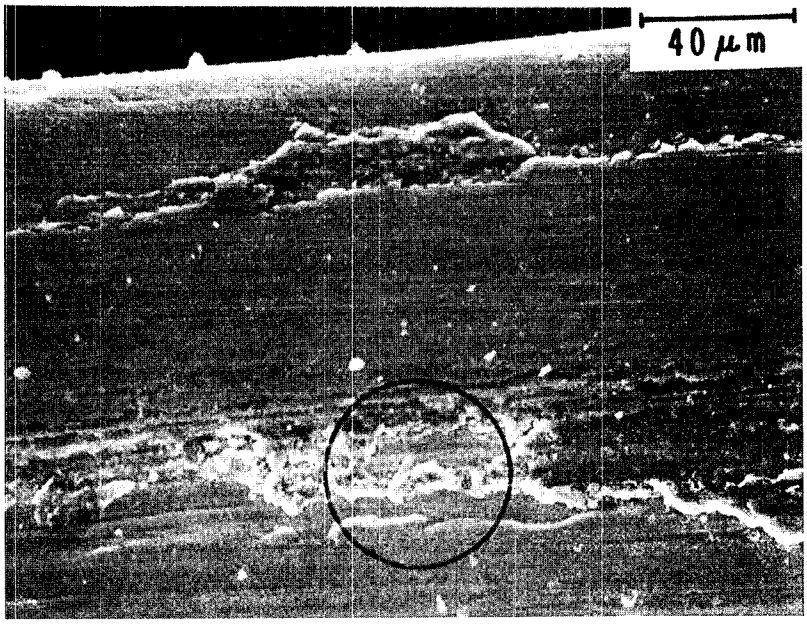

(b)

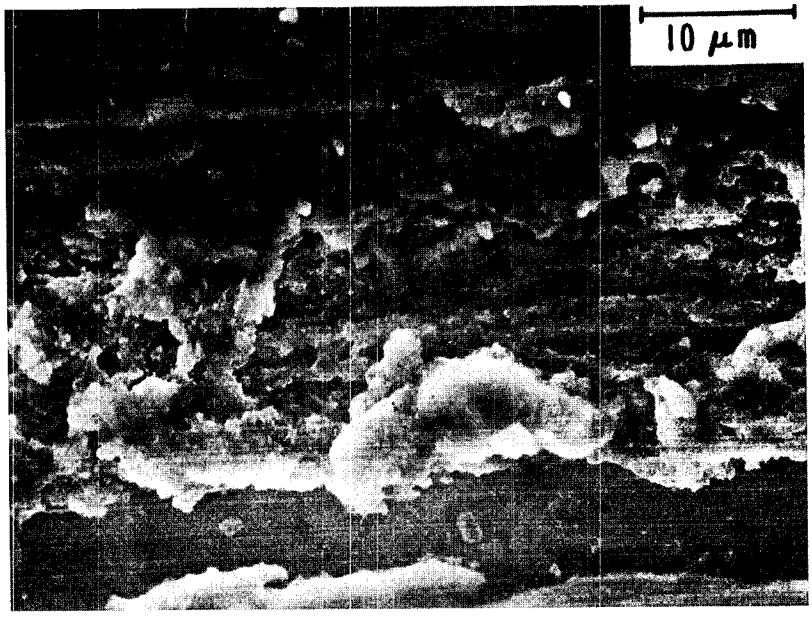

Figure E.2 SEM Micrographs Showing a Transfer Layer on the Turbine Side of the Disk (Periphery of disk at or above top of photo)

(b) higher magnification view of circled region in (a)

(a)

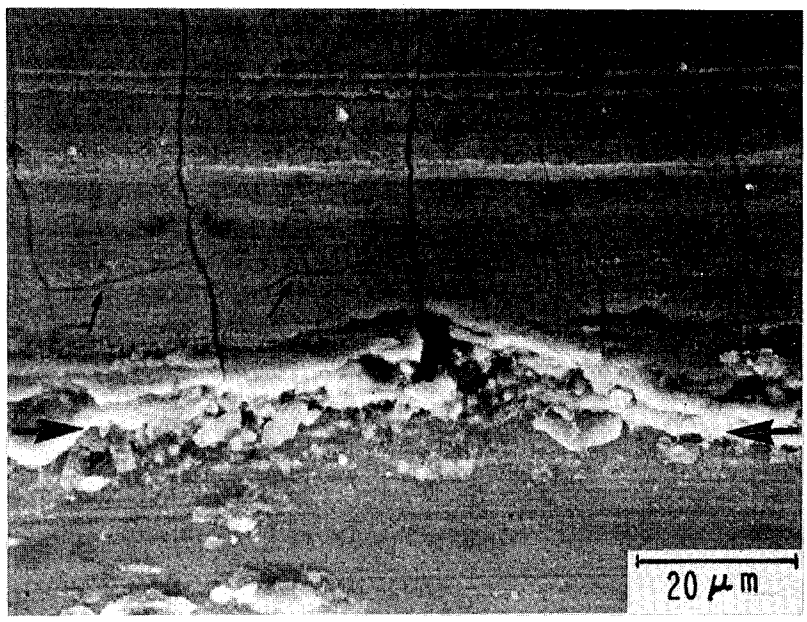

(b)

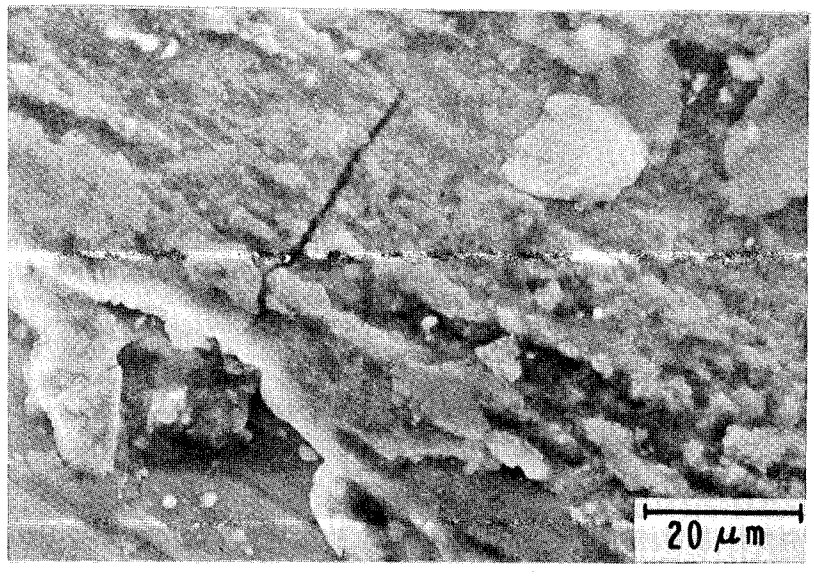

Figure E.3 SEM Micrographs of Transfer Layer on the Turbine Side of Disk Showing Cracks in the Layer. (Two separate locations, about 180° apart, near the periphery of the disk.

(a)

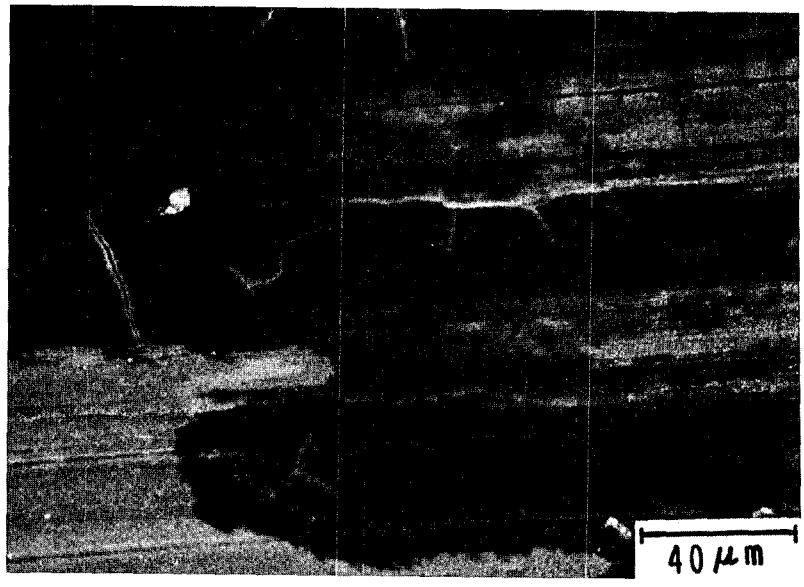

(b)

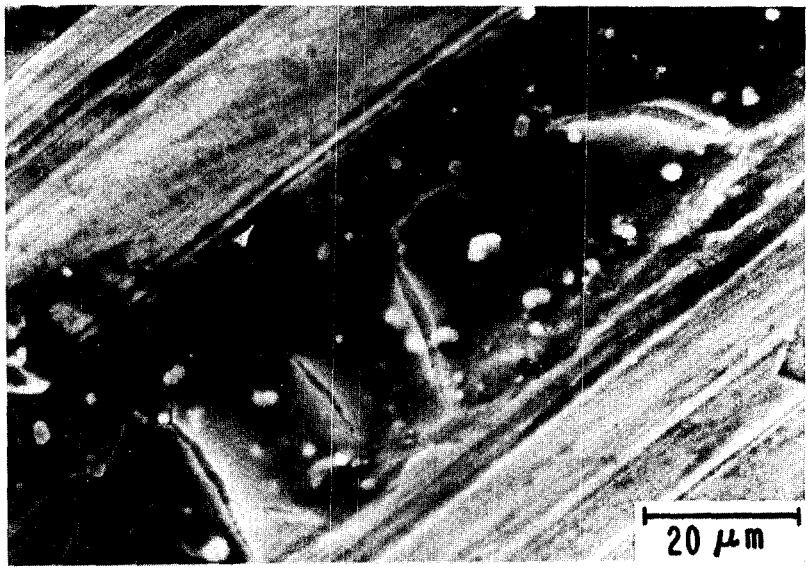

Figure E.4 SEM Micrographs Showing Cracks in Thin Films on the Side of the Disk Opposite the Turbine (Two separate areas)

Figure E.5 SEM Micrograph Showing Incision-Like Crack Within a Thin Film on the Side of the Disk (Note the transparency of the film)

(a)

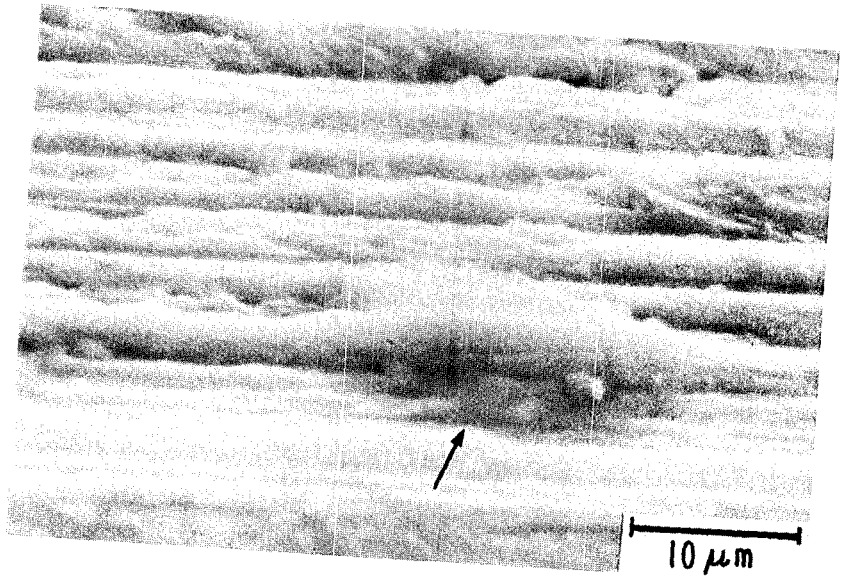

(b)

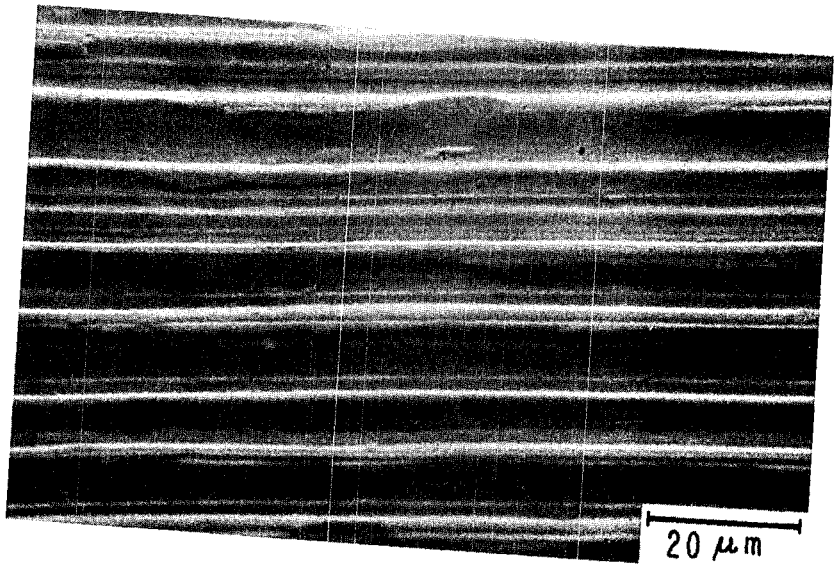

Figure E.6 SEM Micrographs: a) showing the periphery of disk No. 1 after rubbing (2200X) Note the pock mark (arrow); (b) showing the periphery of a disk which was not rubbed (1000X)

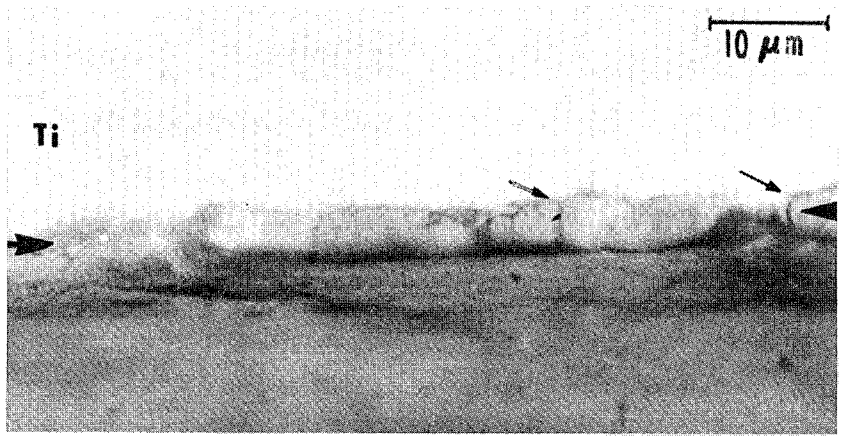

Figure E.7 Optical micrograph showing the interface between an Al (2024) transfer layer and a Ti(5Al-2.5 Sn) disk. Note the cracks (fine arrows) within the transfer layer (heavy arrows).

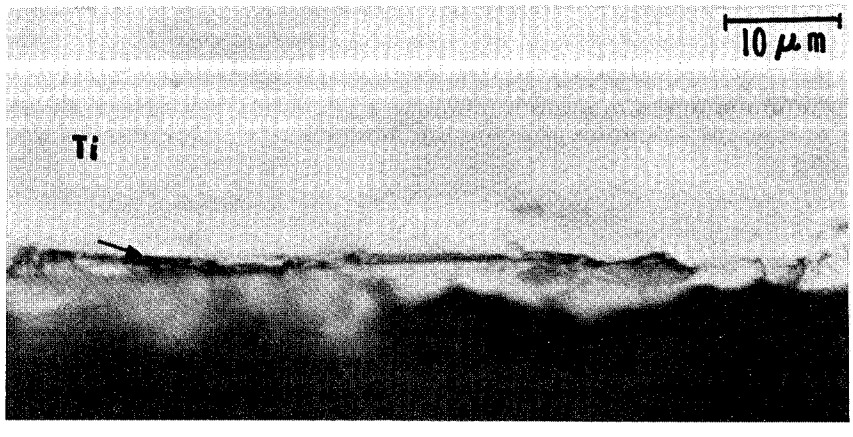

Figure E.8 As Figure E.7 but at a different location along the layer/disk interface. Note the crack (arrow) which lies along the layer/disk interface.

APPENDIX F

SEM PHOTOMICROGRAPHS OF WEAR SPECIMENS

APPENDIX F

SEM Photomicrographs of Wear Specimens

This Appendix contains photographs of the rubbed knife edge and wear ring surfaces taken with a scanning electron microscope. SEM micrographs from 14 of the rub interaction tests are displayed here; photographs of the titanium and aluminum wear surfaces from test TIAL03 are shown separately in Appendix E.

The photographs in this Appendix are grouped to show the mating wear ring and knife edge surfaces from one test as parts (a) and (b) of each figure, respectively. Most figures have views of the wear surfaces at several magnifications and with common magnifications for many of the specimens. A length scale is included on each photograph as an aid to measuring surface features and for comparison of features on different specimens. The test materials, interaction rate and test number are also identified on the figures.

Following is a compilation of brief comments recorded during the examinations of the wear components. The dominant feature observed is the evidence of melting of the aluminum and copper wear surfaces, indicative of high surface temperatures during the rubs. Also, the aluminum/silicon/graphite composite wear ring surface appeared to be least damaged as a result of the rub interaction tests.

Summary of Comments from SEM Examination of Wear Components

Test	Comments
TIAL02	• wear scar filled with tiny cracks transverse to rub direction • evidence of melting on pad and disk
TIAL13	• wear scar filled with "mud flat" type cracks • evidence of melting • smearing on pad and disk
TIAL23	• cracks in scar but fewer than TIAL12 and TIAL02 • again melting and smearing on pad and disk
TIAL04	• found no cracks in scar • smearing on pad and disk • evidence of melting on pad and disk
TICU03	• cracks in scar • evidence of melting in scar • smearing on disk
TIAG02	• clean scar, but smeared; no ridges along edge • titanium transferred to pad (determined from SEM/EDS)
TIAG03	• similar to TIAG02 (no SEM/EDS)
TIYZ03	• pad badly cracked • deposit, presumed to be YSZ at one position on circumference of disk (see Figure 4-9)
TNAL02	• cracks in scar • evidence of solidified metal droplets on pad and disk; smeared droplets
TNAL03	• crack in base of scar; smearing but fewer than TNAL02 • again evidence of melting on pad and disk
AOAL02	• melting and smearing on pad and disk • cracks on disk
AOAL03	• cracks in scar on pad • melting and smearing on pad and disk
TCAL02	• cracks in scar • flaky and cracked ridge along edge of scar • melting and smearing on pad and disk
TCAL03	• no cracks found in scar • melting and smearing • aluminum transfer to disk (determined from SEM/EDS)

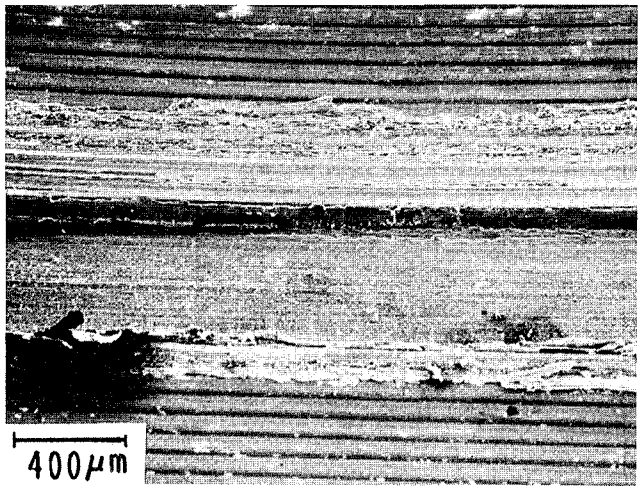

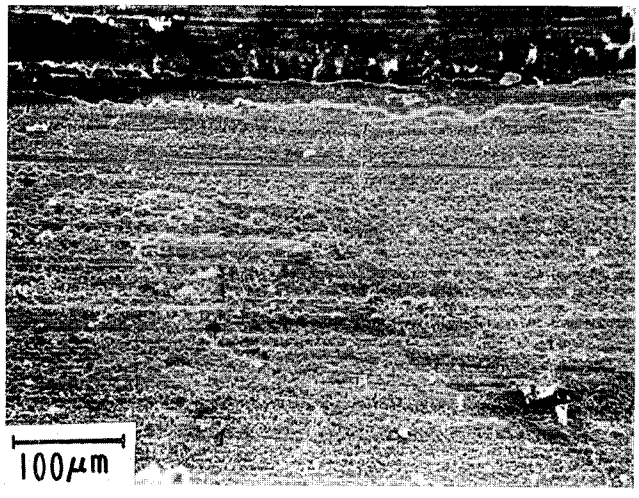

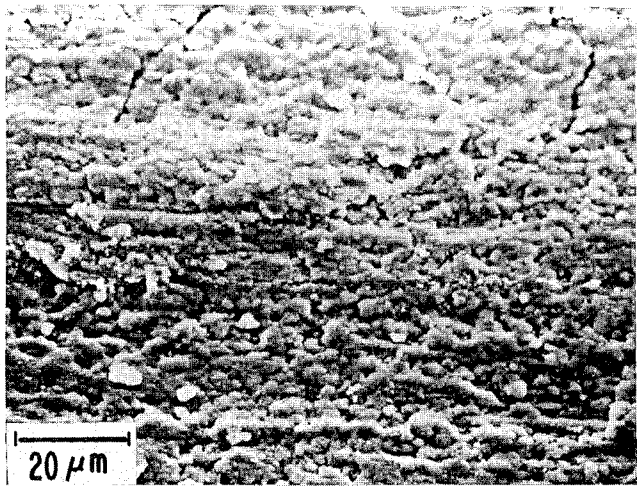

WEAR RING MATERIAL:
2024-T351 ALUMINUM

KNIFE EDGE MATERIAL:
Ti-5Al-2.5Sn ALLOY, ANNEALED

INTERACTION RATE:
1.3×10^{-1} mm/sec

FIGURE F-1a. SEM MICROGRAPH OF WEAR RING SURFACE
TEST NO. TIAL02

WEAR RING MATERIAL:
2024T351 ALUMINUM

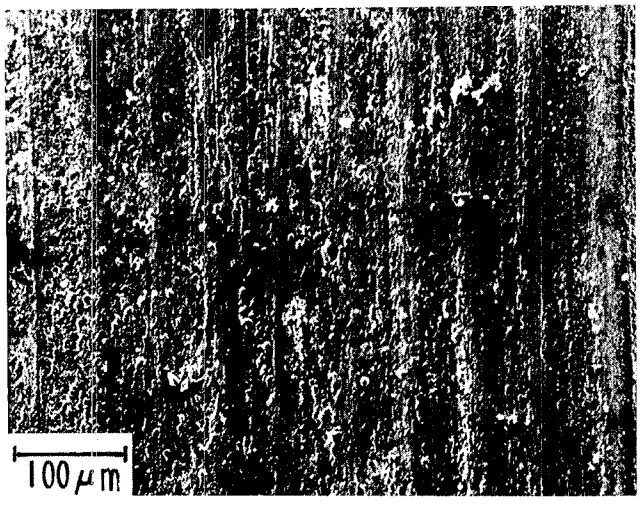

KNIFE EDGE MATERIAL:
Ti-5Al-2.5Sn ALLOY, ANNEALED

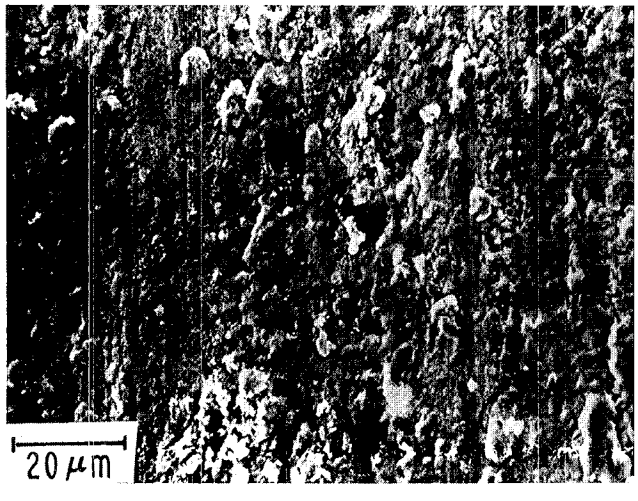

INTERACTION RATE:
1.3×10^{-1} mm/sec

FIGUREF-1b. SEM MICROGRAPH OF KNIFE EDGE SURFACE
TEST NO. TIAL02

WEAR RING MATERIAL:
2024T351 ALUMINUM

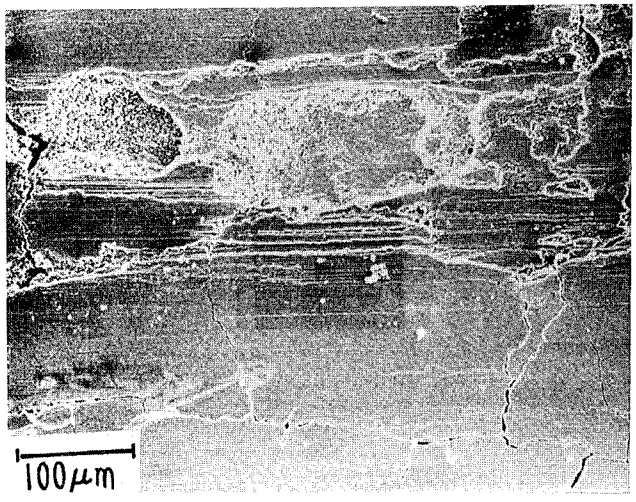

KNIFE EDGE MATERIAL:
Ti-5Al-2.5Sn ALLOY, ANNEALED

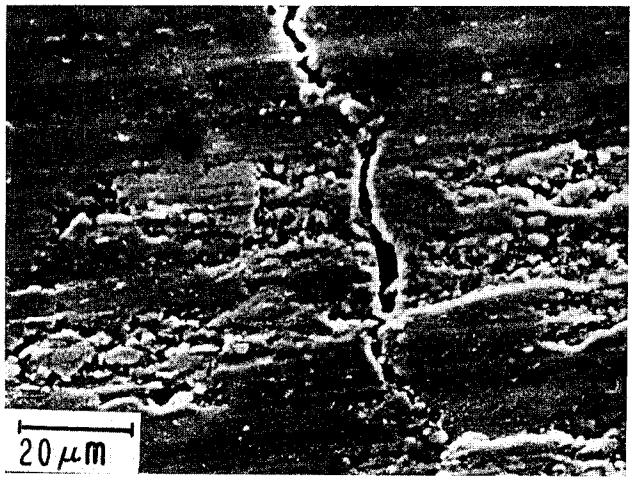

INTERACTION RATE:
0.99×10^{-2} mm/sec

FIGUREF-2a. SEM MICROGRAPH OF WEAR RING SURFACE
TEST NO. TIAL13

WEAR RING MATERIAL:
2024T351 ALUMINUM

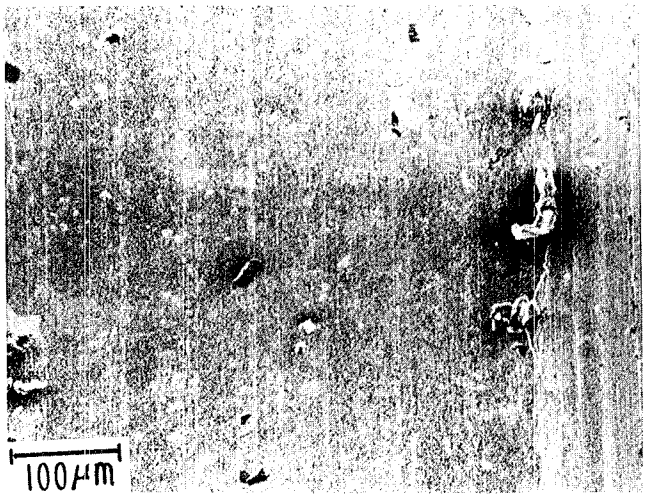

KNIFE EDGE MATERIAL:
Ti - 5Al - 2.5Sn ALLOY, ANNEALED

INTERACTION RATE:
0.99×10^{-2} mm/sec

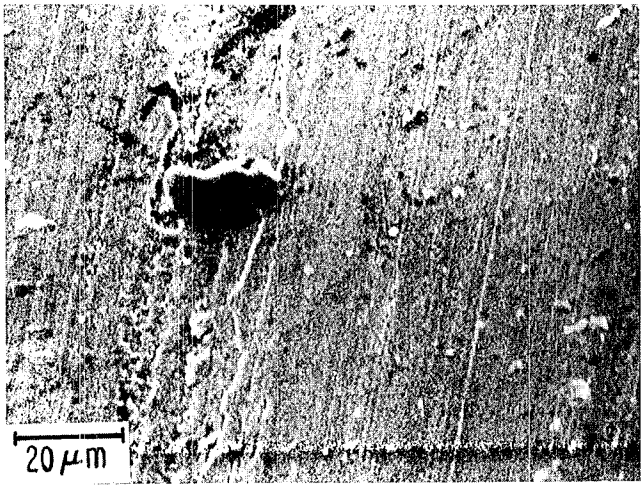

FIGURE F-2b. SEM MICROGRAPH OF KNIFE EDGE SURFACE
TEST NO. TIAL13

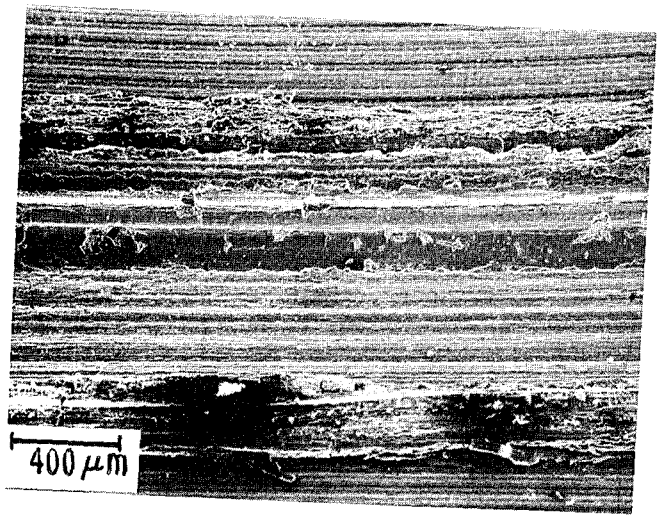

WEAR RING MATERIAL:
2024 T351 ALUMINUM

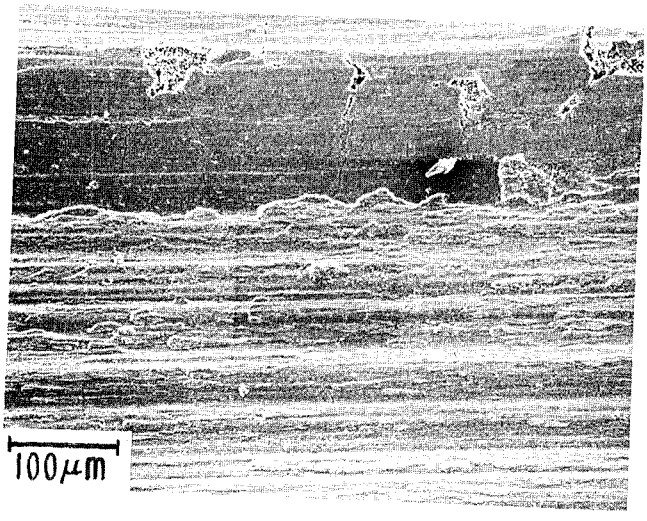

KNIFE EDGE MATERIAL:
Ti-5Al-2.5Sn ALLOY, ANNEALED

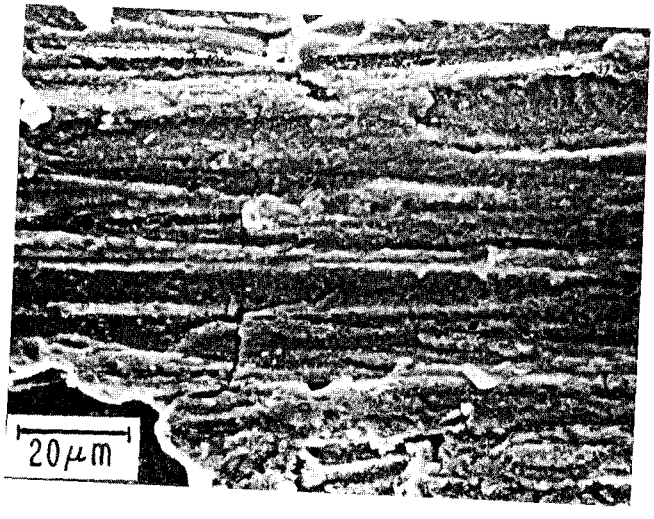

INTERACTION RATE:
1.09×10^{-2} mm/sec

FIGURE F-3a. SEM MICROGRAPH OF WEAR RING SURFACE
TEST NO. TIAL23

WEAR RING MATERIAL:
2024T351 ALUMINUM

KNIFE EDGE MATERIAL:
Ti-5Al-2.5Sn ALLOY, ANNEALED

INTERACTION RATE:
1.09×10^{-2} mm/sec

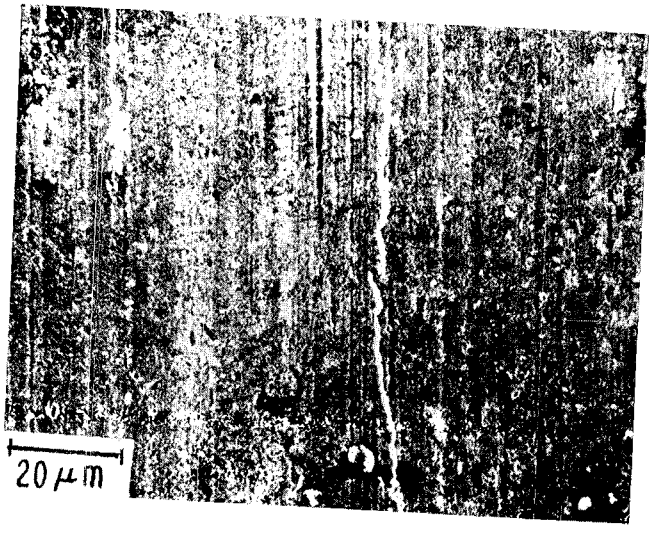

FIGURE F-3b. SEM MICROGRAPH OF KNIFE EDGE SURFACE
TEST NO. TIAL23

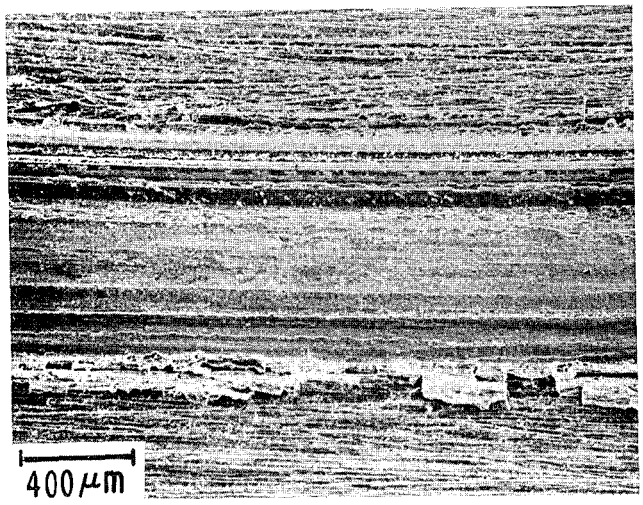

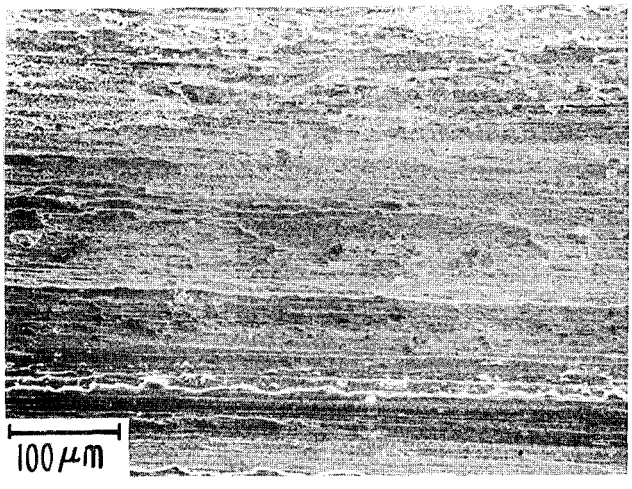

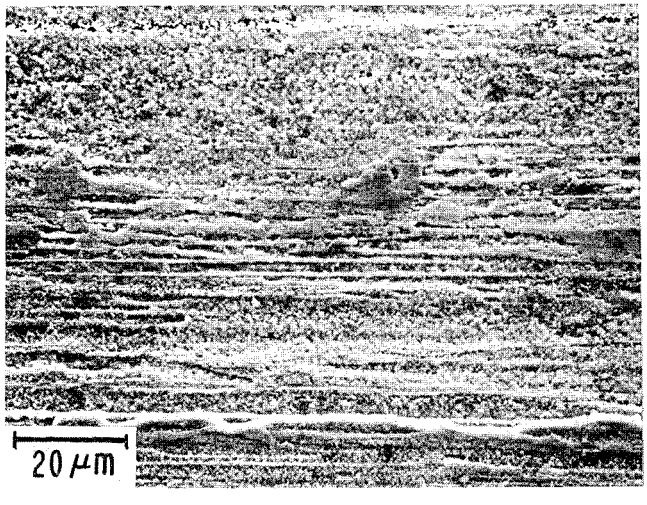

WEAR RING MATERIAL:
2024 T351 ALUMINUM

KNIFE EDGE MATERIAL:
Ti-5Al-2.5Sn ALLOY, ANNEALED

INTERACTION RATE:
1.65×10^{-3} mm/sec

FIGURE F-4a. SEM MICROGRAPH OF WEAR RING SURFACE
TEST NO. TIAL04

WEAR RING MATERIAL:
2024 T351 ALUMINUM

KNIFE EDGE MATERIAL:
Ti-5Al-2.5 Sn ALLOY, ANNEALED

INTERACTION RATE:
1.65×10^{-3} mm/sec

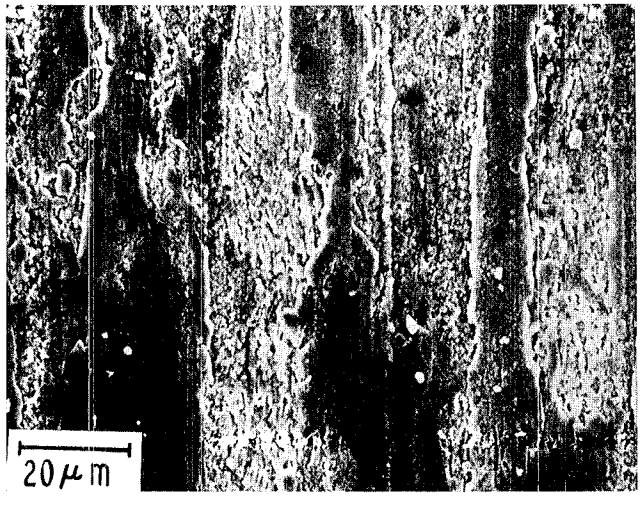

FIGURE F-4b. SEM MICROGRAPH OF KNIFE EDGE SURFACE
TEST NO. TIAL04

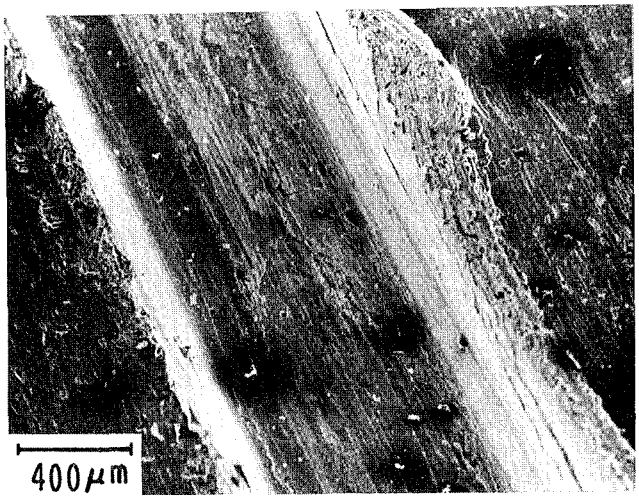

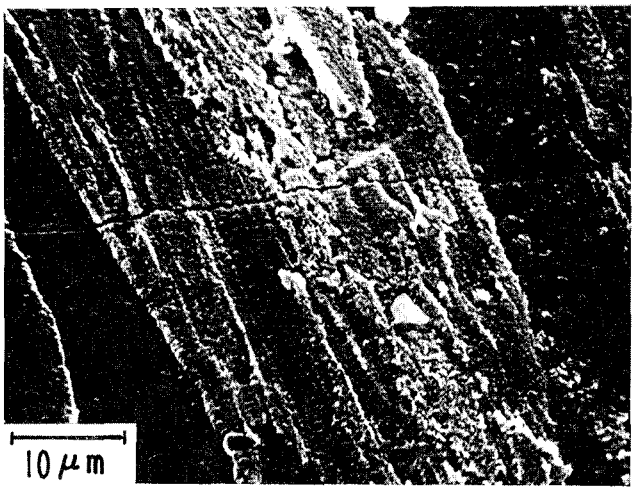

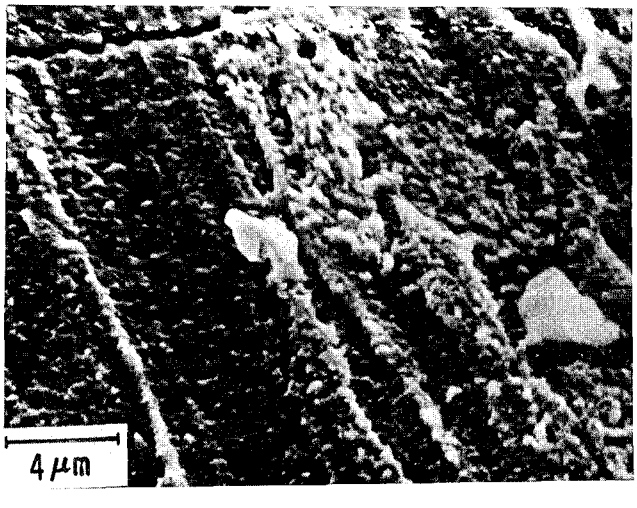

WEAR RING MATERIAL:
99.99% PURE COPPER,
OXYGEN FREE

KNIFE EDGE MATERIAL:
Ti - 5Al - 2.5Sn ALLOY, ANNEALED

INTERACTION RATE:
2.54×10^{-2} mm / sec

FIGURE F-5a. SEM MICROGRAPH OF WEAR RING SURFACE
TEST NO. TICU03

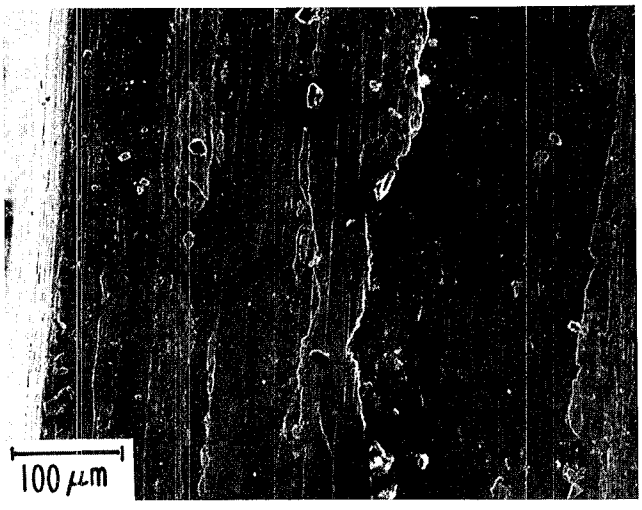

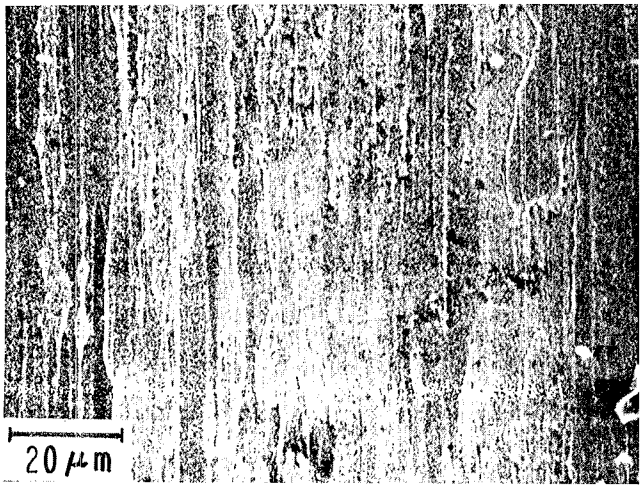

WEAR RING MATERIAL:
99.99% PURE COPPER,
OXYGEN FREE

KNIFE EDGE MATERIAL:
Ti-5Al-2.5Sn ALLOY, ANNEALED

INTERACTION RATE:
2.54×10^{-2} mm/sec

FIGURE F-5b. SEM MICROGRAPH OF KNIFE EDGE SURFACE
TEST NO. TICU03

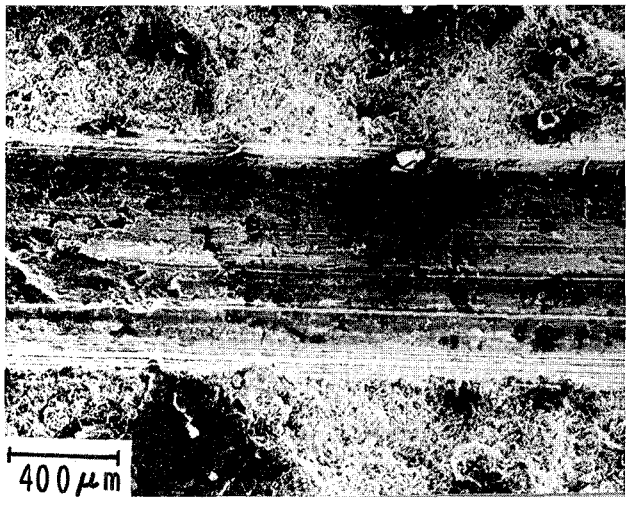

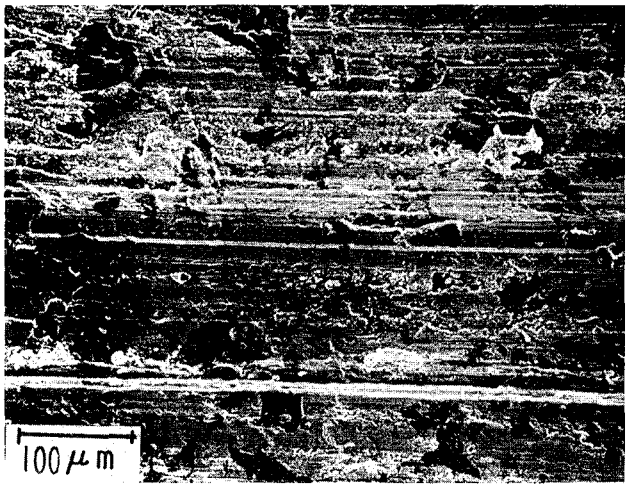

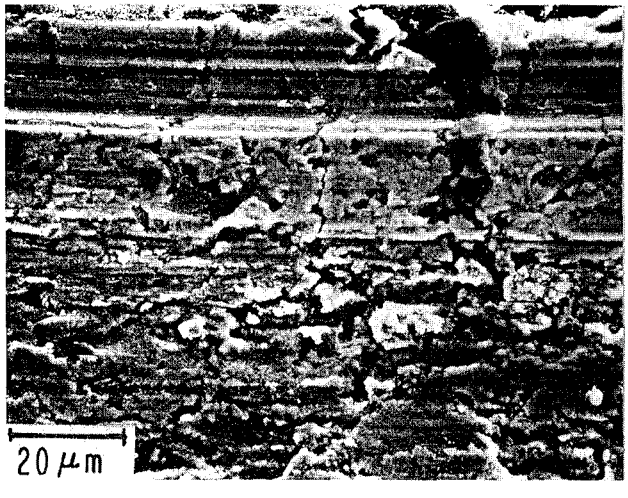

WEAR RING MATERIAL:
ALUMINUM / SILICON/
GRAPHITE COATING,
METCO CE-2198A

KNIFE EDGE MATERIAL:
Ti-5Al-2.5Sn ALLOY, ANNEALED

INTERACTION RATE:
1.45×10^{-1} mm/sec

FIGURE F-6a. SEM MICROGRAPH OF WEAR RING SURFACE
TEST NO. TIAG02

WEAR RING MATERIAL:
ALUMINUM / SILICON / GRAPHITE COATING, METCO CE-2074 A

KNIFE EDGE MATERIAL:
Ti-5Al-2.5Sn ALLOY, ANNEALED

INTERACTION RATE:
1.45×10^{-1} mm / sec

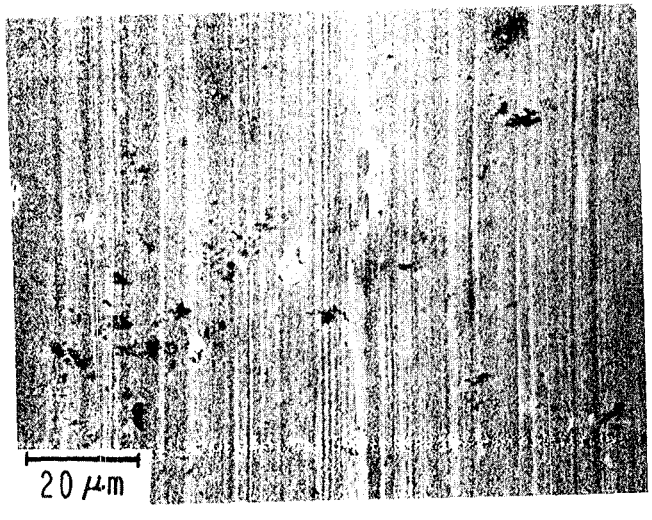

FIGURE F-6b. SEM MICROGRAPH OF KNIFE EDGE SURFACE
TEST NO. TIAG02

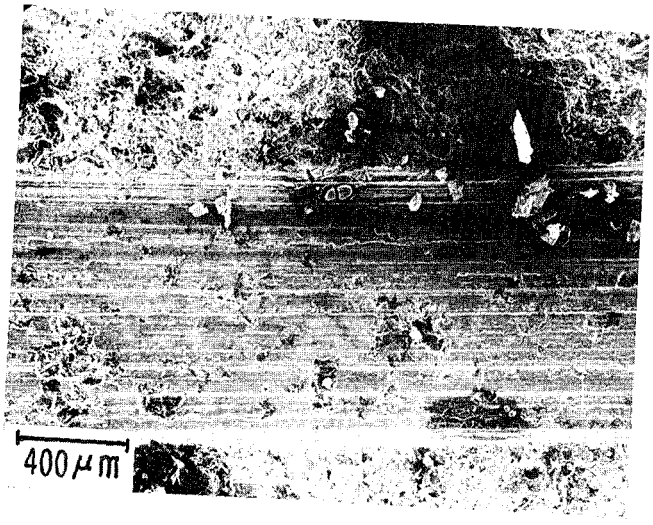

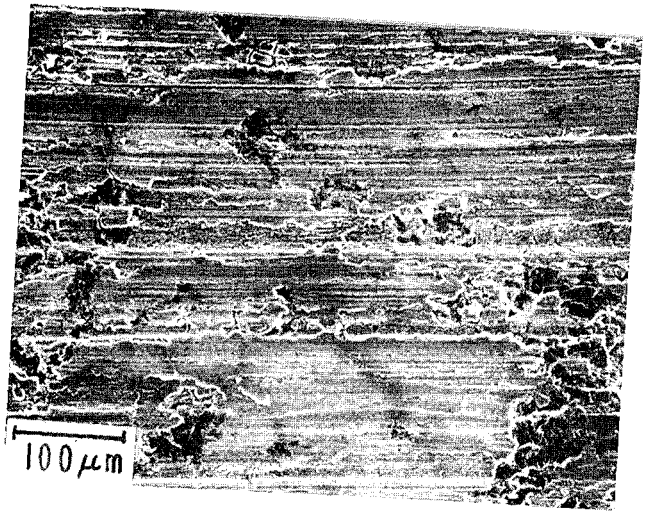

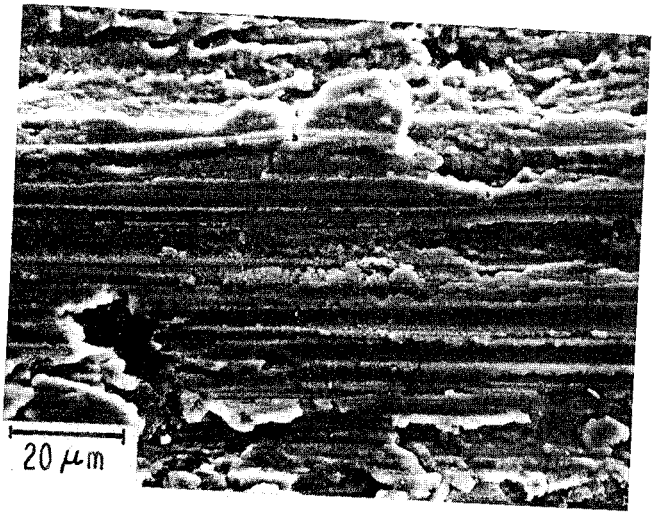

WEAR RING MATERIAL:
ALUMINUM / SILICON / GRAPHITE COATING, METCO CE-2074A

KNIFE EDGE MATERIAL:
Ti-5Al-2.5Sn ALLOY, ANNEALED

INTERACTION RATE:
1.8×10^{-2} mm / sec

FIGURE F-7a. SEM MICROGRAPH OF WEAR RING SURFACE
TEST NO. TIAG03

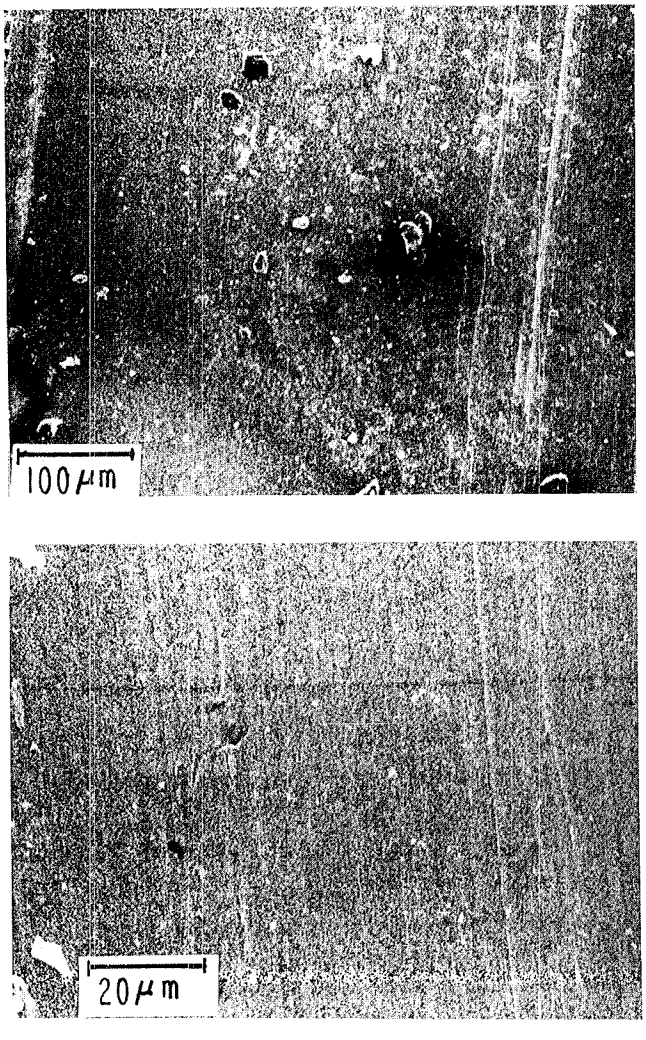

WEAR RING MATERIAL:
ALUMINUM / SILICON /
GRAPHITE COATING,
METCO CE-2074 A

KNIFE EDGE MATERIAL:
Ti-5 Al-2.5 Sn ALLOY, ANNEALED

INTERACTION RATE:
1.8×10^{-1} mm / sec

FIGURE F-7b. SEM MICROGRAPH OF KNIFE EDGE SURFACE
TEST NO. TIAG03

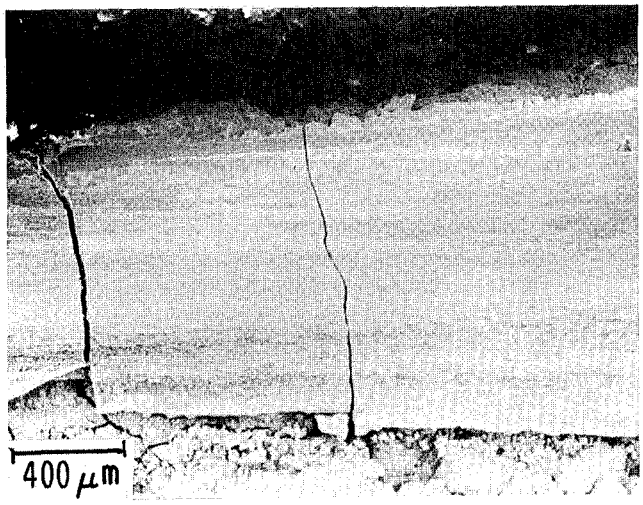

WEAR RING MATERIAL:
Yttria -STABILIZED
ZIRCONIA COATING,
METCO CE-2198A

KNIFE EDGE MATERIAL:
Ti-5Al-2.5Sn ALLOY, ANNEALED

INTERACTION RATE:
2.24×10^{-2} mm/sec

FIGURE F-8a. SEM MICROGRAPH OF WEAR RING SURFACE
TEST NO. TIYZ03

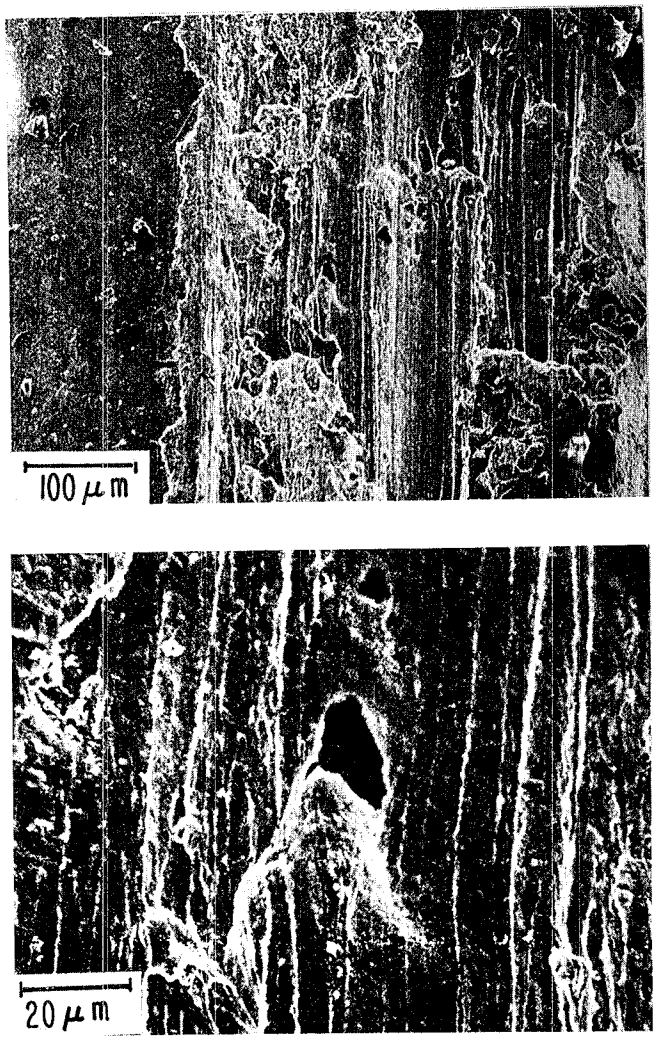

WEAR RING MATERIAL:
Yttria-STABILIZED
ZIRCONIA COATING,
METCO CE-2198A

KNIFE EDGE MATERIAL:
Ti-5Al-2.5Sn ALLOY, ANNEALED

INTERACTION RATE:
2.24×10^{-2} mm/sec

FIGURE F-8b. SEM MICROGRAPH OF KNIFE EDGE SURFACE
TEST NO. TIYZ03

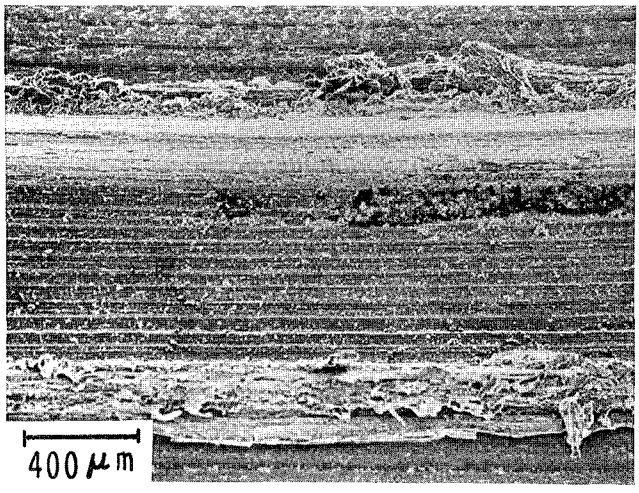

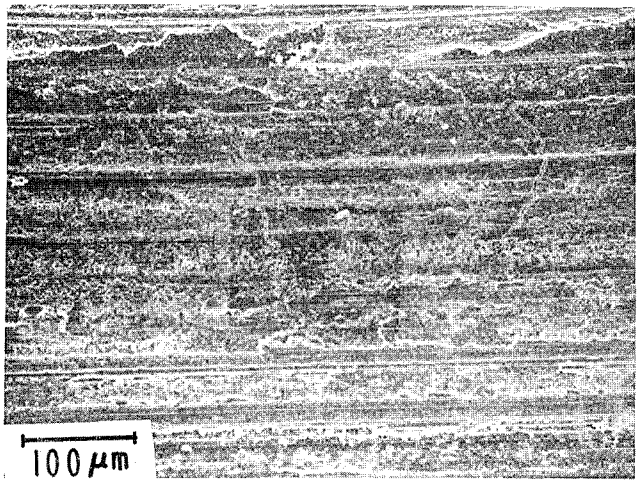

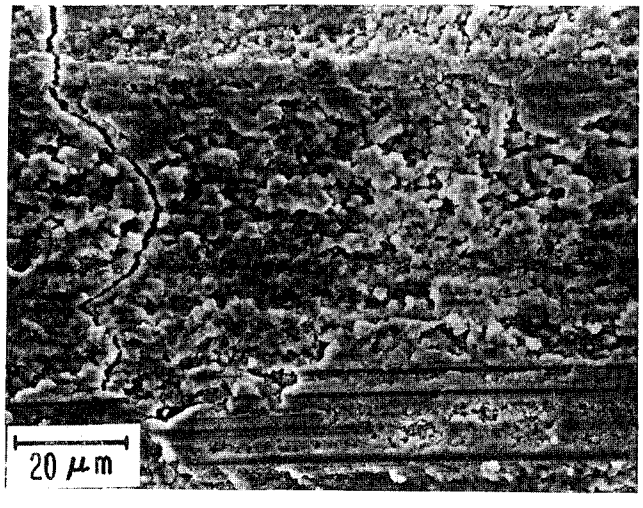

WEAR RING MATERIAL:
2024-T351 ALUMINUM

KNIFE EDGE MATERIAL:
Ti-5Al-2.5Sn ALLOY, ANNEALED

INTERACTION RATE:
1.04×10^{-1} mm/sec

FIGUREF-9a.SEM MICROGRAPH OF WEAR RING SURFACE
TEST NO. TNAL02

WEAR RING MATERIAL:
2024-T351 ALUMINUM

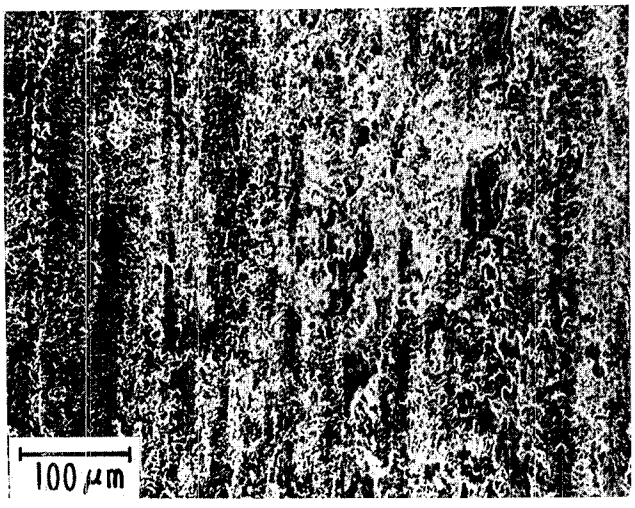

KNIFE EDGE MATERIAL:
Ti-5Al-2.5Sn ALLOY, ANNEALED

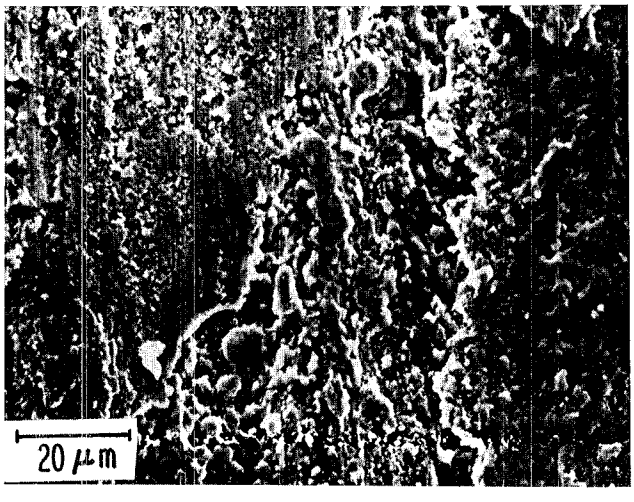

INTERACTION RATE:
1.04×10^{-1} mm/sec

FIGURE F-9b. SEM MICROGRAPH OF KNIFE EDGE SURFACE
TEST NO. TNAL02

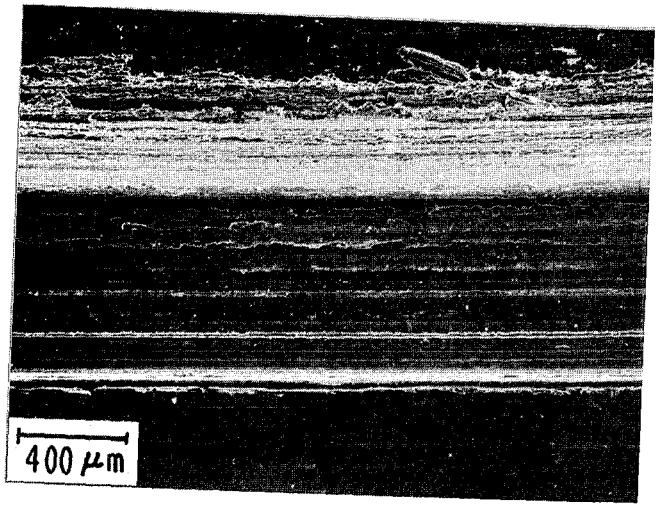

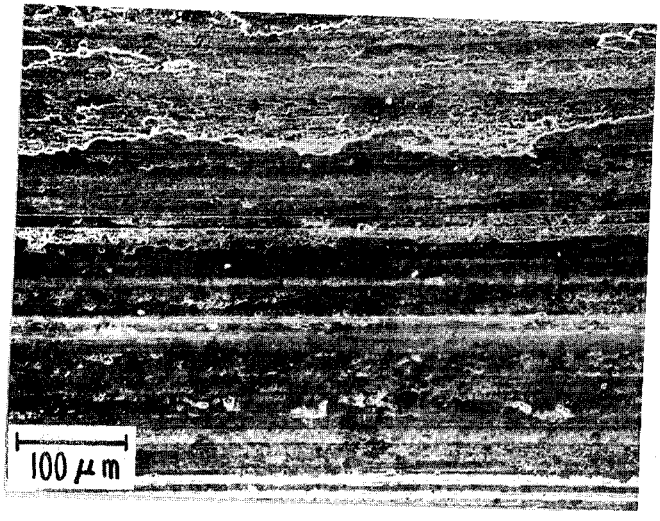

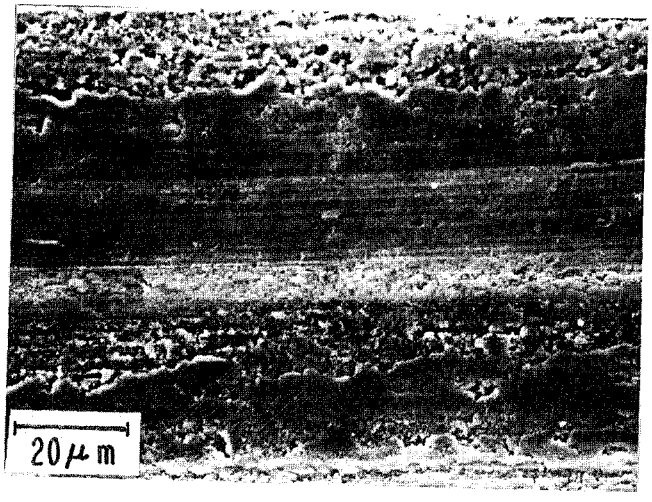

WEAR RING MATERIAL:
2024-T351 ALUMINUM

KNIFE EDGE MATERIAL:
In NITRIDED TITANIUM ALLOY

INTERACTION RATE:
2.1×10^{-2} mm/sec

FIGURE F-10a. SEM MICROGRAPH OF WEAR RING SURFACE
TEST NO. TNAL03

WEAR RING MATERIAL:
2024-T351 ALUMINUM

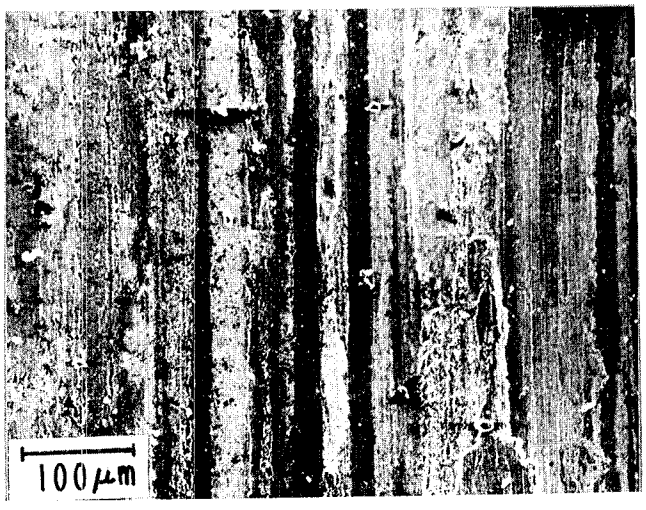

KNIFE EDGE MATERIAL:
In NITRIDED TITANIUM ALLOY

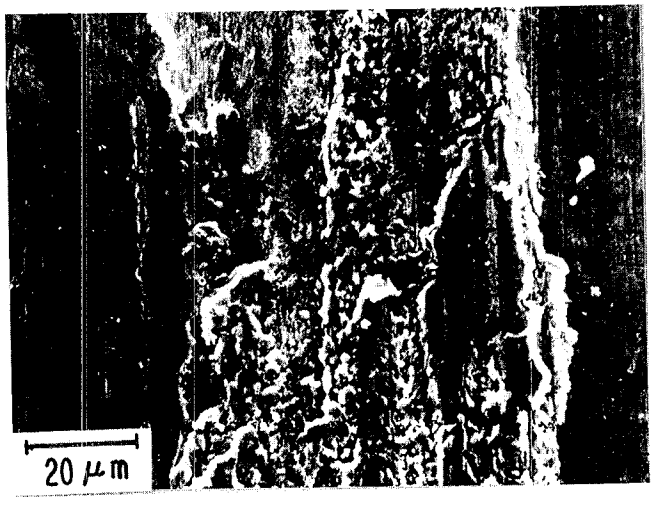

INTERACTION RATE:
2.1×10^{-2} mm/sec

FIGURE F-10b. SEM MICROGRAPH OF KNIFE EDGE SURFACE
TEST NO. TNAL03

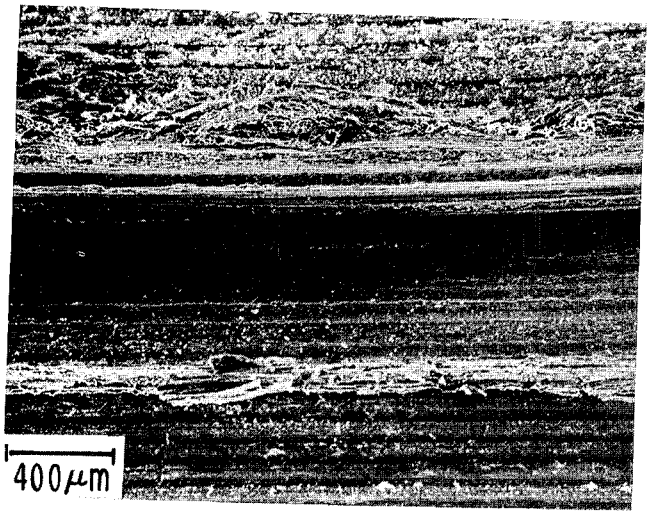

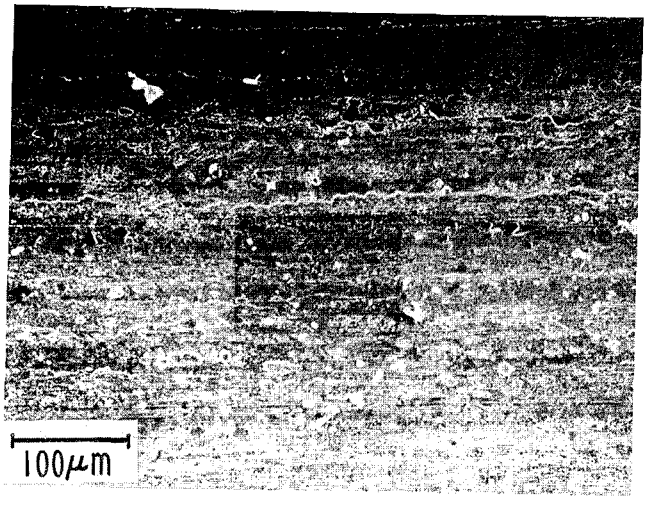

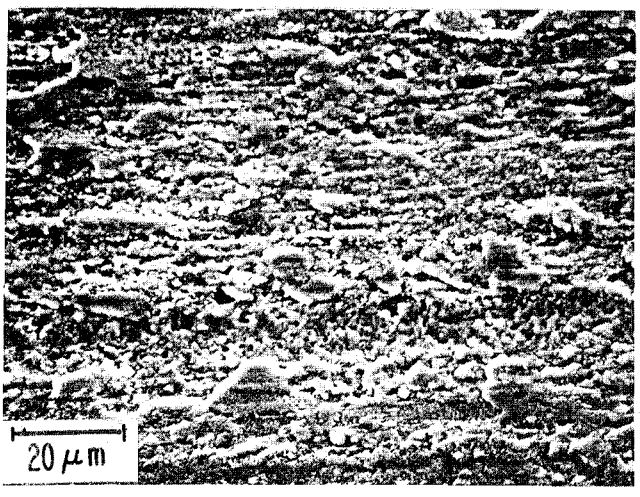

WEAR RING MATERIAL:
2024T 351 ALUMINUM

KNIFE EDGE MATERIAL:
ALUMINA / TITANIA COATING,
METCO 101B-NS

INTERACTION RATE:
1.06×10^{-1} mm / sec

FIGURE F-11a. SEM MICROGRAPH OF WEAR RING SURFACE
TEST NO. A0AL02

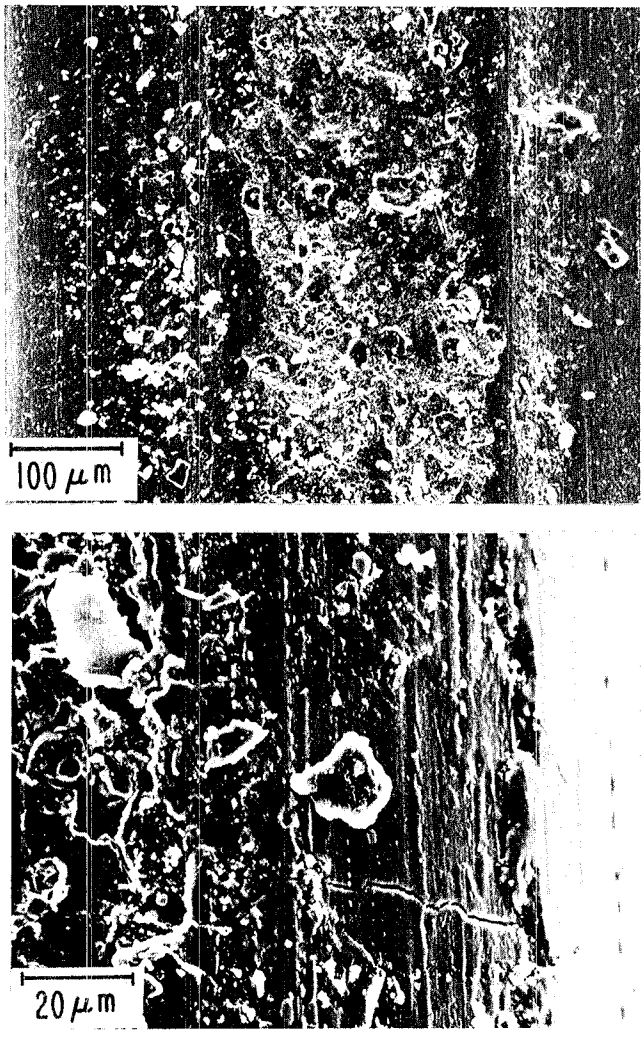

WEAR RING MATERIAL:
2024 T351 ALUMINUM

KNIFE EDGE MATERIAL:
ALUMINA/TITANIA COATING,
METCO 101B-NS

INTERACTION RATE:
1.06×10^{-1} mm/sec

FIGURE F-11b. SEM MICROGRAPH OF KNIFE EDGE SURFACE
TEST NO. AOAL02

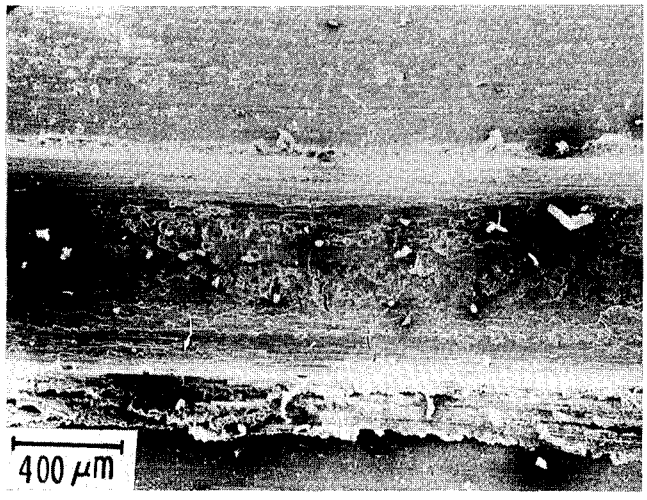

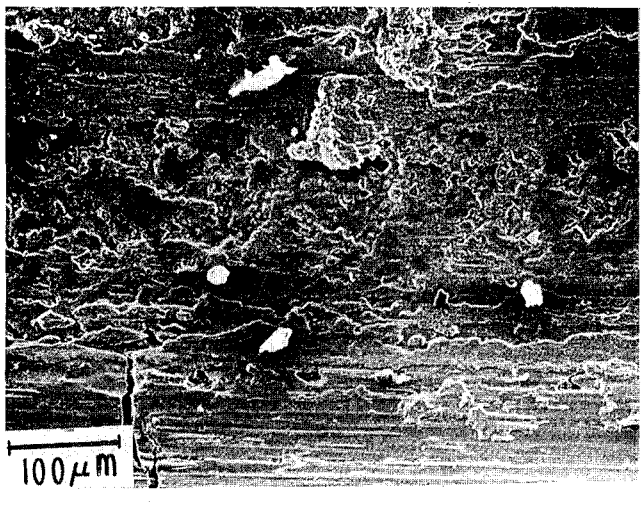

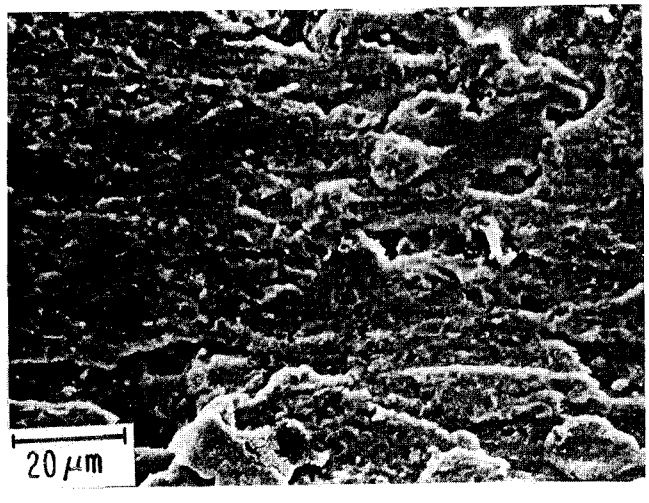

WEAR RING MATERIAL:
2024-T351 ALUMINUM

KNIFE EDGE MATERIAL:
ALUMINA/TITANIA COATING,
METCO 101B-NS

INTERACTION RATE:
1.75×10^{-2} mm/sec

FIGURE F-12a. SEM MICROGRAPH OF WEAR RING SURFACE
TEST NO. A0AL03

WEAR RING MATERIAL:
2024 T 351 ALUMINUM

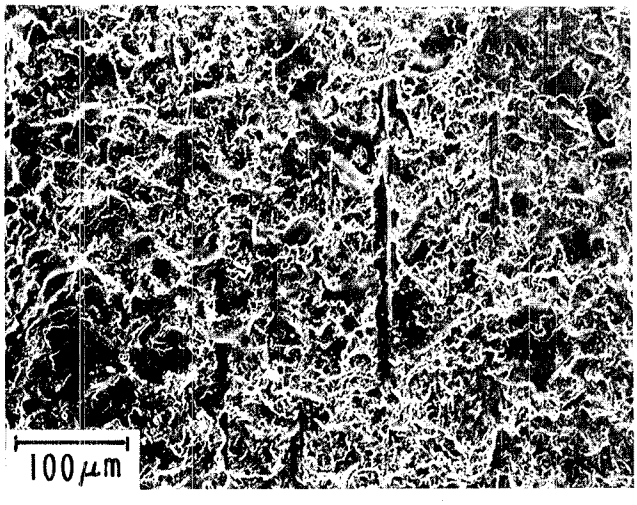

KNIFE EDGE MATERIAL:
ALUMINA / TITANIA COATING,
METCO 101B-NS

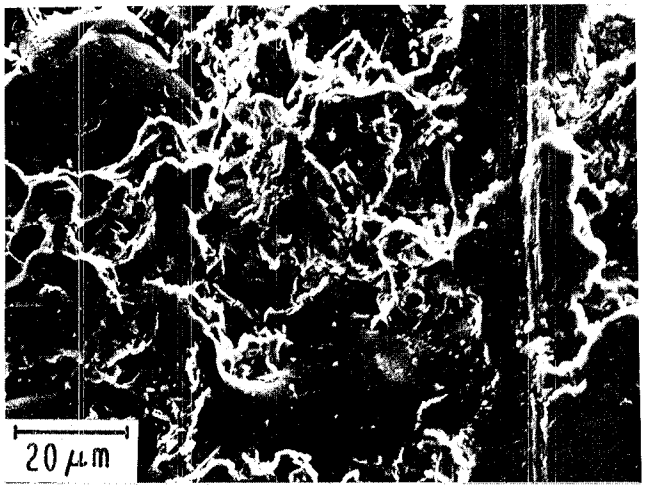

INTERACTION RATE:
1.75×10^{-2} mm / sec

FIGURE F-12b. SEM MICROGRAPH OF KNIFE EDGE SURFACE
TEST NO. A0AL03

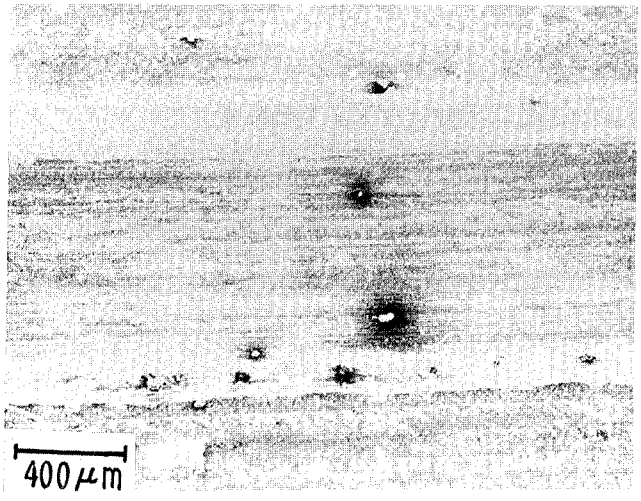

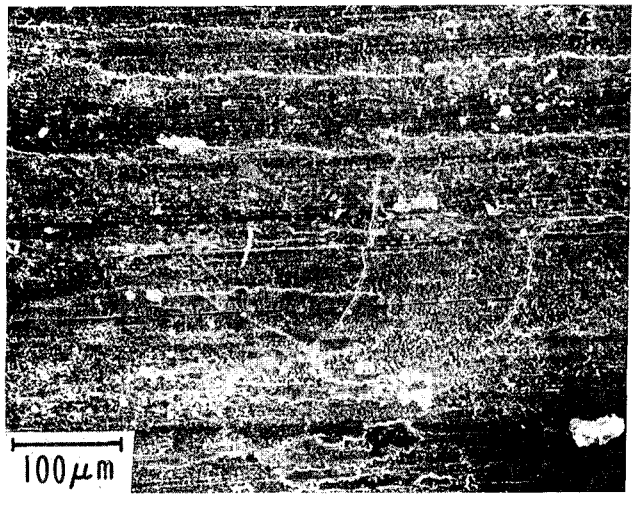

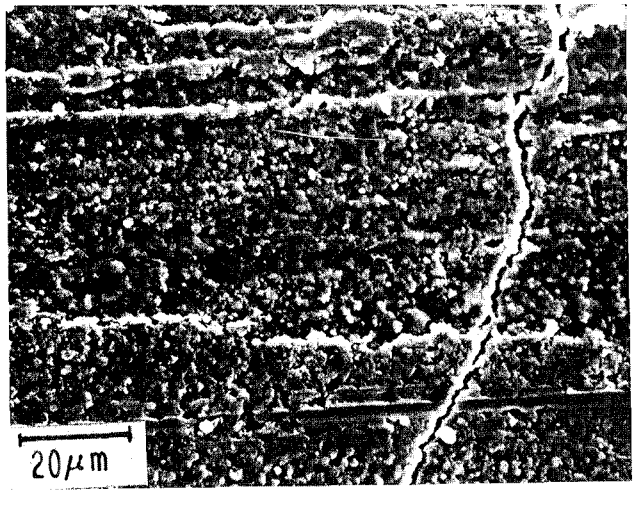

WEAR RING MATERIAL:
2024T351 ALUMINUM

KNIFE EDGE MATERIAL:
TUNGSTEN CARBIDE+
COBALT-CHROMIUM COATING,
UCAR LW-15

INTERACTION RATE:
1.21×10^{-1} mm/sec

FIGURE F-13a. SEM MICROGRAPH OF WEAR RING SURFACE
TEST NO. TCAL02

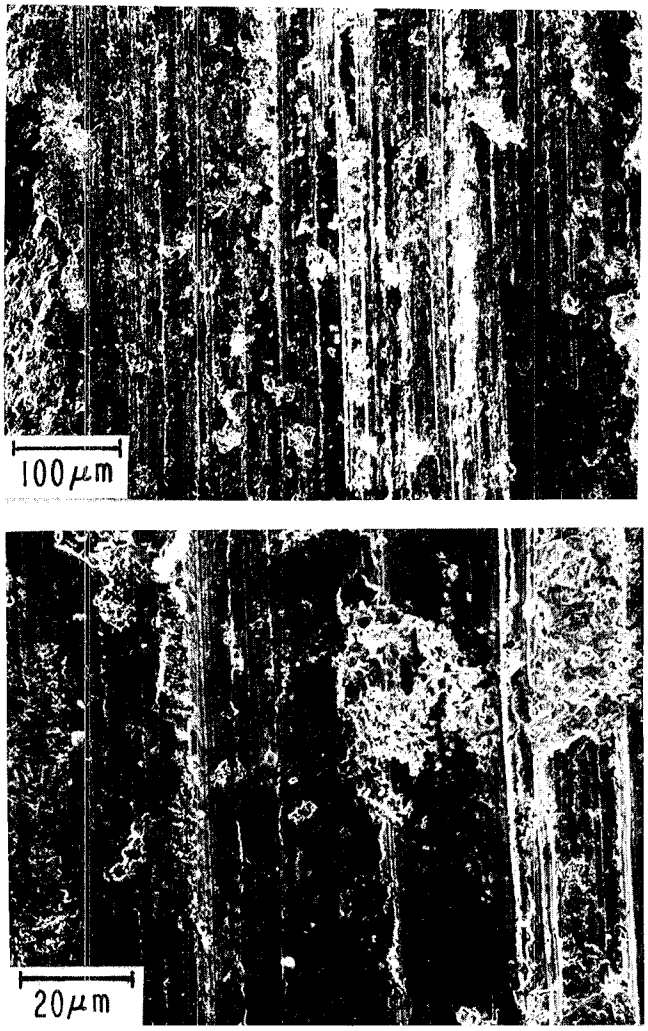

WEAR RING MATERIAL:
2024T351 ALUMINUM

KNIFE EDGE MATERIAL:
TUNGSTEN CARBIDE +
COBALT CHROMIUM COATING,
UCAR LN-15

INTERACTION RATE:
1.21×10^{-1} mm/sec

FIGURE F-13b. SEM MICROGRAPH OF KNIFE EDGE SURFACE
TEST NO. TCAL02

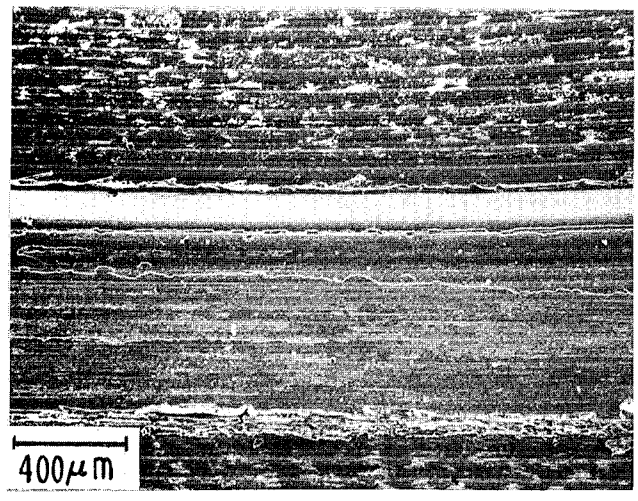

WEAR RING MATERIAL:
2024T351 ALUMINUM

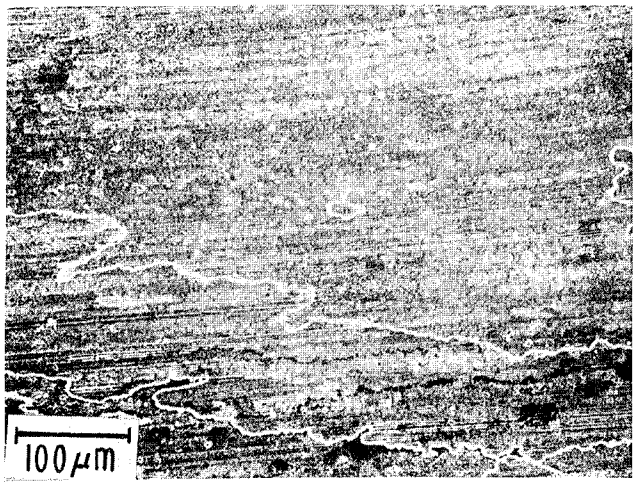

KNIFE EDGE MATERIAL:
TUNGSTEN CARBIDE+
COBALT-CHROMIUM COATING,
UCAR LW-15

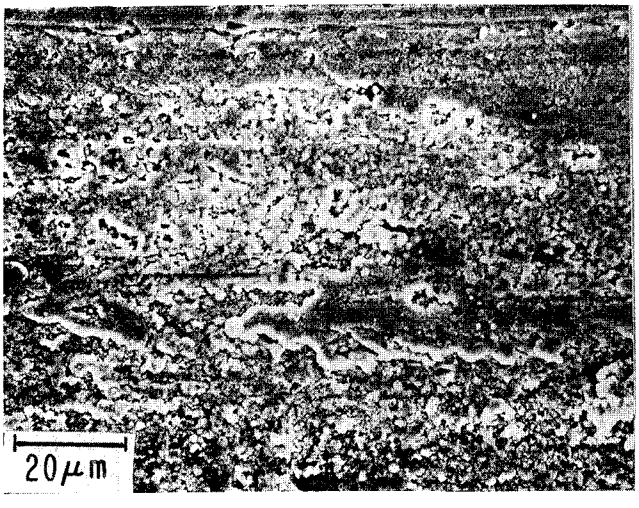

INTERACTION RATE:
1.1×10^{-2} mm/sec

FIGURE F-14a. SEM MICROGRAPH OF WEAR RING SURFACE
TEST NO. TCAL03

WEAR RING MATERIAL:
2024T351 ALUMINUM

KNIFE EDGE MATERIAL:
TUNGSTEN CARBIDE+
COBALT-CHROMIUM COATING,
UCAR LW-15

INTERACTION RATE:
1.1×10^{-2} mm/sec

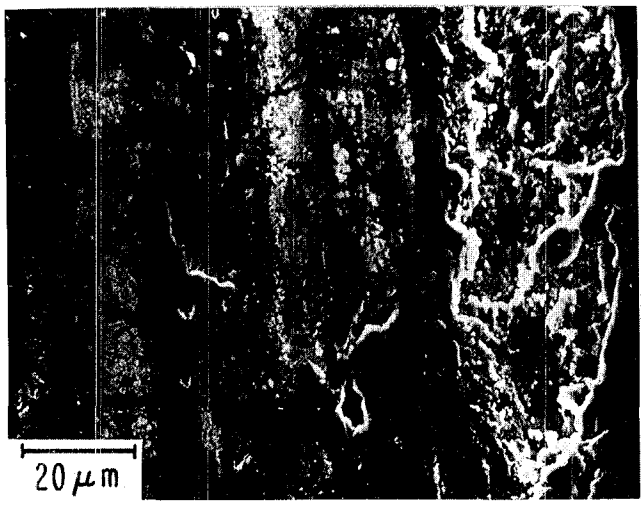

FIGURE F-14b. SEM MICROGRAPH OF KNIFE EDGE SURFACE
TEST NO. TCAL03

End of Document